Terms and Conditions of Use of Digitised Theses from Trinity College Library Dublin

Copyright statement

All material supplied by Trinity College Library is protected by copyright (under the Copyright and Related Rights Act, 2000 as amended) and other relevant Intellectual Property Rights. By accessing and using a Digitised Thesis from Trinity College Library you acknowledge that all Intellectual Property Rights in any Works supplied are the sole and exclusive property of the copyright and/or other IPR holder. Specific copyright holders may not be explicitly identified. Use of materials from other sources within a thesis should not be construed as a claim over them.

A non-exclusive, non-transferable licence is hereby granted to those using or reproducing, in whole or in part, the material for valid purposes, providing the copyright owners are acknowledged using the normal conventions. Where specific permission to use material is required, this is identified and such permission must be sought from the copyright holder or agency cited.

Liability statement

By using a Digitised Thesis, I accept that Trinity College Dublin bears no legal responsibility for the accuracy, legality or comprehensiveness of materials contained within the thesis, and that Trinity College Dublin accepts no liability for indirect, consequential, or incidental, damages or losses arising from use of the thesis for whatever reason. Information located in a thesis may be subject to specific use constraints, details of which may not be explicitly described. It is the responsibility of potential and actual users to be aware of such constraints and to abide by them. By making use of material from a digitised thesis, you accept these copyright and disclaimer provisions. Where it is brought to the attention of Trinity College Library that there may be a breach of copyright or other restraint, it is the policy to withdraw or take down access to a thesis while the issue is being resolved.

Access Agreement

By using a Digitised Thesis from Trinity College Library you are bound by the following Terms & Conditions. Please read them carefully.

I have read and I understand the following statement: All material supplied via a Digitised Thesis from Trinity College Library is protected by copyright and other intellectual property rights, and duplication or sale of all or part of any of a thesis is not permitted, except that material may be duplicated by you for your research use or for educational purposes in electronic or print form providing the copyright owners are acknowledged using the normal conventions. You must obtain permission for any other use. Electronic or print copies may not be offered, whether for sale or otherwise to anyone. This copy has been supplied on the understanding that it is copyright material and that no quotation from the thesis may be published without proper acknowledgement.

Semliki Forest Virus Based Gene Therapy of Rat Glioma

A thesis submitted to the University of Dublin, Trinity College for the Degree of Doctor of Philosophy

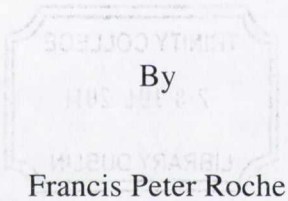

By

Francis Peter Roche

School of Genetics and Microbiology,
Moyne Institute of Preventive Medicine,
Trinity College, Dublin

October 2009

Abstract

Glioblastoma multiforme (GBM) is an invariably fatal neoplastic lesion of the CNS. Despite advances in the treatment of cancer in the recent years, the prognosis of GBM has changed little and patients who undergo surgical resection and adjuvant chemo- or radiotherapy eventually succumb to tumor recurrence.

The Semliki Forest virus - virus-like particle is a replication-incompetent suicidal expression system based on the Semliki Forest virus. The SFV VLP system allows for transient, high-level expression of the encoded transgene and, designed to encode immunostimulatory cytokines, has been successfully used in a number of immunotherapeutic anti-tumor strategies. This study utilised the VLP system encoding interleukin 12 (IL-12), interferon gamma (IFN-γ) and interferon beta (IFN-β) as a therapeutic intervention in two rat GBM models. IL-12, IFN-γ and IFN-β genes were cloned into the VLP expression system which demonstrated the ability to induce expression of biologically active cytokines from infected cells.

The RG2 and F98 rat glioma models are currently considered the most representative *in vivo* models of human GBM and are produced by the intracerebral inoculation of F98 or RG2 cells into syngeneic Fischer 344 rats. The VLP system demonstrated the ability to infect, mediated transgene expression from and induce cell death in both glioma cell lines *in vitro* and *in vivo*. IL-12 encoding VLP therapy of RG2 gliomas resulted in a significant reduction in tumor volume that was associated with a statistically significant extension in survival. This effect was dependant upon IL-12 expression and did not appear to result from the induction of a host anti-tumor response. Additionally, VLP delivery resulted in the occurrence of treatment-related toxicity, particularly in high-dose treated animals. Treatment-related deaths were unrelated to replication-competent virus (RCV) production or IL-12 expression but appeared to be the result of VLP induced damage within the CNS.

The SFV VLP system has also examined as an anti-tumor therapy using the non-invasive intranasal (i.n.) delivery route. IFN-β, IFN-γ and IL-12 encoding VLPs were delivered intranasally to tumor-bearing rats and the effect on tumor volume analysed. No significant reduction in tumor volume was observed because of intranasal treatment. The absence of efficacy appeared to be related to the inefficient transfer of the VLP encoded cytokine into the CNS and suggested that the VLP system may not be suitable for use in rat models.

Publications and Presentations

Presentations:

Oral Presentation ;

1. **Meeting of the Irish Society of Gene and Cell Therapy (ISGCT). 15-16th May 2008, Cork, Ireland.**

   'Gene therapy of RG2 and F98 glioma models using the Semliki Forest Virus – Virus-Like Particle (SFV-VLP) system expressing immuno-stimulatory cytokines.'
   Roche FP, Sheahan BJ, O'Mara SM , Atkins GJ.

Poster presentation ;

1. **The sixteenth meeting of the European Society of Cell and Gene Therapy (ESCGT). 13-16th November 2008, Brugges, Belgium.**

   'RNA based immuno-gene therapy of rat glioma.'
   Roche FP, Sheahan BJ, O'Mara SM , Atkins GJ.

For my parents and for my family

Declaration

This thesis is submitted by the undersigned to the University of Dublin, Trinity College for the examination of Doctorate of Philosophy. The work herein is entirely my own work and has not been submitted as an exercise for a degree to any other university. The librarian of Trinity College Dublin has my permission to lend or copy this thesis upon request.

Acknowledgements

I would like to thank Prof. Gregory Atkins for providing me with the opportunity to pursue my studies, which I have enjoyed immensely and will always fondly remember. Also thank you for the guidance, knowledge and support throughout the years.

I would also like to thank Prof. Shane O' Mara for his assistance in the development of the glioma model and for his assistance in troubleshooting the occasional problems that arose throughout the project.

Brian, I truly appreciate all the help, expertise and guidance you have given me throughout the years.

Dot, what can I say, it's been a blast. You're the second mother I never asked for but couldn't have done without. Thank you so much for your continual support, whether it be in the guise of listening to me rant about something, helping me when I hit a wall, keeping the chocolate drawer well-stocked or just the laughs we had. I will always think of you when I hear the words "I didn't do anything, it just stopped working". I wish you all the best in this, your 3rd age, and hope that it brings you and those you love all the happiness you have given to others throughout the years.

To Ann, Barbara, Caroline, Christina, David, Eavan, Guniz, James, Joanne, Michael and Rory (in alphabetical order), you are my dearest friends who have put up with me for these last four years and provided me with the laughs and entertainment that were, at times, desperately needed. I love you guys very much and appreciate all you have done for me and all the support you have given me.

A special thank you to Marina and Barbara; Thank you so much for everything throughout the years, for the help, the chats and for the laughs. X

Thanks to all those who have contributed to the virology lab and the TCIN who I have had the pleasure of working with; Andrea, Charlotte, Johannes, Kathrina, Ollie, Sally, Sara and Wen, thanks for all the help and laughs, it's been a blast.

To whom this thesis is dedicated; my parents and family. Your support and love is unparalleled and I appreciate it more than I can say.

"The scientist does not study nature because it is useful; he studies it because he delights in it, and he delights in it because it is beautiful. If nature were not beautiful, it would not be worth knowing, and if nature were not worth knowing, life would not be worth living."

Jules Henri Poincaré (1854 –1912)

Abstract

Glioblastoma multiforme (GBM) is an invariably fatal neoplastic lesion of the CNS. Despite advances in the treatment of cancer in the recent years, the prognosis of GBM has changed little and patients who undergo surgical resection and adjuvant chemo- or radiotherapy eventually succumb to tumor recurrence.

The Semliki Forest virus - virus-like particle is a replication-incompetent suicidal expression system based on the Semliki Forest virus. The SFV VLP system allows for transient, high-level expression of the encoded transgene and, designed to encode immunostimulatory cytokines, has been successfully used in a number of immunotherapeutic anti-tumor strategies. This study utilised the VLP system encoding interleukin 12 (IL-12), interferon gamma (IFN-γ) and interferon beta (IFN-β) as a therapeutic intervention in two rat GBM models. IL-12, IFN-γ and IFN-β genes were cloned into the VLP expression system which demonstrated the ability to induce expression of biologically active cytokines from infected cells.

The RG2 and F98 rat glioma models are currently considered the most representative *in vivo* models of human GBM and are produced by the intracerebral inoculation of F98 or RG2 cells into syngeneic Fischer 344 rats. The VLP system demonstrated the ability to infect, mediated transgene expression from and induce cell death in both glioma cell lines *in vitro* and *in vivo*. IL-12 encoding VLP therapy of RG2 gliomas resulted in a significant reduction in tumor volume that was associated with a statistically significant extension in survival. This effect was dependant upon IL-12 expression and did not appear to result from the induction of a host anti-tumor response. Additionally, VLP delivery resulted in the occurrence of treatment-related toxicity, particularly in high-dose treated animals. Treatment-related deaths were unrelated to replication-competent virus (RCV) production or IL-12 expression but appeared to be the result of VLP induced damage within the CNS.

The SFV VLP system has also examined as an anti-tumor therapy using the non-invasive intranasal (i.n.) delivery route. IFN-β, IFN-γ and IL-12 encoding VLPs were delivered intranasally to tumor-bearing rats and the effect on tumor volume analysed. No significant reduction in tumor volume was observed because of intranasal treatment. The absence of efficacy appeared to be related to the inefficient transfer of the VLP encoded cytokine into the CNS and suggested that the VLP system may not be suitable for use in rat models.

Publications and Presentations

Presentations:

Oral Presentation ;

1. **Meeting of the Irish Society of Gene and Cell Therapy (ISGCT). 15-16th May 2008, Cork, Ireland.**

   'Gene therapy of RG2 and F98 glioma models using the Semliki Forest Virus – Virus-Like Particle (SFV-VLP) system expressing immuno-stimulatory cytokines.'
   Roche FP, Sheahan BJ, O'Mara SM , Atkins GJ.

Poster presentation ;

1. **The sixteenth meeting of the European Society of Cell and Gene Therapy (ESCGT). 13-16th November 2008, Brugges, Belgium.**

   'RNA based immuno-gene therapy of rat glioma.'
   Roche FP, Sheahan BJ, O'Mara SM , Atkins GJ.

Table of Contents

Chapter 1
General Introduction

Chapter 2

Cloning of interferon beta, interferon gamma and interleukin-12 into the SFV enhanced expression vector system

Chapter 3

In vitro analysis of the expression and activity of SFV VLP encoded cytokines

Chapter 4

Characterisation of SFV VLP infection and apoptosis induction in two rat glioma cell lines

Chapter 5

Intracerebral treatment of glioma models using the SFV VLP system

Chapter 6

Intranasal treatment of glioma models using the SFV VLP system

Chapter 7

General discussion

Chapter 8

Bibliography

Index of tables

Chapter 1

Chapter 2

Chapter 3

Chapter 5

Index of figures

Chapter 1

Chapter 2

Chapter 3

Chapter 4

Chapter 5

Chapter 6

Abbreviations

AA	anaplastic astrocytoma
aa	amino acid
Ad	adenovirus
ADCC	antibody-dependant cell-mediated cytotoxicity
ADP	adenosine diphosphate
AICD	Activation-induced cell death
APC	antigen-presenting cell
ATCC	American type culture collection
ATP	adenosine triphosphate
BBB	blood brain barrier
BCG	bacillus calmette-guérin
BHK	baby hamster kidney
βME	beta mercaptoethanol
bp	base pair
BSA	bovine serum albumin
CD	cluster of differentiation antigen
CDK	cyclin-dependent kinase
cDNA	complementary DNA
CNS	central nervous system
Con A	concanavalin A
CPE	cytopathic effect
CSF	cerebrospinal fluid
CTL	cytotoxic T lymphocyte
CVO	circumventricular organ
DAB	3,3'-diaminobenzidine
DAPI	4',6-diamidino-2-phenylindole
dATP	deoxyadenosine triphosphate
DC	dendritic cell
DLN	draining lymph node
DMEM	Dulbecco's minimal essential medium
DNA	deoxyribonucleic acid
dNTP	deoxynucleoside triphosphate

dsDNA	double stranded DNA
dsRNA	double stranded RNA
DTT	dithiothreitol
ECACC	European collection of cell cultures
ECM	extracellular matrix
EDTA	ethylene-di-amine tetra-acetic acid
EGFP	enhanced green fluorescent protein
ELISA	enzyme-linked immunosorbent assay
EPC	endothelial precursor cell
ER	endoplasmic reticulum
FACS	fluorescence-activated cell sorter
FasL	Fas ligand
FCS	foetal calf serum
FGF	fibroblast growth factor
FGFR	FGF receptor
FITC	fluorescein isothiocyanate
FMDV	foot and mouth disease virus
g	gravitational force
G	gauge
GBM	glioblastoma multiforme
GDP	guanosine diphosphate
GFAP	glial fibrillary acidic protein
GFP	green fluorescent protein
GM-CFS	granulocyte-macrophage colony stimulating factor
GTP	guanosine triphosphate
H&E	haematoxylin and eosin
h.p.i.	hours post infection
H_2O_2	hydrogen peroxide
hepes	4-(2-hydroxyethyl)-1-piperazineethanesulfonic acid
HIV	human immunodeficiency virus
HLA	human leukocyte antigen
HPV	human papillomavirus
HRP	horseradish peroxidase
HSV	herpes simplex virus

i.c.	intracerebral
i.m.	intramuscular
i.n.	intranasal
i.t.	intratumoral
ICE	interleukin-converting enzyme
IFN	interferon
Ig	immunoglobulin
IGF	insulin-like growth factor
IHC	immunohistochemistry
IL	interleukin
iNOS	inducible nitric oxide synthase
IP-10	interferon-gamma-inducible protein-10 (CXCL10)
IRSE	interferon-stimulated response element
ISGF3	interferon-stimulated gene factor-3
I-TAC	interferon-inducible T cell alpha chemoattractant (CXCL11)
IU	international units
kb	kilo base pairs
LPS	lipopolysaccharide
MOI	multiplicity of infection
MCS	multiple cloning site
MCP-1	monocyte chemotactic protein-1
MDA5	melanoma-differentiation-associated gene 5 RNA helicase
MEM	minimal essential medium
MHC	major histocompatibility complex
MIG	monokine induced by interferon-gamma (CXCL9)
MMP	matrix metalloprotease
MRI	magnetic resonance imaging
mRNA	messenger RNA
miRNA	micro RNA
NDV	Newcastle disease virus
NGS	normal goat serum
NHS	normal horse serum
NK	natural killer cell
NKT	natural killer T cell

NMS	normal mouse serum
NO	nitric oxide
NRS	normal rabbit serum
nsP	SFV non-structural protein
OAS	oligoadenylate synthetase
ORF	open reading frame
p.f.u.	plaque forming units
p.i.	post infection
PAMP	pathogen-associated molecular pattern
PBS	phosphate buffered saline
PBST	PBS containing 0.05% Tween 80
PCR	polymerase chain reaction
PDGF	platelet-derived growth factor
PDGFR	platelet-derived growth factor receptor
PEG_2	prostaglandin E_2
PFA	paraformaldehyde
PKR	protein kinase R
rpm	revolutions per minute
RBC	red blood corpuscle
RCV	replication competent virus
RH	relative humidity
RIG-1	retinoic acid-inducible gene-1
RNA	ribonucleic acid
RT	room temperature
RT-PCR	reverse transcription polymerase chain reaction
s.c.	subcutaneous
SCID	severe combined immunodeficiency
SFV	Semliki Forest virus
SIN	Sindbis virus
STAT	signal transducer and activator of transcription
TAA	tumour-associated antigen
TADC	tumour-associated DC
TAM	tumour-associated Macrophage
TGF	transforming growth factor

Th	T helper
TIL	tumour-infiltrating lymphocyte
TLR	toll-like receptor
TMB	trimethyl benzidine
TNF	tumour necrosis factor
TRAIL	TNF-related apoptosis-inducing ligand
Tris	Tris-(hydroxymethyl)-aminomethane
UTR	untranslated region
VEGF	vascular endothelial growth factor
VEGFR	vascular endothelial growth factor receptor
VLP	virus-like particle
WHO	world health organisation

Chapter 1

General Introduction

1.1 Semliki Forest virus

Semliki Forest virus (SFV) is one of at least twenty-six members of the *Alphavirus* genus, family Togavirade. Alphaviruses have a diverse host range and arthropods, in which infection is life-long, are the primary transmission vectors. Vertebrate hosts typically undergo acute infection and viral pathogenesis and disease severity are dependent upon the alphavirus strain and host-specific factors. SFV was first isolated in 1942 from the Semliki crown forest in Uganda (Smithburn and Haddow, 1944) and a number of isolates have subsequently been identified in Africa, the USSR and India. SFV infection is not known to cause lethal encephalitis in humans but produces a mild febrile disease accompanied by headache, myalgia and arthalgia (Mathiot *et al.*, 1990). Additionally, laboratory strains of SFV are considered avirulent in humans with the exception of an individual case of lethal SFV-mediated encephalitis reported in a laboratory worker (Willems *et al.*, 1979). SFV is a single-stranded, positive-sense RNA virus and the approximately 11kb genome is encapsidated by 240 copies of the capsid protein surrounded by a plasma-membrane-derived lipid bi-layer studded with virus encoded glycoproteins. The SFV genome is 5' capped, 3' polyadenylated and consists of two non-overlapping open reading frames (ORFs) encoding nine proteins. The 5' two-thirds of the SFV genome encodes the non-structural ORF, translated to produce the replicase complex, and the 3' one-third ORF encodes the structural proteins. Both open reading frames are translated as polyprotein precursors, which are post- and co-translationally cleaved into individual proteins by virus encoded and host proteases. The SFV genome also contains the 5' and 3' untranslated regions (UTRs) and the junction between the non-structural and structural reading frames, which includes the sub-genomic transcriptional promoter, subgenomic translational start site and 5' non-translated leader sequence.

The natural infection route via arthropod vectors is initiated by subcutaneous deposition of virus by an infected vector, following blood feeding. Initially, viral replication occurs in the subcutaneous tissue and is transported to the local draining lymph node (DLN) either as free virus or by exploiting the migratory potential of activated innate immune cells such as dendritic cells (DCs) or macrophages (Ryman and Klimstra, 2008). Within the DLN, virus replication seeds blood viremia followed by systemic infection of permissive cells. Infection of the CNS typically occurs late in the infection cycle, resulting in infection and replication in neurons and oligodendrocytes (Fazakerley, 2004); however, the degree of encephalitis and its ultimate clinical outcome are dependent on the alphavirus

strain and virus-host interactions. Figure 1.1 represents the infection cycle of SFV; following the introduction of genomic ($42S^+$) RNA into the host-cell cytoplasm, the non-structural ORF is directly translated into the nsP1-4 polyprotein. The nsP2's protease activity efficiently cleaves the nsP3/4 junction liberating the nsP1-3 and nsP4 proteins which form the replicase complex responsible for the production of negative-sense genomic ($42S^-$) RNA. Negative strand synthesis proceeds for approximately 4 hours at which point further nsP1-3 cleavage, mediated by the nsP2 protease, redirects the replicase activity towards the production of $42S^+$ genomic and $26S^+$ subgenomic RNA, using the $42S^-$ RNA as template (Strauss and Strauss, 1994; Meritis *et al.*, 2001; Vasiljeva *et al.*, 2003). Although the stable replicase complex persists throughout the infection cycle (Strauss and Strauss, 1994) translation of the replicase complex is terminated as a result of the inhibition of cap-dependent translation by the dsRNA dependent protein kinase R (PKR) system (Ventoso *et al.*, 2006). The production of $26S^+$ subgenomic RNA is followed by translation of the structural proteins; a stable RNA hairpin loop located within the capsid sequence of the $26S^+$ RNA is responsible for overcoming the cap-dependent translation inhibition allowing for efficient translation of the structural proteins (Ventoso *et al.*, 2006). The capsid protein is cotranslationally liberated from the nascent polyprotein by its serine auto-protease activity producing the capsid and E3-E2-6k-E1 proteins. The capsid protein diffuses into the cytoplasm and specifically interacts with a sequence present in the 5' region of the $42S^+$ RNA non-structural ORF, known as the packaging signal, resulting in the encapsidation of the genomic RNA. The E3-E2-6k-E1 polyprotein, also designated p62-6k-E1, is shuttled, by virtue of the E3 N-terminal signal sequence, to the endoplasmic reticulum (ER). Polyprotein maturation occurs within the ER and involves various cleavage and glycosylation events carried out by cellular enzymes to produce the individual mature E3, E2, 6k and E1 proteins. These mature glycoproteins are trafficked through the golgi apparatus and become associated with the cell membrane. The viral spike complex is composed of three E1/E2/E3 trimers possessing a cytoplasmic domain that interacts with the viral nucleocapsid and initiates budding from the cell. Newly produced virus is then capable of initiating infection in permissive cells.

Alphavirus entry is achieved by receptor-mediated endocytosis; studies have demonstrated a large variety of cell receptors used by the alphaviruses family and within a single virus strain a number of possible receptors can be used (Strauss and Strauss, 1994). Although the lamin receptor has been identified as at least one of the Sindbis (SIN) virus cellular receptors, SFV receptors are currently undefined only to say there are likely to be a

number of different receptors. Following virus entry, the virion-containing endosome fuses with cellular lysosomes ultimately releasing the viral RNA into the cytoplasm, initiating genome replication and virion production.

1.2 Alphaviruses and the immune system

The interaction between alphavirus infection and host immune responses has been examined primarily using the two prototypic new world alphaviruses; SIN virus and SFV. Host innate responses are the initial and most rapidly induced following virus infection; innate responses are initiated by the detection of various pathogen-associated molecular patterns (PAMPs) by toll-like receptors (TLRs) or cytoplasmic sensors. As a consequence of alphavirus infection, TLR3 (recognising ssRNA), TLR7/8 (recognising dsRNA) and the cytoplasmic sensors PKR (protein kinase R system), OAS (2'-5' oligoadenylate synthetase family), RIG-1 (retinoic acid-inducible gene-1 RNA helicase) and MDA5 (melanoma-differentiation-associated gene 5 RNA helicase) within host cells are all capable of detecting and responding to alphavirus replication products. The stimulation of the innate immunity in this manner is an important factor in initially controlling alphavirus infection and results in the priming of adjacent, uninfected cells to efficiently resist subsequent infection. Additionally, innate activation promotes innate and adaptive immune cell infiltration and phagocytosis, important for the induction of a specific adaptive response essential for virus clearance and protection from re-infection. SFV infection induces a Th1 type, cell mediated adaptive response; although the involvement of B cells, through their production of IgM antibodies, is the major mechanism of clearing blood viremia (Fazakerley, 2002). CNS infection proceeds primarily within neurons and oligodendrocytes and, in avirulent strains, produces a non-lytic infection. Cytolytic effector cells, such as natural killer (NK) or T cells, can eliminate dispensable infected cells, however the essential nature of neurons prohibits their removal; as a result, neuronal infection is cleared by non-cytolytic mechanisms. Both *in vivo* and *in vitro*, anti-E2 antibodies, of varying isotypes, are capable of clearing infection within neurons of the brain parenchyma and spinal chord; the mechanism appears to involve the inhibition of virus budding and the restoration of cellular membrane potential, host cell translation and interferon responsiveness allowing for the induction of cellular anti-viral mechanisms (Griffin *et al.*, 1997). $CD8^+$ T cells are also involved in clearing neuronal infection, in a non-cytolytic IFN-γ-dependent manner, although this is only relevant to neurons of the

spinal cord (Binder and Griffin, 2001). Although these non-cytolytic mechanisms are capable of eliminating viremia they are inefficient and SIN RNA is detectable up to 17 months after acute infection (Levine and Griffin, 1992).

Despite the obvious essential contribution of the immune system to protection against alphavirus infection, immune responses initiated in an attempt to limit infection have been linked to the induction of lethal and sub-lethal pathologies. High level interferon induction following infection with interferon-insensitive alphaviruses has been linked to the induction of a systemic inflammatory response-like syndrome resulting in significant mortality in murine models. The development of demyelinating lesions in the CNS following infection with the aviralent SFV strain A7(74) has been demonstrated; although severity and duration appear to be mouse strain dependent, pathology is contingent upon $CD8^+$ T cells, which mediate the demyelinating process (Amor *et al.*, 1996).

1.3 The Semliki Forest virus – virus-like particle system

The use of a replicating virus in any setting raises a number of safety concerns; the potential for virus escape into the general population, especially if the virus is not endemic, and the possibility of toxicity related to uncontrolled infection, particularly in immunocompromised or immunosuppressed individuals, are important concerns for the use of a replicating virus. From a therapeutic standpoint, the incorporation of transgenes into a replicating virus has the potential for gene loss making the therapy less controlled, predictable and possibly efficacious. For these reasons the Semliki Forest virus was developed into a suicidal vector system called the SFV virus-like particle (SFV VLP) system, first described in 1991 (Liljestrom and Garoff). Because of the mRNA genome of SFV, all manipulations are carried out on a DNA plasmid clone of the virulent SFV4 genome. The SFV virus-like particle is composed of an enveloped virion structurally identical to that of the wild-type replicating SFV. In an attempt to produce a suicidal vector prohibited from productive infection, the structural ORF was removed from the genomic sequence. The truncated structural ORF, which retains all the regulatory elements required for sub-genomic expression, is the site of cloning for heterologous genes. The plasmid containing the truncated structural ORF, heterologous gene and SFV4 backbone sequence was termed the expression plasmid and a number of revisions have been produced. The most recent expression plasmid is pSFV-b12a/pSFV-Enh and is composed of the modified SFV4 backbone sequence, however the truncated structural ORF has been modified for

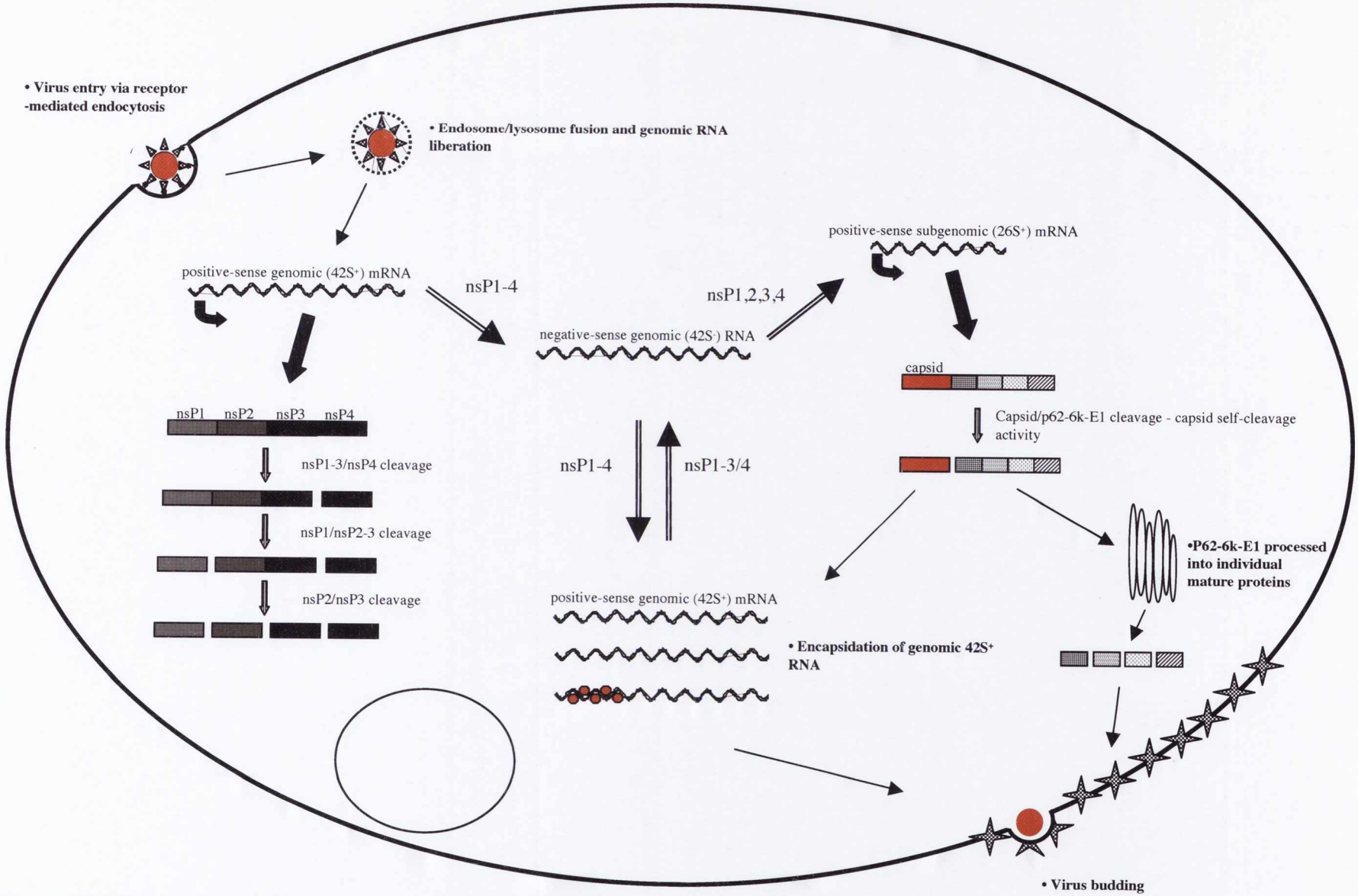

Figure 1.1: Schematic of infection cycle of replicating SFV.

ease of cloning and enhanced expression. Because of the inherent translational enhancer ability of the 5' capsid sequence, it was reintroduced into the subgenomic promoter of the expression plasmid, located upstream of the multiple cloning site. The absence of the remaining capsid sequence, which normally liberates the capsid protein from the remainder of the structural polyprotein, necessitated the inclusion of the foot-and-mouth disease virus (FMDV) 2A autoprotease. The FMDV 2A protease is a 17 amino acid sequence that co-translationally self-cleaves between the $16/17^{th}$ amino acid. As a result, the capsid sequence and FMDV protease are removed from the heterologous protein, with the exception of a single proline.

The removal of the structural genes from the expression plasmid requires their inclusion, in some form, during VLP production. Consequently, the structural genes are included on two helper plasmids, known together as the split helper system. Both plasmids contain a truncated non-structural ORF that prevents replicase production and, because of the packing sequence removal, incorporation into the newly synthesised virion. For additional safety, the structural ORF was divided between two plasmids, pSFV-Capsid and pSFV-Spike, encoding the capsid and E3-E2-6k-E1 genes respectively. For the production of VLPs, the expression and helper plasmids are *in vitro* transcribed to produce three distinct mRNA species used to transfect, typically Swedish baby hamster kidney (S-BHK), cells by electroporation (Figure 1.2). Following transfection, the replicase complex is translated directly from the expression mRNA molecule, which amplifies all three RNA species. Subsequently, transcription of the subgenomic RNA occurs followed by capsid and spike protein translation. Virion production then follows a route identical to that of replicating SFV although, importantly, only the expression RNA is encapsidated. The split helper VLP system allows for the production of high-titre VLPs with the relatively low frequency of replication-competent virus (RCV) production of approximately 10^{-13} or about 1 RCV in every 100 - 1000 batches of particles (Smerdou and Liljestrom, 1999).

The nascent VLP is then capable of initiating infection in permissive cells in a manner, at least initially, identical to wild-type replicating virus. Following VLP infection and the uncoating, the liberated mRNA is directly translated to produce the non-structural replicase responsible for negative-sense 42S RNA production. From this $42S^-$ RNA, positive-sense RNA is transcribed serving as template for further negative-sense 42S RNA. Approximately six hours post infection, nsP processing results in the switch to subgenomic $26S^+$ RNA production exclusively. Subgenomic RNA is translated into the transgene protein product that accounts for approximately 30-40% of cellular protein production

(Ventoso *et al.*, 2006). Additionally, all the hallmarks of replicating virus infection are preserved including host protein shutdown and apoptosis induction mediated by dsRNA production (Jacobs and Langland, 2000) and RNA replication (Urban *et al.*, 2008) respectively.

Host immune responses will inevitably be initiated against the VLPs and it has been demonstrated that the innate responses are effectively stimulated following SFV VLP infection (Hidmark *et al.*, 2005). Additionally this innate stimulation, mediated primarily by interferons, is an important factor in the adjuvant effect of SFV VLPs when co-administered with an un-related antigen (Hidmark *et al.*, 2006). The adaptive immune system will also become primed against the SFV VLPs although, in the absence of productive infection, the initial stages of antigen processing and presentation within APCs may be more likely to result from cross-priming. Despite the low levels of the structural proteins, relative to replicating SFV, neutralising antibodies are efficiently induced and have been shown to impact upon systemic i.v. readministration. However, it has also been demonstrated that intratumoral delivery of VLPs results in lower neutralising antibody levels and only moderately inhibits transgene expression when VLPs were readministered by the intratumoral route (Rodriguez-Madoz *et al.*, 2007).

1.4 Cancer

In single-celled organisms, the replication efficiency of individual cells is the determinant in their natural selection and evolution. For multicellular organisms, in which replication of the entire organism is the substrate of natural selection, the maintenance of the organism can proceed only under tightly controlled individual cell proliferation. The correct and functional formation of tissues is dependent upon the orchestration of several cell types and involves a multitude of complex heterotypic signalling that both positively and negatively regulate cell proliferation and tissue formation. Cancer is a disease arising from the unregulated proliferation of host cells, which have become independent of factors which normally regulate cell turnover. Given that the multitude of normal regulatory controls which cancer must overcome to progress to a clinically relevant disease, it is not surprising that the development of cancer itself is a complex process whose understanding has drawn on various disciplines of biology (Weinberg, 2006).

Cancer has been recently redefined as a genetic disease and its etiology has been the subject of extensive study. Cancer initiation occurs at a cellular level wherein

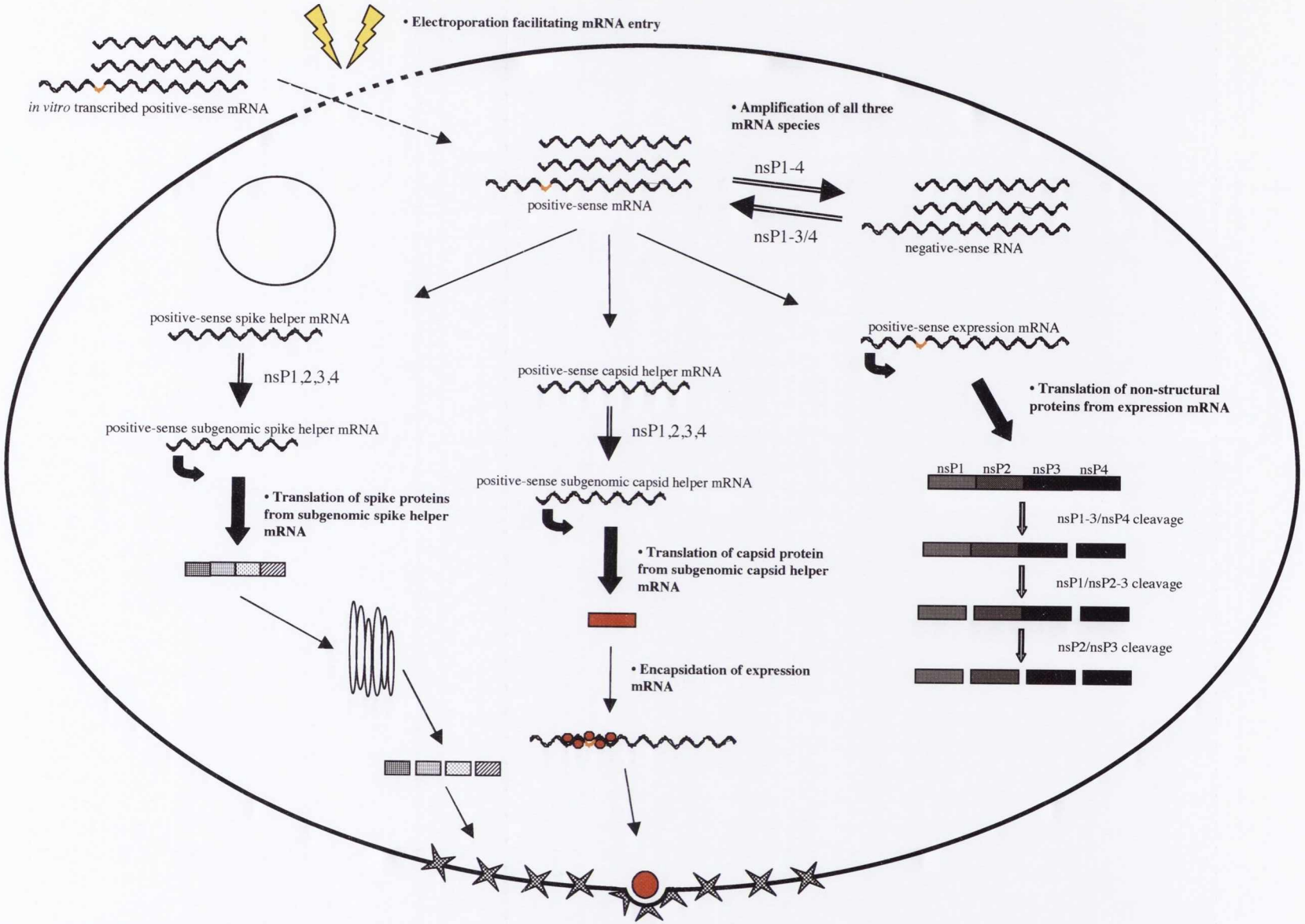

Figure 1.2: Schematic of VLP production.

stochastic mutations impart novel cellular geno- and phenotypes. Mutational events can be single point mutations, frame shift mutations, large nucleotide deletions, amplifications or inversions, or cytogenetic rearrangements. Additionally, heritable epigenetic mutations, such as promoter methylation, can directly influence the expression of genes without DNA sequence changes. Those mutated cells that have acquired some selective growth advantage will undergo clonal expansion during which the further acquisition of mutations can lead to further rounds of clonal expansion potentially leading to a clinically relevant disease. Although this is a drastic oversimplification of the initiation and progression of cancer, it embodies the key elements in cancer development.

Mutations may occur as a consequence of the cell's inherently fallible DNA replication machinery or due to chemical or physical insult and are typically distributed stochastically throughout the genome. The majority of mutational events are likely to have no effect on cancer development, occurring within 'junk' DNA or synonymously within coding DNA. Alternatively, mutations may occur at non-essential sites within a gene or within non-essential genes and may have no phenotypic effect or relevance to cancer formation. However, the occurrence of mutations in three main categories of gene has been shown to play a pivotal role in neoplasia. Two such categories, whose names derive from their involvement in oncogenesis, are the oncogenes and tumor-suppressor genes. Oncogenes are genes that normally, in their active state, positively influence cell division, replication or pro-neoplastic processes. Mutations within these genes that engender constitutive activation, upregulation or a resistance to inactivation can contribute to oncogenesis and are typically dominant, with mutation in one allele being sufficient for an aberrant phenotype. It is important to note that correctly functioning genes of this class are more aptly termed proto-oncogenes, whereas the term oncogene normally designates the mutated and deregulated forms. Tumor-suppressor genes are those whose gene products are involved in negatively regulating cell growth and division, and comprise numerous proteins involved in the regulation of cell cycle progression and detection of cell dysfunction. Mutations in tumor-suppressor genes that constitutively inactivate or downregulate protein function are oncogenic, although normally mutation of both alleles is required for complete phenotypic effect. Obviously, genes involved in the prevention and correction of mutations, known as DNA repair genes, that are dysregulated by mutation will increase the likelihood of further mutagenesis and of cancer development. The importance of DNA repair genes is highlighted in individuals suffering from the autosomally recessive genetic disease xeroderma pigmentosum that have a mutational

defect in the UV-activated DNA repair pathway and, as a result, a 1000-fold increased risk of non-melanoma and melanoma skin cancers (Tuteja and Tuteja, 2001).

The development of cancer is a complex process and the large number of regulatory elements that must be overcome in order to develop into a clinically relevant disease is mirrored by the fact that tumors may require decades to progress to full blown malignancy. It is not surprising then that no single mutation is cancer causing *per se* but only increases the risk of developing a neoplastic phenotype. Even in the presence of germline mutations in key regulatory genes there is only an increased risk of cancer development, with the precise risk ratio and site of tumor formation dependent upon the specific mutation. The major advances in molecular biology research in the last 30 years have allowed for large scale analysis of the human genome, its proteome and the identification of genetic and proteomic factors contributing to cancer. Consequently, there are a large number of known and putative genes involved in oncogenesis and an even greater number of specific genetic/epigenetic lesions responsible for their dysfunction. As a result, it is more pertinent to consider these mutational events in terms of the regulatory pathways they disrupt. Because the majority of cellular pathways involve various intermediate members involved in initiation, signal transduction and effector mechanisms, mutations in individual pathway members can result in almost identical phenotypes and there is significant convergence of oncogenic mutations upon specific pathways (Vogelstein and Kinzle, 2004). Additionally, mutations may result in the disruption of specific downstream elements within a pathway while retaining other potentially pro-neoplastic elements.

Since the net rate of cell proliferation is a balance of cell division and cell death, it is not surprising that the pathways involved in both these processes are necessarily dysregulated in cancer cells. Cell division and progression through the cell cycle, involves a number of checkpoints that ensure previous stages of the cell cycle are complete before continuation to the next. Cell cycle progression through these checkpoints depends upon various mitogenic signals, ensuring an adequate environment for replication, and internal checks, such as genome integrity, particularly important during DNA replication and chromosome segregation (reviewed in Vermeulen *et al.*, 2003). One of the most important checkpoints occurs between the G_1, the phase directly after cell division, and S phases, wherein genomic DNA replication is carried out, and is known as the restriction point or 'R point'. At this juncture cells may continue irrevocably through replication or enter a reversible quiescent phase, termed G_0; it is during the G_1 phase that cells are most sensitive

to extracellularly derived mitogenic and anti-mitogenic signals (Figure 1.3). The retinoblastoma protein, pRb, is an essential gatekeeper in the decision to, or not to, progress through the R point and was one of the first identified genes involved in cancer.

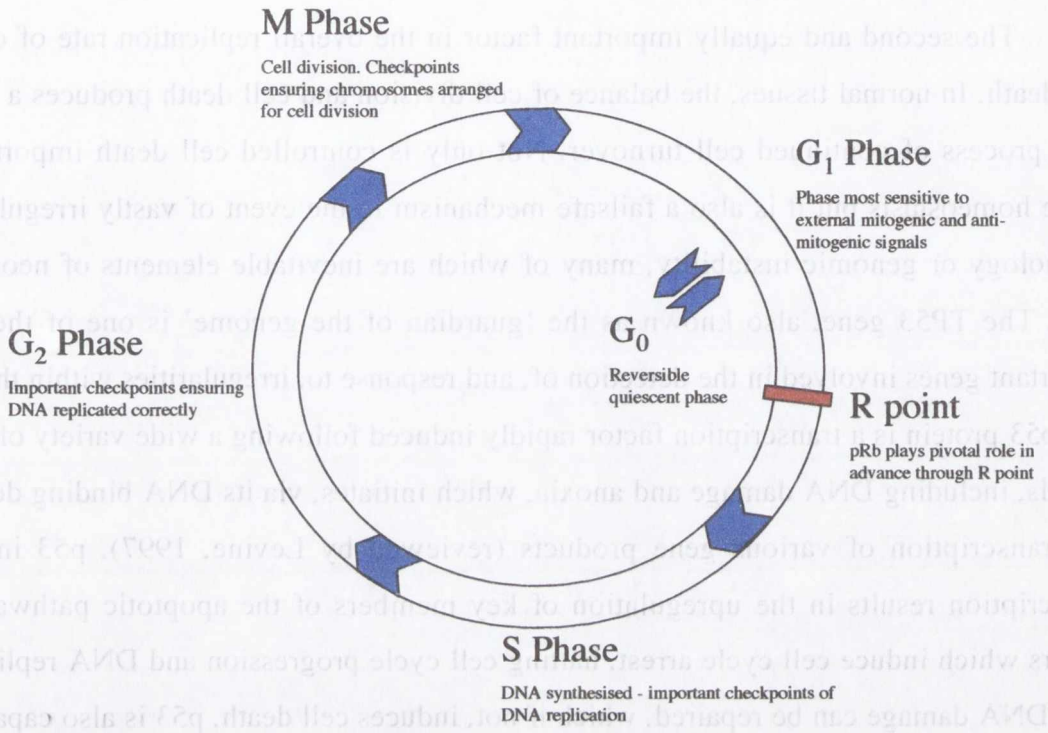

Figure 1.3: Schematic of cell cycle.

The phosphorylation state of pRb determines its ability to sequester the E2F group of transcription factors, which are essential mediators of the transition through the R point. Hypophosphorylated pRb sequesters the E2F transcription factors and upon hyperphosphorylation and E2F release, the transcription of a wide variety of genes results in the eventual progression into S phase (Weinberg, 1995). Thus, the Rb gene is an important tumor-suppressor gene and its downregulation, inability to bind E2F, or constitutive or unregulated hyperphosphorylation leads to a perturbation in the cell cycle control and excessive cell proliferation. The importance of the Rb tumor suppressor gene is highlighted by the observation that mutations affecting Rb directly are present in over 50% of all human tumors (Sherr and McCormick, 2002). Interestingly, pRb hyperphosphorylation is a downstream effect of mitogenic signalling and a key mediator in the signal transduction is the Ras protein. Activated Ras induces downstream signalling which results in the hyperphosphorylation of pRb and consequently the activation state of Ras is an indirect effector of cell cycle progression. The Ras gene, a proto-oncogene, is commonly mutated in cancer to acquire constitutive activation resulting in the induction of

excessive cell proliferation (Bos, 1989). Rb and Ras are just two genes involved in the cell cycle regulatory pathways whose mutation can result in part of the phenotypic behaviour associated with neoplastic cells and demonstrates that pathways are sensitive to perturbation at multiple stages.

The second and equally important factor in the overall replication rate of cells is cell death. In normal tissues, the balance of cell division and cell death produces a steady state process of continued cell turnover. Not only is controlled cell death important in tissue homeostasis but it is also a failsafe mechanism in the event of vastly irregular cell physiology or genomic instability, many of which are inevitable elements of neoplastic cells. The TP53 gene, also known as the 'guardian of the genome' is one of the most important genes involved in the detection of, and response to, irregularities within the cell. The p53 protein is a transcription factor rapidly induced following a wide variety of stress signals, including DNA damage and anoxia, which initiates, via its DNA binding domain, the transcription of various gene products (reviewed by Levine, 1997). p53 induced transcription results in the upregulation of key members of the apoptotic pathway and factors which induce cell cycle arrest, halting cell cycle progression and DNA replication until DNA damage can be repaired, which if not, induces cell death. p53 is also capable of detecting deregulation of other cellular pathways such as the pRb pathway discussed. pRb dysfunction and subsequent E2F release causes, via E2F1, the inactivation of Mdm2, the mouse double minute 2 protein, which normally acts to ubiquitinate the p53 protein for degradation. pRb pathway disruption results in the rapid rise in p53 levels and induction of cell death; as a result it is thought that pRb dysfunction cannot successfully arise with an intact p53 pathway. Mutation of the TP53 gene is evident in approximately 50% of clinical tumors although this does not include epigenetic changes, which are though to present in a large proportion of clinical tumors not demonstrating TP53 gene mutation (Lemke, 2004).

The pathways and genes described represent just a subset of those involved in the regulation of proliferation; the ability to overcome the inherent controls of proliferation are not alone sufficient to generate a malignant disease and, at a cellular level, there are at least two further limitations. Firstly, cells can only undergo a finite number of divisions before the loss of replicative viability. This cell division limit is inherent in all somatic cells and mediated by the gradual loss of chromosomal flanking sequences termed telomeres. Telomeres are essential for chromosome stability and become progressively shortened following successive rounds of DNA replication and subsequent mitosis. After a certain number of cell divisions, known as the Hayflick limit, the telomeres become so short that

they no longer protect chromosomes from chromosome-chromosome fusion events which, in a non-specific manner, produce repeated breakage-fusion-bridge cycles resulting in random karyotypic anomalies. These gross and irreversible abnormalities result in the rapid induction of cell death mediated by, among others, the p53 protein. Although cancer cells harbouring mutations in key regulatory genes may resist the induction of apoptosis, at some point the random karyotypic events will negatively impact upon the cell's ability to consistently transmit genetic information through subsequent cell divisions. Telomere length is shortened progressively in all cells, with the exception of stem cells, which express the telomerase holoenzyme. Telomerase is responsible for the reconstruction of telomeres, which results in the immortalisation of cells endowing a nearly infinite replicative capacity. If neoplastic cells are to continue to grow and divide they will, at some point, be required to overcome this fundamental restriction and it has been demonstrated that the expression of telomerase occurs in around 85% of tumors (Shay and Bacchetti, 1997). An alternative strategy, know as alternative lengthening of telomeres (ALT, first described by Bryan *et al.*, 1997), has also been described although it appears to be less frequent than the reactivation of the telomerase enzyme.

As mentioned above, one cell population that continually express the telomerase holoenzyme is stem cells. Stem cells are multipotent cells that retain the ability for unlimited replication and are the cells responsible for repopulating tissues. Stem cell are capable of both symmetric and asymmetric division giving rise to identical daughter cells or further differentiated progenitor cells. Progenitor cells are capable of rapid division and amplification becoming progressively more differentiated and eventually producing fully differentiated cells. There has been significant interest in the determination of the precise populations of cells that are the cancer initiating cells and there exists a number of lines of evidence in support of the theory that stem or precursor cells are the initial cancer initiator cells. Given the stochastic nature of the mutational events required for the development of a malignant disease it would follow that longer-lived cells would be more likely to develop all the mutations required for cancer development. Additionally, the observation that tumors are composed of phenotypically diverse tumor cell populations would be in line with undifferentiated stem or precursor cells being the etiological origin of tumors. Probably the most compelling evidence for the stem cell theory are the numerous examples of stem cell isolation from clinical tumors which are capable of repopulating an entire heterogeneous tumor, while non-stem cancer cells can not. However, the evidence mentioned above is also justifiable under the assumption of differentiated cells being the

cancer initiator cells, which, through mutation, attain a less differentiated precursor phenotype. Continued experimentation is likely to further define the contribution of the respective cell populations to oncogenesis.

Although cancer related death may occur as a result of a single tumor mass, particularly when located in anatomical locations that compromise organ function, the main cause of cancer related death is the result of metastatic disease (Mehlen and Puisieux, 2006). The ability of tumors to develop an invasive nature is probably the least elucidated aspect of cancer and is complicated by a number of factors that hinder accurate portrayals of the process in *in vivo* models. However, it has been postulated that tumor cells undergo a reversible phenotypic transition called the epithelial-mesenchymal transition gaining independence of adherence signals and the ability to migrate and metastasise. This transition represents a re-activation of a cellular pathway normally active only during embryogenesis although the acquisition of mutations resulting in other migratory phenotypes is also possible. Interestingly liquid cancers, such as hematopoietic leukemias, appear to require fewer mutational 'hits' in order to acquire malignancy, which is though due to their inherent migratory potential (Vogelstein and Kinzler, 2004). Although this is the least defined process, it is nonetheless a fundamental restriction that must be, and is, overcome in the majority of clinical malignancies.

1.5 Angiogenesis and Cancer

Despite the acquisition of mutations that enhance cancer cell survival and proliferation, cell growth is ultimately dependent upon access to nutrients and the removal of waste products. In normal tissues, cells are typically no more than 0.2mm from their closest blood vessel, which represents the limit of diffusion of nutrients though living tissue. The expansion of the blood supply is achieved by the process of angiogenesis and is an absolute requirement during embryogenesis and growth. In humans, this is particularly evident following the use of thalidomide, a potent angiogenic inhibitor (Gelati *et al.*, 2003), in pregnant women that restricted neovascularisation in the developing foetus and resulted in numerous birth defects. Additionally, transgenic mice lacking key components of the angiogenic pathway are non-viable and embryos do not survive beyond 8 days post-implantation when the embryo outgrows its blood supply (Carmeliet *et al.*, 1996). In adults, angiogenesis is restricted to a small number of physiological and pathological events including ovulation, wound healing and arteriosclerosis (Folkman, 2006). The angiogenic process is normally tightly regulated and is dependent upon the interaction of

numerous pro- and anti-angiogenic signals, the balance of which ultimately deciding the outcome.

In a seminal paper published by Judah Folkman in 1971 the involvement of angiogenesis in cancer progression was first theorised; subsequently, there has been notable scientific investment in the study of both normal and neoplastic angiogenesis. The acquisition of carcinogenic mutations, clonal expansion and the preferential unregulated proliferation of cancerous cells leads to the development of solid tumors, the notable exception being liquid cancers such as leukemias. However, as solid tumors increase in size, the limited diffusion of nutrients, in the absence of a sufficient blood supply, becomes the major inhibitory factor in further growth. For this reason, the development of macroscopic tumors is reliant upon the acquisition and development of blood vessels in the expanding tumor. Blood vessel formation is a process not only dependent upon angiogenic signals, supplied by tumor cells or non-tumor cells such as reactive stroma or infiltrating immune cells, but also the non-tumor host cells that comprise the developing structures, such as endothelial cells and their supporting mural cells.

Angiogenesis is a normal consequence of wounding and inflammation; in this paradigm, the release of growth factors and chemokines such as platelet-derived growth factor, PDGF, and TGF-β, transforming growth factor-beta, by platelets is involved in tipping the balance towards the initiation of the angiogenic process. PDGF stimulates and attracts fibroblasts while TGF-β induces their activation and release of FGFs, fibroblast growth factors, and MMPs, matrix metalloproteases. The MMPs are essential enzymes in tissue remodelling and mediate the degradation of the extracellular matrix (ECM), important in vasculature rearrangement and release of ECM sequestered growth factors that include basic fibroblast growth factor, bFGF, vascular endothelial growth factor, VEGF, and TGF-β. Vascular neogenesis may arise from the sprouting of endothelial cells from existing vessels or the recruitment of endothelial precursor cells EPCs from circulation (Goh *et al.*, 2007) and VEGF is an important mediator of both these processes. The newly formed endothelial cell microvasculature is initially immature and requires the mobilization of mural cells, through endothelial derived PDGF, which recruits supporting pericytes to produce trophins that stabilise newly formed vessels. During this maturation process, microvessels are extremely unstable and blockade of trophins, including VEGF and Ang-1, results the rapid collapse and regression of newly formed microvessels (Bergers and Benjamin, 2003).

Platelet-derived growth factors and those liberated from the ECM play an additional role as immune cell attractants that mobilise monocyte, macrophage, mast cell and lymphocyte infiltration into the wound site (reviewed by O'Byrne *et al.*, 2000). The protective role of immune cell infiltration into sites of potential infection is obvious but infiltrating immune cells also produce additional VEGF and FGFs further stimulating fibroblast activation, endothelial proliferation and angiogenesis. It is apparent then that the initial wounding event results in the rapid cascading of pro-angiogenic factors that tip the balance in favour of angiogenesis. Under normal tissue physiology however, the pro-angiogenic environment reverts to an environment that no longer supports active angiogenesis; a number of ECM cleavage products are themselves potent angiogenic inhibitors demonstrating the presence of negative feedback loops ensuring only limited physiological angiogenesis (Nyberg *et al.*, 2000). In fact, histological and biochemical similarities between wound healing and the tumor microenvironment had been observed for a number of years (Balkwill and Mantovani, 2001). Indeed, it appears that tumors, rather than reinventing angiogenic pathways, which involve a number of non-mutated, non-tumor cells, invoke the stimulation of the wound healing programs resulting in reactive stroma, immune cell infiltration and other factors capable of overcoming the inhibitory environment and producing active angiogenesis. It has been demonstrated that tumor cells can produce a variety of growth factor and mitogens that are directly involved in the wound healing/angiogenic process and include, FGFs, PDGFs, VEGF and placental growth factor, the latter shown to be associated only with pathological angiogenesis (reviewed by Folkman, 2003).

1.6 Cancer and the immune system

Cancer is a disease that severely impacts upon the host's longevity and normal function. It is obvious then, that there would be a large selective advantage imparted on organisms able to stymie or eliminate newly developed tumors. Multicellular organisms possess safeguards against neoplastic transformation in the guise of tumor-suppressor and housekeeping genes, which are necessarily mutated, in the initial stages of neoplasia. The immune system, whose function it is to guard against pathogens and disease manifestations, too plays an essential role in tumor surveillance and elimination. The production of transgenic animals in the late 1970s allowed for the incorporation of specific genetic lesions into animals providing a greater understanding of some of the hugely

complex organism-wide processes. The creation of mice with specific genetic alterations in key elements of the immune system, while leaving other elements intact, has elucidated the nature of some of the interactions between cancer and the immune system. Animals lacking functional cytokine pathways, including the interferons and IL-12, specific immune cell subsets, including T, B, NK and natural killer T (NKT) cells or combinations thereof, are associated with increased cancer development (reviewed in Dunn *et al.*, 2006). These and other observations have led to the conclusion that the immune system actively participates in the detection and elimination of cancer, known as cancer immunosurveillance. While tumors derived from virus-initiated oncogenesis express non-self proteins, cancers of non-viral etiology may only express host-derived proteins. However, mutations required for tumor initiation and progression, particularly those resulting in amino acid changes, have the potential to provide novel antigens to which the immune system has not been tolerised during lymphocyte development in the thymus. These tumor antigens can be broadly divided into two classes; tumor antigens (TAs) and tumor-associated antigens (TAAs). Tumor antigens are classified as those expressed specifically by tumor cells and are derived from non-host proteins, such as the human papilloma virus E6 and E7 proteins or mutated cellular proteins, such as the products of tumor suppressor or oncogene mutagenesis. Tumor-associated antigens are classified as those which, although expressed on non-tumor cells, are upregulated in tumor cells and include host cell products involved in the cell cycle, such as cyclin dependent kinase-4, or antigens normally limited to specific cell types, such as members of MAGE gene family whose expression is normally restricted to the testis (Jungbluth *et al.*, 2000). Palpable tumors however, do not spontaneously develop but evolve within the organism and are constantly faced with host immunosurveillance; it is thought that this selective pressure results in immunoselection whereby, at the initial stages of tumor development, newly arising antigenic neoplastic cells are eliminated, selecting for less immunogenic or immunoevasive cells.

Immune evasion and suppression by tumor cells has been described at various stages in the development and propagation of innate and adaptive immune responses. The tumor microenvironment can lead directly to the dysregulation of innate immune cell functions and tumor-associated dendritic cells (TADCs) have been shown to be poor mediators of T cell re-stimulation and proliferation (Gabrilovich, 2004) while tumor associated macrophages (TAMs) also exhibit functional defects compared to their systemic counterparts (Mantovani, 1994). Even in the presence of primed anti-tumor effector T

cells, engagement and destruction is reliant upon the correct presentation of tumor antigens for recognition by CTLs and potentially antigenic tumor cells may disrupt the cellular processing and presentation pathway in order to avoid adaptive effector functions. It has been demonstrated that clinical tumors are capable of downregulating or producing functionally inactive forms of human leukocyte antigen (HLA, equivalent to MHC discussed previously) class I or essential co-stimulatory molecules (Marincola *et al.*, 2000). Additionally, members of the cytosolic processing machinery such as transporter-associated with antigen presentation-1, TAP-1, maybe lost (Korkolopoulou *et al.*, 1996). Interestingly, Hoffmann *et al.* (2000) demonstrated that specific p53 mutations are capable of abolishing the processing of a normally immunogenic p53 peptide fragment suggesting that at various stages in antigen presentation there are a number of potential mechanisms capable of subverting immune detection. Additionally, the alternative expression of pro- and anti-apoptotic genes may allow tumors to persist despite immune cell derived pro-apoptotic signals, rendering anti-tumor cytotoxic T cells ineffective.

Tumor derived factors have also been implicated in the direct dysregulation of adaptive responses. The induction of interleukin 10 (IL-10) and TGF-β, among others, within the tumor microenvironment has been implicated in biasing locally developing T cells towards a Th2 profile, typical of a humoral response and inefficacious in tumor eradication (Shurin *et al.*, 1999). Additionally, tumor-infiltrating lymphocytes (TILs) derived from clinical samples, despite being enriched for TAA reactive clones, are poorly stimulated *ex vivo* and lack expression of IL-2 or its receptor, an important factor for T cell activation and expansion (Chiou *et al.*, 2005). Tumors may also produce microvesicles containing membrane-bound FasL or secret soluble FasL capable of inducing apoptosis in local and systemic lymphocyte populations (Whiteside, 2002). The immune systems own safeguards may also contribute to an ineffective immune response. The chronic stimulation of T cells may result in activation-induced cell death (AICD) because of high-dose antigen exposure, in the absence of co-stimulation or complementary cytokines, thereby eliminating tumor-specific T cell populations. Additionally the presence of regulatory T cells, important in regulating auto-immunity, may play an active role in the dampening of anti-tumor immune responses to antigens which are considered self.

It is obvious then that the immune system is a key player in tumor prevention; however, the development of neoplastic cells within the host can evade detection and proceed to actively subvert host defences in a number of complex processes that are the subject of ongoing experimental investigation. In fact, the negation of tumor initiated

immunosuppression and the stimulation of effective host immune response is currently an approach under much investigation in both *in vivo* and clinical settings.

1.7 Cancer etiology and epidemiology

Global cancer rates in 2002 demonstrated that lung, breast (women), and colorectal cancers were the most frequently diagnosed cancers while lung, stomach and liver cancers were the major cause of cancer related deaths worldwide (Parkin *et al.*, 2005). Globally, cancer is responsible for 12% of deaths while in the US it represents 22.9% of deaths second only to heart disease (Scottenfeld and Beebe-Dimmer, 2005). Because mutational events are the initiating factors in cancer, any physical or chemical insults that increase the mutational frequency, known as mutagens, are likely to increase the risk of cancer and are termed carcinogenic. While a mutagen is inherently carcinogenic, carcinogens are not necessarily mutagenic and these are known as promoters. Promoters can act as potent mitogens resulting in excessive cell proliferation and increasing the risk of neoplastic development and progression. Epidemiological data has identified a number of environmental factors contributing to cancer. Exposure to carcinogens from tobacco smoke, asbestos and UV and X ray radiation in addition to lifestyle factors such as a BMI index above 25 or alcohol consumption are associated with increased cancer incidence (Peto, 2001). It is thought that approximately 40% of clinical cancers are the result of lifestyle factors, such as diet and smoking, and considered preventable. A number of familial syndromes have been identified stemming from germline mutations in key tumor-suppressor or oncogenes. Known hereditary predispositions represent approximately 5-10% of all diagnosed cancers (Garber and Offit, 2005) and include Li-Fraumeni syndromes, a germline mutation of TP53, and familial adenomatous polyposis, a germline mutation of the tumor suppressor gene APC. By far however, the majority of cancers are sporadic in nature occurring because of successive rounds of mutation and clonal expansion eventually giving rise to a clinically relevant disease.

While cancer is not a communicable disease, the involvement of pathogens in the development of cancer was one of the first identified mechanisms for oncogenesis and allowed for the initial progression in cancer research. Pathogens can directly participate in the oncogenic process or may induce environments favouring the development of malignant disease. The former process is typically virus-mediated and these 'tumor viruses' have been identified in a variety of animals. Viral initiated oncogenesis can occur

in two ways as viral infection may act as a mutagen or promoter, or both. Viruses may unintentionally or intentionally integrate entire or partial genomic DNA sequences into to the host genome. Integration events may occur within tumor-suppressor or house-keeping genes, resulting in loss of function, or in proximity to proto-oncogenes or their promoters resulting in oncogenes under the control of viral promoter elements and independent of host control. Integration events are common among retroviruses and are, at least potentially, possible in all viruses requiring a DNA intermediate for replication. A second mechanism in viral oncogenesis may occur because of virus-encoded genes designed to dysregulate the cell's regulatory pathways. While viral gene products may be entirely novel, a number of virally encoded genes are almost identical to cellular proto-oncogenes, although importantly they include mutations that impart oncogenic activity. Additionally, viral and non-viral infectious agents have been linked to sporadic cancer incidence mediated by the induction of a chronic inflammatory response providing an environment more likely to complement, or participate in, the development of malignant disease. A number of pathogens have been directly linked to cancer in humans including the human papilloma viruses, human herpes virus 8, liver fluke, *Helicobacter* pylori and a number of hepatic viruses including hepatitis B and C. In 1990, pathogen-related cancer incidence represented 20-25% and 7-10% of cancer related deaths in developing and industrialised countries respectively (Pisani *et al.*, 1997).

1.8 The central nervous system

The central nervous system (CNS) is a fundamental and essential element in respiration, the processing of stimuli and the coordination of bodily functions, and is composed of two major cell types; neurons and glia. Neurons represent approximately 10% of the cells of the CNS and are the components responsible for conducting stimuli and information processing. Glial cells function in a supportive role and consist of oligodendrocytes, astrocytes and microglia. Oligodendroglia or oligodendrocytes have the primary role of myelinating neuronal axons, vastly increasing impulse transmission speed. Astrocytes are important biochemical supporters of neurons and endothelial cells of the blood brain barrier (BBB), and are involved in the repair of CNS damage. While oligodendroglia and astroglia are of neuroectodermal origin, microglia are derived from hematopoietic precursor cells, which early during development, migrate to and become resident within the brain parenchyma. Microglia are essentially CNS resident macrophages with similar

functions to peripheral macrophages and capable of detecting and responding to various noxious stimuli within the brain.

Given the crucial importance of the CNS, it is not surprising that it is the most heavily protected organ in the body. Physical trauma is reduced by the presence of the skull, cushioning of the brain with cerebrospinal fluid (CSF) and the somewhat physical and biochemical separation from the rest of the body provided by the BBB. The confined space and low cell renewal potential within the CNS provides an important dichotomy in vertebrates. The absolute necessity to protect the CNS from infectious pathogens, which would rapidly colonise and damage the delicate architecture, is countered by the potential for substantial bystander cytotoxicity as a direct consequence of immune intervention. In systemic organs, inadvertent damage is typically well tolerated and is a small cost when balanced against the consequences of uncontrolled pathogen proliferation. The thermogenic response, complement system and reactive species production can all participate in the toxicity and death of non-target cells. Additionally, the limited space within the skull may result in elevated intracranial pressure following inflammatory oedema. These factors can all contribute to the loss of essential neurons, supporting cells and important neural pathways, potentially leading to neurological dysfunction and death. As a result, there must be some balance between allowing essential immune intervention and limiting the adverse effects of an uncontrolled immune response. These problems are somewhat mirrored in the eye, testis and developing foetus which are all granted some amount of immune privilege, although the specific mechanisms appear to be differentially regulated. Obviously, some immune intervention must be allowed and 'immune privilege' is a relative rather than absolute term and compared to the systemic immune response the brain is more selective in terms of the infiltration of immune cells and the extent of effector mechanisms (Walker *et al.*, 2003). It is also necessary to draw a distinction between the CNS in general and brain parenchyma as both are not as equally separated from the systemic immune response. The circumventricular organs (CVOs), including the ventricular system, and the choroid plexus have a somewhat incomplete BBB and are relatively open to systemic immune surveillance and responses, however the brain parenchyma is considered much more privileged (Carson *et al.*, 2006). The CVOs are also populated by peripherally derived, renewable immune cells capable of initiating a rapid pro-inflammatory response as a result of the peripheral presence of pathogens, which can propagate into the parenchyma resident immune cells.

Like peripheral tissues, innate immune cells of the CNS play an important role in the orchestration and development of adaptive immune responses and the major innate cells within the CNS are microglia and astrocytes. Microglia reside within the brain parenchyma, are typically in a ramified state and undergo little cell turnover; a second type of microglia/macrophage population is also present and contributes to the perivascular cells lining the BBB. These, unlike parenchymal microglia, are continuously lost and replaced by bone marrow derived precursor cells and are the first innate cells to experience peripherally derived material (Guillemin and Brew, 2004). The CNS is fully capable of initiating innate immune responses to peripheral and intracerebral pathogens (Nguyen *et al.*, 2002b). Microglia, like systemic macrophages, possess a variety of TLRs and upon engagement initiate activation and pro-inflammatory cytokine secretion; IL-1, TNFs, IL-12 and a number of important chemokines are induced following TLR stimulation, although cytokine expression profiles are dependent upon the specific subset of TLRs activated (Jack *et al.*, 2005). The pro-inflammatory cytokines direct the upregulation of adhesion molecules on endothelial cells, which are important for lymphoid and myeloid cell extravasation. Additionally, subsequent exposure of activated microglia to IFN-γ induces MHC class I and II and co-stimulatory molecule upregulation making microglia efficient antigen-presenting cells for T cell restimulation. Although astrocytes also possess TLR subsets, *in vivo* findings suggest they may respond to TLR ligation by the production of anti-inflammatory and neuroprotective mediators such as IL-10, IFN-β and prostaglandins, such as PGE_2. Additionally, microglia can induce an expression profile switch from pro- to anti-inflammatory producing repressors of its own activation. The overall consequence of this signalling crosstalk is likely dependent on the strength and origin of the activating signals and their continued presence, with unnecessary inflammation being rapidly suppressed. There are several mechanisms in place to ensure that inadvertent and unnecessary damage does not occur within the brain. Neurons express surface proteins that inhibit complement-mediated toxicity and NK cell-mediated cytotoxicity, although they remain sensitive to bystander effects (Lebbink and Meyaard, 2007). Additionally, complement protein and antibody concentrations are significantly reduced in the CSF compared to peripheral levels, which may limit complement activation, via the classical pathway, and the induction of antibody-dependent cell-mediated cytotoxicity (ADCC) by innate cells such as NK cells and monocytes.

Since the adaptive immune response can act only in an antigen-dependent manner and there is limited access of antigen to the systemic lymphoid organs, it raises the

question as to how antigen originating within the CNS is presented to the adaptive immune system. Within the CNS, the limited traffic of immune cells is less restricted during an inflammatory process (Aloisi *et al.*, 2000); DCs, typically absent from the CNS, appear and are capable of presentation and priming T cells *ex vivo* suggesting their migration to lymphoid organs may be responsible for initial T cell priming. Additionally, antigen placed directly into the CNS is capable of reaching the cervical lymph nodes carried by draining CFS, although without sufficient 'danger signals', T cell anergy may be initiated (Walker *et al.*, 2003). Whatever the mechanism of initial T cell priming and subsequent migration to the antigen site, it is at this juncture that the development of a cell mediated or humoral adaptive response occurs. Within the CNS, the divergence of adaptive responses involves crosstalk between astrocytes and microglia; the exact functions of CNS-derived APCs *in vivo* has not been fully determined as sufficient numbers of APC populations are difficult to isolate for *ex vivo* analysis. However, it is known that activated microglia are efficient APCs capable of restimulating T cells by upregulating MHC class II and I molecules and co-stimulatory factors such as CD80 and CD86 (Williams *et al.*, 1993). Although astrocytes are capable of upregulating MHC class II molecules and presenting antigen *in vitro* it is unknown, and thought improbable, that astrocytes are the APCs that mediate T cell restimulation within the CNS and that where $CD4^+$ T cell priming does occur it tends to induce a Th2-type/anti-inflammatory response (Aloisi *et al.*, 1999). Additionally, astrocytes are capable of expressing TGF-β, IL-10 and PGE_2, which inhibit microglia/macrophage antigen-presentation function.

Given the limited renewal of neurons and the importance of immune surveillance within the brain, it is not surprising that the outcome of infection must be heavily controlled in order to produce a proportional response, the magnitude of which is determined by danger signals, feedback loops and crosstalk among microglia, astrocytes and infiltrating immune cells.

1.9 Cancer and the CNS

Tumors of the CNS can be broadly divided into three categories; non-CNS-derived tumors, non-glial tumors and glial tumors. Non-CNS-derived tumors result from peripherally derived metastatic disease, which infiltrates the CNS; metastases are phenotypically and histologically similar to the tissue of origin and are most commonly the result of lung cancer (40-50%), breast cancer (14-20%) and melanoma (10%) (Lemke, 2004). Non-glial

tumors are those putatively arising from, and histologically and biochemically similar to, non-glial cells such as neurons or Schwann cells and include medulloblastoma and schwannomas/neurilemoma. Non-gliomas represent one-third of primary brain tumors and although generally benign may result in malignancy and fatality (CBTRUS, 2009). Glial tumors, or gliomas, represent the majority of newly diagnosed CNS tumors and may be phenotypically and histologically similar to mature glial cells or may be anaplastic in nature. Glioma nomenclature is typically based upon histological resemblance to glial cells and may be classified as oligodendrogliomas, astrocytomas or mixed tumors known as oligoastrocytomas. Brain tumors are categorised using the World Health Organisation (WHO) classification system, the most recent revision of which was published in 2007 (Louis *et al.*, 2007). The WHO classification grades tumors according to histology, cellularity, mitoses, necrosis and endothelial proliferation (Table 1.1). While grade I and II CNS tumors are considered benign and low-grade respectively, grade III and IV are considered high-grade and have the worst prognosis.

Grade I CNS tumors are typically well-circumscribed, benign tumors associated with the best prognosis and, although can be fatal due to mass induced compression, surgical resection is typically curative (Buckner *et al*, 2007). Grade I tumors are typically non-gliomas, including meningiomas and pituitary adenomas although several gliomas may also be well circumscribed grade I neoplasms. Grade II gliomas are diffusely infiltrative and include low-grade astrocytomas, oligodendrogliomas and oligoastrocytomas which have median survival times of 5, 10 and 8 years respectively (Buckner *et al.*, 2007). Clinical therapy of grade II gliomas is complicated by the fact that the majority of these lesions eventually develop into anaplastic astrocytoma (grade III) or glioblastoma (grade IV) to which surgical and therapeutic intervention has extremely limited efficacy. As a result, neurological symptoms may be treated with anticonvulsant, corticosteroid or anticoagulant medication, designed to reduce tumor related seizures, oedema and thrombosis, while harsh therapeutic interventions such as radiation therapy or ressective surgery, which may result in neurological impairment, be delayed until progression to grade III or IV gliomas (Buckner *et al.*, 2007). Grade III gliomas are generally distinguished from low-grade astrocytoma by the presence of mitoses and anaplastic cells, hence the term anaplastic astrocytoma/oligodendroglioma. Anaplastic astrocytoma (AA) has a median age at diagnosis of 45 years with standard initial treatment being maximum surgical debulking, without increasing neurological deficit, and adjuvant radiation therapy (Buckner *et al.*, 2007). The use of adjuvant chemotherapy for the

WHO grade	Malignancy	Example	Histological Characteristics
I	Beign	Pilocytic astrocytoma, schwannoma, meningenoma	Well-circumscribed, low proliferatve potential
II	Low-grade	Astrocytoma/oligodendroma/oligoastrocytoma	Typically inflitrative, low-level proliferative
III	High-grade	Anaplastic astrocytoma/oligodendroma/oligoastrocytoma/meningenoma	Infiltration, nuclear plemorphsism, frequent mitoses
IV	High-grade	Glioblastoma multiforme, gliosarcoma, medullablastoma	Grade III plus widespread infiltration, necrosis and endothelial proliferation

Table 1.1: Classification of CNS tumors by the WHO classification system (from Louis *et al.*, 2007).

treatment of AA following primary surgical resection has produced conflicting results in a number of clinical trials and meta-analyses although it is still under investigation; however, the use of chemotherapy following tumor recurrence after primary surgical and radiotherapeutic treatment has demonstrated some moderate survival enhancement (Yung *et al.*, 1999). In a American epidemiological study, AA patients demonstrated a median survival time of 20 months and 5-year survival rate of 11% (Ohgaki and Kleihues, 2005). Anaplastic oligodendrogliomas and oligoastrocytomas tend, unlike other gliomas, to be chemosensitive although the median survival and survival rates closely approximate those of AA. Grade IV CNS tumors are generally distinguished from lower grade lesions by marked endothelial proliferation, primarily at the tumor perimeter, numerous mitoses, nuclear pleomorphism, cellular anaplasia, extensive central necrosis and include gliosarcoma, glioblastoma multiforme (GBM) and medulloblastoma. Both gliosarcoma and medulloblastoma represent less than 1% of all CNS neoplasms; GBM is the most frequently diagnosed grade IV lesion and represents 17.6% of all primary CNS tumors (CBTRUS, 2009). Whereas medulloblastoma has a median age of diagnosis of 9 years, both gliosarcoma and GBM have a median age of diagnosis of 50-60 years (Roberts *et al.*, 1991; Hess *et al.*, 2004). As with the majority of high-grade gliomas, surgical resection is the primary therapeutic intervention, however, the infiltrative capacity of high-grade gliomas typically makes complete surgical resection impossible. The recurrence of tumors following resection and the limited efficacy of radio- and chemotherapeutic interventions accounts for the extremely high lethality associated with grade IV CNS tumors.

1.10 Gliomagenesis

Given the low level of cell proliferation in the normal CNS and the classical model of oncogenesis involving rounds of mutagenesis and clonal expansion there has been significant interest in the cells responsible for gliomagenesis, that is, the first mutant or pool of mutants that eventually develop into clinical tumors. There are currently considered two potential sources of cells initiating gliomagenesis; mature CNS cells and neuroectodermal precursor or stem cells. Although limited proliferation of astrocytes does occur during pathological conditions, there is no definite epidemiological link between inducers of reactive astrocytosis and glioma incidence (Esiri, 2000). Additionally, brain tumors histologically similar to neurons, such as medulloblastomas, that are putatively derived from neural cells, which are in a post-mitotic state in the developed brain, initially

suggested that mature glia or neurons may not be the initiating cancer cells which underwent progressive rounds of clonal expansion. However, limited cell replication does occur within the developing CNS, providing a potential 'oncogenic window' and the relative frequency and age of on-set of neural and glial tumors is in line with the timing and length of this oncogenic window in immature neurons and glia (Russel and Rubinstein, 2007). Interestingly, observations have shown that mature astrocytes with mutations in $p16^{INK4a}$ and $p19^{ARF}$ are capable of dedifferentiation in response to EGFR activation and forming a heterogeneous tumor mass (Bachoo *et al.*, 2002). The alterative mechanism is that CNS tumors are derived from neuroectodermal precursor or stem cells, which have the ability to self-renew, proliferate and differentiate into mature neural or glia cells. The belief that the developed CNS was fixed and immutable was reconsidered following the seminal paper published by Joseph Altman (Alman and Das, 1965) demonstrating ongoing neurogenesis in the hippocampus and olfactory bulbs of rats. Subsequent studies have demonstrated ongoing neurogenesis in the dentate gyrus of the hippocampus and the subventricular zone initiated by resident neuroectodermal stem cells (Martin-Villalba *et al.*, 2008). This population of proliferating cells, capable of differentiation into neural or glia cells, has received much interest as putative tumor initiating cells, also called cancer stem cells. Cancer stem cells, generally isolated by CD133 expression and the demonstration of enhanced dye efflux, have been isolated from numerous clinical CNS tumors including GBM (Martin-Villalba *et al*, 2008) and are capable of regenerating a heterogeneous tumor population with stem-cell frequencies similar to that isolated from the primary tumors (Galli *et al.*, 2004). There are thus two potential sources of glioma initiating cells and experimental evidence has not yet ruled out either although a greater understanding of the events involved in gliomagenesis may provide further insight.

1.11 Glioma etiology and epidemiology

Given the relative isolation of the brain to peripherally present genotoxic and mutagenic substances, in comparison to peripheral organs, it is not surprising that a number of factors causally linked to systemic tumors do not demonstrate an equivalent correlation with primary brain tumors. The only unequivocal link to an increased brain tumor risk is therapeutic X ray irradiation of the CNS, used as a prophylactic treatment in childhood acute lymphoblastic leukaemia and associated with a greater than 20-fold increased risk of subsequent CNS tumor development (Ohgaki and Kleihues, 2005). Interestingly, ionizing

radiation induces the production of reactive oxygen species in the brain that increases neural stem cell expansion (Zhang *et al.*, 2004b) suggesting X ray irradiation may act as a cancer promoter in addition to a direct mutagen. Other factors associated with a minor increase in CNS tumor risk are parental occupation (Ohgaki and Kleihues, 2005) and although tobacco smoke has not been causally linked to CNS tumor development, some studies suggest a possible moderate increased risk. Additionally dietary factors, associated with the majority of systemic cancers, are associated with a moderate increased risk of CNS tumors and include the consumption of *N*-nitroso compounds (Ohgaki and Kleihues, 2005). The involvement of viruses in primary CNS tumor formation has been the subject of much investigation and putative connections between simian virus, SV40 a contaminant in early polio vaccines, John Cunningham (JC) virus and BK virus have been examined although no definitive, reproducible correlation has been produced (Martin-Villalba *et al.*, 2008). Interestingly, an inverse correlation between CNS tumor incidence and allergies, IgG antibodies to varicella-zoster virus and high serum IgE levels have been noted although a causal relationship has not been identified (Swartzbaum *et al.*, 2006). Primary CNS lymphomas, although relatively rare, are associated with HIV infection although this is related to the associated immunocompromisation (Baumgartner *et al.*, 1990).

A number of genetic syndromes are associated with an increased occurrence of glioma, although these are thought to represent only a small proportion of clinical diagnoses (Ohgaki, 2009). Li-Fraumeni syndrome, neurofibromatosis 1 and 2 and Turcot syndrome are all associated with increased CNS tumor incidence (Ohgaki and Kleihues, 2005). Like systemic cancers, mutation in the p53 gene is common among gliomas and 50% of grade II gliomas and 75% of GBM demonstrate mutation in the p53 gene (von Deimling *et al.*, 1992; Lemke, 2004). Additionally, the PTEN, phosphatase and tensin homolog detected on chromosome 10, is an important target of disruption in gliomas. Pten is a pleiotropic, tumor-suppressor protein involved in cell cycle regulation, angiogenesis, cell adhesion and migration and homozygous loss is an indicator of extremely poor prognosis in grade II and III gliomas (Knobbe *et al.*, 2002).

1.12 Glioma angiogenesis and invasion

The infiltrative capacity of gliomas is the major determinant in their lethality and is evident even in low-grade diffuse astrocytomas (grade II), which typically progress to invariably fatal grade III and IV lesions. The precise infiltrative patterns vary among gliomas and can

involve crossing into the contralateral hemisphere producing 'butterfly lesions', may remain restricted to white matter areas, preferentially grow around neurons in the grey matter or display a preference for perivascular growth (Louis, 2006). Although the ECM of the CNS is less well defined than systemic tissues, with the exception of perivascular and subpial regions, invasion and migration are thought to proceed similarly to peripheral tumors. Proteases responsible for remodelling the ECM, facilitating glioma cell invasion, are upregulated in clinical gliomas and include the MMPs and cathepsin B, a lysosomal cystine protease (Rao, 2003). Integrin receptors, which upon ligation to ECM ligands promote cytoskeleton rearrangement and locomotion, are upregulated in glioma cells (Paulus and Tonn, 1994). Additionally, mitogens can participate in the migration and invasion processes. Gliomas may express mitogenic proteins in an autocrine manner and the most frequently amplified gene in AA encodes the EGF mitogen, which is a potent stimulator of astrocytoma cell proliferation, migration and invasion (Hoelzinger *et al.*, 2007). Additionally, the insulin-like growth factor (IGF) pathway, involving two ligands, their receptors and a number of binding proteins, has demonstrated particular importance in glioma cell proliferation, glucose metabolism, apoptosis resistance and migration (Trojan *et al.*, 2007).

Gliomas represent one of the most vascularised clinical tumors (Brem *et al.*, 1972) and angiogenesis plays an important role in gliomagenesis, tumor expansion and resultant death. It is sufficient to note that the expression of a large variety of pro-angiogenic molecules have been demonstrated in clinical glioma samples and this is especially pronounced in GBM. VEGF, thought to be the most important factor in glioma neovascularisation (Bernsen and van der Kogel, 1999), and its receptor, are upregulated on glioma tissue and tumor associated vasculature, respectively (Hoelzinger *et al.*, 2007). Additionally, PDGF, PDGFR, FGF and FGFR have all demonstrated upregulation in high-grade clinical gliomas (Fischer *et al.*, 2005) suggesting that there are a multitude of angiogenic factors involved in glioma-induced angiogenesis.

1.13 Gliomas and the immune system

The analysis of clinical glioma patients and tissues has provided much direct and indirect evidence of the involvement of gliomas in the suppression of host immune responses. Being the primary innate immune cells in the brain and the first to encounter newly formed tumors, microglia play an important role in the initiation and promotion of efficient anti-

tumor responses. Microglia can represent one-third of cells in clinical gliomas (Graeber *et al.*, 2002) and gliomas may actively recruit microglia, monocytes and macrophages by the expression of chemoattractants such as monocyte chemoattractant protein-1 (Leung *et al.*, 1997). Despite the relative abundance of microglia in glioma tissue, gliomas are almost invariably fatal suggesting that microglial functions are either downregulated within the tumor microenvironment or may actively support glioma growth. Clinical glioma associated microglia have demonstrated numerous functional deficits that can be mimicked by *ex vivo* co-culture with glioma cell lines. Glioma derived factors including TGF-β and PGE_2 are potent suppressors of microglial activation and function (Bogdan and Nathan, 1993) inhibiting pro-inflammatory cytokine and reactive species production, co-stimulatory molecule expression, TLR stimulation responsiveness and T cell stimulation (Hussain *et al.*, 2006). In addition to demonstrating dysfunction in elements important in glioma eradication, glioma associated microglia themselves can be a source of factors promoting glioma growth. Microglia are a major source of IL-10 in gliomas (Wagner *et al.*, 1999) and are thought to promote ECM remodelling enhancing glioma invasion (Graeber *et al.*, 2002). Additionally, both clinical glioma explant cultures and primary tissues have demonstrated enhanced lectin-like transcript-1 mRNA and protein expression, which is an inhibitory ligand for NK cells (Roth *et al.*, 2007) providing an additional immunoevasive mechanism and potentially allowing for the downregulation of MHC class I molecules without resultant NK cell targeting.

Immunosuppressive effects upon the adaptive immune system have additionally been demonstrated in glioma patients and in *in vivo/ex vivo* studies. The adaptive immune system is limited to targeting only antigens that have been correctly presented in the lymphoid organs; this raises the question as to the immunogenicity of CNS tumors and whether there is an opportunity for the development of an adaptive immune response. Unlike the majority of pathogen derived antigens, which arise peripherally and subsequently breach the BBB, the *de novo* development of tumors is likely to be an immunologically silent event given the limited traffic of immune cells into the non-inflamed CNS. However, the typically ill-formed vascularisation and necrotic potential of malignant tumors results in increased permeability of the BBB and lymphoid and myeloid cell entry. The extent of glioma expressed tumor/tumor-associated antigens, their identification and antigenic relevance are important factors given their relevance for the development of immunotherapeutic treatments. To date, a number of TAAs have been identified in clinical glioma samples; however, this screening has been carried out against

known tumor-associated antigens using immunohistochemistry and mRNA analysis and for much of the TAAs their ability to elicit host T cell responses is unknown (Walker *et al.*, 2003). Although the immunosuppression of host T cells by gliomas has limited the analysis of *ex vivo* antigen reactivity, Pannetier *et al.* (1995) have demonstrated T cell receptor enrichment within the CNS indicative of the clonal expansion of CNS antigen specific T cells. Additionally, anti-TAA antibodies have been identified in glioma patients and studies indicate that gliomas do express tumor antigens to which the immune system is capable of mounting a response. Despite the presence of an immune system capable of targeting gliomas, curative immunologic intervention is rarely, if ever realized. Suppression of the adaptive immune system, mediated by gliomas, may be indirect, via the effects on innate cells discussed, or may occur directly upon cells of the adaptive immune system. Serum IL-12 and IL-10 levels are measurably lower in clinical AA and GBM patients compared to controls, indicative of a systemic Th1 type immune suppression (Kumar *et al.*, 2006). The induction of apoptosis in glioma-infiltrating T cells has been demonstrated in numerous clinical samples as a result of tumor cell-expressed Fas Ligand, FasL, capable of binding Fas receptor on incoming T cells and inducing apoptosis (Didenko *et al.*, 2002). The destruction of infiltrating T cells is not the only mechanism capable of inhibiting host adaptive responses, and effects upon resident APCs, as discussed above, can prevent efficient activation of adaptive immune responses by skewing T cell development towards inefficacious Th2 type immune responses. In fact, IL-10, the key cytokine involved in Th2 type response development, can be expressed by both tumor and non-tumor cells. Additionally, the induction of regulatory T cells (Tregs), which actively suppress adaptive immune responses, can promote glioma growth and immune evasion. The induction of regulatory immune cells has been observed in a number of animal glioma models following peripheral vaccination before i.c. challenge; this resulted in the enhancement of glioma growth and lethality compared to unvaccinated controls that could be overcome by the blockade of Tregs (Fecci *et al.*, 2007). Additionally, while absolute numbers of $CD4^+$ T cells are reduced in glioma patients there is a greater proportion of Treg cells (Fecci *et al.*, 2006) and known glioma expressed immunosuppressive factors such as TGF-β and IL-10 are essential cytokines in the development of $CD4^+$ Treg cells (Wan and Flavelle, 2006).

1.14 Glioblastoma multiforme

Glioblastoma multiforme represents 54% of gliomas and is the most common and most malignant clinical glioma (CBTRUS, 2009); approximately 10-20% of GBM are considered to be derived from pre-existing hyper/neoplastic lesions and are termed secondary GBM (Dropcho and Soong, 1996). GBM is invariably fatal and can produce devastating neurological consequences, particularly if the tumor is located in an indispensable anatomical location. Typically, GBM first presents because of neurological symptoms such as headaches, seizures or neurological defects. The initial therapeutic intervention for GBM is surgical resection, where amenable, designed to attain tissue for histological grading and to reduce mass effects, which can significantly improve neurological symptoms. Surgical resection is typically supplemented by adjuvant radiotherapy and various clinical trials have attempted to develop optimal radiotherapeutic regiments ultimately producing a moderate but significant survival benefit (Laperriere *et al.*, 2002). While additional chemotherapy has historically provided little survival benefit, newer chemotherapeutic agents and dosing regimens have demonstrated an increased median survival and greater 2 and 5-year survival and are now included as standard care for GBM (Stupp *et al.*, 2005; Erpolat *et al.*, 2009). Following initial treatment, even resulting in MRI negative lesions, recurrence is inevitable and further resection and adjuvant therapy may be considered and are associated with significant survival benefits, although palliative care may be the most appropriate action. Despite advances in therapeutic interventions in the last 20 years survival benefit has changed nominally, producing a median survival time increase from 12 to 18 months and rarely producing long-term cures. Given the minimal therapeutic benefit provided by conventional therapies, it is not surprising that a number of clinical trials are currently under investigation involving a variety of approaches, a subset of which is discussed below.

The use of oncolytic replication-restricted viruses has been examined in early phase I/II clinical trials and includes herpes simplex virus-1 (HSV-1), Newcastle disease virus (NDV), adenovirus and reovirus. The primary purpose of these trials was dose escalation and toxicity assessment and in most cases the minimum toxic dose was not reached nor did treatment result in viral encephalitis; however, one strain of NDV, PV701, resulted in serious adverse events including a treatment related death (Pecora *et al.*, 2002) while NDV MTH-68/H demonstrated no such events. Although the clinical trials were small, some promising results were obtained including 4/14 GBM patients with survival time of 5-9

years when treated with NDV MTH-68/H (Csatary *et al.*, 2004) and extended disease-free survival in HSV-1 treated patients (Harrow *et al.*, 2004). Adenovirus, although proven safe, did not result in statistically significant survival extension (Chiocca *et al.*, 2004), possibly related to the immunogenicity and rapid clearance of adenovirus from the CNS. An alternative strategy involved the use of replication-incompetent virus capable of infecting tumor cells *in vivo* and inducing heterologous protein expression capable of interfering with tumor growth. One strategy employed by Lang *et al.* (2003) was to incorporate the TP53 gene into an adenovirus vector in an attempt to repair the glioma cell's p53 functional status and although safe, the nature of the phase I trial did not allow for determination of efficacy. By far however, the most frequently incorporated gene is the HSV thymidine kinase (HSV-TK) gene encoding the Tk phosphotransferase protein. Tk is an enzyme capable of converting the prodrug ganciclovir (GCV) into GCV triphosphate, an inhibitor of DNA replication, resulting in the induction of cell death. Transfection of cancer cells with the TK gene, followed by GCV delivery, results in local activation of GCV and cell death in transfected cells, although it has been shown that bystander and immune adjuvant effects may also play an essential part in the anti-tumor process (Mensil and Yamasaki, 2000; Barzon *et al.*, 2006). Both retrovirus and adenovirus vectors have been used for TK gene transfer in clinical trials and although both demonstrated safety, only the latter produced survival enhancement, which increased median survival time from 38 to 62 weeks (Sandmair *et al.*, 2000; Immonen *et al.*, 2004).

The major obstacle in the treatment of malignant glioma is the invasive pattern of growth; despite initial treatment, infiltrating cells rapidly and effectively reseed large tumors and therapies that require the transduction of entire glioma cell populations are inherently limited. One potential therapeutic intervention is the induction of specific and efficacious anti-tumor immune responses capable of eliminating the primary tumor mass and invading tumor cells. To this end, direct immunotherapeutic approaches for the treatment of GBM have been examined in clinical trials and produced encouraging results (reviewed by Ehtesham *et al.*, 2004). Initial attempts at adoptive immunotherapy involved the transfer of autologous or heterologous lymphocytes, which had been activated and expanded *ex vivo*, into the tumor resection cavity. Results were largely negative and thought to be the result of non-specific *ex vivo* lymphocyte expansion and the immunosuppressive tumor microenvironment. Active vaccination therapy was examined using irradiated autologous tumor cells delivered subcutaneously in combination with immune stimulants such as BCG, GM-CSF and IL-2. Dendritic cell vaccines were

examined using autologous DCs pulsed with tumor peptide or tumor lysates; when administered peripherally or intratumorally these vaccination strategies proved safe and resulted in increased tumor-infiltrating lymphocytes and prolonged survival times (Barzon *et al.*, 2006). Given the limited effectiveness of conventional radio- and chemotherapeutic intervention in the treatment of high-grade glioma and the elucidation of some of the contributing factors to glioma lethality, it is not surprising that novel treatment modalities have recently entered a variety of clinical trials which represent interesting and potentially beneficial therapies.

1.15 *In vivo* brain tumor models

Before progression of any therapeutic modality toward clinical trials, efficacy and safety must be demonstrated in *in vivo* models and there are currently a large number of brain tumor models in a variety of host animals. Metastatic disease can be easily modelled by the inoculation of systemically originating tumor cells into the CNS, although for primary CNS tumors there are 3 major types of CNS models in use; those derived from primary human CNS tumors or human glioma cell lines; those arising spontaneously, typically in susceptible strains or induced by mutagens; and gliomas induced using non-human glioma cell lines originally induced, isolated and propagated from a variety of rodent species. Although human glioma explant cultures or cells lines are the most representative of human gliomas, the complications of host versus graft immune responses necessitates implantation into immunocompromised animals. This obviously limits the investigation of immunotherapeutic strategies or may underestimate the immunological adjunctive mechanisms of treatments not directly targeting the immune system. Additionally, the presence of pro- and anti-tumor immunological components, lacking in immunocompromised animals, may be unaccounted for. Despite these caveats, the xenograft model is an important tool in the investigation of therapeutics designed specifically against tumor cells, such as pharmacological agents; additionally the genetic manipulation of tumor cells *in situ* or before implantation can be extremely informative, especially concerning basic biochemical research.

Endogenously arising tumors have the primary advantage of being initiated similarly to clinical human tumors; that is, evolving within an immunocompetent host and undergoing successive rounds of mutation, clonal expansion and immunoediting within the CNS. Tumors may be induced by any number of biological or chemical mutagens or

promoters delivered locally or systemically and may be carried out in a variety of immunocompetent hosts. Alternatively, animals with increased susceptibility to certain tumors, due to some accidental or intentional genetic lesion, can be used without invoking the use of antigenic pathogens or non-specific chemical carcinogens. One major drawback however is the potential variation between animals in terms of the tumor geno- and phenotype that may complicate the interpretation of results. Although an important model in the study of oncogenesis and tumor development, there are a number of limitations in its use in a therapeutic setting.

Gliomas derived from cultured cell lines represent the most common *in vivo* glioma model and is the model employed in this study. Gliomas derived from cell lines may incorporate the use of immunocompetent, immunocompromised, syngeneic or allogeneic hosts; in combination with cell lines derived from virally or chemically induced tumors, which maybe inherently immunogenic in syngeneic hosts. Due to the ability of immunogenic cell lines to form lethal tumors in the host animal's CNS, immunogenicity is typically determined by the ability of peripheral vaccination to protect animals from i.c. challenge. Gliomas derived form cultured cell lines hold a number of advantages above other models; the reproducibility and short incubation time required for lethal tumor formation, the ability to readily characterise and/or modify cell lines *in vitro* before implantation and their wide availability allows for greater inter-laboratory comparison. Whereas tumors derived from human tissues are primarily implanted in immunocompromised mice, both mice and rats represent commonly used hosts for non-human glioma cell line implantation models. Rats, the host animal used in this study, have an obvious advantage in terms of their size and docility when considering surgical procedures and non-surgical manipulation.

There are in excess of eight commonly used rat brain tumor cell lines (reviewed by Barth, 1998 and summarised in table 1.2); of these, two were derived from chemically induced tumors, the 9L and T9 cell lines, and are considered WHO grade IV gliosarcoma while the reminder are considered equivalent to WHO grade III (anaplastic astrocytoma) or IV (GBM). The C6 glioma cell line was isolated from an out-bred Wister rat and as a result there is no syngeneic host; consequently the immunogenicity of C6 gliomas in allogeneic hosts has somewhat limited its use as an experimental model. The RT-2 tumor cell line was isolated from Fischer 344 rat pups following i.c. inoculation with avian sarcoma virus (ASV), is considered an anaplastic astrocytoma and, as a result of ASV antigen expression, is immunogenic in syngeneic hosts (Watts and Merchant, 1992). The RG2, alternatively

named D74-RG2 or D74, and F98 glioma cell lines were isolated from Fischer 344 rat pups inoculated transplacentally with N-ethyl-N-nitrosourea and the resultant tumor cells isolated and propagated *in vitro* (Ko *et al.*, 1980). Both RG2 and F98 gliomas are classified as high-grade undifferentiated astrocytoma based upon histological analysis in syngeneic hosts. Gene expression analysis has also been carried out on both cell lines and demonstrated a marked increase in the expression of a number of genes known to be involved in human gliomas including PDGFβ, cyclin D1 and D2, MMPs, Ras and EGFR (Sibenaller *et al.*, 2005). While F98 cells are considered weakly immunogenic, with peripheral vaccination marginally extending survival, RG2 cells are non-immunogenic, with extensive vaccination failing to extend survival following i.c. challenge (Tzeng *et al.*, 1991). *In vivo* tumors from both cell lines have demonstrated remarkable resistance to treatment; both chemo- and radiotherapy have generally resulted in little or no survival benefit with rapid tumor regrowth and death. Recently however, significant progress has been made in the treatment of F98 tumors and produced long-term survival following radiotherapeutic interventions combined with radiosensitisers or i.c. delivered chemotherapeutics. Irradiation combined with *cis*-diamminedichloroplatinum II (Biston *et al.*, 2004), boron compounds (Barth *et al.*, 1997) or carboplatin (Rousseau *et al.*, 2007) resulted in a 34, 10 and 17% long-term survival respectively. There is currently no published literature demonstrating a curative therapy for RG2 glioma, although its usage is less common in therapeutic models. Interestingly, despite being considered non-immunogenic, peripheral vaccination with RG2 cells is capable of inducing tumor infiltration of cytotoxic T cells into i.c. tumors which demonstrate specific cytolytic activity *ex vivo* (Tzeng *et al.*, 1991). Additionally, TLR ligands, LPS or zymosan A, delivered to s.c. RG2 tumors results in complete regression in syngeneic animals accompanied by immunological memory and protection from subsequent s.c. challenge (Mariani *et al.*, 2007). Although treatment of or protection from subsequent i.c. challenge was not examined in this study it nonetheless demonstrates the ability to induce an antigen-dependent adaptive immune response capable of clearing the tumor.

The invasive nature of tumor growth, resistance to chemo- and radiotherapies and the fact that death is caused by an expanding intracranial mass, are all characteristic of clinical human GBM (Wesseling *et al.*, 1997). It is for this close resemblance to human GBM that the F98 and RG2 glioma cell lines are currently considered the most suitable model for therapeutic *in vivo* experimentation (Barth, 1998) and were chosen as the experimental models in this study.

1.16 Immunotherapy and cancer

Given that the immune system is an inherent anti-cancer defence and an efficient immune response should clear the tumor and invading or metastising cancer cells it is not surprising that much research has explored the possibility of modulating the host's immune system to effectively mount and propagate an efficient anti-tumor response, termed cancer immunotherapy. A number of immunotherapeutic strategies have been examined both in *in vivo* models and in clinical trials and can be broadly categorised into either active or passive immunotherapy, although some strategies have included elements of both. Active immunotherapy involves vaccination of tumor bearing hosts with known individual tumor-associated antigens or unknown pools of tumor antigens arising from tumor cell surface proteins, whole irritated tumor cells or tumor lysates. Vaccination may additionally incorporate cytokine co-administration designed to enhance immune cell activation, infiltration or proliferation. Vaccination strategies have also incorporated the use of autologous or heterologous professional APCs, primarily DCs (reviewed by Gilboa, E., 2007), pulsed with tumor antigens, *ex vivo* stimulated and re-administered ensuring that, at least, initial antigen capture and presentation are efficiently accomplished. An alternative approach is passive immunotherapy involving the use of immune components that possess some anti-tumor activity and include antibodies (reviewed by Adams and Weiner, 2005), possibly linked to cytotoxic molecules, or immune cells (reviewed by Rosenberg *et al.*, 2008) that demonstrate oncolytic activity. These effector molecules can be host derived or obtained from allogeneic or xenogeneic hosts and in the case of effector cells may be *ex vivo* expanded or activated prior to infusion. The use of immunotherapeutic intervention, in one form or another, has been carried out in clinical settings for at least 30 years and, although generally less effective than pre-clinical studies, have provided clinically relevant results.

The central role of immune cytokines in the development, regulation and determination of host effector mechanisms in response to immunological challenges highlights their potential use in anti-cancer immunotherapeutic strategies, termed cytokine therapy. Given the complexity of the immune system and the responsibility of cytokines in orchestrating these responses, it is not surprising that each cytokine has multiple effects on a variety of cell populations. In fact, tumor cells are a novel 'pathogen' in that they can, and do, respond to host cytokines and as a result, cytokine therapy cannot only modify host immune and non-immune cells but potentially the tumor cells themselves. As a result,

Cell Line	Carcinogen	Species and strain	Histological grade (WHO grade)	Syngeneic model	Immunogenic*	Reference
CNS-1	N-nitroso-N-methylurea	Inbred Lewis	Uncharacterised	Yes	Not determined**	Kruse *et al.*, 1994
C6	N-methylnitrosourea	Outbred Wistar	Astrocytoma	No	Yes	Schmidek *et al* ., 1971
RG2 (D74, RG2-D74)	N-ethyl-N-nitrosourea	Fischer 344	Anaplastic glioma (grade IV)	Yes	No	Ko *et al* ., 1980
F98	N-ethyl-N-nitrosourea	Fischer 344	Anaplastic glioma (Grade IV)	Yes	Moderately	Ko *et al* ., 1980
RT-2	Avian Sarcoma Virus	Fischer 344	Anaplastic Astrocytoma (Grade III)	Yes	Yes	Copeland *et al* ., 1976
T9	N-methylnitrosourea	Fischer 344	Gliosarcoma (Grade IV)	Yes	Yes	Benda *et al* ., 1971
9L	N-methylnitrosourea	Fischer 344	Gliosarcoma (Grade IV)	Yes	Yes	Benda *et al* ., 1971

Table 1.2: Summary of rat glioma cell lines currently used in experimental neuro-oncology.

* - as determined by protection from i.c. challenge following vaccination in syngeneic animal
** - although successful immunotherapy has been achieved resulting in immunological memory

cytokines are considered potential therapeutic effector molecules and have been examined in a variety of pre-clinical and clinical anti-tumor settings. There are currently a large number of cytokines described in scientific literature and at least 20 of which have entered phase I clinical trials as cancer therapies, although this discussion will be limited to the three cytokines examined in this study which are, interferon gamma (IFN-γ), interferon beta (IFN-β) and interleukin-12 (IL-12).

1.17 Interferon gamma

Interferon gamma is the sole member of the type II interferon group and is expressed by a subset of immune cells including NK and T cells (reviewed by Schroder *et al.*, 2004). First identified for its ability to protect cells from viral infection *in vitro,* the functions of IFN–γ have been elucidated more extensively and include, among others, antiviral, antiproliferative and antineoplastic effects as well as modulating elements of the innate and adaptive immune responses. Although IFN-γ expressed by a limited number of cells the IFN-γ receptor, composed of the two subunits IFNGR1 and IFGR2, is ubiquitously expressed. The functional IFNGR is composed of a two IFNGR1 and two IFNGR2 chains and specifically binds the IFN-γ homodimer to initiate signal transduction. Initially, the ligand-receptor interaction causes a conformational change resulting in the rapid autophosphorylation of the IFNGR2-associated Janus tyrosine kinase, Jak2. Jak2 then transphosphorylates the IFNGR1-associated Jak1 which directly phosphorylates residue 440 on the IFNGR1 intracellular region, required for recruitment of the unphosphorylated STAT (signal transducer and activator of transcription), STAT1. STAT1 is in turn phosphorylated at residue 701, thought to be mediated by Jak2, which dissociates from the IFNGR1 chain. The primary STAT complex induced by IFNGR engagement is the STAT1 homodimer, also know as γ-IFN activation factor, which enters the nucleus and to bind promoter elements bearing the GAS, interferon-gamma activated site, sequence allowing for transcriptional suppression or enhancement. It should be noted that although STAT1 homodimers are essential for much of the IFN-γ mediated transcriptional regulation other member so the STAT family and non-STAT co-factors are capable of forming multimer complexes capable of transcriptional regulation; these include, but are not limited to, STAT1:STAT2, STAT2:STAT2:IRF-9, STAT1:STAT1:IRF-9. Interestingly, although it was thought that the STAT1:STAT2:IRF-9 complex, also called ISGF3 (interferon-stimulated gene factor-3) which binds the ISRE (interferon-stimulated response element)

sequence was exclusively an element of the type I IFN signal pathway it now appear to be an, albeit minor, component of the type II IFN signal pathway demonstrating some overlap between the two cytokine receptor systems. Figure 1.4 is a schematic of the signal transduction of following IFN-γ/IFNGR engagement, additionally a subset of IFN-γ-induced genes important in various physiological effects of IFN-γ are listed (Schroder *et al.*, 2004).

IFN-γ has demonstrated, albeit typically in an *in vitro* setting, direct antiproliferative and pro-apoptotic effects on a variety of tumor cells lines. IFN-γ induced CDK inhibitors, such as p21 and p17, and pro-apoptotic proteins, such as caspase-8, and Fas/FasL are though to be responsible for the anti-proliferative and pro-apoptotic effects, respectively (Chin *et al.*, 1996; Chin *et al.*, 1997; Xu *et al.*, 1998b). A second effector function relevant to cancer immunotherapy is the upregulation, by tumor and antigen-presenting cells, of members of the antigen presentation pathway including mediators of antigen processing, loading and ultimate presentation at the cell surface (reviewed by Boehm *et al.*, 1997). The antigen presentation capacity of tumor cells directly impacts the ability of adaptive and innate cells to mediated antigen specific cell cytotoxicity; *in vivo* experiments incorporating IFN-γ–insensitive tumors into wild-type mice have demonstrated that tumor cell responsiveness to IFN-γ is crucial in IFN-γ cytokine therapy (Dunn *et al.*, 2006).

IFN-γ also induces antiangiogenic/angiostatic effects upon developing tumors *in vivo* which is again dependent upon tumor cell sensitivity to IFN-γ (Beatty and Paterson, 2001). The angiostatic effects of IFN-γ are mediated by members of the chemokine CXC family and the induction of IP-10, interferon-gamma-inducible protein-10 or CXCL10, MIG, monokine induced by interferon-gamma or CXCL9, and I-TAC, interferon-inducible T cell alpha chemoattractant or CXCL11. The CXC ligands also play important roles as lymphocyte chemoattractants and their contribution to tumor elimination appears obligatory, at least in some tumor models, although the relative contribution of the angiostatic and chemoattractant effects remain to be fully defined.

IFN–γ has numerous effects upon cells of the immune system, some of which are themselves endogenous IFN–γ producers. IFN–γ is a direct activator of macrophages, inducing production of reactive species and the upregulation of cytotoxic ligands such as TNF-α and FasL (Farrar and Schreiber, 1993). NK and NKT cells have demonstrated an important role in protection from, and rejection of, induced or transplanted tumors. These effects depend upon, although not exclusively, IFN–γ expression which acts as an

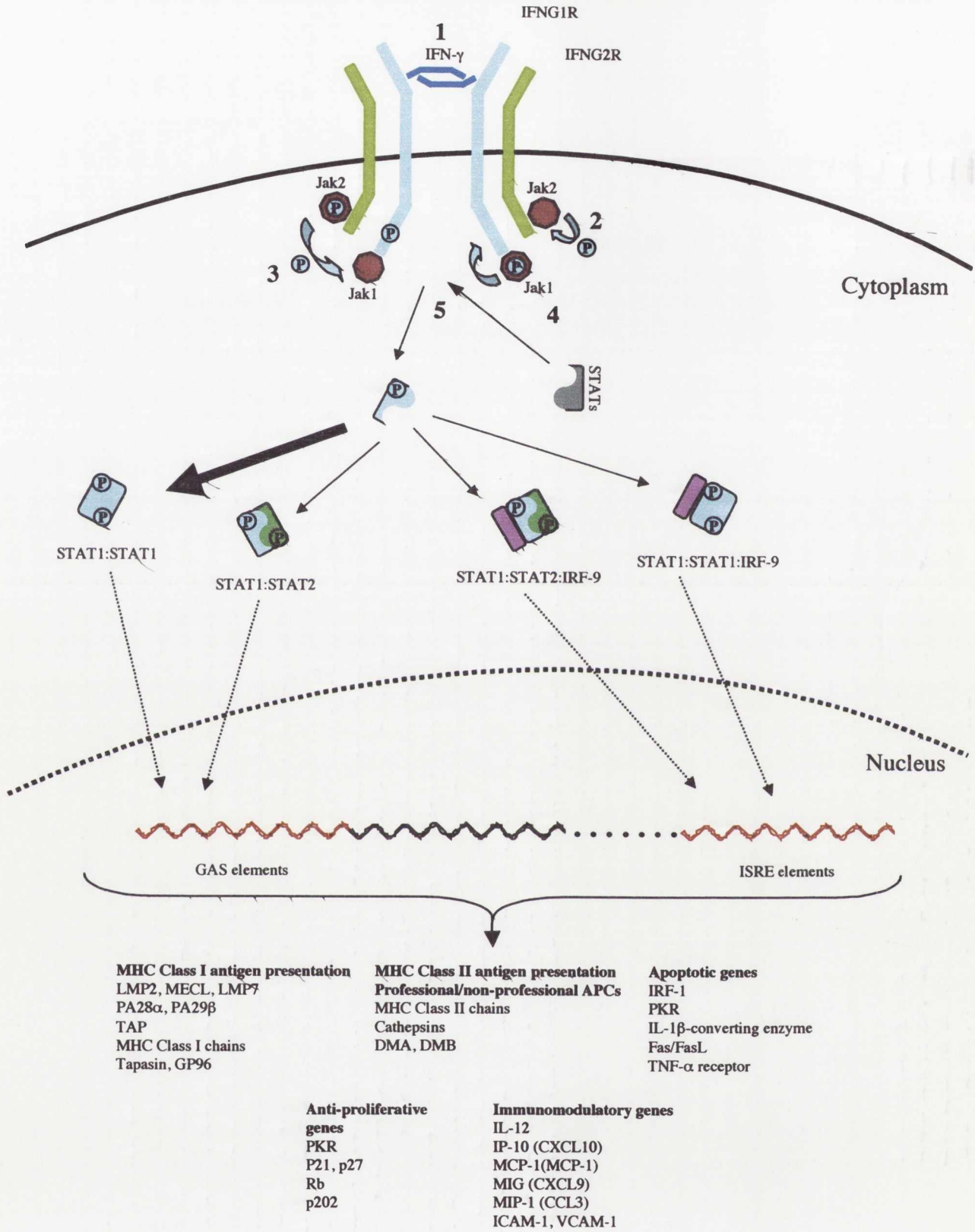

Figure 1.4: Schematic of type II interferon signal transduction system

IFN-γ/IFNR engagement (**1**) initiates receptor rearrangement and autophosphorylation of Jak2 (**2**). Jak2 transphosphorylates Jak1 (**3**) which mediates IFNGR1 chain phosphorylation (**4**) allowing for STAT docking to the receptor complex and subsequent phosphorylation by Jak2 (**5**). Various STAT homo/heterodimers associate and mediate transcriptional activation/repression by binding conserved sequences in gene promoters, although STAT1:STAT1 dimers are the major transcriptional regulator induced by IFN-γ.

important mediator of the NK/NKT cell activation cascade (Smyth *et al.*, 2000B). IFN-γ is also an essential component in the development and propagation of adaptive immune responses. As discussed previously, the upregulation of members of the MHC class I presentation pathway allows for enhanced propagation of CTL effector mechanisms. Additionally, and unlike type I interferons, IFN–γ also upregulates the expression of members of the MHC class II pathway (Boehm *et al.*, 1997) in APCs, thereby enhancing T cell restimulation and the development of an active adaptive response. The polarisation of the adaptive immune response also relies upon members of the IFN-γ signalling pathway and various studies have demonstrated the requirement for IFN–γ, or its downstream products, in the development of a Th1 adaptive immune response (reviewed by Dunn *et al.*, 2005) and the inhibition of Th2 cell development (Del Vecchio *et al.*, 2007). Additionally, IFN–γ has been shown to directly block the activation and development of regulatory T cells, which can play an important role in tumor growth and immune escape (Nishikawa *et al.*, 2005).

Previous experimentation has elucidated some of the key effector functions of IFN–γ in transplantable and induced tumors although the use of IFN–γ as a recombinant protein or via gene therapy has been somewhat limited, especially relative to the type I interferons. Early clinical trials involving systemic delivery of rIFN–γ demonstrated dose limiting toxicities and overall poor responses (Goldstein and Laszlo, 1986) although more recent clinical trails have demonstrated some adjuvant activity such as the i.p. administration of IFN-γ in the treatment of ovarian cancer which extended time to progression and increased overall survival rates (Windbichler *et al.*, 2000). A number of phase one clinical trials have examined adenovirus or retroviral mediated transduction of tumor cells with the IFN-γ gene. Fujii *et al.* (2000) demonstrated host anti-tumor-antigen immunity following retroviral transduction of *in situ* malignant melanoma and Khorana *et al.* (2003) demonstrated the safety of adenovirus use in a similar setting accompanied by encouraging results, despite being early phase trials.

IFN-γ cytokine therapy has additionally been examined as a therapeutic intervention against brain tumors both in pre-clinical and clinical trials. Initial attempts at systemic delivery of rIFN–γ for the treatment of recurrent gliomas did not demonstrate an objective response (Mahaley *et al.*, 1988) nor did the direct intratumoral delivery of IFN-γ in newly diagnosed GBM patients (Farkkila *et al.*, 1994). Clinical trials of glioma therapy have thus far examined only the use of recombinant IFN–γ delivery, although a number of pre-clinical studies using IFN-γ gene therapy have demonstrated some efficacy. Tjuvajev

et al. (1995) demonstrated an initially effective anti-tumor response following implantation of IFN-γ encoding retrovirus, although IFN-γ expression resulted in lethal vasogenic oedema. Oshiro *et al.* (2001) demonstrated an inhibition of RG2 glioma growth and survival extension, although long term survival was not assessed, following intracarotid infusion of recombinant rat IFN-γ. Ehtesham *et al.* (2002) used an adenovirus vector encoding IFN-γ for direct intratumoral delivery into GL-26 glioma and resulted in reduced tumor size, lymphocyte infiltration and extended survival, although no complete tumor regressions were observed. Saleh *et al.* (2000) demonstrated the complete eradication of C6 glioma following treatment with an IFN-γ encoding retroviral vector found to be mediated by B/T cells and angiogenic effects.

1.18 Interferon Beta

Interferon beta (IFN-β) is a member of the type I interferons which include at least 16 other members, the majority of which are IFN-α subtypes, and all bind a common receptor, IFNAR. The functional type I interferon receptor is composed of two subunits IFNAR1 and IFNAR2 and is capable of binding numerous type I interferon proteins. The IFNAR1 and IFNAR2 chains are associated with the Janus tyrosine kinases Tyk2 and Jak1 respectively. Upon ligand/receptor engagement, Tyk2 and Jak1 are autophosphorylated followed by phosphorylation of the IFNAR1 subunits allowing for STAT2 recruitment and Tyk2-mediated phosphorylation. Phosphorylated STAT2 then serves to attract STAT1 to the receptor complex where it is phosphorylated by Jak1. Phosphorylated STATs can then form homo- and heterodimers that may or may not associate with additional cellular co-factors. The most important complex is the STAT1:STAT2:IRF-9 complex, also called ISGF3, that is the only transcriptional complex capable of binding the ISRE DNA sequence. Additionally, STAT1 homodimers and STAT1:STAT3 heterodimers may bind the GAS DNA sequence although this is though to be only a minor component of the type I interferon signalling pathway. Figure 1.5 is a schematic of the signal transduction pathway of the type I interferon system, additionally a subset of type I IFN induced genes important in various physiological effects are listed (Stark *et al.*, 1998).

The type I interferons play important roles in almost all immunological responses including those to viral, bacterial, schistosome infections and neoplastic transformation. Whereas the investigation and elucidation of the mechanisms of endogenous and exogenous type II IFNs in cancer formation and elimination has produced an

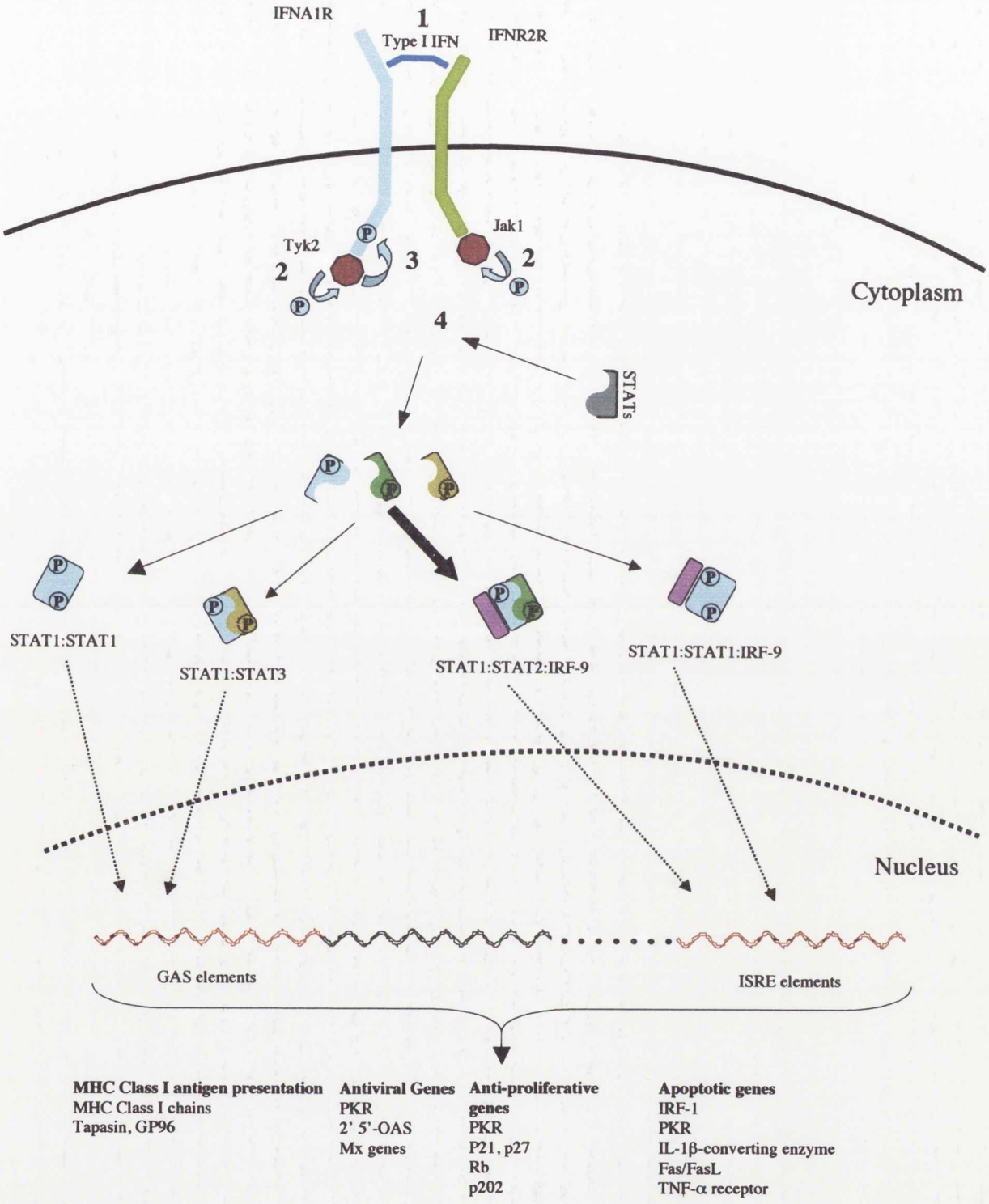

Figure 1.5: Schematic of type I interferon signal transduction system

Type I IFN/IFNR engagement (**1**) initiates receptor rearrangement and autophosphorylation of Tyk2 and Jak1 (**2**). Tyk2 phosphorylates the IFA1R chain (**3**) allowing for STAT2 docking to the receptor complex and phosphorylation by Tyk2 (**4**). Phosphorylated STAT2 recruits STAT1 that is itself phosphorylated. Various STAT homo/heterodimers associate and mediate transcriptional activation/repression by binding conserved sequences in gene promoters although the STAT1:STAT2:IRF-9 complex is the major transcriptional regulator induced by type I interferon receptor engagement.

understanding of the complex host-tumor interactions, the equivalent functions of the type I IFN system are less well defined. In contrast to IFN-γ, the type I IFNs appear to have no influence on tumor cell immunogenicity (Dunn *et al.*, 2005). Furthermore, ablation and reconstitution experiments in mice have demonstrated that type I interferon responsiveness is required only by members of the haematological compartment for the anti-tumor effects of type I interferons and that blockade of the type I receptor prevents lymphocyte-dependent elimination of highly immunogenic tumors (Dunn *et al.*, 2005). Although the involvement of the type I interferons in pathologic infections have largely been elucidated, the exact cell populations and molecular functions required for the type I interferon anti-tumor responses remain to be fully determined. As a result, the specific anti-tumor functions of exogenous IFN-β maybe best determined by the analysis of IFN-β tumor therapy models. Despite this, a number of effects of IFN-β upon immune and host cells have been elucidated, although their relative contributions in an anti-tumor therapy remain to be fully determined.

Interferon beta has demonstrated direct anti-proliferative and pro-apoptotic effects *in vitro* (Takaoka *et al.*, 2003). Interestingly, unlike IFN-γ, the anti-tumor effects of the type I interferons do not require tumor cells to be sensitivity to the type I interferons suggesting that the direct anti-proliferative and pro-apoptotic effects mediated by type I interferons are not essential mediators of the anti-tumor effects elicited by IFN-β. The anti-angiogenic and chemoattractant chemokines induced by IFN-γ are also induced following signalling via the interferon type I receptor and will additionally play some role in the overall anti-neoplastic effects of IFN-β. Given the requirement for interferon responsiveness of the haematological compartment it is not surprising that the type I interferons would have various effects on these cellular components. The type I interferons activate NK cells, inducing the development of cytotoxic competency and cytokine production (Nguyen *et al.*, 2002A). IFN-β may also have inhibitory or stimulatory effects on macrophages, however the eventual outcome appears to depend upon other signals and can potentially induce cell activation, IL-12 and inducible nitrous oxide synthetase (iNOS) production (Bogdan *et al.*, 2004). Type I interferons may also stimulate the activation, maturation and differentiation of DCs into efficient antigen-presenting cells, important for adaptive immunity development (Luft *et al.*, 1998). The effector functions of adaptive immunity are also influenced by type I IFNs that enhance T-cell proliferation, Th1 development, migration and cytotoxicity (Bogdan *et al.*, 2004).

Cao *et al.* (2001) demonstrated reduced microvessel density and increased apoptotic index, resulting in an overall reduction of metastases and, in some animals, complete regression of orthotopic prostate cancer model in nude mice following adenovirus mediated IFN-β (Ad-IFNβ) gene delivery. These results suggested a tumorcidal and anti-angiogenic effect that was independent of T lymphocytes. Olson *et al.*, (2006) later demonstrated this inhibitory effect to be dependent upon nitric oxide synthetase activity and correlated with decreased mRNA levels of a number of pro-angiogenic factors including MMP-9, TGF-β and VEGF. Xu *et al.* (1998A) provided additional evidence in an ovarian cancer model that NOS production was mediated by macrophages. Lu *et al.* (1999) independently corroborated these observations in an immunocompetent murine model (Kito *et al.*, 2002), which demonstrated the ability to induce regression of fibrosarcomas in immunocompetent mice accompanied by immunological memory, following Ad-IFNβ vector delivery.

IFN-β gene therapy has also been examined in pre-clinical glioma models and as a therapeutic intervention in malignant glioma patients. Natsume *et al.* (2000) delivered lipoencapsulated IFN-β encoding DNA into established GL261 murine gliomas resulting in complete tumor regression and long-term survival. Initial clinical trials utilising recombinant IFN-β produced mixed results with some trials producing statistically significant enhancement in survival (Duff *et al.*, 1986; Packer *et al.*, 1996; Yung *et al.*, 1991; Yung *et al.*, 1990). The use of adenovirus mediated IFN-β gene delivery has also been examined in a small phase I/II clinical trials and demonstrated safety and a significant reduction (>50%) in two of four treated patients.

1.19 Interleukin 12

Interleukin 12 (IL-12) is a pro-inflammatory cytokine produced by a number of immune cells including macrophages, DCs and B cells in response to both pathogenic and immunostimulatory molecules (Trinchieri, 1998). The active IL-12 protein is a heterodimer composed of two disulphide linked subunits, p40 and p35. Both subunits are regulated separately; the p35 subunit is constitutively expressed in a wide variety of cells while the inducible subunit, p40, is expressed only by IL-12 producing cells. The IL-12 receptor is composed of two subunits IL-12Rβ1 and IL-12Rβ2 and is expressed on a limited number of immune cells including T cells, macrophages, NK cells and NKT cells (Portielje *et al.*, 2003). Signal transduction is mediated, like the IFNs, by the JAK-STAT

pathway however, unlike IFN signal transduction the biochemical events initiated by IL-12/IL-12R engagement largely remain to be elucidated (Watford *et al.*, 2003). IL-12R engagement occurs via binding to both IL-12Rβ1 and IL-12Rβ2 subunits via the IL-12 p40 and IL-12 p35 subunits respectively. Following receptor binding the receptor-associated Jaks, Tyk1 and Jak2 become transphosphorylated which lead to IL-12Rβ1 chain phosphorylation facilitating STAT docking and phosphorylation by Jak2. STAT1, STAT3, STAT4 and STAT5 have been reported to undergo phosphorylation following IL-12 binding however STAT4:STAT4 homodimers are though to be the most important transcription factors induced as a result of IL-12R engagement. STAT complexes then migrate to the nucleus mediating transcriptional activation/repression of target genes. Figure 1.6 is a schematic representation of the signal transduction cascade following IL-12R/IL-12p70 binding.

Cellular expression of active IL-12p70 protein is reliant upon pathogenic signals, cytokines and cell-cell interactions, combinations of which are especially important for efficient and optimal production (Del Vecchio *et al.*, 2007). IL-12 receptor engagement results in a variety of downstream effects including the expression of pro-inflammatory cytokines such as granulocyte-macrophage colony stimulating factor (GM-CSF), TNF-α, IL-8, 6, 15 and 18 (Portielje *et al.*, 2003). Additionally, IL-12 is a potent immune cell activator/stimulant (reviewed by Watford *et al.*, 2003) inducing neutrophil activation and chemoattractant production and NK and NKT migration, cytotoxicity and cytokine production. IL-12 has demonstrated the capacity to stimulate, directly and in-directly, dendritic cells inducing their maturation and enhancement of their antigen presentation capacity. IL-12 is also of importance in the development and stimulation of T cells and is an essential cytokine for the development of naive $CD4^+$ T cells toward a Th1 phenotype as well as their subsequent activation and proliferation. IL-12 is also involved in the priming, expansion and differentiation of Th1 effector cells, namely $CD8^+$ CTLs responsible for cell-mediated immunity.

In addition to the direct effects of IL-12, there are a number of important in-direct effects mediated primarily by IL-12 induced IFN-γ, discussed in section **1.17**. Unlike IL-12R, the IFN-γ receptor is present on the majority of cells including tumor cells allowing for the amplification of downstream effects and enhancement of immune mediated detection and elimination of neoplastic cells. The importance of IFN-γ in IL-12 anti-tumor therapy is highlighted by the fact that IFN-γ blockade inhibits IL-12 mediated tumor regression (Nastala *et al.*, 1994). In fact, IL-12 and IFN-γ are intimately linked and

function in a mutual positive amplification loop and IFN-γ upregulates the β chain of the IL-12 receptor, further enhancing IL-12 binding and function (Afkarian *et al.*, 2002).

The use of IL-12 in pre-clinical anti-tumor models has been extensive. Toxicity as a result of systemic delivery, mediated primarily by IFN-γ induction, has been demonstrated in a variety of animal models and human clinical trials (Car *et al.*, 1990). As a result of systemic toxicity, local delivery by the direct intratumoral injection of rIL-12, transduced IL-12 expressing non-tumor cells or viral vector mediated transduction of tumor cells has taken favour in pre-clinical and clinical investigations. The delivery of IL-12 expressing fibroblasts to the tumor bed has produced encouraging results accompanied by limited toxicity (Zitvogel *et al.*, 1995; Tahara *et al.*, 1995) and was the subject of a phase I clinical trial (Kang *et al.*, 2001) demonstrating initial safety. Given the labour-intensive requirements for the production of transduced fibroblasts under GMP conditions and the inherent batch-to-batch variability, the use of viral vectors for local delivery has received much attention. In pre-clinical models, various neoplastic malignancies have been treated with adenovirus (Caruso *et al.*, 1996), retrovirus (Tahara *et al.*, 1995), herpes simplex virus (Toda *et al.*, 1998), vaccinia virus (Chen *et al.*, 2001), Semliki Forest virus (Chikkanna-Gowda *et al.*, 2005) and non-viral vectors (Iwashita *et al.*, 2004) encoding the IL-12 gene and have demonstrated impressive results.

IL-12 treatment of CNS tumors has also been examined; neural stem cells transduced to express IL-12 and co-implanted or subsequently implanted into gliomas demonstrated significant growth inhibition accompanied by an influx of $CD4^+$ and $CD8^+$ T cells (Ehtesham *et al.*, 2002; Yang *et al.*, 2004). Herpes virus and vaccinia virus vectors encoding the IL-12 gene have also been examined and demonstrated survival enhancement and lymphocyte infiltration (Parker *et al.*, 2000; Chen *et al.*, 2001). Liu *et al.* (2002) examined the effect of IL-12 gene transfer by a replication-incompetent adenoviral vector encoding IL-12 in a GL-26 murine glioma model. This treatment protocol produced a 50% long-term survival rate accompanied by the elicitation of an adaptive memory response.

The extensive use of IL-12 gene therapy in *in vivo* models has allowed for an elucidation of the molecular events following the therapeutic use of IL-12. In peripheral anti-tumor models, cellular mediated immunity has been shown to be $CD8^+$ CTL dependent and $CD4^+$ T cell and NK cell independent. The Th1 cell mediated regression mechanism has been further elaborated and additionally involved activated macrophages with nitrous oxide (NO) being the major effector molecule (Tsung *et al*, 1997). In contrast to above, other studies have found that both NK and NKT cells are essential for tumor

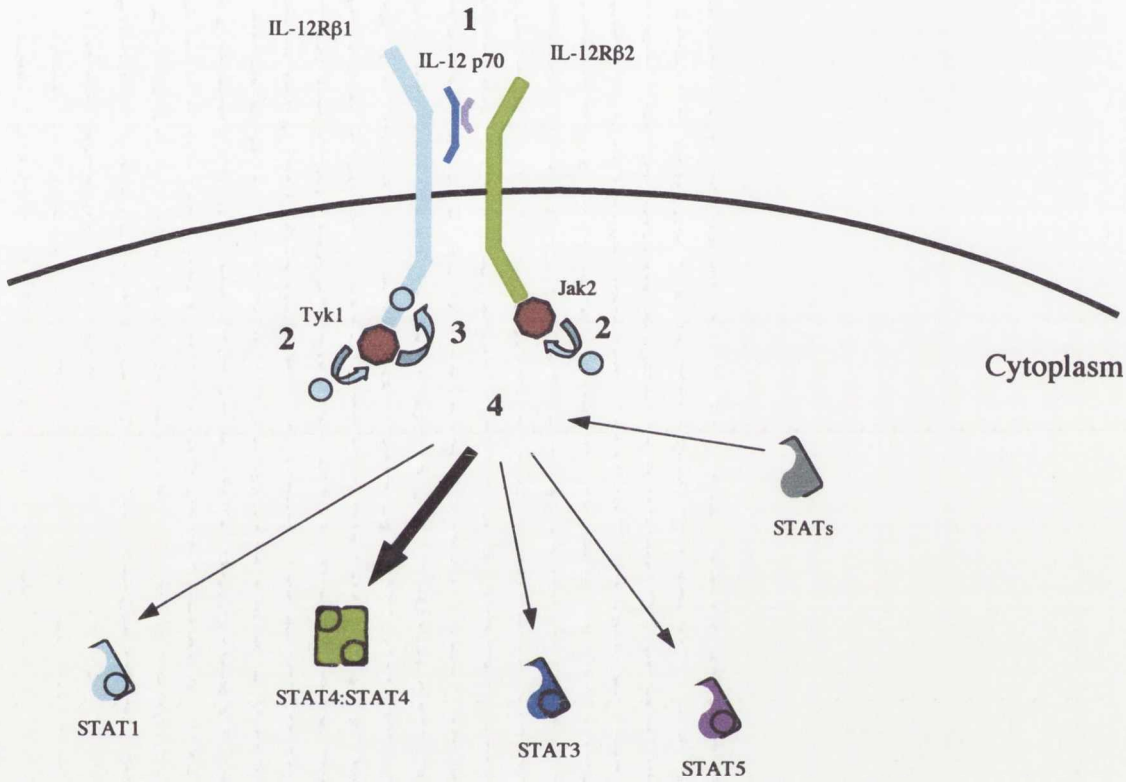

Figure 1.6: Schematic of IL-12 signal transduction system

IL-12 p70/IL-12R engagement (**1**) initiates receptor rearrangement and transphosphorylation of Tyk1 and Jak2 (**2**). Tyk1 phosphorylates the IL-12Rβ1 chain (**3**) allowing for STAT docking to the receptor complex and phosphorylation by Jak2 (**4**). Various STAT homo/heterodimers associate and mediate transcriptional activation/repression by binding conserved sequences in gene promoters although the STAT4:STAT4 homodimer complex is the major transcriptional regulator induced by IL-12 receptor engagement.

inhibition (Smyth *et al.*, 2000a), although both agree on the necessity of $CD8^+$ T cells for immunological memory. It has been suggested that the specific innate cell subpopulations directly responsible for tumor regression are model dependent and may be particular to the genetic lesions/expression profiles of tumors as well as the concentration of IL-12 achieved during treatment (Smyth *et al.*, 2000a).

1.20 Immunogene Therapy

Immunogene therapy differs from direct cytokine delivery in one significant way; in place of administering the therapeutic protein, nucleic acid encoding the cytokine is delivered resulting in cytokine production from transfected cells. While gene delivery can be mediated by direct intratumoral or systemic injection, ideally with some degree of tumor targeting, cell transfection can be carried out by biophysical means, such as electroporation or ultrasound; chemical transfection, such as liposome encapsulated DNA/RNA, or by the use of viral vectors which have their own inherent transfection potential. The particular viral vector used for gene transfer is also subject to variation and can result in transient protein expression, typically accompanied by virally initiated host-cell death, or long-term integrative or non-integrative protein expression. Additionally, cytokine expression levels will depend upon the gene promoters included, which may be virally derived or specific host cell promoters included in the viral vector design. This study uses the viral vector system based on the Semliki Forest virus, termed SFV virus-like particles. VLPs are produced specifically to encode a transgene in place of the virus' own structural genes. Following infection, the transgene, encoded by the RNA genome, is expressed under control of the subgenomic promoter resulting in rapid and high level expression of the protein product. Ultimately, infected host-cells will undergo apoptosis initiated by the viral non-structural replicase resulting in cell death by approximately 72 hours post-transfection. The use of viral vectors to mediate cytokine expression may have additional, albeit potential, therapeutic effects or caveats compared with direct cytokine delivery. Because of apoptosis induction in transfected cells, expression will be limited and will require re-administration in order to achieve prolonged cytokines expression. However, this apoptosis induction has the advantage of providing cellular material for phagocytosis and allowing some control over expression levels by the cessation of treatment. Anecdotal observations of virus infection coinciding with spontaneous tumor regression were the initiating factor in the use of replicating viruses in virotherapy. Obviously then, viral infection has the

potential to produce some anti-tumor effects, possibly due to tumor oncolysis or adjuvant effects in the initiation of a host anti-tumor immune response. The induction of a local anti-viral response accompanied by interferon, pro-inflammatory cytokine and chemokine release in association with innate, and later, adaptive immune cell infiltration and activation, have advantages in providing a suitable environment of the initiation of immune responses as well as increasing cytokine-target cell populations. The cross-presentation process, in which apoptotic material can be phagocytosed and presented by APCs, which have been sufficiently activated by internal TLR binding or cytokine activation, to T cells, may provide tumor antigen in the context of 'danger signals'. Additionally, epitope spreading may occur, in which the immune response, initially initiated against a single or multiple antigens, can develop to include antigen(s) not present in the initial antigen challenge. Epitope spreading may have an important role in the use of the SFV VLP system in an anti-cancer setting by providing an initial immune response to the viral vector, infection with which is associated with 'danger signals' and the induction of an immune response targeting antigen at the tumor environment. Additionally, these cytokine/vector interactions may be synergistic and may not be fully represented by analysis of either alone. An additional advantage of viral vector-mediated cytokine delivery is the provision of local high-dose cytokine expression while reducing systemic levels avoiding systemic toxicity which can limit administration to sub-optimal doses.

Objectives of study

This study has been designed and carried out to investigate a number of primary and secondary goals that include;

- The cloning and production of SFV VLPs encoding the interferon beta, interferon gamma and interleukin 12 genes and an assessment of their *in vitro* and *in vivo* expression.
- To examine the ability of the SFV VLP system to infect, mediate transgene expression from, and induce apoptosis in glioma cells lines *in vitro* and *in vivo*.
- To develop two intracranial glioma models suitable for repeated intracranial treatment with SFV VLPs.
- To determine the safety of direct intracerebral delivery of SFV VLPs, and the relative contributions, if any, of the VLPs and the encoded transgene.
- To determine the efficacy of intracranial SFV VLP mediated IL-12 gene delivery as an anti-tumor agent and, where possible, determine the effector mechanisms responsible for these effects.
- To examine the use and efficacy of the SFV VLP system encoding IFN-β, IFN-γ and IL-12 as an anti-glioma therapy when delivered via the non-invasive intranasal route and, where possible, determine the effector mechanisms responsible for these effects.

The overall objective of this study was to examine the hypothesis that IL-12 expression within the CNS, mediated by the SFV VLP expression system, could inhibit the growth of gliomas in a rat model.

Chapter 2

Cloning of interferon beta, interferon gamma and interleukin-12 into the SFV enhanced expression vector system

2.1 Introduction

SFV VLPs are produced by the co-transfection of S-BHK cells with three distinct mRNA species, two of which encode the structural proteins required for virion production. The third mRNA molecule is the SFV expression RNA, into which transgenes are cloned, and is the only mRNA species encapsidated during virion production. There have been several generations of SFV expression plasmid produced, each successively modified to enhance transgene expression and ease of cloning. The SFV expression plasmids contain a SP6 RNA polymerase promoter for *in vitro* transcription, an ampicillin resistance gene for plasmid selection, the SFV 5' and 3' untranslated regions and the SFV non-structural ORF, which includes the packaging signal sequence. The first produced SFV expression plasmid, pSFV1, had a small multiple cloning site in place of the structural ORF and was flanked by the subgenomic ORF sequence. pSFV3 was subsequently cloned including a Kozak sequence for enhanced transgene translation, however cloning was cumbersome due to the necessity to maintain frame and the limited number of cloning sites. Following this, the pSFV4.2/pSFV10 expression plasmid was created containing a larger multiple cloning site, for ease of cloning, but lacking the Kozak sequence. The most recent plasmid, and the one used in this study, is pSFV10-b12a/pSFV-Enh. To allow for ease of cloning, a larger multiple cloning site was included comprising approximately 7 unique endonuclease restriction sites into which transgenes can be ligated. Additionally, the 5' 102 nucleotide capsid sequence (b1 sequence) has been included which enhances transgene expression by approximately ten-fold. This translational enhancer sequence then forms the translational start site located upstream of the multiple cloning site. For this reason, the foot-and-mouth disease virus (FMDV) 2A protease sequence was cloned directly downstream of the capsid enhancer sequence. The 2A sequence is 17 amino acids in length and contains an autocatalytic protease that specifically and co-translationally cleaves between the 16^{th} (glycine) and 17^{th} (proline) residues. This allows for the removal of the b1 and 2A sequence from the transgene protein product.

The rat IFN-γ, IFN-β and IL-12 genes were cloned into the enhanced expression vector. Cloning of the IFN-β and IFN-γ genes was carried out by PCR amplification of gene-encoding cDNA followed by in-frame ligation into the pSFV-Enh vector. The IL-12 protein is a heterodimer composed of two subunits, p35 and p40, both encoded by individual genes and processed differentially (Murphy *et al.*, 2000). Due to the potential production of p40 homodimers, which antagonistically bind the IL-12 receptor (Ling *et al.*,

1995), optimal IL-12 p70 production is dependant upon equimolar expression of both subunits. For this reason a pSFV-Enh double construct was produced incorporating both subunits under the control of individual sub-genomic promoters. This strategy has been successfully employed for the production of multiple transgene-encoding SFV-Enh plasmids including mouse IL-12 (Chikkanna-Gowda *et al.*, 2005; Rodriguez-Madoz *et al.*, 2005).

2.2 Experimental Procedures

2.2.1 Materials

2.2.1.1 Cell lines and bacterial cultures

Baby hamster kidney (BHK-21) cells were obtained from the American type culture collection (ATCC, USA) and propagated in Glasgow minimum essential medium (GMEM) supplemented with 5% (v/v) newborn calf serum (NCS), 5% (v/v) tryptose phosphate broth, 2mM L-glutamine and 100 units/ml penicillin/streptomycin. Swedish BHK (S-BHK) cells were a kind gift from Prof. P. Liljeström (Karolinska Institute, Sweden) and maintained in GMEM supplemented with 5% (v/v) fetal calf serum (FCS), 5% (v/v) tryptose phosphate broth, 20mM hepes, 2mM L-glutamine and 100 units/ml penicillin/streptomycin. Overlay medium was composed of 20% minimum essential medium (MEM), 8% (v/v) NCS, 10% (v/v) tryptose phosphate broth, 100 units/ml penicillin/streptomycin, 2mM L-glutamine and 0.4% $NaHCO_3$ in sterile distilled water. Infection medium was composed of MEM supplemented with 0.2% (v/v) bovine serum albumin (BSA), 20mM hepes, 2mM L-glutamine and 100 units/ml penicillin/streptomycin. All tissue culture flasks and dishes were purchased from Sarstedt (Germany). E. coli DH5α cells and S.O.C. medium were obtained from Invitrogen (UK). XL-10 Gold® ultracompetent E. coli cells were purchased from Stratagene® (USA). 1.8% Difco agar, Luria-Bertani broth (LB-broth), Luria-Bertani broth agar (LB-agar) and NZY^+ broth were obtained in house. Dulbecco's PBS (D-PBS), PBS with Ca^{2+}/Mg^{2+} and all medium and supplements were purchased from Invitrogen. Ampicillin and trypan blue were purchased from Sigma-Aldrich (USA).

2.2.1.2 Semliki Forest virus and the SFV enhanced expression vector

The SFV enhanced expression vector plasmid, pSFV-Enh, and map were a kind gift from Prof. P. Liljeström. A seed stock of SFV4 virus was obtained in house.

2.2.1.3 Animals

Male Fischer 344 rats were obtained from Harlan (UK). Animals were maintained in temperature-controlled rooms and given food and water *ad libitum*.

2.2.1.4 Molecular biology reagents

The QIAprep® spin Miniprep and Midiprep kits, QIAquick® PCR purification kit, QIAquick® nucleotide removal kit and TripleMaster® enzyme PCR system were purchased from Qiagen (UK). The Improm-II™ reverse transcription system, nuclease free water and agarose were purchased from Promega (USA). TRIzol® reagent was purchased from Invitrogen. All restriction endonucleases, endonuclease reaction buffers, 1 kb and 100 bp DNA ladders, Taq DNA polymerase, ThermoPol® buffer, $MgCl_2$, Quick Ligase® kit, Klenow, antarctic phosphatase and antarctic phosphatase buffer were purchased from New England Biolabs (NEB, UK). SP6 polymerase, RNA polymerase buffer, CAP analogue, rNTPs and RNasin were also purchased from NEB.

Agarose gels were run on a Bio-Rad® electrophoresis apparatus (Bio-Rad®, USA) and ethidium bromide was purchased from Bio-Rad®. Gels were visualised using the MiniBis Bio-Imaging system and GelCapture v4.25 software (DNR Bio-Imaging Limited, Israel). Electroporation was carried out on a GenePulser XCell™ (Bio-Rad®) electroporation apparatus using 4mm electroporation cuvettes (Cell Projects, UK).

Bacterial cultures were agitated in an Innova 2300 orbital shaker (New Brunswick Scientific, USA). QIAquick® and QIAprep® kit protocols were carried out using the ALC® 4214 microCENTRIFUGETTE® microcentrifuge (Thermo Scientific, USA), bacterial and tissue culture cells were centrifuged using the ALC® PK131R centrifuge and RNA and DNA centrifugation carried out using the ALC® PK 121R centrifuge. Tissue homogenisation was carried out using Lysing Matrix D in a FastPrep™ FP120 homogenising apparatus (Q-Bio gene, USA).

Reverse transcription and PCR primers were synthesised by MWG Biotech, Germany (Table 2.1). Site-directed mutagenesis primers (HPLC purified) were also purchased from MWG biotech. All thermocycle reactions were carried out on a Hybaid gradient PCR machine (Hybaid Limited, UK).

Target gene	Direction	Restriction site	Primer sequence (5' – 3')
IL-12 p35	Forward	XmaI	CAT GTG CCC GGG ATG TGT CAA TCA CGC TAC C
IL-12 p35	Reverse	XhoI	GAC GTG CTC GAG TTA GGA GGA GCT CAG ATA G
IL-12 p40	Forward	XmaI	GAT ACA CCC GGG ATG TGT CAT CAG AAG TTA AC
IL-12 p40	Reverse	SpeI	TAC AAG ACT AGT TTA GGA TCG GCC CCT GC
IFN-γ	Forward	XhoI	TCG ATA CTC GAG ATC CAT GAG TGC TAC ACG
IFN-γ	Reverse	NotI	GTC TAA GCG GCC GCA GAA TCA GCA CCG ACT CC
IFN-β	Forward	XhoI	AGT GGC TTC TCG AGC ATG GCC AAC AGG TGG
IFN-β	Reverse	SpeI	TGG CTC ACT AGT GGT CTT CAG TTC TGG

Table 2.1: Primers used for PCR amplification.

Red bases signify restriction sites for directional cloning, blue bases signify start/stop codons.

2.2.1.5 ELISA reagents

The BD OptEIA™ set rat IFN-γ ELISA was purchased from BD Biosciences (USA) and the rat IL-12 p70 CytoSet™ purchased from BioSource International (USA). ELISAs were carried out on Nunc™ MaxiSorp™ flat-bottomed 96-well plates (Thermo Fischer Scientific, USA). ELISA buffers were produced in house. ELISA ancillary reagents including 3,3',5,5'-tetramethylbenzidine (TMB) liquid substrate system, NaCl, Tween® 20, $Na_2HPO_4 \cdot 2H_2O$ and KH_2PO_4 were purchased from Sigma-Aldrich. $NaHCO_3$, Na_2CO_3, KCl and H_2SO_4 were purchased from BDH (UK). ELISAs were read on a Multiskan EX plate reader using the Ascent software v2.6 (Thermo Labsystems, USA). IL-12 ELISAs were incubated on the Titramax 1000 orbital shaker (Heidolph Instruments, Germany).

2.2.1.6 Immunofluorescence reagents

Neutralising polyclonal rabbit IgG anti-rat interferon beta (ab-25470) was purchased from Abcam (UK). Biotinylated mouse anti-rabbit IgG and streptavidin/FITC were purchased from DAKO (Denmark). Normal rabbit and mouse sera were purchased from Sigma-Aldrich. VECTASHIELD® Hard Set™ mountant with DAPI was purchased from Vector Laboratories (USA). Glass slides and 22x22 mm coverslips were purchased from Menzel-Gläser® (Germany).

2.2.1.7 Microscopy

A Nikon Eclipse E400 epifluorescence microscope was used for both bright field and fluorescence microscopy. Green fluorescent protein (GFP, emission wavelength 460-500 nm) and 4',6-diamidino-2-phenylindole (DAPI, emission wavelength 340-380 nm) Nikon filters were used for fluorescence detection.

2.2.1.8 Miscellaneous

Isopropanol, ethanol, acetone, acetic acid, paraformaldehyde and crystal violet dye were purchased from BDH. Dithiothreitol (DTT) was purchased from Sigma-Aldrich.

2.2.2 Methods

2.2.2.1 Cell culture techniques

Cells were thawed rapidly in a 37°C water bath and placed into appropriate medium. 12-24 hours later medium was changed to remove residual DMSO. Cells were grown to confluence and sub-cultured at a ratio of 1/8-1/12. For sub-culturing of cell lines, incubation medium was removed, cells washed twice in D-PBS and incubated for 2-5 minutes in 1ml/75cm^2 of 0.05% trypsin. Once cells had detached 9ml of appropriate medium was added per 1ml of trypsin, the cells pipetted 10 times, divided into sterile tissue culture flasks and maintenance medium added.

2.2.2.2 Virus production

2.2.2.2.1 Virus infection

A seed culture of SFV4 was obtained in house and used to infect a confluent 150cm^2 tissue culture flask of BHK cells. Cells were infected with 2x10^6 p.f.u. of SFV4 in 1ml of infection medium for 1 hour with gentle rocking every 15 minutes. Following infection, the inoculum was removed and cells replenished with 30ml of BHK medium. Cells were placed in an incubator (37°C, 7.5% CO_2, 100% RH) for 18 hours after which medium was removed, centrifuged at 4000rpm (2934.4g) at 4 °C for 5 minutes, sterile filtered through a 0.22μm filter, aliquoted and frozen at –70 °C.

2.2.2.2.2 Virus titration

A confluent 150cm^2 flask of BHK cells was trypsinised and divided into 60mm^2 sterile petri dishes in a total volume of 2ml of BHK medium per dish. Cells were grown until confluent, the medium removed and infected with 10-fold serial dilutions of virus stock in 0.5ml of infection medium. Cells were infected for 1 hour in a 37 °C incubator with gentle rocking every 15 minutes. Following infection, the inoculum was removed and 3ml of 1.8% Difco agar/overlay medium (1:1) added gently to each dish. Dishes were placed in a 37°C incubator for 48 hours followed by fixation with 3ml of 4% PFA for 10 minutes at RT. PFA and agar were removed using gently running water followed by the addition of

3ml of crystal violet dye for 5 minutes. Dishes were washed extensively with tap water and dried overnight at 37°C. Plaques were counted and used to calculate virus titers.

2.2.2.3 Cloning of interferon beta, interferon gamma and IL-12 into the SFV enhanced vector

2.2.2.3.1 Cloning strategies for the production of pSFV-Enh-IFNβ, pSFV-Enh-IFNγ, pSFV-Enh-IL12(p35) and pSFV-Enh-IL12(p40)

2.2.2.3.1.1 SFV enhanced expression vector

Figure 2.1 shows a schematic of pSFV-Enh indicating the non-structural ORF, the sub-genomic translation start site and the multiple cloning site. Figure 2.2 indicates the restriction sites used for cloning and for the conformation of correct inserts.

2.2.2.3.1.2 Interferon beta cloning

Figure 2.3 is a schematic of the cloning strategy used for the production of pSFV-Enh-IFNβ. Briefly, IFN-β mRNA was reverse transcribed with primers incorporating the XhoI and SpeI restriction sites into the forward and reverse primers, respectively. Both the SFV-Enh plasmid and PCR product were digested with XhoI and SpeI, ligated and screened for the correct insert. Figure 2.4 is a schematic of the completed pSFV-Enh-IFNβ construct. The 4th year undergraduate student Ms. Michelle Cashin-Cox carried out the interferon beta cloning under my planning and supervision.

2.2.2.3.1.3 Interferon gamma cloning

Figure 2.5 is a schematic of the cloning strategy used for the production of pSFV-Enh-IFNγ. Briefly, IFN-γ mRNA was reverse transcribed with primers incorporating the XhoI and NotI restriction sites into the forward and reverse primers, respectively. Both the SFV-Enh plasmid and PCR product were digested with XhoI and NotI, ligated and screened for the correct insert. Figure 2.6 is a schematic of the completed pSFV-Enh-IFNγ construct. The 4th year undergraduate student Ms. Sarah Leonard carried out the interferon gamma cloning under my planning and supervision.

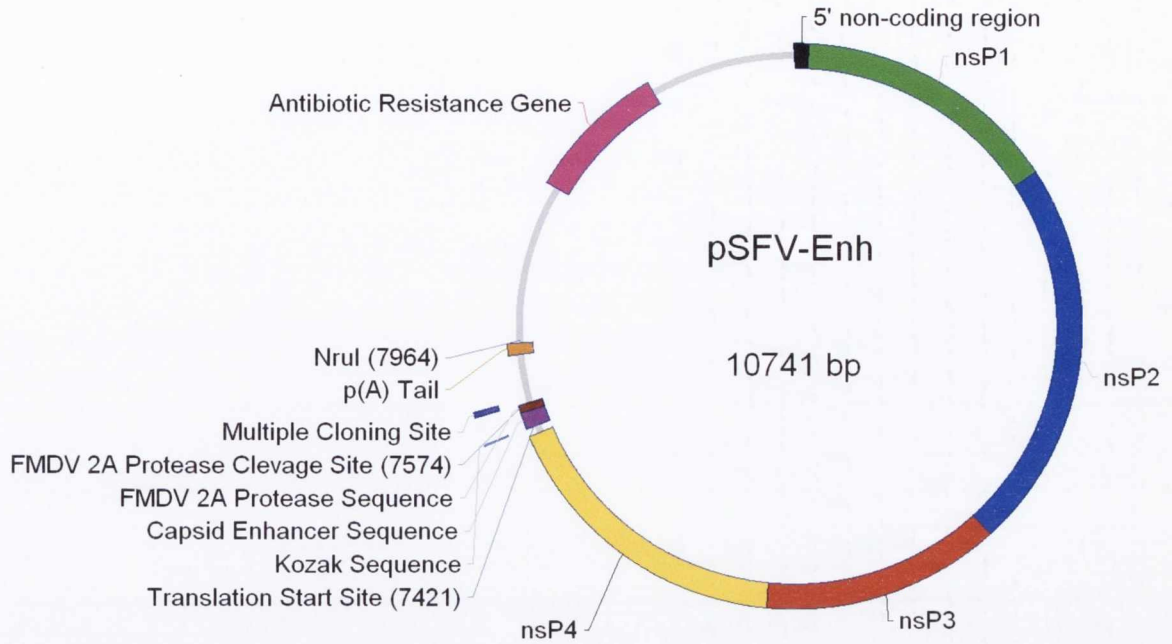

Figure 2.1: Schematic of pSFV-Enh.

Shown are the nonstructural ORF, sub-genomic promoter region and the multiple cloning site.

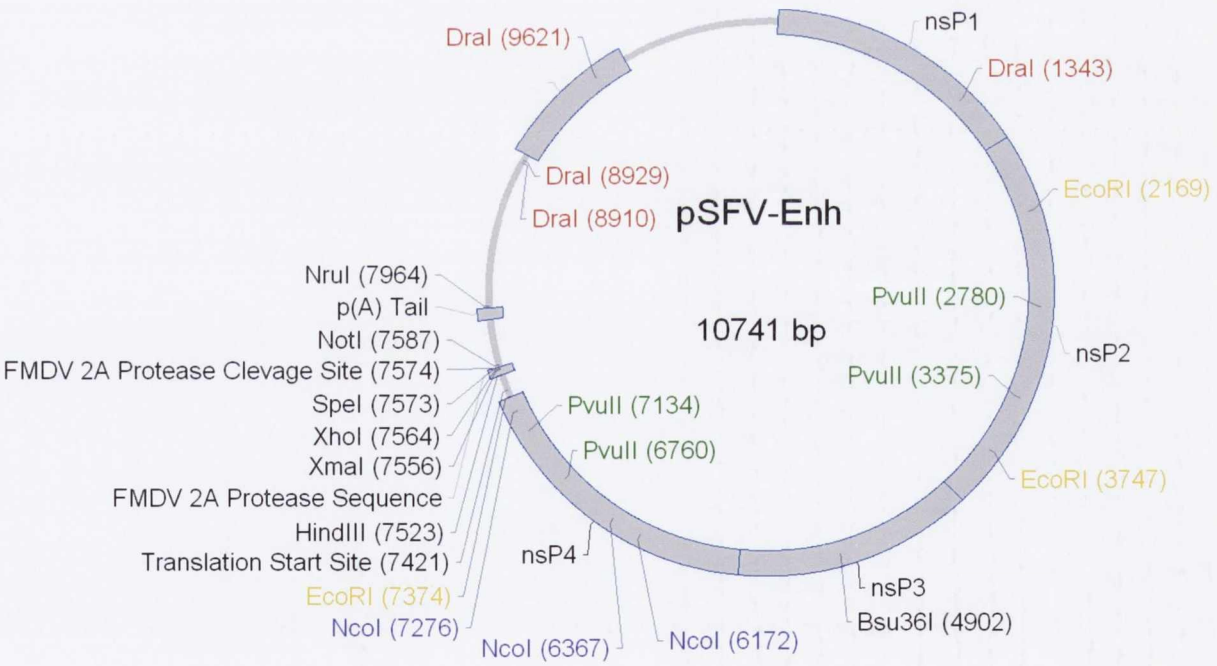

Figure 2.2: Schematic of pSFV-Enh.

Shown are the restriction sites used for cloning and conformation of correct insertions.

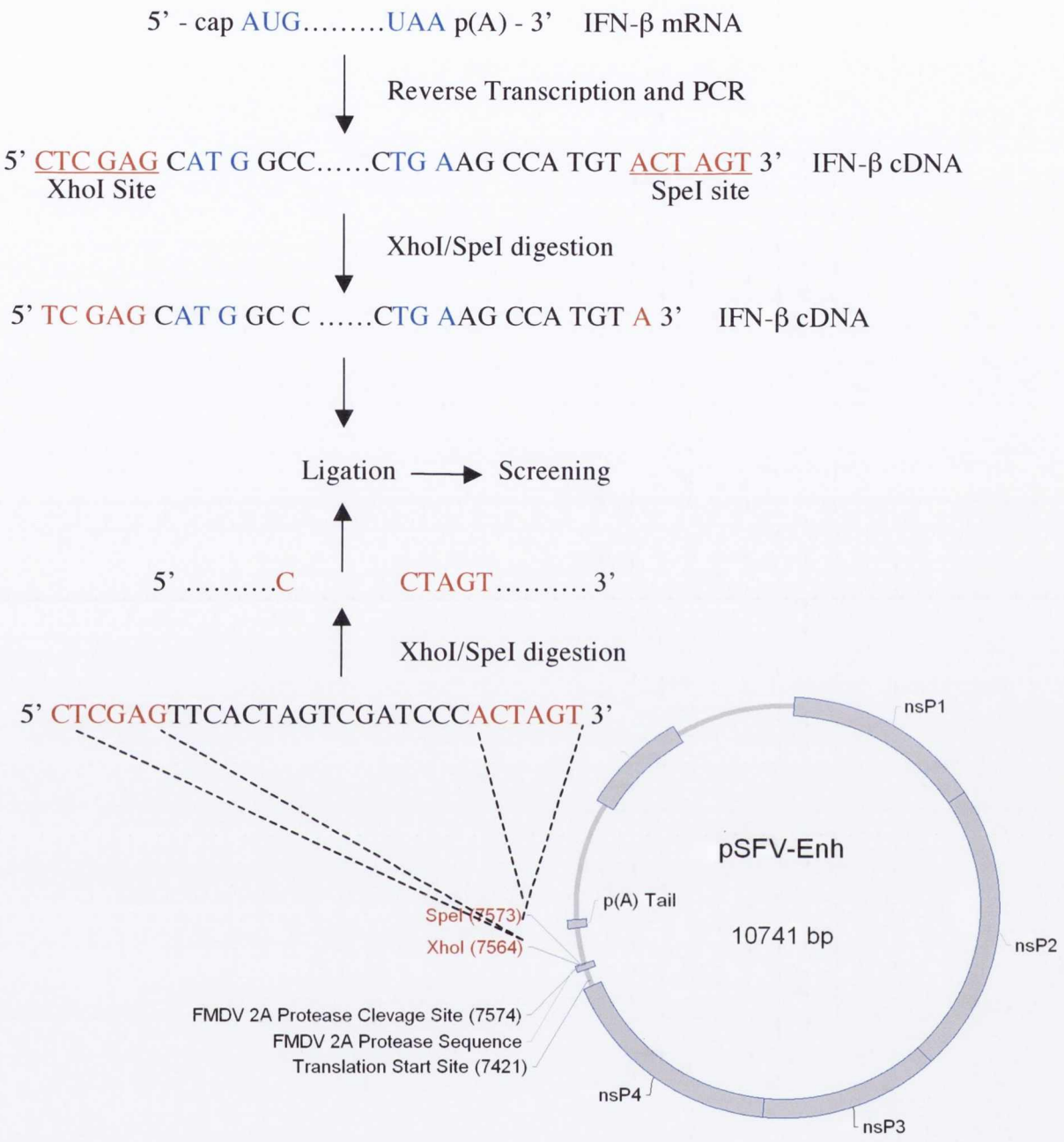

Figure 2.3: Schematic representation of IFN-β cloning strategy.

IFN-β mRNA was reverse transcribed with primers incorporating the XhoI and SpeI restriction sites into the forward and reverse primers, respectively. Both the SFV-Enh plasmid and PCR product were digested with XhoI and SpeI, ligated and screened for the correct insert. Blue bases signify start/stop codons; red bases signify restriction sites used for cloning.

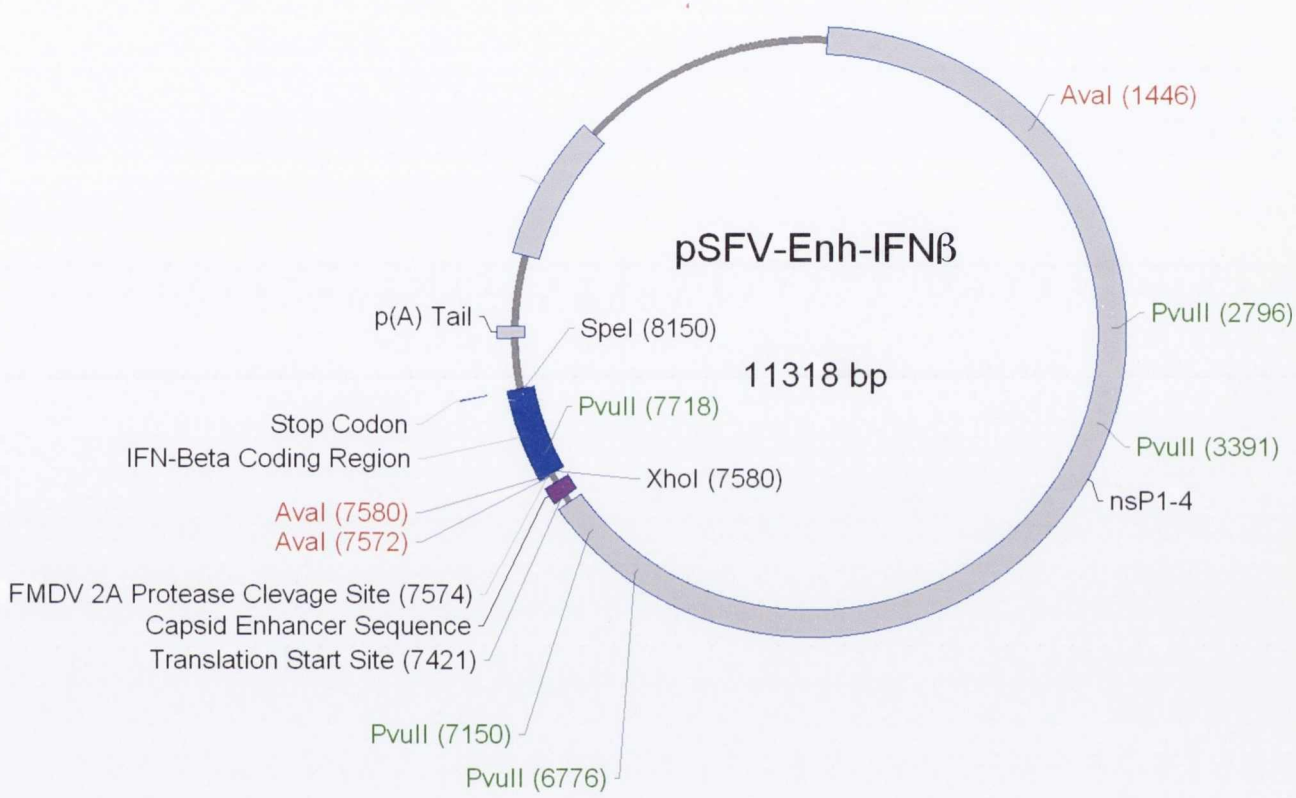

Figure 2.4: Schematic of pSFV-Enh-IFNβ.

Image represents constructed SFV-Enh-IFNβ plasmid. Indicated are the restriction sites used for cloning and conformation of the correct insert.

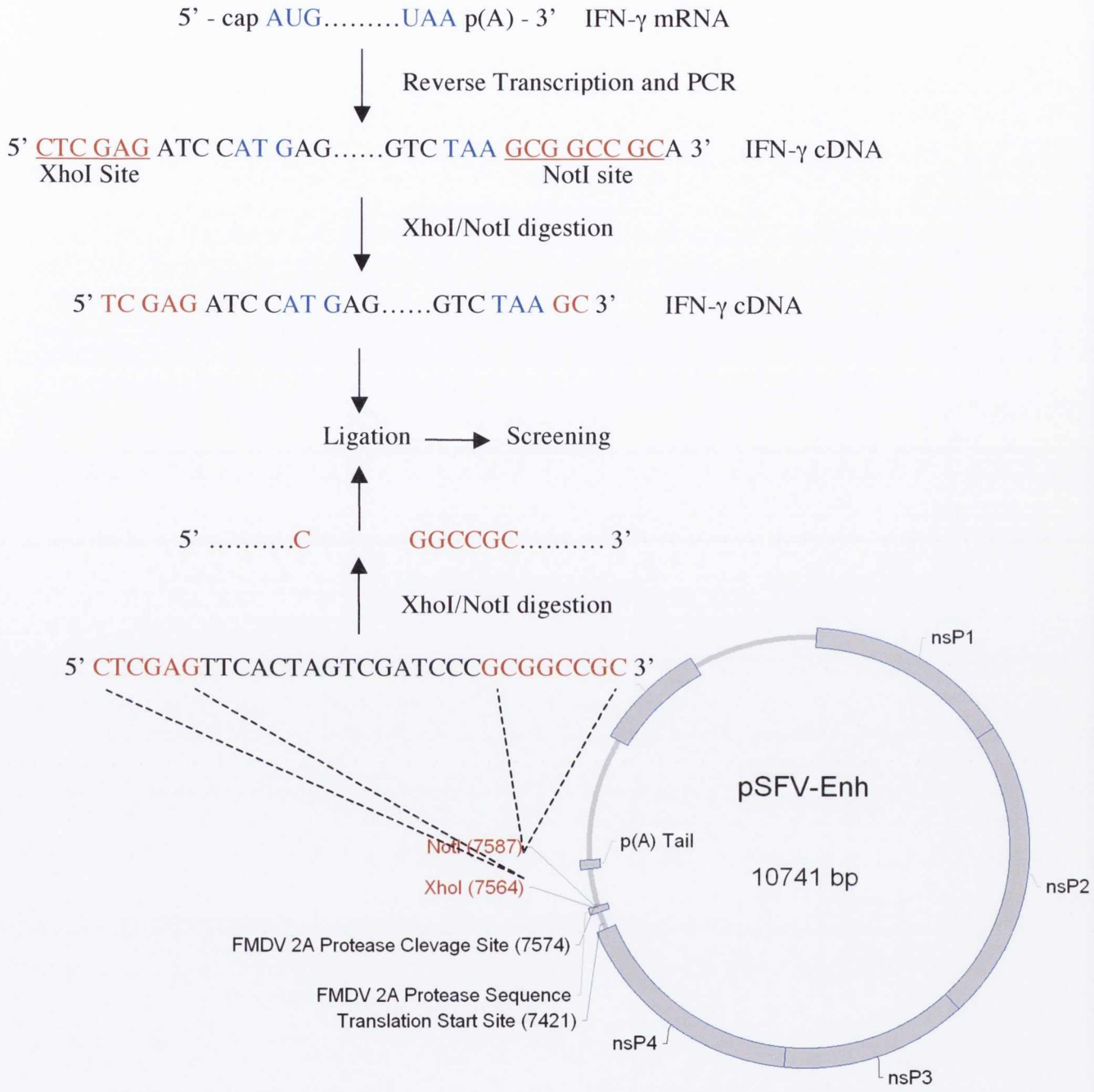

Figure 2.5: Schematic representation of IFN-γ cloning strategy.

IFN-γ mRNA was reverse transcribed with primers incorporating the XhoI and NotI restriction sites into the forward and reverse primers, respectively. Both the SFV-Enh plasmid and PCR product were digested with XhoI and NotI, ligated and screened for the correct insert. Blue bases signify start/stop codons; red bases signify restriction sites used for cloning.

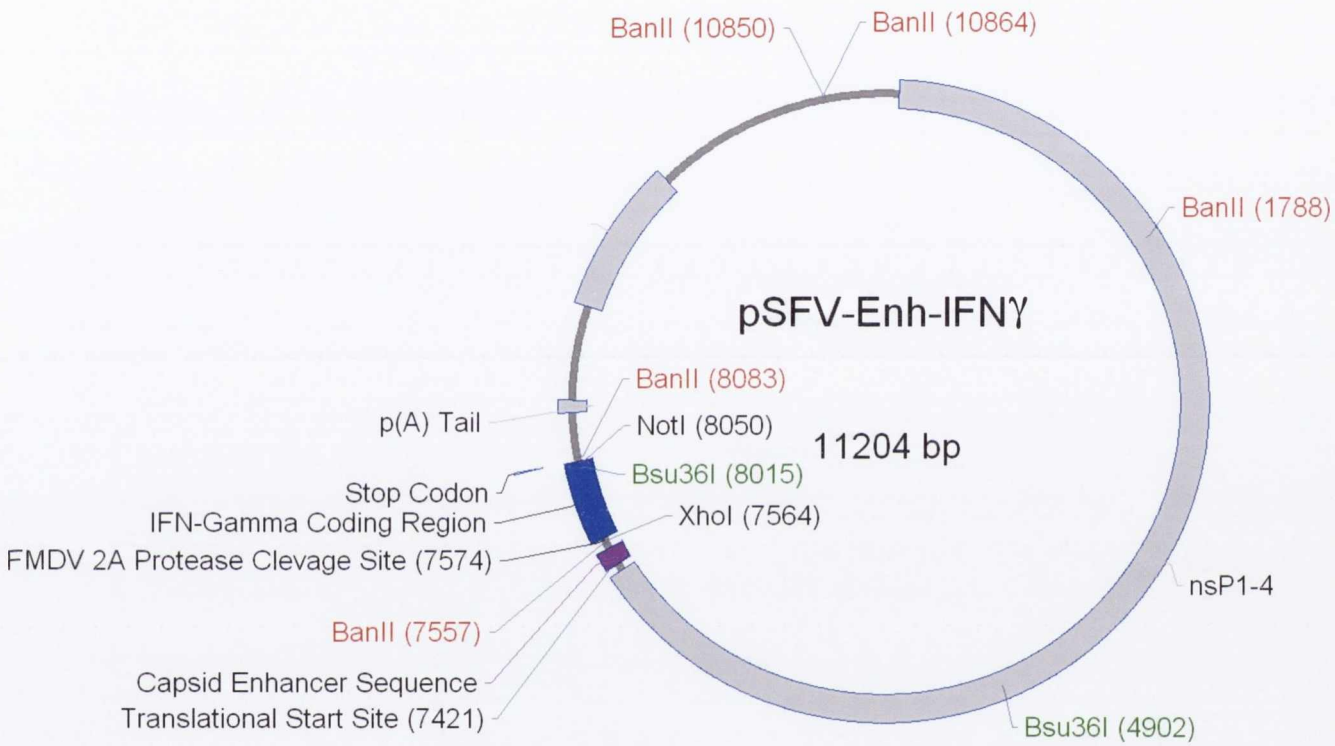

Figure 2.6: Schematic of pSFV-Enh-IFNγ.

Image represents constructed SFV-Enh-IFNγ plasmid. Indicated are the restriction sites used for cloning and conformation of the correct insert.

2.2.2.3.1.4 IL-12 cloning

Figures 2.7 and 2.8 are schematic representations for the construction of pSFV-Enh-IL12(p35) and pSFV-Enh-IL12(p40). For the construction of pSFV-Enh-IL-12(p35), IL-12 p35 mRNA was reverse transcribed with primers incorporating the XmaI and XhoI restriction sites. Both the SFV-Enh plasmid and PCR product were digested with XmaI and XhoI, ligated and screened for the correct insert. pSFV-Enh-IL12(p40) was constructed similarly using the XmaI and SpeI restriction sites. Schematics of the completed pSFV-Enh-IL12(p35) and pSFV-Enh-IL12(p40) are shown (Figure 2.9 and 2.10 respectively) and include the restriction sites used for cloning, insert confirmation and the production of pSFV-Enh-IL12.

Figure 2.11 is the cloning strategy for the production of the double construct pSFV-Enh-IL12. Briefly, the 26S sub-genomic promoter, translational enhancer and IL-12 p40 sequence were excised by BglII/SpeI digestion and ligated into the SpeI linearised SFV-Enh-IL12(p35) plasmid. Figure 2.12 is a schematic representation of the SFV-Enh-IL12 plasmid encoding both the p35 and p40 IL-12 subunits.

2.2.2.3.2 Growth of expression plasmids

2.2.2.3.2.1 Transfection of E. coli DH5α cells

Competent E. coli DH5α cells were thawed on ice and 30-100 ng of plasmid, in no more than 1µl, added to 100µl of cells. Cells remained on ice for 30 minutes followed by incubation at 42°C for 90 seconds. Cells were incubated for 2 minutes on ice, added to 800µl of S.O.C. buffer in a 20ml test tube and placed in an orbital shaker at 37°C and 200rpm for 1 hour. 10-fold serial dilutions of cells were made in L-broth and 200µl of each dilution plated onto LB-agar (100µg/ml ampicillin) plates. Control plates included LB-broth alone and LB-agar plates without ampicillin. Plates were allowed to dry and incubated overnight at 37 °C.

2.2.2.3.2.2 Isolation of transfected colonies

Individual colonies were picked, placed in 50ml of LB-broth plus ampicillin in 250ml baffled conical flasks and grown overnight in an orbital shaker at 200 rpm and 37 °C.

2.2.2.3.2.3 Plasmid extraction and purification

Cultures were centrifuged at 4000rpm (2934.4g) for 10 minutes, plasmids extracted and purified using the Qiagen Midiprep™ kit and resuspended in 1ml of nuclease-free water. DNA concentrations were determined using the NanoDrop™ system.

2.2.2.3.2.4 Confirmation of correct plasmid

EcoRI and NruI restriction endonucleases were used to produce digestion patterns sufficient for the gross confirmation of the SFV-Enh plasmid. Plasmid digests were run on a 1% agarose (0.4 mg/ml EtBr) gel at 90 volts for 30-60 minutes. 0.5µg per lane of 1 kb and 100 bp DNA ladders were run concurrently.

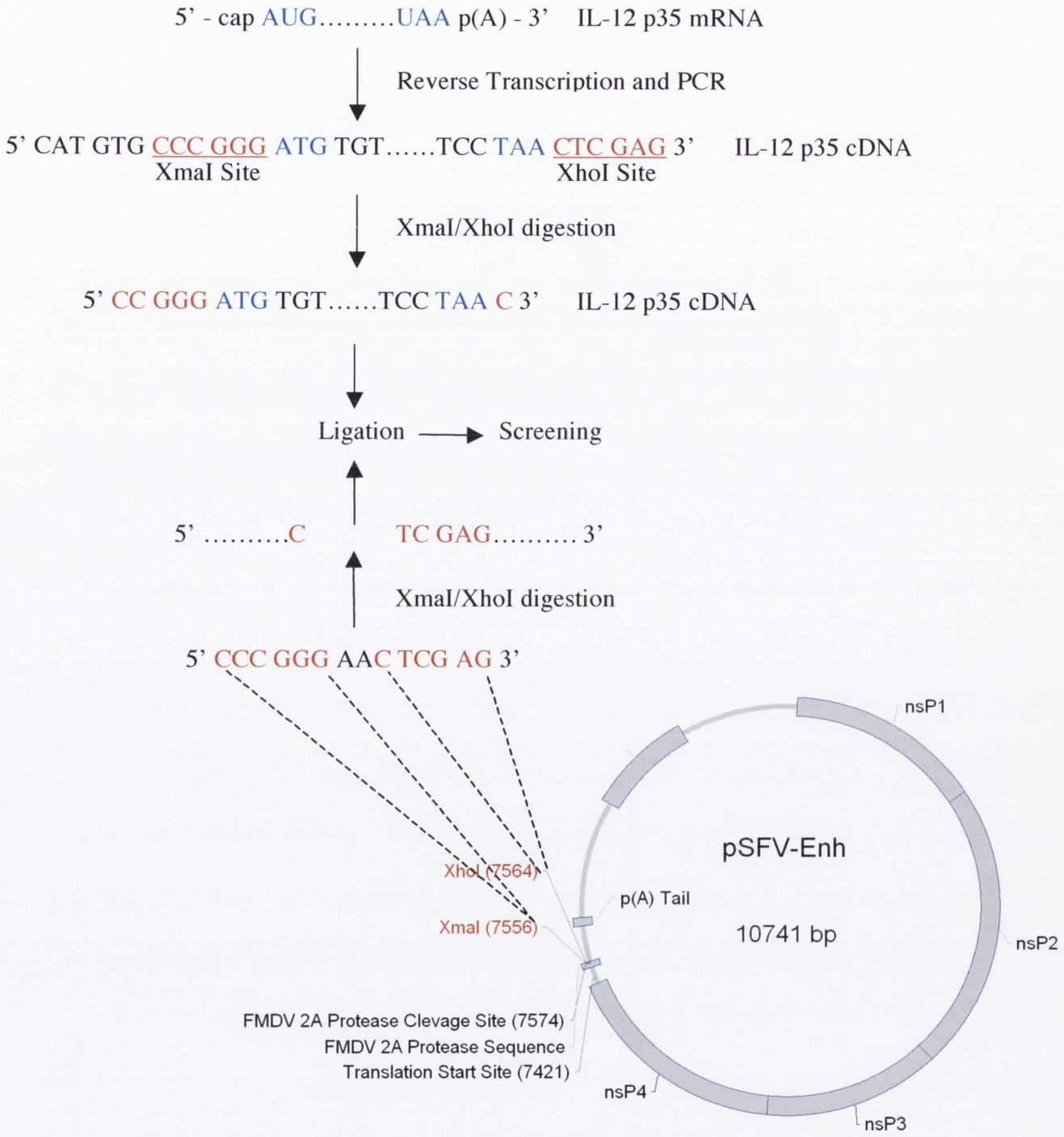

Figure 2.7: Schematic representation of IL-12 p35 cloning strategy.

IL-12 p35 mRNA was reverse transcribed with primers incorporating the XmaI and XhoI restriction sites. Both the SFV-Enh plasmid and PCR product were digested with XmaI and XhoI, ligated and screened for the correct insert. Blue bases represent start and stop codons; red bases represent restriction sites used for cloning.

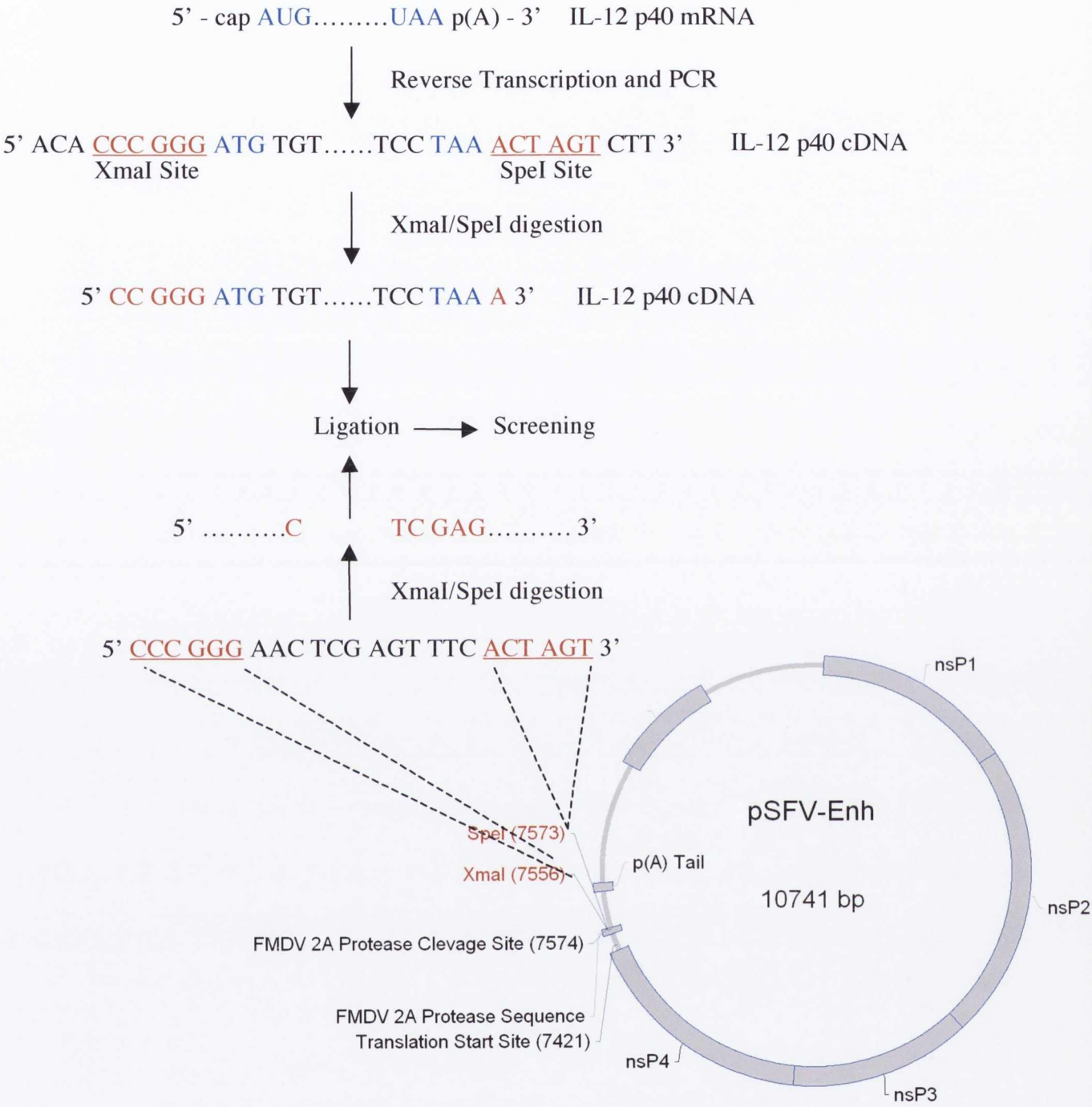

Figure 2.8: Schematic representation of IL-12 p40 cloning strategy.

IL-12 p40 mRNA was reverse transcribed with primers incorporating the XmaI and SpeI restriction sites. Both the SFV-Enh plasmid and PCR product were digested with XmaI and SpeI, ligated and screened for the correct insert. Blue bases represent start and stop codons; red bases represent restriction sites used for cloning.

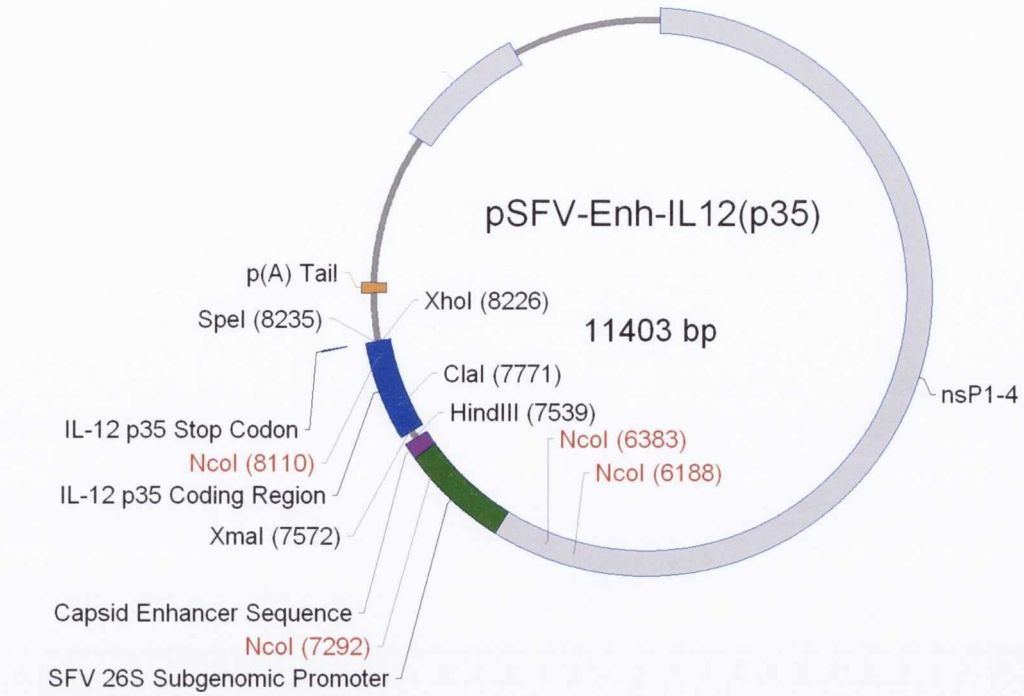

Figure 2.9: Schematic of SFV-Enh-IL12(p35).

Image represents constructed SFV-Enh-IL12(p35) plasmid. Indicated are the restriction sites used for cloning and conformation of the correct insert.

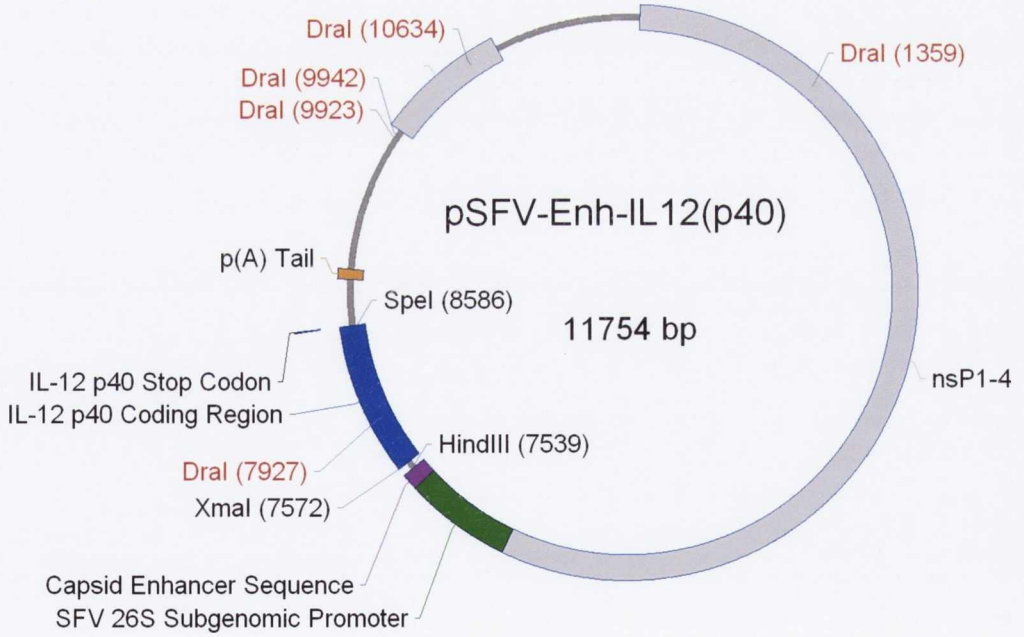

Figure 2.10: Schematic of SFV-Enh-IL12(p40).

Image represents constructed SFV-Enh-IL12(p40) plasmid. Indicated are the restriction sites used for cloning and conformation of the correct insert.

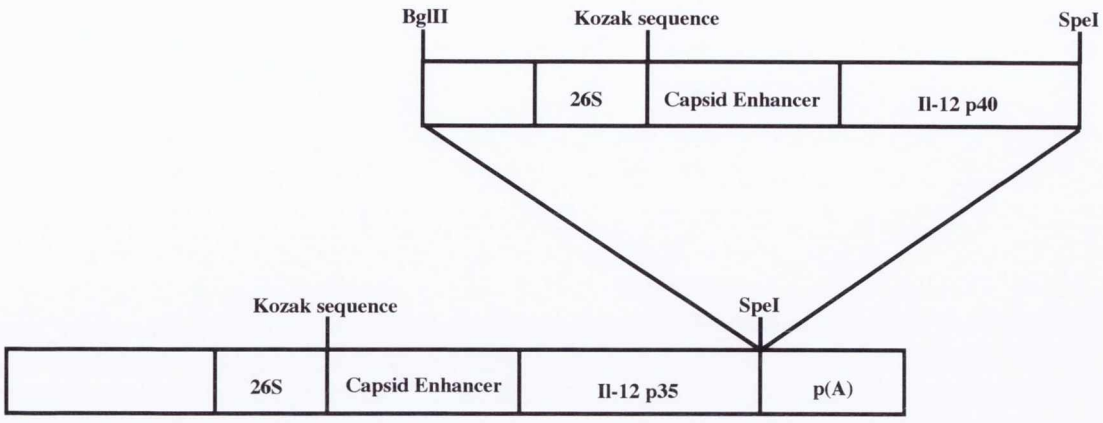

Figure 2.11: Schematic for the construction of pSFV-Enh-IL12.

The 26S sub-genomic promoter, translational enhancer and IL-12 p40 sequence were excised by BglII/SpeI digestion and ligated into the SpeI linearised SFV-Enh-IL12(p35) plasmid.

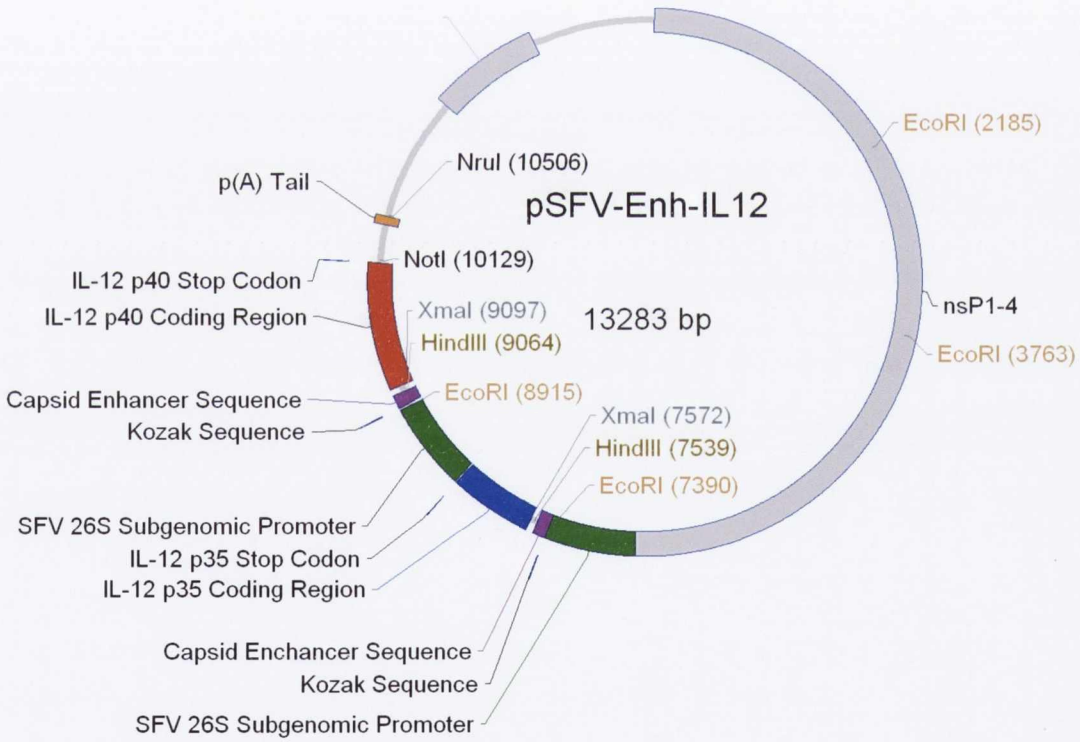

Figure 2.12: Schematic of pSFV-Enh-IL12.

Image represents constructed SFV-Enh-IL12 plasmid. Indicated are the restriction sites used for cloning and conformation of the correct insert.

2.2.2.3.3 Isolation of cytokine encoding DNA

2.2.2.3.3.1 Inoculation of rats with SFV4

Two 250-300g male Fischer 344 rats were injected intraperitoneally (i.p.) with 5 x 10^6 p.f.u. of SFV4 in 500µl of TNE buffer.

2.2.2.3.3.2 Isolation of total splenic RNA

72 hours post-inoculation animals were culled by anesthetic overdose and cervical dislocation. Spleens were removed, divided into three and placed in TRIzol® buffer (100mg tissue/ml). Splenic tissue plus TRIzol® reagent was placed in Lysing Matrix and homogenised in a FastPrep™ FP120 apparatus.

Homogenised spleen tissue RNA was extracted with TRIzol® as per manufacturer's instructions. Briefly, homogenate was brought to room temperature and allowed to stand for 5 minutes before the addition of 200µl of chloroform per 1ml of tissue homogenate. Samples were briefly vortexed and allowed to stand at RT for 2-3 minutes before centrifugation at 12,000g and 4°C for 15 minutes. Following centrifugation the aqueous phase was removed and isopropanol added (0.5ml per 100 mg homogenised tissue). Samples were incubated at RT for 10 minutes and centrifuged as above. Following centrifugation the supernatant was discarded, the pellet washed with 1ml of 100% EtOH per 100mg tissue and centrifuged at 7,500g at 4°C for 5 minutes. The EtOH was discarded and the RNA pellet air-dried for 5 – 10 minutes. RNA was resuspended in 20µl of nuclease-free water.

2.2.2.3.3.3 *In vitro* reverse transcription of RNA

Purified total splenic RNA was reversed transcribed using the Improm II™ reverse transcription system. Reverse transcription was carried out according to manufacturer's instructions with 5µl/reaction of RNA using oligo$(dT)_{15}$ primers (0.5µg/reaction, supplied) or gene specific primers, 1µM (Table 2.2). Reverse transcription reactions were incubated at 25°C for 5 minutes, 42°C for 1 hour and 70°C for 15 minutes in a PCR thermocycler.

Gene	Primer sequence (5' – 3')
IFN-β	ACA GGT CTT CAG TTC TGG
IFN-γ	A GAA TCA GCA CCG ACT CC
IL-12 p35	TTA GGA GGA GCT CAG ATA G
IL-12 p40	TTA GGA TCG GCC CCT GC

Table 2.2: Reverse transcription primers for primary strand cDNA synthesis.

Blue bases signify stop codon.

2.2.2.3.4 Cloning of cytokine encoding DNA into pSFV-Enh

2.2.2.3.4.1 PCR amplification of the IFN-β coding region

Reverse transcribed cDNA was PCR amplified using primers specific for the IFN-β coding sequence and included 5' and 3' restriction sites for directional cloning into pSFV-Enh (Table 2.3).

Gene	Direction	Restriction site	Tm (°C)	Primer sequence (5' – 3')
IFN-β	Forward	XhoI	52°C	AGT GGC TTC TCG AGC ATG GCC AAC AGG TGG
IFN-β	Reverse	SpeI	54°C	TGG CTC ACT AGT ACA GGT CTT CAG TTC TGG

Table 2.3: IFN-β PCR primers.

Blue bases signify start/stop codons; red bases signify restriction sites.

PCR amplification was carried out using the TripleMaster® PCR System, as per manufacture's instructions. PCR amplification was carried out in 1x TripleMaster® high-fidelity buffer with Mg^+ with the addition of 500μM of each dNTP, 200nM of each forward and reverse primer, 0.05u/μl of TripleMaster® polymerase and approximately 1ng of template cDNA. PCR reactions conditions are shown in Table 2.4.

Cycle	Step	Temperature	Duration	Description
	1	94°C	2 min	Initial template denaturation
30x	2	94°C	30 sec	Template denaturation
	3	48°C	30 sec	Primer annealing
	4	72°C	1 min	Primer extension
	5	72°C	2 min	Final primer extension

Table 2.4: PCR reaction conditions for IFN-β gene amplification.

Successful PCR amplification was confirmed by agarose gel electrophoresis, the specific PCR product excised and purified using the QIAquick® PCR purification kit.

2.2.2.3.4.2 PCR amplification of the IFN-γ coding region

PCR amplification of the IFN-γ coding region was carried out using the TripleMaster® PCR System, as per **2.2.2.3.4.1**. Amplification was carried out using primers specific for the IFN-γ coding sequence (Table 2.5). PCR reaction conditions were as per Table 2.4 using an annealing temperature of 50 °C. Successfully amplified PCR product was gel purified.

Gene	Direction	Restriction site	Tm (°C)	Primer sequence (5' – 3')
IFN-γ	Forward	XhoI	54°C	TCG ATA CTC GAG ATC CAT GAG TGC TAC ACG
IFN-γ	Reverse	NotI	56°C	GTC TAA GCG GCC GCA GAA TCA GCA CCG ACT CC

Table 2.5: IFN-γ PCR primers.

Blue bases represent start/stop codons; red bases represent restriction sites.

2.2.2.3.4.3 PCR amplification of IL-12 p35 coding region

The IL-12 p35 coding region was amplified using Taq DNA polymerase. The PCR reaction was carried out in 1x ThermoPol buffer (20 mM Tris-HCl, 10 mM $(NH_4)_2SO_4$, 10

mM KCl, 2 mM $MgSO_4$, 0.1 % Triton X-100) supplemented with 1.5mM $MgCl_2$, 100µM of each dNTP, 200nM each forward and reverse primer (Table 2.6) and 0.025 u/µl Taq DNA polymerase. PCR amplification conditions were as per **2.2.2.3.4.1** using an annealing temperature of 50°C.

Gene	Direction	Restriction site	Tm (°C)	Primer sequence (5' – 3')
IL-12 p35	Forward	XmaI	54°C	CAT GTG CCC GGG ATG TGT CAA TCA CGC TAC C
IL-12 p35	Reverse	XhoI	56°C	GAC GTG CTC GAG TTA GGA GGA GCT CAG ATA G

Table 2.6: IL-12 p35 PCR primers.

Blue bases represent start/stop codons; red bases represent restriction sites.

2.2.2.3.4.4 PCR amplification of IL-12 p40 coding region

The IL-12 p40 subunit coding region was amplified and purified as per **2.2.2.3.4.1**. IL-12 p40 subunit primers (Table 2.7) were used at an annealing temperature of 50°C.

Gene	Direction	Restriction site	Tm (°C)	Primer sequence (5' – 3')
IL-12 p40	Forward	XmaI	54°C	GAT ACA CCC GGG ATG TGT CAT CAG AAG TTA AC
IL-12 p40	Reverse	SpeI	56°C	TAC AAG ACT AGT TTA GGA TCG GCC CCT GC

Table 2.7: IL-12 p40 PCR primers.

Blue bases represent start/stop codons; red bases represent restriction sites.

2.2.2.3.4.5 Ligation of PCR amplified cytokine-encoding DNA into pSFV-Enh

Successfully amplified fragments were digested with restriction enzymes recognising the 5' and 3' recognition sites incorporated during PCR amplification (Tables 2.3, 2.5, 2.6 and 2.7). pSFV-Enh was similarly digested with combinations of restriction enzymes to allow

the directional ligation of PCR inserts. Following digestion of pSFV-Enh and PCR products, DNA was purified using the QIAquick® nucleotide removal kit. Ligation was carried out using the T4 DNA quick ligation kit as per manufacture's instructions. Ligation reactions were carried out in 1x quick ligation buffer (66mM Tris-HCl, 10mM $MgCl_2$, 1mM DTT, 1mM ATP, 7.5% polyethylene glycol) using a 3:1 molar excess of insert and 1µl Quick T4 DNA ligase in a total volume of 20µl. Ligation proceeded for 12-16 hours at room temperature.

2.2.2.3.4.6 Transformation of ligation products

Ligation reactions were used to transform XL-10 Gold® ultracompetent cells, as per manufacture's instructions. Briefly, XL-10 Gold® ultracompetent cells were thawed on ice and 50µl of cells per transformation reaction aliquoted into pre-chilled 14ml BD Falcon® polypropylene round-bottomed tubes. 2µl of beta mercaptoethanol (β-ME) was added to each tube, stored on ice for 10 minutes with gentle swirling every 2 minutes. 2µl of ligation reaction was added; the cells swirled gently and incubated on ice for 30 minutes. Cells were heat shocked at 42 °C for 30 seconds and placed on ice for 2 minutes. 450µl of preheated NZY^+ broth was added to each tube and incubated at 37 °C for 1 hour in an orbital shaker at 200rpm. Cultures were plated on LB-agar plates containing 1mg/ml ampicillin, allowed to dry and incubated at 37 °C overnight.

2.2.2.3.4.7 Screening of colonies

Following transformation of competent cells, individual colonies were used to inoculate 15ml of L-broth (1 mg/ml ampicillin) and grown overnight at 37 °C in an orbital shaker at 200rpm. The resultant cultures were centrifuged for 10 minutes at 4000rpm (2934.4g), the plasmids extracted and purified using the QIAprep® spin Miniprep kit. Multiple colonies from each transformation reaction were grown and minipreped for screening. In order to detect the presence of the correct insert, ligation products underwent restriction digestion and insert positive clones were additionally digested with an enzyme that cut within the expected insert. Digestion reactions were run on a 1% agarose gels with the inclusion of an appropriate DNA ladder.

2.2.2.3.5 Confirmation and correction of pSFV-Enh inserts

2.2.2.3.5.1 DNA sequencing

Lark Cogenics (UK) carried out all DNA sequencing and additional primer synthesis. Sequencing was carried out using the primers used for PCR amplification and primers recognising a sequence within the expected insert. DNA sequencing was analysed using Chromas Pro 2.23 and blasted against the NCBI database (www.ncbi.nlm.nih.gov). Multiple alignment was carried out using the Clustal W (www.ebi.ac.uk/clustalw) and Box shade (www.ch.embnet.org/software/BOX_form.html) online programs.

2.2.2.3.5.2 Site-directed mutagenesis.

Site-directed mutagenesis was carried out using the Quickchange® XL site-directed mutagenesis kit, as per manufacture's instructions. Primer design used the online Quickchange® primer design program (http://www.stratagene.com/qcprimerdesign) (Table 2.8). Where possible, corrected mutations were screened for by restriction digest. Sequencing was used to confirm the correction of all mutations.

Within the IL-12 p35-containing plasmid, both the –5 insertion and 374 substitution corrections were confirmed by XmaI and NcoI digestion, respectively. Following the third correction at 535, the plasmid was sequenced to confirm all 3 corrections. Following sequencing, the corrected IL-12 p35 subunit was excised from pSFV-Enh-IL12(p35) and re-ligated into pSFV-Enh that had not undergone PCR amplification, as described in **2.2.2.3.4.5**.

Base Change	%GC content	Tm (°C)	Direction	Primer sequence (5' – 3')
-5_-4_{insC}	62	79	Forward	GTC CAA CCC TGG GCC CGG GAT GTG TCA AT
-5_-4_{insC}			Reverse	ATT GAC ACA TCC CGG GCC CAG GGT TGG AC
$374_{(T\Rightarrow A)}$	46	78	Forward	CCT TGG TAG CAT CTA TGA GGA CTT GAA GAT GTA CC
$374_{(T\Rightarrow A)}$			Reverse	GGT ACA TCT TCA AGT CCT CAT AGA TGC TAC CAA GG
$535_{(G\Rightarrow A)}$	58	82	Forward	GCA CCA GAA AGC TCC CAT GGG AGA AGC AGA TCC
$535_{(G\Rightarrow A)}$			Reverse	GGA TCT GCT TCT CCC ATG GGA GCT TTC TGG TGC

Table 2.8: Site-directed mutagenesis primers.

Base change designated from adenine of start codon. Blue bases signify the start codon, green bases signify an insertion correction and red bases signify a substitution correction.

2.2.2.3.6 Production of pSFV-Enh-IL12

2.2.2.3.6.1 Digestion of plasmids

pSFV-Enh-IL12(p35) was linearised by SpeI digestion. The sub-genomic promoter, b12a sequence, 2A protease and p40 gene fragment was excised from pSFVEnh-IL12(p40) by BglII/SpeI digestion. Backbone (pSFV-Enh-IL12(p35)) and insert (pSFV-Enh-IL12(p40) fragment) were gel purified following digestion.

2.2.2.3.6.2 Pre-ligation modification of DNA

Backbone and insert were blunt-ended using DNA polymerase I, large (Klenow) fragment. The Klenow reaction was carried out in 1x NEB buffer 2 (10 mM Tris-HCl, 50 mM NaCl, 10 mM $MgCl_2$, 1 mM DTT) supplemented with 33μM dNTPs and 2.5 units of Klenow. Reactions were carried out for 30 minutes at 37 °C followed by heat inactivation for 20

minutes at 75 °C. Blunt-ended backbone was dephosphorylated by supplementing the Klenow reaction mixture with 10x antarctic phosphatase buffer to a 1x concentration and 1u of antarctic phosphatase per μg of backbone. Reactions were incubated at 37 °C for 30 minutes followed by heat inactivation at 65 °C for 5 minutes. Backbone and insert were purified using the QIAquick® nucleotide removal kit and quantified by agarose gel electrophoresis.

2.2.2.3.6.3 Ligation of pSFV-Enh-IL12(p40) gene fragment into pSFV-Enh-IL12(p35)

Backbone and insert ligation was carried out as per **2.2.2.3.4.5** and used to transform XL-10 Gold® ultracompetent cells, as per **2.2.2.4.6**. Individual colonies were isolated and grown overnight in LB-broth containing 1 mg/ml ampicillin.

2.2.2.3.6.4 Screening of colonies for correct insert

Plasmids were extracted and purified from overnight cultures as per **2.2.2.3.4.7**. Restriction enzyme analysis was used to determine the correct insert and orientation. Briefly, plasmids were digested with HindIII and examined for the presence of insert and its correct orientation. Insert-positive plasmids were further digested with EcoRI and XmaI/XhoI before sequencing.

2.2.2.4 Analysis of transgene expression

2.2.2.4.1 *In vitro* transcription of expression plasmids

1.5μg of each expression plasmid was linearised with NruI, cleaned using the QIAquick® nucleotide removal kit and used as template for the *in vitro* transcription reaction. *In vitro* transcription was carried out in 1x RNA polymerase reaction buffer (40 mM Tris-HCl, 6 mM $MgCl_2$, 10 mM DTT, 2 mM spermidine) supplemented with 5mM DTT, 1mM CAP, 1mM rATPs, 1mM rUTP, 1mM rCTP, 0.5mM rGTP, 1.2 units/μl RNasin and 1.59 units/μl SP6 polymerase with 1.5μg DNA template per 50μl reaction. Reactions proceeded for 90 minutes at 37 °C and 1μl of the transcription reaction run on a 0.6% agarose gel to confirm a sufficient quantity of RNA for electroporation.

2.2.2.4.2 Electroporation of S-BHK cells

For each electroporation, one 75cm^2 of S-BHK cells was grown to 90-95% confluence. The medium was removed, cells washed twice with D-PBS, trypsinised, pipetted 10 times and 9ml of S-BHK medium and 40ml D-PBS added. Cells were centrifuged at 1,500rpm (412.65g) for 5 minutes at RT. Following centrifugation supernatant was discarded and cells resuspended in 50ml of D-PBS followed by centrifugation as before. Supernatant was discarded and cells resuspended in 750µl of D-PBS followed by the addition of freshly thawed mRNA. The suspension was transferred to a 4mm electroporation cuvette and electroporated. Electroporation used two 850-volt pulses of 4 milliseconds each with an inter-pulse interval of 5 seconds. Electroporated cells were pipetted into 9ml of pre-warmed S-BHK medium and the cuvette washed 3 times with 1ml of S-BHK medium. Electroporated cells were divided into 6 wells of a 6-well tissue culture dish with 22x22mm sterile coverslips placed on the floor of each well. pSFV-Enh RNA, lacking any transgene, and PBS alone were used as controls.

2.2.2.4.3 Immunofluorescent analysis of IFN-β expression by SFV-Enh-IFNβ mRNA

18 hours post-electroporation, cell supernatant was removed, cells washed twice in D-PBS (with Ca^{2+}/Mg^{2+}) and fixed/permeabilised in 100% cold acetone for 5 minutes at –20 °C. Cells were washed twice further in D-PBS and blocked with 5% normal mouse serum (NMS) in D-PBS for 1 hour at RT. Following blocking, coverslips were incubated with a 1/200 dilution of rabbit anti-rat IFN-β antibody in blocking buffer for 1 hour in a humidified chamber at RT. Cells were washed twice for 5 minutes in PBS-T (0.05% Tween® 20 in PBS), coverslips incubated in a 1/100 dilution of biotinylated mouse anti-rabbit IgG antibody in blocking buffer for 1 hour as before. Following two washes as before, cells were incubated in a 1/100 dilution of streptavidin/FITC in PBS for 40 minutes. Cells were washed twice for 15 minutes each in high salt/hepes buffer (0.5M NaCl, 10mM hepes) followed by two 7.5 minute washes in PBS-T, two 5 minute washes in PBS and dipped in distilled water before being air-dried and mounted on glass slides with mountant containing DAPI. Cells were examined by fluorescent microscopy.

2.2.2.4.4 ELISA analysis of IFN-γ expression by SFV-Enh-IFNγ mRNA

Medium was harvested from electroporated cells at 0, 16, 24, 48 and 72 hours post-electroporation, snap frozen in liquid nitrogen and stored at –80 °C until assayed. A commercial rat IFN-γ ELISA was used to measure IFN-γ production in supernatant samples. 96-well ELISA plates were coated with 100µl of a 1/250 dilution of capture antibody in coating buffer overnight at 4 °C. Plates were aspirated and washed five times with 300µl/well of wash buffer and blocked with 300µl/well of blocking buffer for 1 hour at RT. Plates were washed as before and samples and IFN-γ standard diluted in blocking buffer and incubated in triplicate with 100µl/well for 2 hours at RT. Plates were washed as before and 100µl/well of a 1/250 dilution of detection antibody added to each well and incubated for 1 hour at RT. Plates were washed and 100µl of a 1/250 dilution of streptavidin/horseradish peroxidase conjugate added to each well and incubated for 30 minutes at RT. Plates were washed seven times with 300µl/well of wash buffer, 100µl TMB substrate added to each well and incubated in the dark for 30 minutes at RT. The HRP reaction was stopped by the addition of 50µl of 2N H_2SO_4 and read at 450nm within 30 minutes. Samples were compared to the standard curve to extrapolate IFN-γ concentrations per ml of sample and figures adjusted per 1 x 10^6 cells.

2.2.2.4.5 ELISA analysis of IL-12 p70 expression by SFV-Enh-IL12 mRNA

Medium was harvested from electroporated cells at 0, 24, 48 and 72 hours post-electroporation, snap frozen in liquid nitrogen and stored at –80 °C until assayed. A commercial rat IL-12 p70 ELISA was used to analyse IL-12 production in supernatant samples. 96-well ELISA plates were coated with 100µl of a 1/500 dilution of capture antibody in coating buffer overnight at 4 °C. Plates were aspirated, washed once with 300µl/well of wash buffer and blocked with 300µl/well of blocking buffer for 2 hours at RT. Plates were washed as before and samples and IL-12 standard diluted in blocking buffer and incubated in triplicate with 100µl/well immediately followed by the addition of 50µl/well of a 1/1250 dilution of biotinylated detection antibody. Plates were incubated in an orbital shaker at 700rpm for 2 hours at RT. Plates were washed four times as before and 100µl/well of a 1/2500 dilution of streptavidin/horseradish peroxidase conjugate added to each well and incubated at 700rpm for 30 minutes at RT. Plates were washed four times with 300µl/well of wash buffer and 100µl TMB substrate added to each well and incubated

in the dark at 700rpm for 30 minutes at RT. The HRP reaction was stopped by the addition of 100µl of 1.8N H_2SO_4 and read at 450nm within 30 minutes. Samples were compared to the standard curve to extrapolate IL-12 concentrations per ml of sample and figures adjusted per 1 x 10^6 cells.

2.3 Results

2.3.1 Virus production

Virus was produced and titers of 10^9 p.f.u./ml were routinely obtained.

2.3.2 Cloning of interferon beta, interferon gamma and IL-12 into the SFV enhanced vector

2.3.2.1 Conformation of pSFV-Enh plasmid

pSFV-Enh was obtained in house and confirmed by digestion with EcoRI and NruI. Restriction digest analysis predicted the presence of 3 bands at 5552, 3627, 1578 bps as a result of EcoRI digestion and linearisation by NruI digestion. Figure 2.13 shows the resultant gel accompanied by uncut plasmid.

2.3.2.2 PCR amplification of cytokine encoding DNA

PCR amplification of the IFN-β, IFN-γ, IL-12 p35 and IL-12 p40 coding regions was carried out and reaction products analysed by agarose gel electrophoresis for IFN-β (Figure 2.14-A), IFN-γ (Figure 2.14-B), IL-12 p35 (Figure 2.14-C) and IL-12 p40 (Figure 2.14-D). PCR fragments of 590pb, 505bp, 672bp and 1032bp were expected following IFN-β, IFN-γ, IL-12 p35 and IL-12 p40 gene amplification.

2.3.2.3 Pre-ligation preparation of pSFV-Enh and PCR amplified cytokine-encoding DNA

Prior to ligation of PCR-amplified cytokine genes into pSFV-Enh, both pSFV-Enh and PCR products were digested with enzymes corresponding to those included in the PCR primers. pSFV-Enh and PCR products were digested with XhoI/SpeI for IFN-β cloning, XhoI/NotI for IFN-γ cloning, XmaI/XhoI for IL-12 p35 cloning and XmaI/SpeI for IL-12 p40 cloning. As a control, single digestions with each enzyme were carried out and are included in each gel (Figure 2.15).

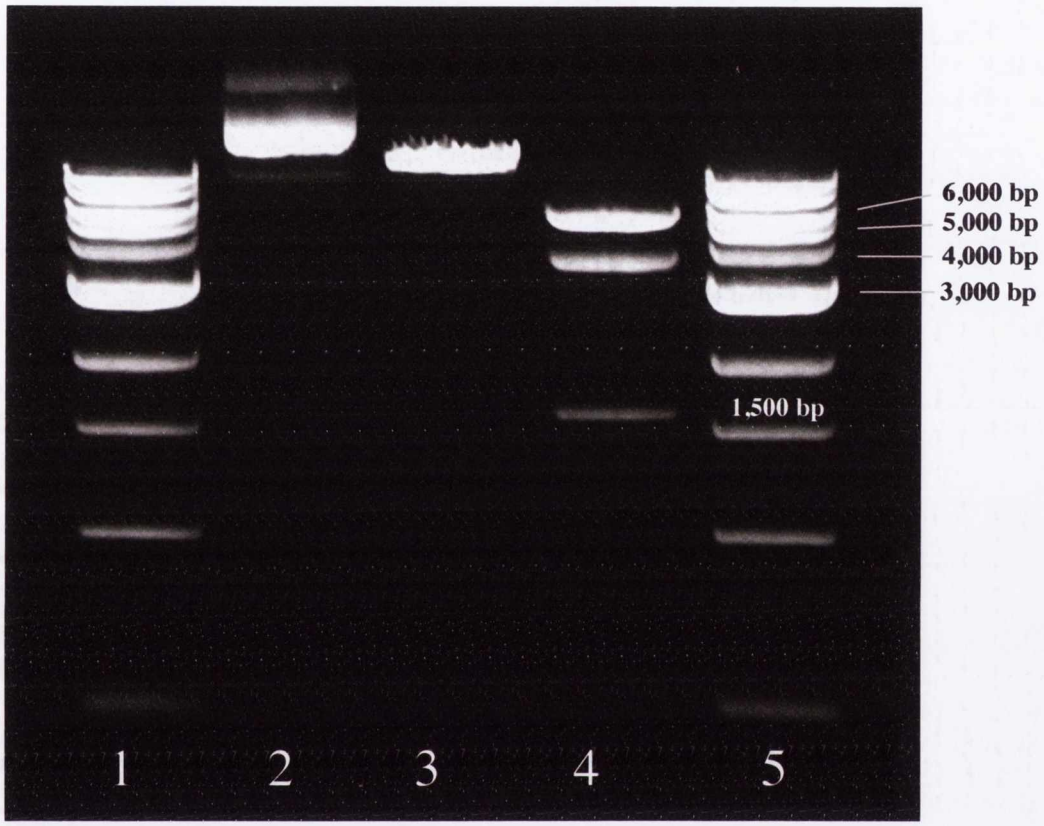

Figure 2.13: Confirmation of pSFV-Enh by restriction digest.

Lanes 1 and *5* are 1 kb DNA ladder, *Lane 2* is uncut pSFV-Enh, *Lane 3* and *4* are NruI and EcoRI digested pSFV-Enh. The presence of a single linearised band following NruI digest and the presence of 3 bands at 5552, 3627 and 1578 bps following EcoRI digestion confirmed the plasmid was pSFV-Enh.

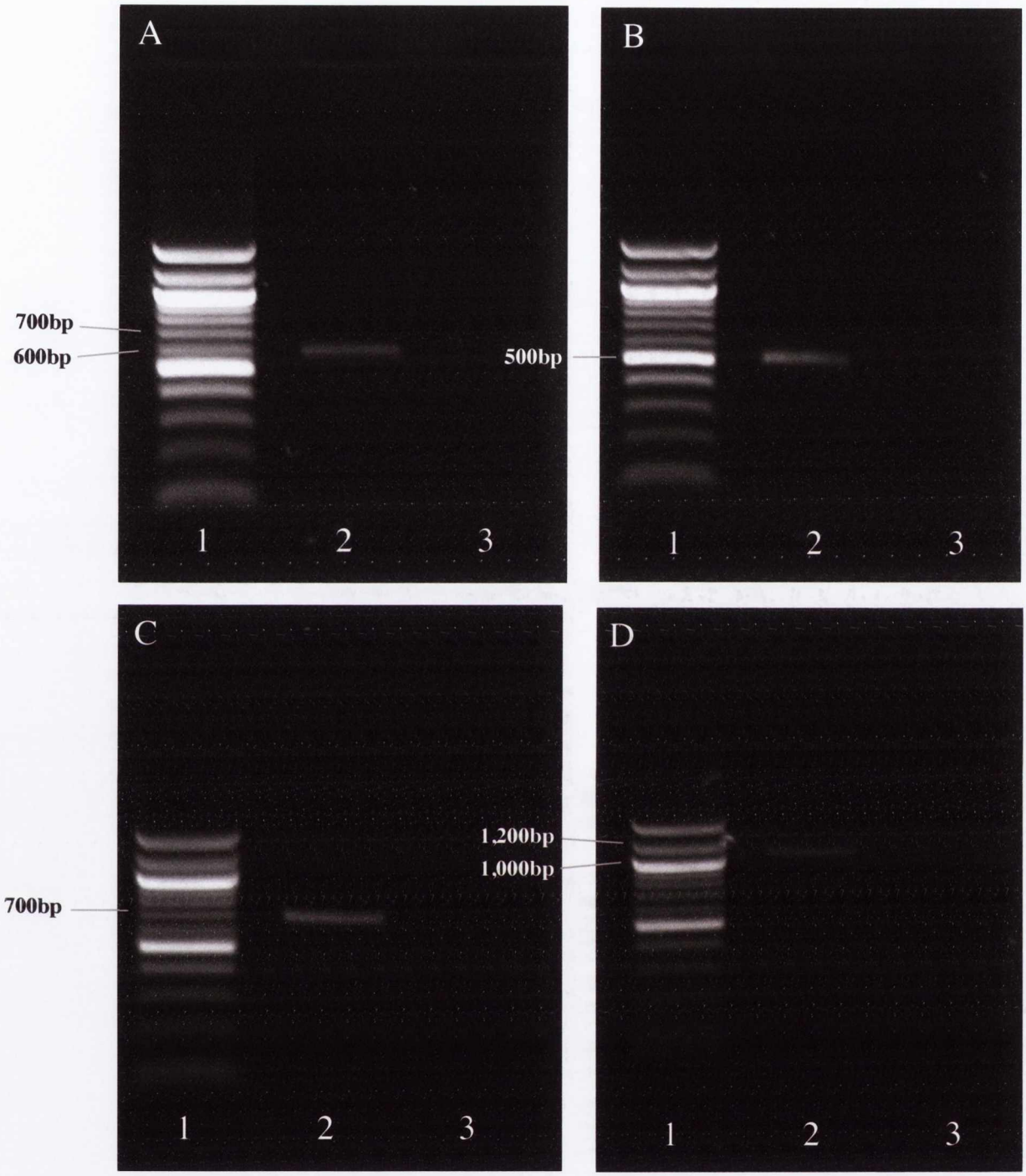

Figure 2.14: PCR amplification of cytokine encoding cDNA.

PCR amplification of the IFN-β, IFN-γ, IL-12 p35 and IL-12 p40 coding regions was carried out following first stand DNA synthesis. PCR reaction products were analysed by agarose gel electrophoresis. *Lanes 1* are 100bp DNA ladder, *Lanes 2* are PCR reaction products for IFN-β *(A)*, IFN-γ *(B)*, IL-12 p35 *(C)* and IL-12 p40 *(D)*. *Lanes 3* are negative control lacking DNA template. PCR fragments of 590pb, 505bp, 672bp and 1032bp were expected following IFN-β, IFN-γ, IL-12 p35 and IL-12 p40 gene amplification.

Figure 2.15: Digestion of pSFV-Enh prior to ligation of PCR products (overleaf).

A – pSFV-Enh digested with XhoI/SpeI for IFN-β cloning. *Lanes 1* and *6* represent 1kb DNA ladder. *Lanes 2, 3 and 4* represent uncut, XhoI digested and SpeI digested pSFV-Enh respectively. *Lane* 5 is pSFV-Enh digested simultaneously with XhoI and SpeI.

B – pSFV-Enh digested with XhoI/NotI for IFN-γ cloning. *Lanes 1* and *6* represent 1kb DNA ladder. *Lanes 2, 3 and 4* represent uncut, XhoI digested and NotI digested pSFV-Enh respectively. *Lane* 5 is pSFV-Enh digested simultaneously with XhoI and NotI.

C – pSFV-Enh digested with XmaI/XhoI for IL-12 p35 cloning. *Lanes 1* and *6* represent 1kb DNA ladder. *Lanes 2, 3 and 4* represent uncut, XhoI digested and XmaI digested pSFV-Enh respectively. *Lane* 5 is pSFV-Enh digested simultaneously with XhoI and XmaI.

D – pSFV-Enh digested with XmaI/SpeI for IL-12 p35 cloning. *Lanes 1* and *6* represent 1kb DNA ladder. *Lanes 2, 3 and 4* represent uncut, XmaI digested and SpeI digested pSFV-Enh respectively. *Lane* 5 is pSFV-Enh digested simultaneously with XhoI and SpeI.

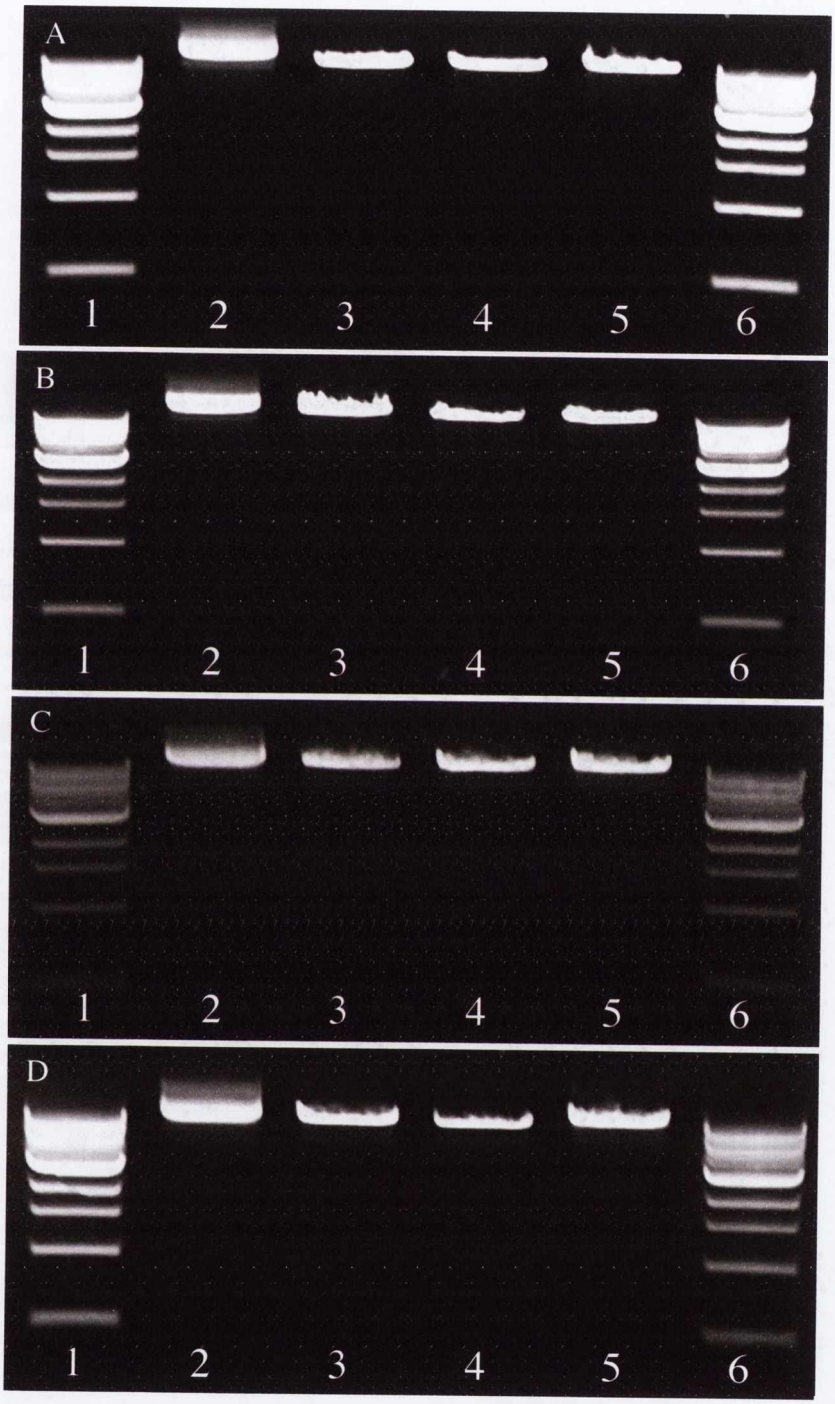
A
1
2
3
4
5
6
B
1
2
3
4
5
6
C
1
2
3
4
5
6
D
1
2
3
4
5
6

2.3.2.4 Screening of ligation reaction products

Following ligation of the insert into pSFV-Enh, colonies were screened for the presence of the insert by restriction digest. 6 colonies were screened from each ligation reaction.

IFN-β insert-positive clones were confirmed by XhoI/SpeI digestion (Figure 2.16). The presence of a band of 570 bps indicated the successful ligation of the IFN-β coding sequence into pSFV-Enh. As an additional confirmation, the 2 insert-positive clones were digested with PvuII, a recognition sequence of which is within the IFN-β coding sequence. Restriction digest analysis predicted the presence of 5 bands at 6396, 3385, 595, 568 and 374 bps following PvuII digestion of pSFV-Enh-IFNβ while the absence of the IFN-β coding sequence produced 4 bands. Figure 2.17 is a representative gel of the PvuII digestion; in both cases the insert was confirmed to contain the PvuII recognition site and both clones underwent DNA sequencing.

IFN-γ insert-positive clones were confirmed by XhoI/NotI digestion (Figure 2.18). The presence of a band of 478 bps indicated the successful ligation of the IFN-γ coding sequence into pSFV-Enh. As an additional conformation, the 2 insert positive clones were digested with Bsu36I, a recognition sequence of which is within the IFN-γ coding sequence. Restriction digest analysis predicted the presence of 2 bands at 8107 and 3113 bps following Bsu36I digestion of pSFV-Enh-IFNγ while the absence of the IFN-γ coding sequence produced a single band. Figure 2.19 is a representative gel of the Bsu36I digestion; in both cases the insert was confirmed to contain the Bsu36I recognition site and both clones underwent DNA sequencing.

IL-12 p35 insert-positive clones were confirmed by HindIII/SpeI digestion (Figure 2.20). The presence of a band of 687 bps indicated the successful ligation of the IL-12 p35 coding sequence into pSFV-Enh. As an additional conformation, the 3 insert-positive clones were digested with ClaI/XhoI, a ClaI recognition sequence is found within the IL-12 p35 coding sequence. Restriction digest analysis predicted the presence of 2 bands at 10948 and 455 bps following ClaI/XhoI digestion of pSFV-Enh-IL12(p35) while the absence of the IL-12(p35) coding region produced a single band. Figure 2.21 is a representative gel of the ClaI/XhoI digestion; in all cases the insert was confirmed to contain the ClaI recognition site and all 3 clones underwent DNA sequencing.

IL-12 p40 insert-positive clones were confirmed by HindIII/SpeI digestion (Figure 2.22). The presence of a band of 1047 bps indicated the successful ligation of the IL-12 p40 coding sequence into pSFV-Enh. As an additional conformation, the 3 insert-positive

clones were digested with DraI, a recognition sequence of which is within the IL-12 p40 coding sequence. Restriction digest analysis predicted the presence of 5 bands at 6568, 2479, 1996, 692 and 19 bps following DraI digestion of pSFV-Enh-IL12(p40) while the absence of the IL-12(p40) coding region produced 4 bands at 6403, 3385, 595 and 374 bps. Figure 2.23 is a representative gel of the DraI digestion; in all cases the insert was confirmed to contain the DraI recognition site and all 3 clones underwent DNA sequencing.

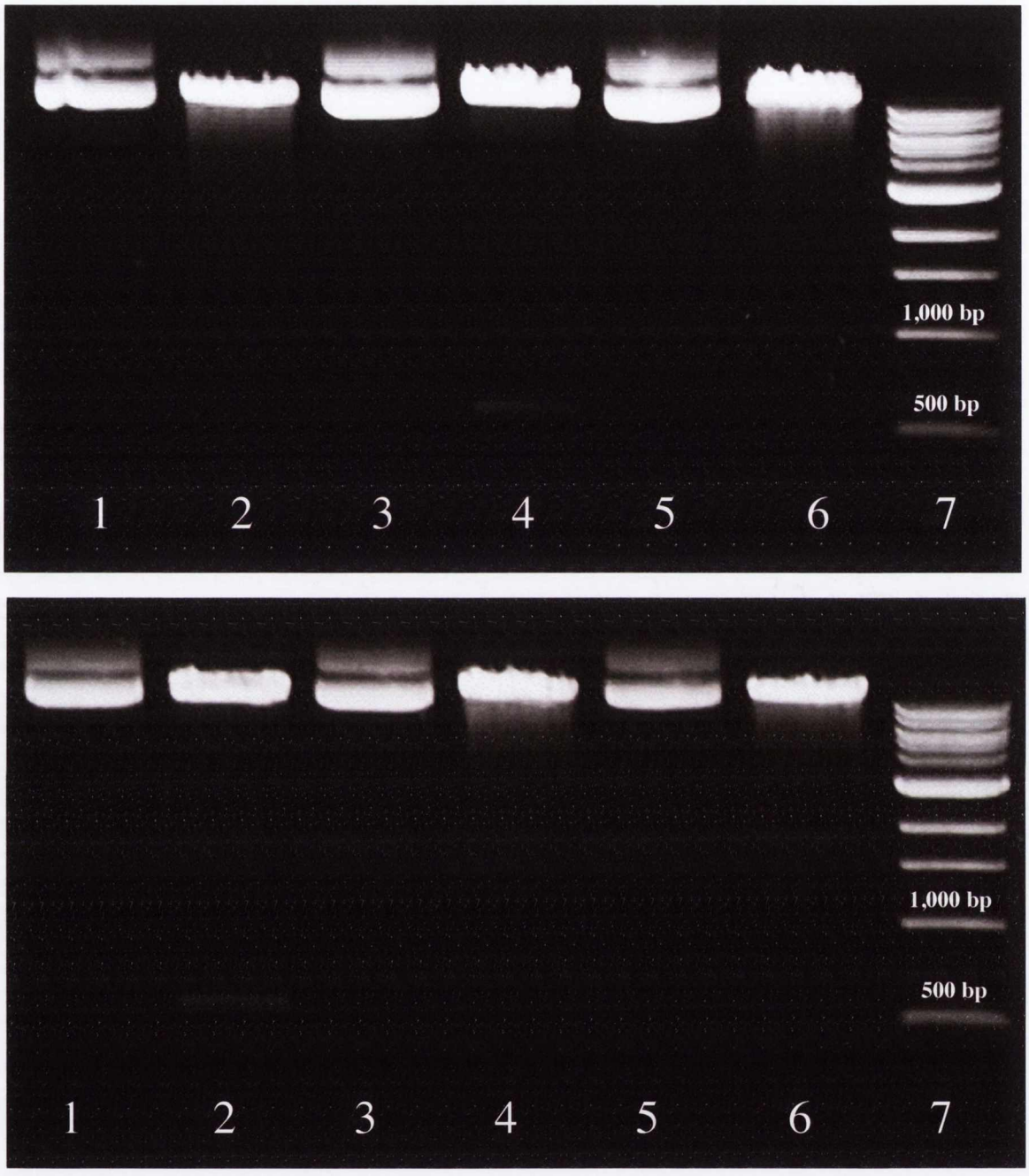

Figure 2.16: Screening of IFN-β ligation reactions by XhoI/SpeI restriction digests.

6 colonies were selected and digested. *Lanes 1, 3* and *5* are uncut plasmid, *Lanes 2, 4, 6* are XhoI/SpeI digested plasmids and *Lanes 7* are 1kb DNA marker. The presence of a 570 bp band indicated the successful ligation of the IFN-β coding sequence into pSFV-Enh.

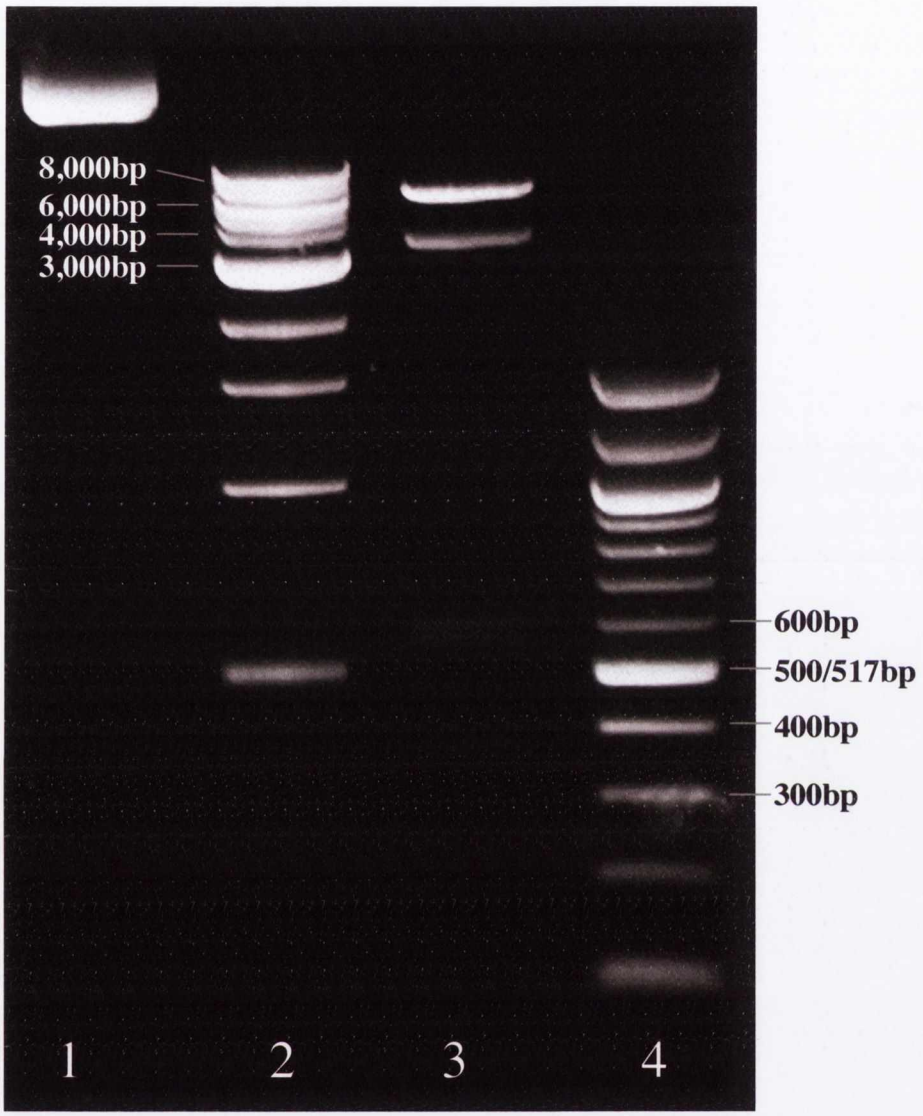

Figure 2.17: Screening of IFN-β insert-positive ligation reactions by restriction digest.

Figure is representative of both insert-positive plasmids. *Lane 2* and *4* are 1kb DNA and 100bp DNA ladder respectively, *Lanes 1* and *3* are uncut and PvuII digested insert-positive plasmid respectively. The presence of 5 bands at 6396, 3385, 595, 568 and 374 bps indicated the successful ligation of the IFN-β coding sequence into pSFV-Enh.

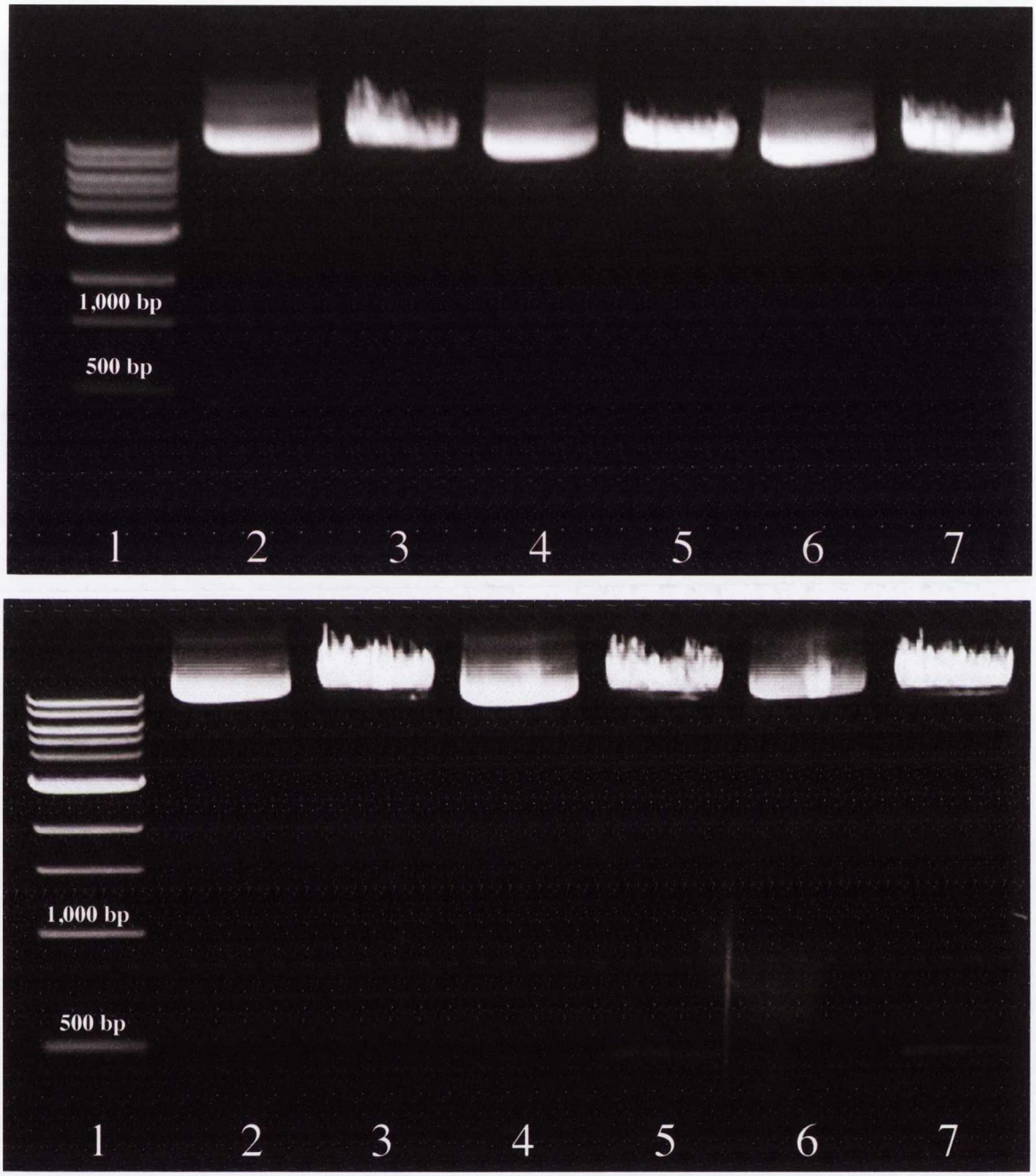

Figure 2.18: Screening of IFN-γ ligation reactions by XhoI/NotI restriction digests.

6 colonies were selected and digested. *Lanes 2, 4* and *6* are uncut plasmid, *Lanes 3, 5, 7* are XhoI/NotI digested plasmids and *Lanes 1* are 1kb DNA marker. The presence of a 478 bp band indicated the successful ligation of the IFN-γ coding sequence into pSFV-Enh.

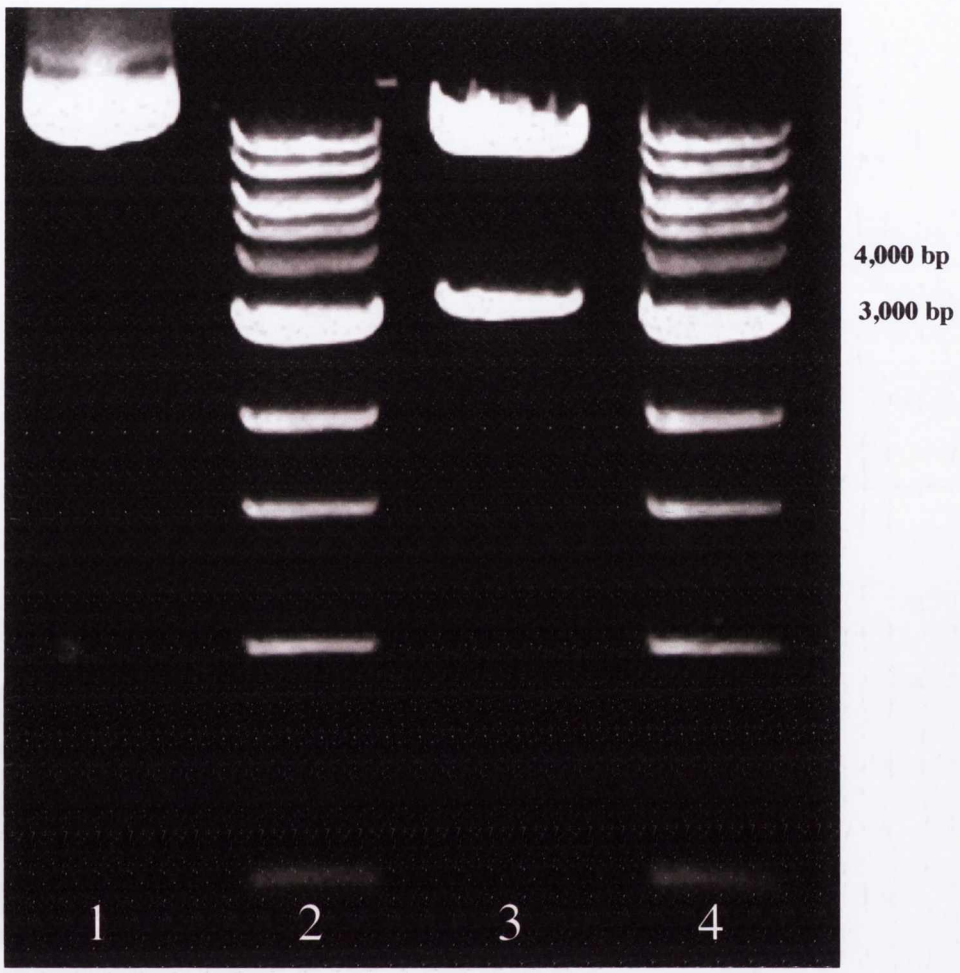

Figure 2.19: Screening of IFN-γ insert-positive ligation reactions by restriction digest.

Figure is representative of both insert-positive plasmids. *Lanes 2* and *4* are 1kb DNA ladder, *Lanes 1* and *3* are uncut and Bsu36I digested insert-positive plasmid respectively. The presence of 2 bands at 8107 and 3113 bps following Bsu36I digestion confirmed the presence of the IFN-γ coding region.

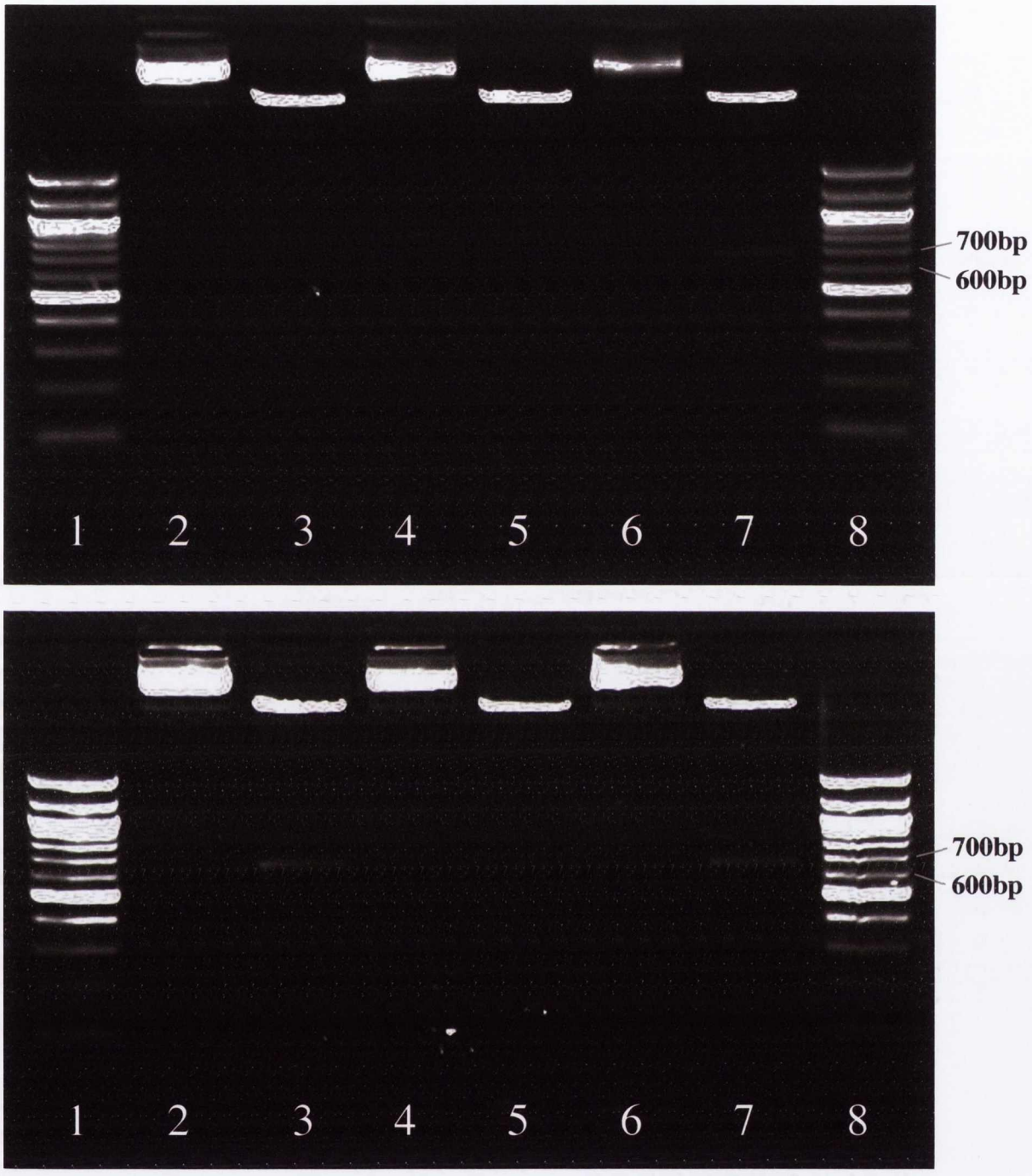

Figure 2.20: Screening of IL-12 p35 ligation reactions by HindIII/SpeI restriction digests.

6 colonies were selected and digested. *Lanes 2, 4* and *6* are uncut plasmid, *Lanes 3, 5, 7* are HindIII/SpeI digested plasmids and *Lanes 1* are 100bp DNA marker. The presence of a 687 bp band indicated the successful ligation of the IL-12 p35 coding sequence into pSFV-Enh.

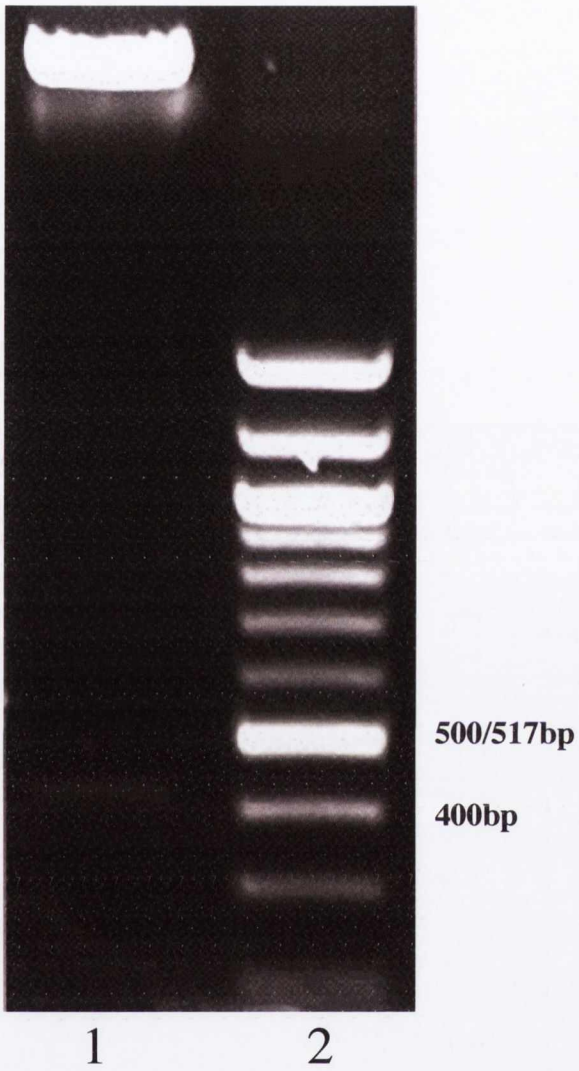

Figure 2.21: Screening of IL-12 p35 subunit insert-positive ligation reactions by restriction digest.

Figure is representative of all 3 insert-positive plasmids. *Lane 1* is ClaI/XhoI digested insert-positive plasmid and *Lane 2* is 100bp DNA ladder, respectively. The presence of a band at 455 bps indicated the successful ligation of the IL-12 p35 subunit coding sequence into pSFV-Enh.

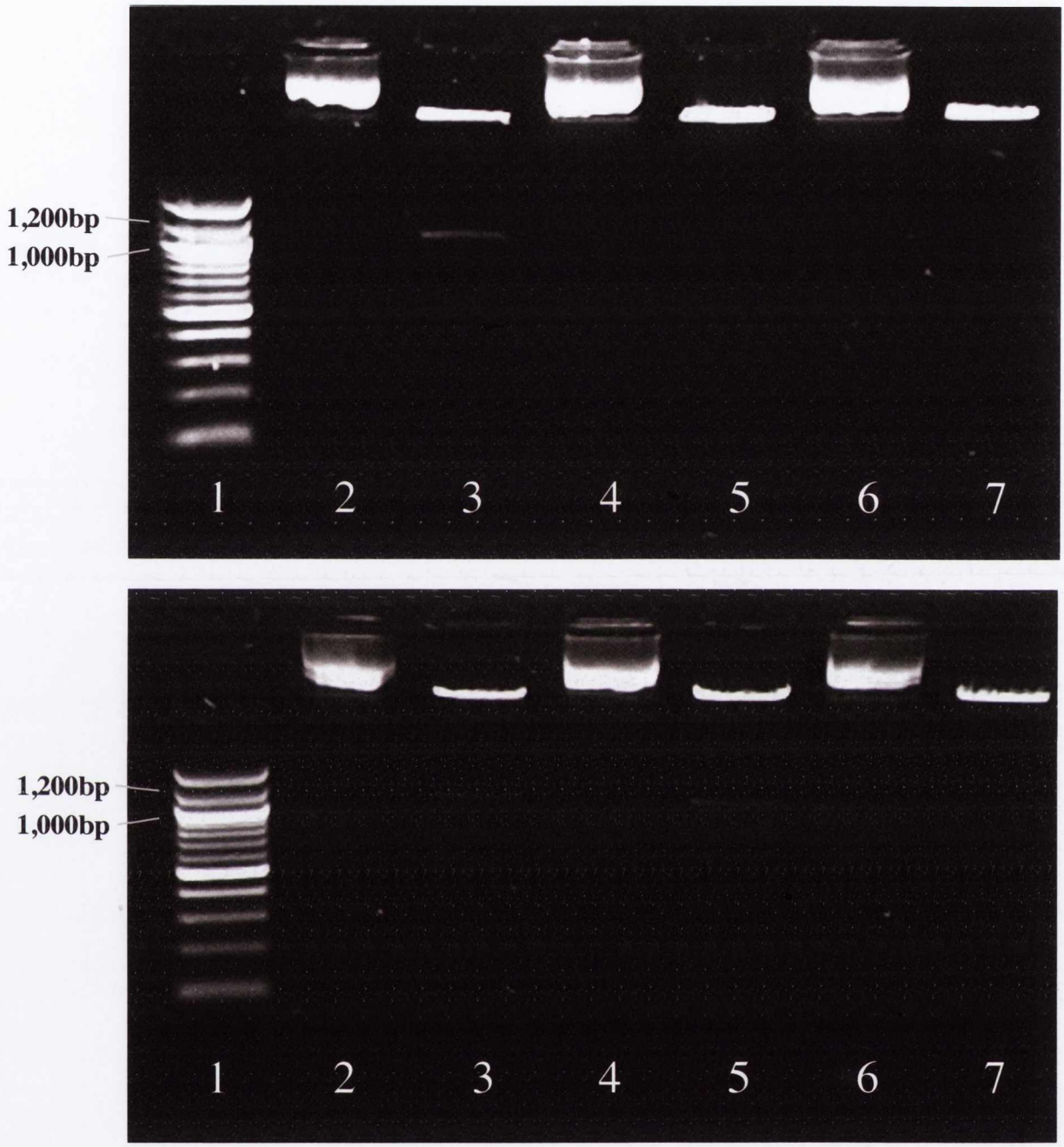

Figure 2.22: Screening of IL-12 p40 ligation reactions by HindIII/SpeI restriction digests.

6 colonies were selected and digested. *Lanes 2, 4* and *6* are uncut plasmid, *Lanes 3, 5, 7* are XhoI/NotI digested plasmids and *Lanes 1* are 100bp DNA marker. The presence of a 1047bp band indicated the successful ligation of the IL-12 p40 coding sequence into pSFV-Enh.

Figure 2.23: Screening of IL-12 p40 subunit insert-positive ligation reactions by restriction digest.

Figure is representative of all 3 insert-positive plasmids. *Lane 1* is 1kb DNA ladder and *Lane 2* is DraI digested insert-positive plasmid respectively. The presence of 5 bands at 6568, 2479, 1996, 692 and 19 bps indicated the successful ligation of the IL-12 p40 subunit coding sequence into pSFV-Enh. The 19bp fragment is not visible on the agarose gel.

2.3.2.5 Confirmation and correction of pSFV-Enh inserts

2.3.2.5.1 DNA sequencing

2.3.2.5.1.1 pSFV-Enh-IFNβ sequencing

Three IFN-β insert-positive SFV-Enh clones were analysed by DNA sequencing. Sequencing results were used to produce contiguous sequences for each plasmid using Chromas Pro, blasted against the NCBI database, aligned using Clustal W and the alignment file used to produce the Box shade representation. The NCBI *Rattus* norvegicus IFN-β mRNA sequence (NM_019127) was included in the multiple alignment. Multiple alignment results include the 5' and 3' sequences containing the restriction sites used for cloning. Additionally, a Box shade representation of the translated plasmid and NM_019127 sequences was produced.

Of the three sequenced plasmids only one contained non-synonymous mutations. Clone 3 contained a single mutation at base 159 (Figure 2.24) which did not produce any changes in the amino acid sequence (Figure 2.25). This clone was designated pSFV-Enh-IFNβ and used for all further work.

2.3.2.5.1.2 pSFV-Enh-IFNγ sequencing

Two IFN-γ insert-positive SFV-Enh clones were analysed by DNA sequencing. Sequencing results were used to produce contiguous sequences for each plasmid using Chromas Pro, blasted against the NCBI database, aligned using Clustal W and the alignment file used to produce the Box shade representation. The NCBI *Rattus* norvegicus IFN-γ mRNA sequence (NM_138880) was included in the multiple alignment. Multiple alignment results include the 5' and 3' sequences containing the restriction sites used for cloning. Additionally, a Box shade representation of the translated plasmid and NM_138880 sequences was produced.

Of the two sequenced plasmids only one contained non-synonymous mutations. Clone 1 contained a single mutation at base 132 (Figure 2.26) which did not produce any changes in the amino acid sequence (Figure 2.27). This clone was designated pSFV-Enh-IFNγ and used for all further work.

2.3.2.5.1.4 pSFV-Enh-IL12(p35) sequencing

Three IL-12 p35 insert-positive SFV-Enh clones were analysed by DNA sequencing. Sequencing results were used to produce contiguous sequences for each plasmid using Chromas Pro, blasted against the NCBI database, aligned using Clustal W and the alignment file used to produce the Box shade representation. The NCBI *Rattus* norvegicus IL-12a (IL-12 p35) mRNA sequence (NM_053390) was included in the multiple alignment. Multiple alignment results include the 5' and 3' sequences including the restriction sites used for cloning. Additionally, a Box shade representation of the translated plasmid and NM_022611 sequences was produced.

All 3 clones contained a number of synonymous and non-synonymous mutations (Figure 2.28, Figure 2.29). Both clone 1 and 3 contained three non-synonymous mutations however clone 1 was chosen for site-directed mutagenesis as two mutations were within endonucleases restriction sites and correction could be confirmed without the need for repeated sequencing.

2.3.2.5.1.3 pSFV-Enh-IL12(p40) sequencing

Three IL-12 p40 insert-positive SFV-Enh clones were analysed by DNA sequencing. Sequencing results were used to produce contiguous sequences for each plasmid using Chromas Pro, blasted against the NCBI database, aligned using Clustal W and the alignment file used to produce the Box shade representation. The NCBI *Rattus* norvegicus IL-12b (IL-12 p40) mRNA sequence (NM_022611) was included in the multiple alignment. Multiple alignment results include the 5' and 3' sequences including the restriction sites used for cloning. Additionally, a Box shade representation of the translated plasmid and NM_022611 sequences was produced.

Clone 2 contained an inversion at bases 505-506 (Figure 2.32) which resulted in a single amino acid change at 125 from valine to glutamic acid (Figure 2.31). This inversion was present in all 3 sequenced clones (not shown) and in the *Rattus* norvegicus IL-12 p40 genomic DNA reference assembly (NW_047334, Figure 2.30). This suggested that the inversion was a genuine polymorphism and as a result was not corrected by site-directed mutagenesis. Clone 2 was designated pSFV-Enh-IL12(p40) and used for all further work.

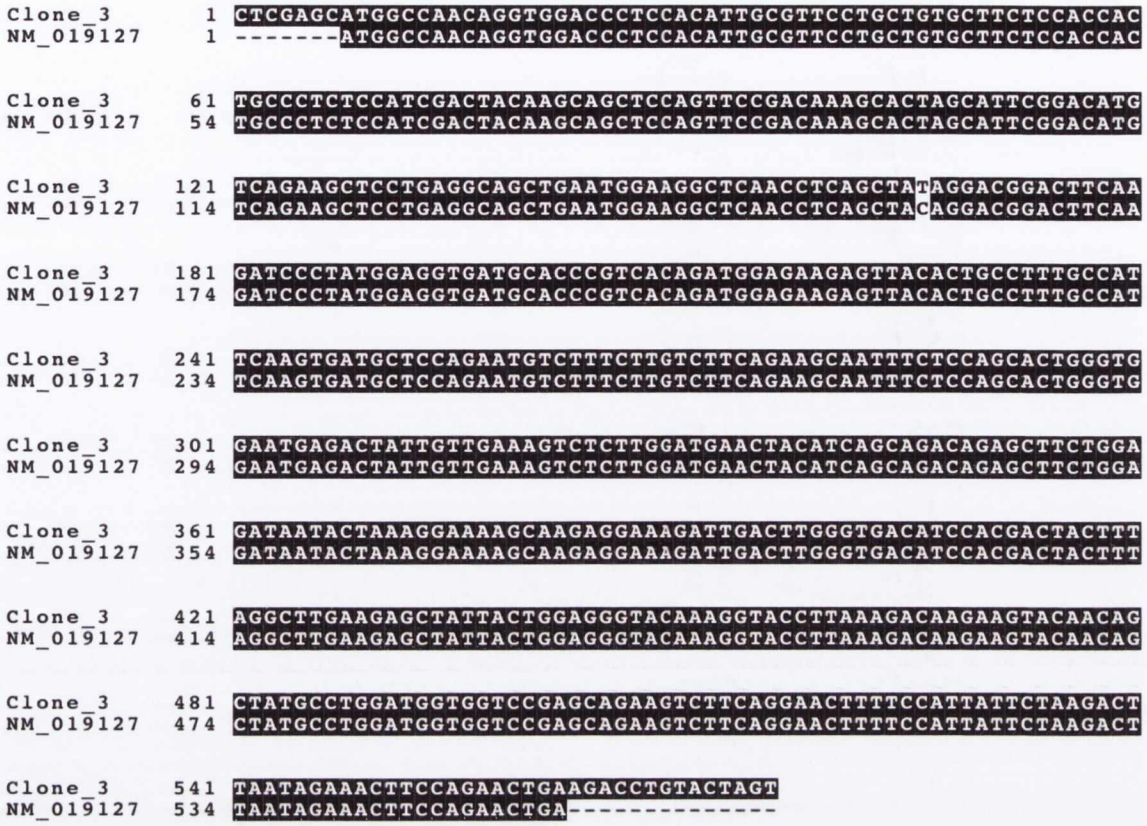

Figure 2.24: IFN-β sequencing.

Multiple alignment and Box shade representation of the IFN-β clone 3 and *Rattus* norvegicus IFN-β mRNA nucleotide sequences (Pubmed accession number NM_019127).

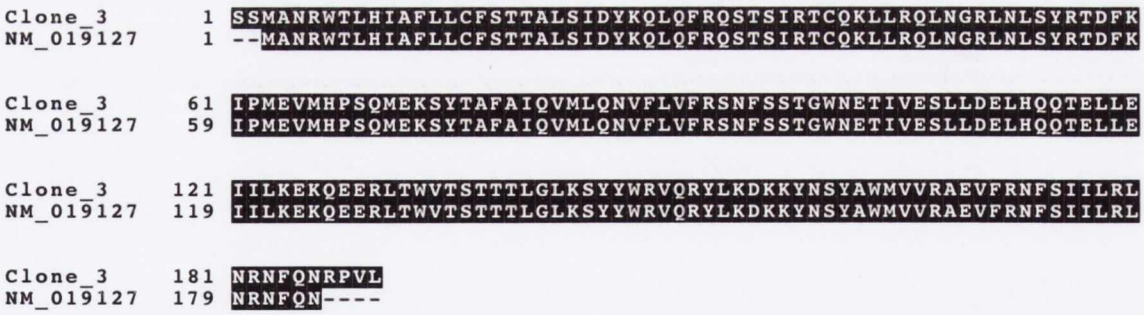

Figure 2.25: IFN-β protein sequence.

Multiple alignment and Box shade representation of the IFN-β clone 3 and *Rattus* norvegicus IFN-β mRNA translated amino acid sequence (Pubmed accession number NM_019127).

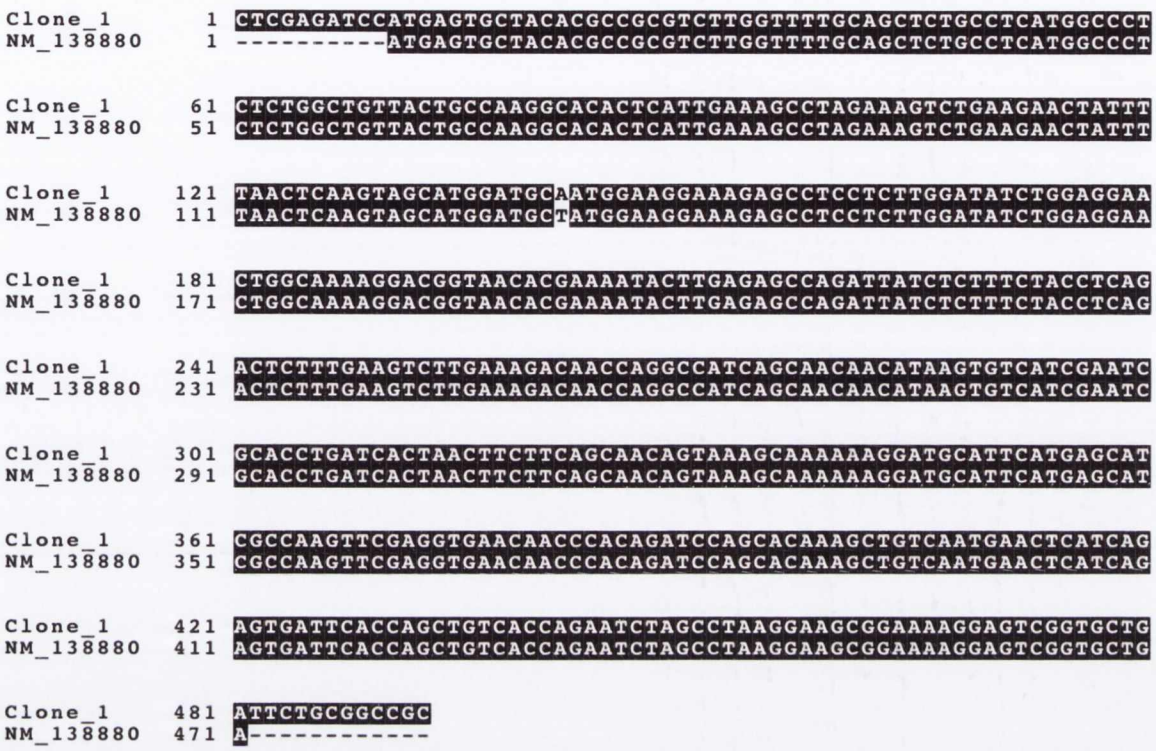

Figure 2.26: IFN-γ sequencing.

Multiple alignment and Box shade representation of the IFN-γ clone 1 and *Rattus* norvegicus IFN-γ mRNA nucleotide sequences (Pubmed accession number NM_138880).

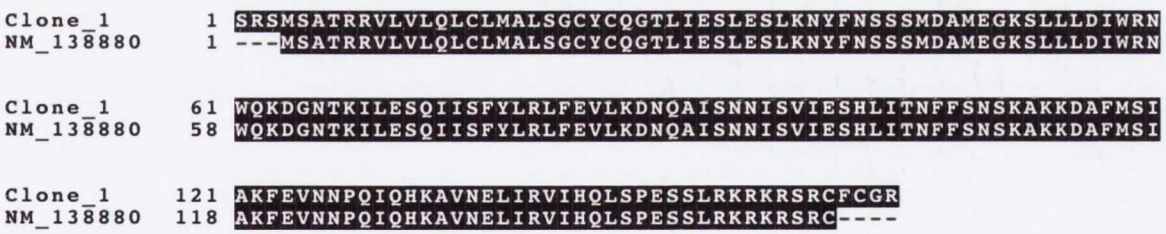

Figure 2.27: IFN-γ protein sequence.

Multiple alignment and Box shade representation of the IFN-γ clone 1 and *Rattus* norvegicus IFN-γ mRNA translated amino acid sequence (Pubmed accession number NM_138880).

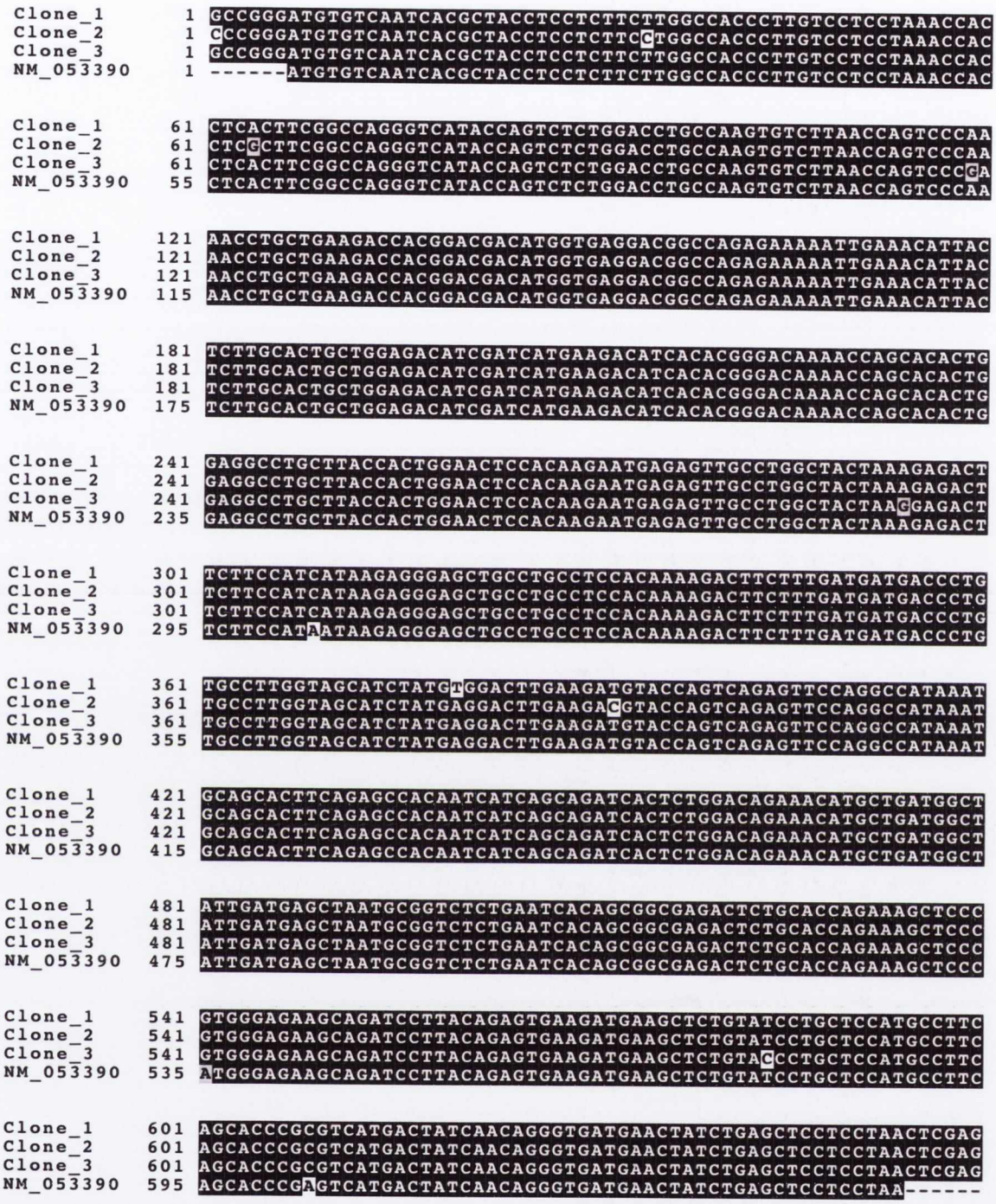

Figure 2.28: IL-12 p35 subunit sequencing.

Multiple alignment and Box shade representation of the IL-12 p35 subunit clones 1-3 and the *Rattus* norvegicus IL-12 p35 subunit mRNA nucleotide sequences (Pubmed accession number NM_053390).

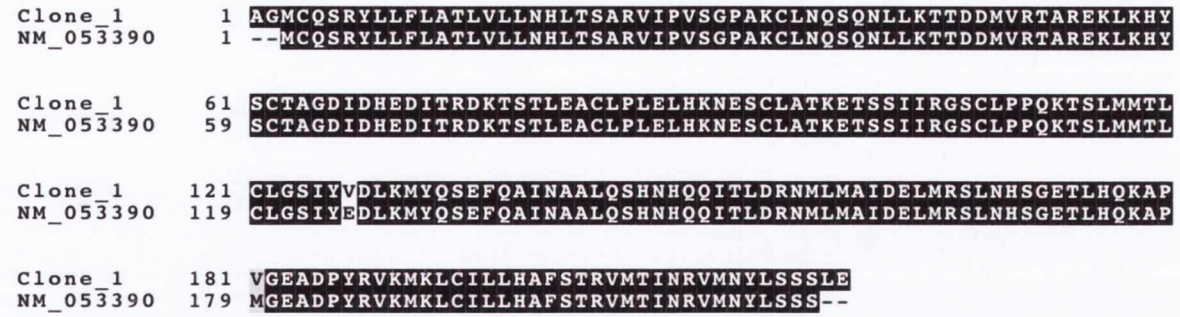

Figure 2.29: IL-12 p35 subunit protein sequence.

Multiple alignment and Box shade representation of the IL-12 p35 subunit clone 1 and *Rattus* norvegicus IL-12 p35 subunit mRNA translated amino acid sequence (Pubmed accession number NM_053390).

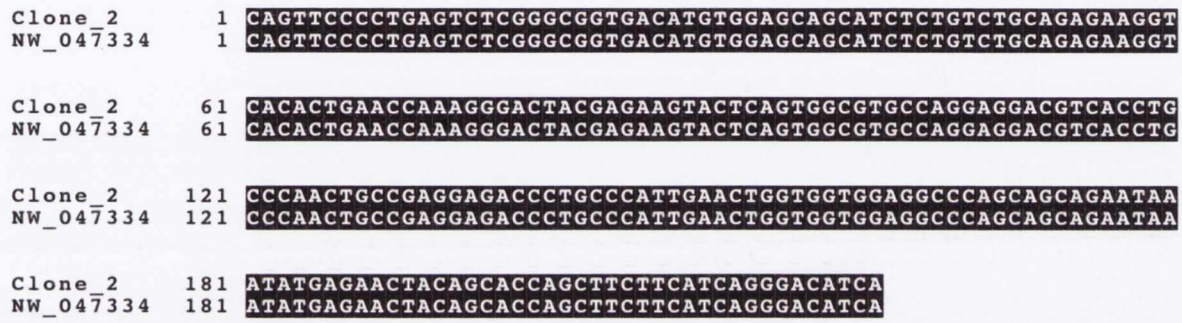

Figure 2.30: IL-12 p40 sequencing.

Multiple alignment and Box shade representation of the IL-12 p40 clone 2 and the partial genomic *Rattus* norvegicus IL-12 p40 DNA nucleotide sequence (Pubmed accession number NW_047334).

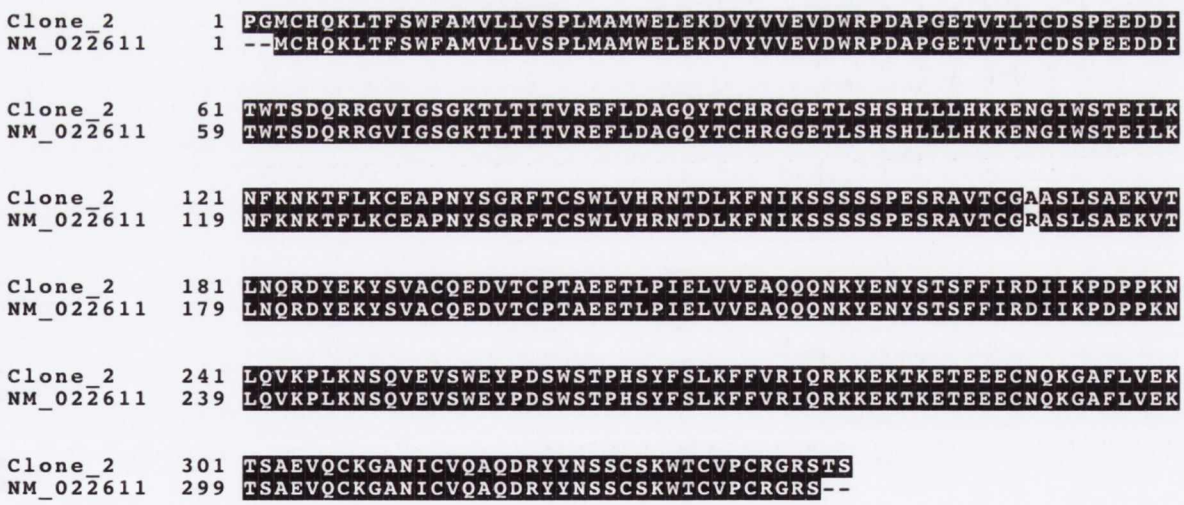

Figure 2.31: IL-12 p40 subunit protein sequence.

Multiple alignment and Box shade representation of the IL-12 p40 subunit clone 2 and the *Rattus* norvegicus IL-12 p40 subunit mRNA translated amino acid sequence (Pubmed accession number NM_022611).

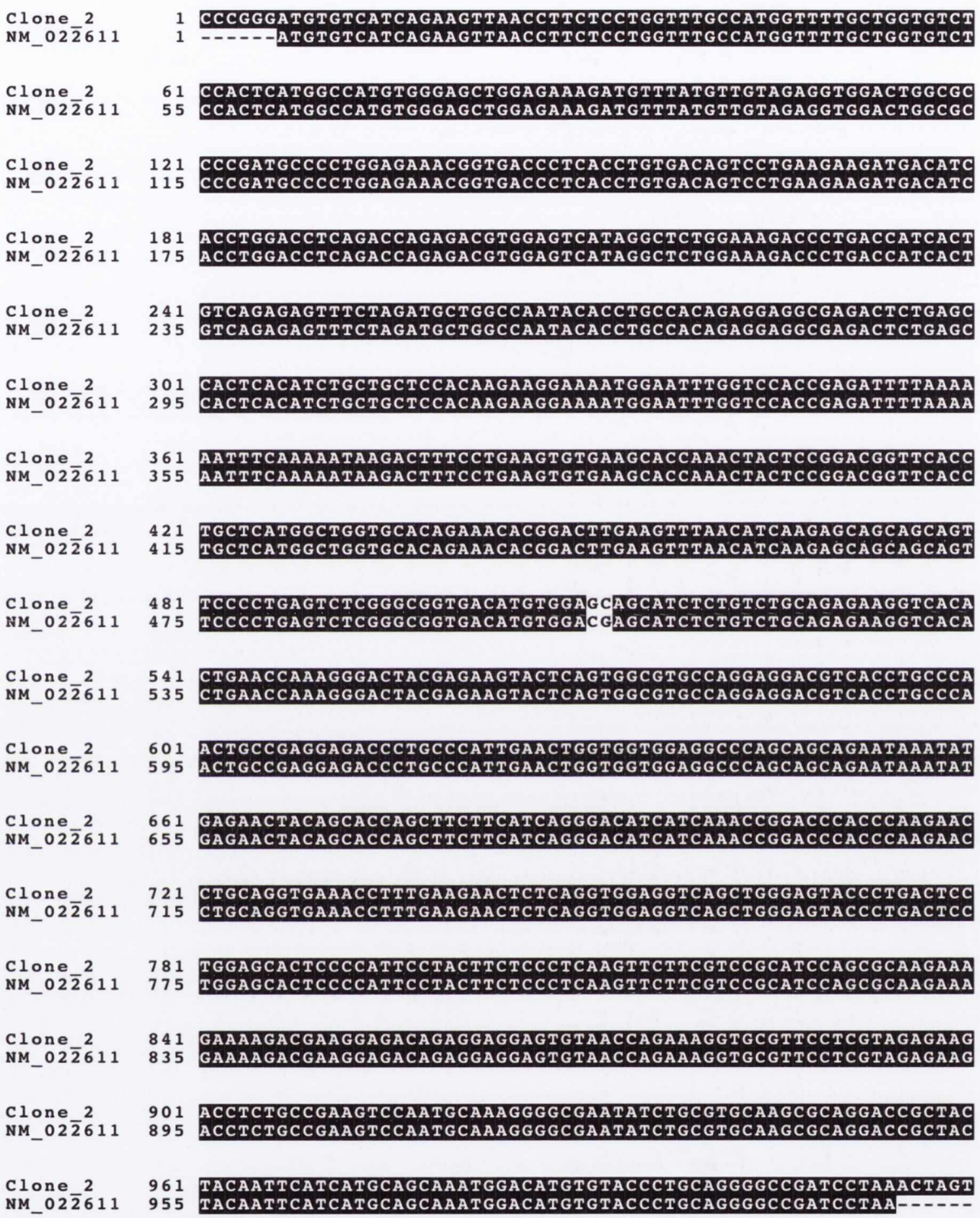

Figure 2.32: IL-12 p40 subunit sequencing.

Multiple alignment and Box shade representation of the IL-12 p40 subunit clone 2 and the *Rattus* norvegicus IL-12 p40 subunit mRNA nucleotide sequences (Pubmed accession number NM_022611).

2.3.2.5.2 Site-directed mutagenesis

Site-directed mutagenesis was carried out by successive rounds of screening and correction. Correction efficiencies of 90% were routinely obtained. The frameshift mutation in pSFVEnh-IL12(p35) at –5bp was corrected and confirmed by XmaI/SpeI restriction digestion (data not shown). The second round of mutagenesis involved the correction of the 535bp substitution and was confirmed by NcoI restriction digest (data not shown). The remaining mutation at 374bp was corrected as above and analysed by DNA sequencing.

2.3.2.5.2 DNA sequencing

Following the final site-directed mutagenesis reaction, six colonies were analysed for the correction of the substitution mutation at 374 by DNA sequencing. Of the six clones sequenced, all showed the correction of all three mutations. Figure 2.33 shows one such clone aligned with the NCBI *Rattus* norvegicus IL-12 p35 mRNA sequence (NM_053390). Figure 2.34 shows the aligned translated DNA sequences for the corrected in-frame IL-12 p35 subunit and NM_053390.

2.3.2.6 Production of pSFV-Enh-IL12

2.3.2.6.1 Pre-ligation preparation of pSFV-Enh-IL12(p35) and pSFV-Enh-IL12(p40)

Prior to the production of pSFV-Enh-IL12 the p35 sequence from the corrected IL-12 p35 subunit-containing plasmid was excised using the restriction sites for cloning and cloned into pSFV-Enh that had not undergone PCR amplification during site-directed mutagenesis (data not shown). This plasmid was designated pSFV-Enh-IL12(p35) and used for all further work.

For the production of pSFV-Enh-IL12, pSFV-Enh-IL12(p35) was linearised by SpeI digestion (Figure 2.35B), blunt ended and dephosphorylated. pSFV-Enh-IL12(p40) was digested with BglII/SpeI (Figure 2.35A) and the 1872 bp fragment gel purified and blunt-ended prior to ligation.

2.3.2.6.2 Screening of ligation reaction

Following ligation, colonies were screened for the presence of the IL-12 p40 subunit insertion by HindIII digestion. Six colonies were analysed by restriction digest and the presence of a 1525 bp band indicated a successful in-orientation ligation (Figure 2.36). Of the six clones analysed, one was positive for the presence of the 26S sub-genomic promoter, capsid enhancer sequence, IL-12 p40 sequence. This clone was further digested with HindIII/XmaI and EcoRI to ensure the correct orientation of the insert. Table 2.9 shows the expected band pattern for the in-orientation and reverse orientation insert of each digestion. Clone 1 produced a digestion pattern expected for the correct in-orientation ligation (Figure 2.37), was designated pSFV-Enh-IL12 and used for all further experimentation.

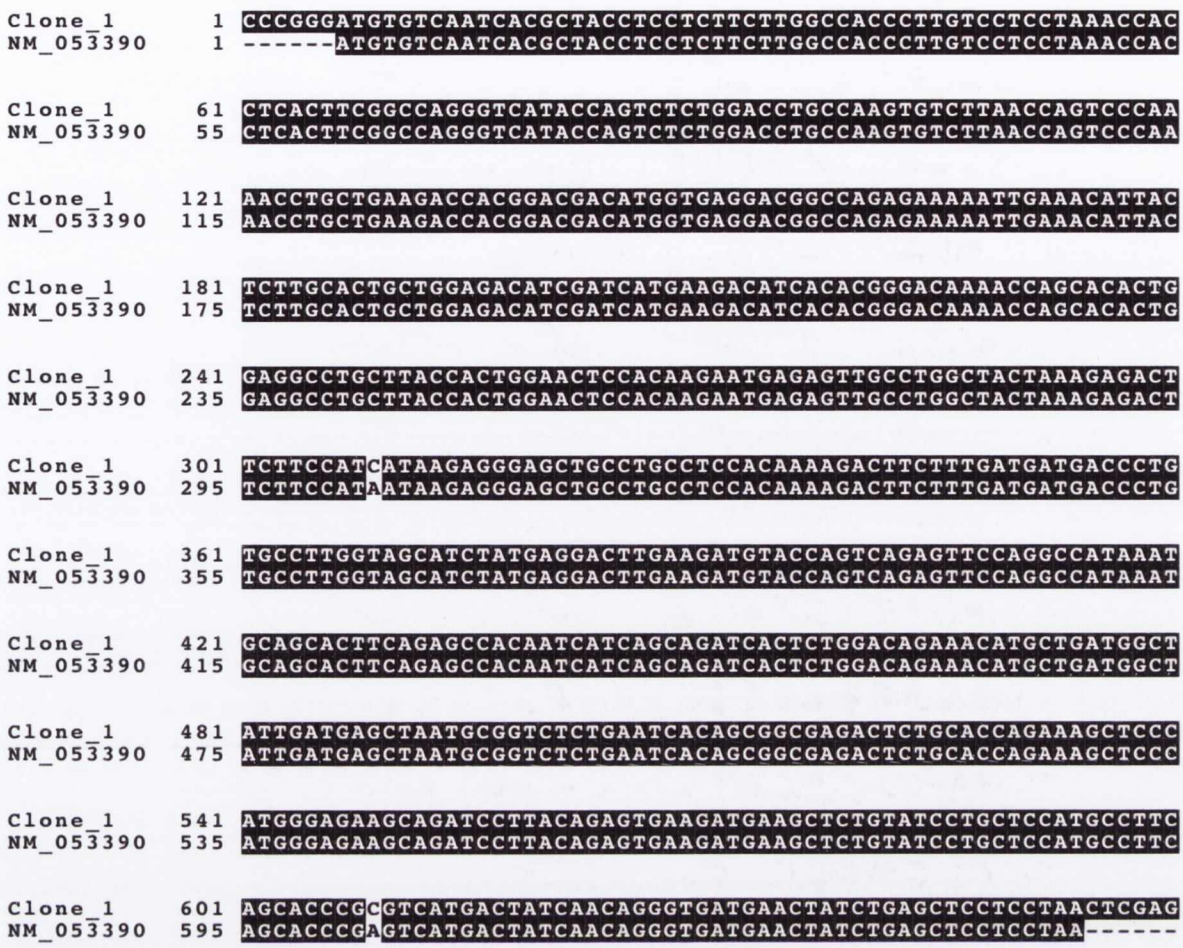

Figure 2.33: IL-12 p35 subunit sequencing following site-directed mutagenesis.

Multiple alignment and Box shade representation of the IL-12 p35 subunit clone 1 and the *Rattus* norvegicus IL-12 p35 subunit mRNA nucleotide sequences (Pubmed accession number NM_053390).

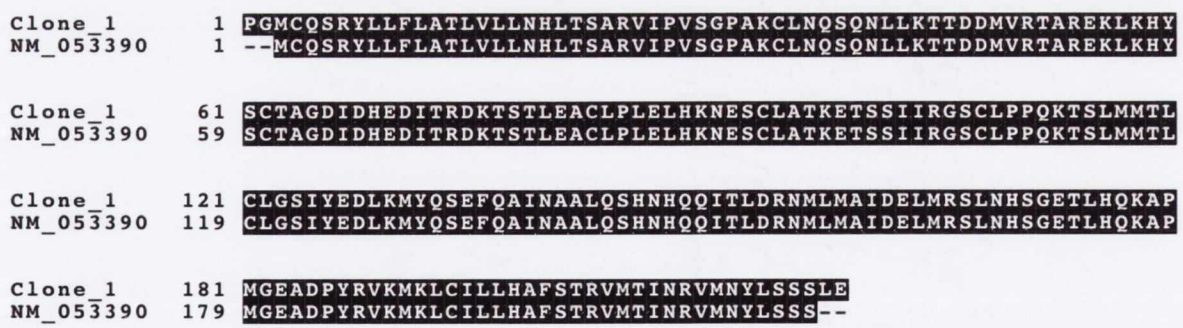

Figure 2.34: IL-12 p35 subunit sequencing following site-directed mutagenesis.

Multiple alignment and Box shade representation of the IL-12 p35 subunit clone 1 and the *Rattus* norvegicus IL-12 p35 subunit mRNA translated amino acid sequence (Pubmed accession number NM_053390).

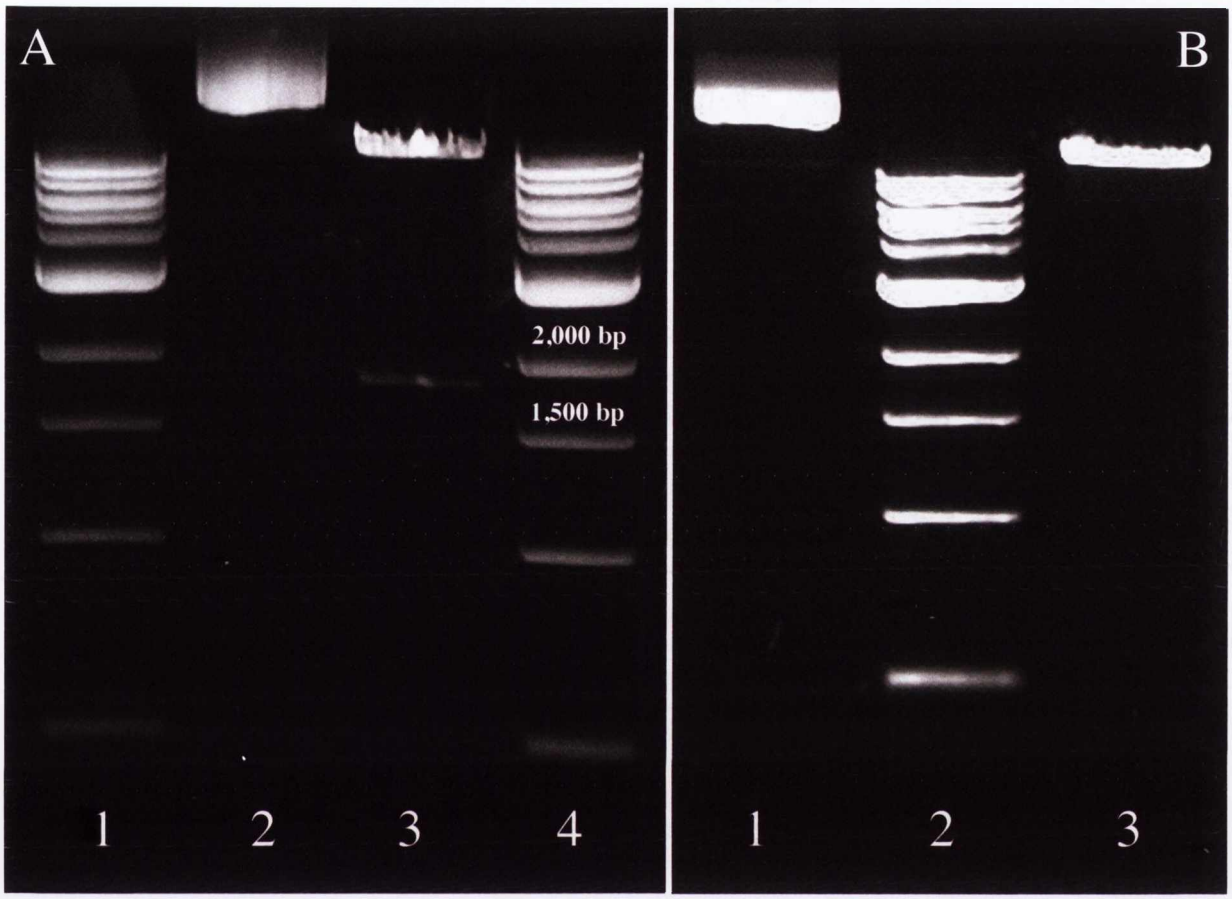

Figure 2.35: Pre-ligation preparation of pSFV-Enh-IL12(p35) and pSFV-Enh-IL12(p40).

A - The 26S sub-genomic promoter, capsid enhancer sequence and IL-12 p40 sequence (1872bp) was excised by BglII/SpeI digest of pSFV-Enh-IL12(p40). *Lanes 1* and *4* are 1kb DNA ladder, *Lane 2* and *3* are uncut and BglII/SpeI digested pSFV-Enh-IL12(p40) respectively.

B – pSFV-Enh-IL12(p35) was linearised by SpeI restriction digest, blunt ended and dephosphorylated prior to ligation. *Lane 2* is 1kb DNA ladder, *Lane 1* and *3* are uncut and SpeI digested pSFV-Enh-IL12(p35) respectively.

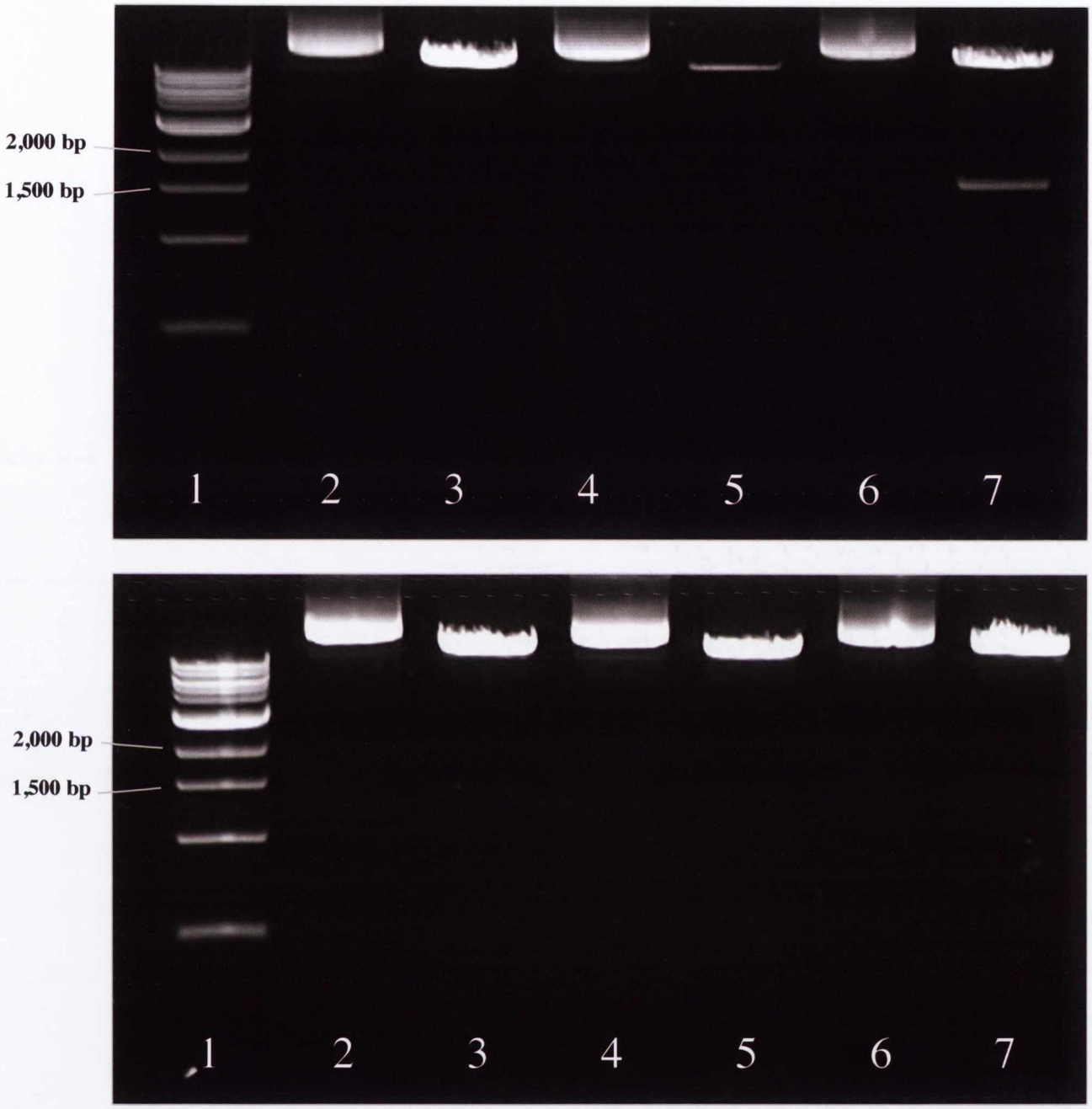

Figure 2.36: Screening of IL-12 ligation reactions by HindIII restriction digest.

6 colonies were selected and digested. *Lanes 2, 4* and *6* are uncut plasmid, *Lanes 3, 5, 7* are HindIII digested plasmids and *Lane 1* is 1 kb DNA marker. The presence of a band at 1525bp indicated the correct ligation of the 26S subgenomic promoter and IL-12 p40 fragment into pSFV-Enh-IL12(p35).

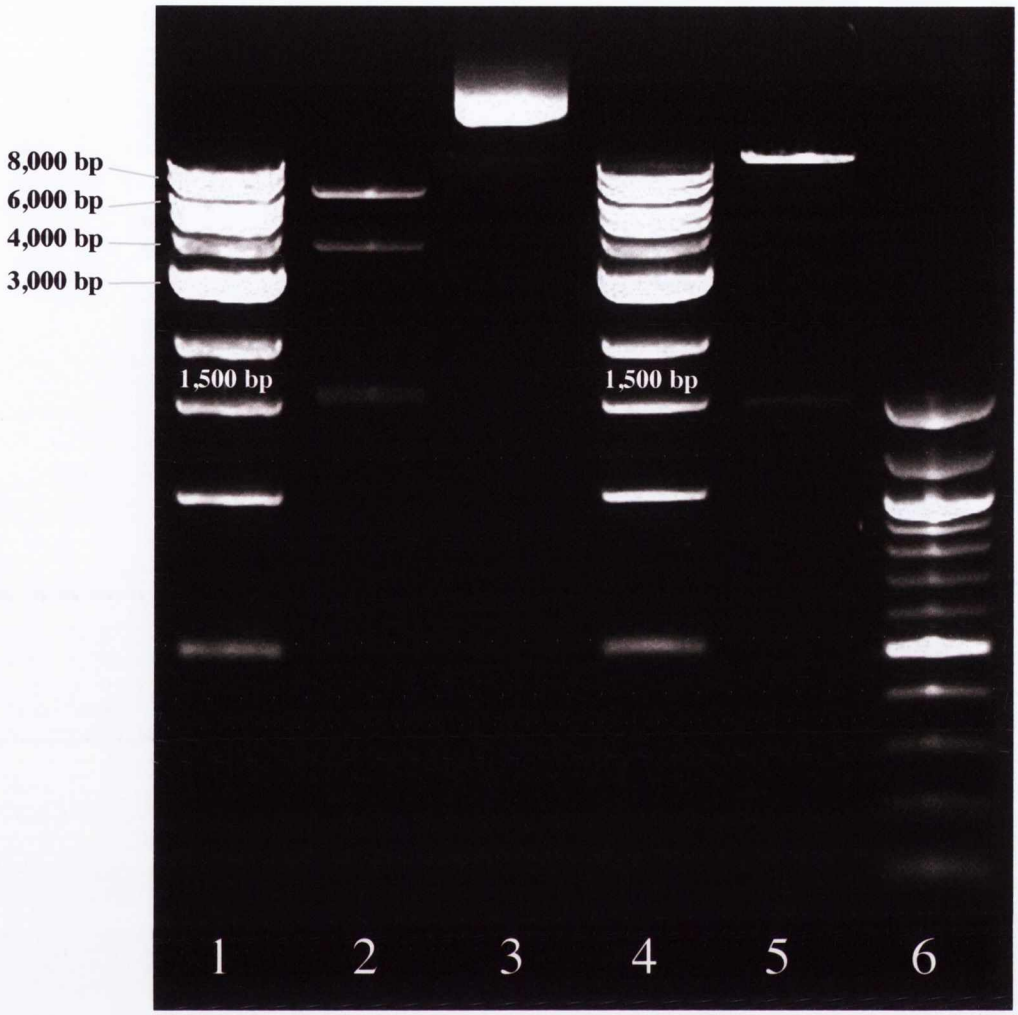

Figure 2.37: Screening of IL-12 ligation reactions for orientation.

The IL-12 p70 insert positive clone was digested with HindIII/XmaI and EcoRI. Table 2.9 represents the expected band pattern for the in-orientation and reverse orientation ligation products. *Lanes 1* and *4* are 1kb DNA ladder, *Lane 4* is 100bp ladder and *Lanes 2* and 5 are HindIII/XmaI and EcoRI digests respectively.

Ligation product	Restriction digest – expected digestion pattern			
	HindIII/XmaI		EcoRI	
PSFV-Enh-IL12	11,725	33	6,553	1,578
P40 fragment in-orientation	1,492	33	3,627	1,525
PSFV-Enh-IL12	7,571	1,021	6,031	2,039
P40 fragment reverse orientation	4,029	654	3,627	1,578

Table 2.9: Expected band pattern for pSFV-Enh-IL12 restriction analysis.

Red bands represent bands not visible by gel electrophoresis

2.3.2.7 Analysis of transgene expression

mRNA from each plasmid was produced by *in vitro* transcription of linearised plasmid. Following electroporation of SFV-Enh-IFNβ mRNA, S-BHK cells were stained for the presence of IFN-β by indirect immunofluorescence. Figure 2.38 shows the resultant DAPI/FITC overlay images. IFN-β detection was negligible in mock electroporated or SFV-Enh mRNA electroporated cells. Staining was pronounced in cells electroporated with SFV-Enh-IFNβ mRNA indicating the presence of intracellular IFN-β.

To examine the expression of IFN-γ, S-BHK cells were electroporated with PBS, empty SFV-Enh mRNA or SFV-Enh-IFNγ mRNA. Cell supernatant was harvested at 0, 16, 24, 48 and 72 hours post-electroporation. Medium was analysed in triplicate for the presence of IFN-γ by commercial rat IFN-γ ELISA (Figure 2.39). IFN-γ expression from mock and empty SFV-Enh mRNA electroporated cells was negligible at all time points. SFV-Enh-IFNγ mRNA electroporated cells showed expression at all time points measured, peaking at approximately 146 ng/10^6 cells of IFN-γ at 48-72 hours, with no significant differences between the two time points ($p=0.3872$).

To examine IL-12 expression, S-BHK cells were electroporated with SFV-Enh-IL12 mRNA or PBS. Medium was harvested at 0, 24, 48 and 72 hours post-electroporation. Medium was analysed in triplicate for the presence of IL-12 by commercial rat IL-12 ELISA (Figure 2.40). IL-12 expression was negligible at all time points in mock electroporated cells. SFV-Enh-IL12 mRNA electroporated cells showed expression at all time points measured with a significantly greater expression at 72 hours than 24 hours ($p=0.0323$).

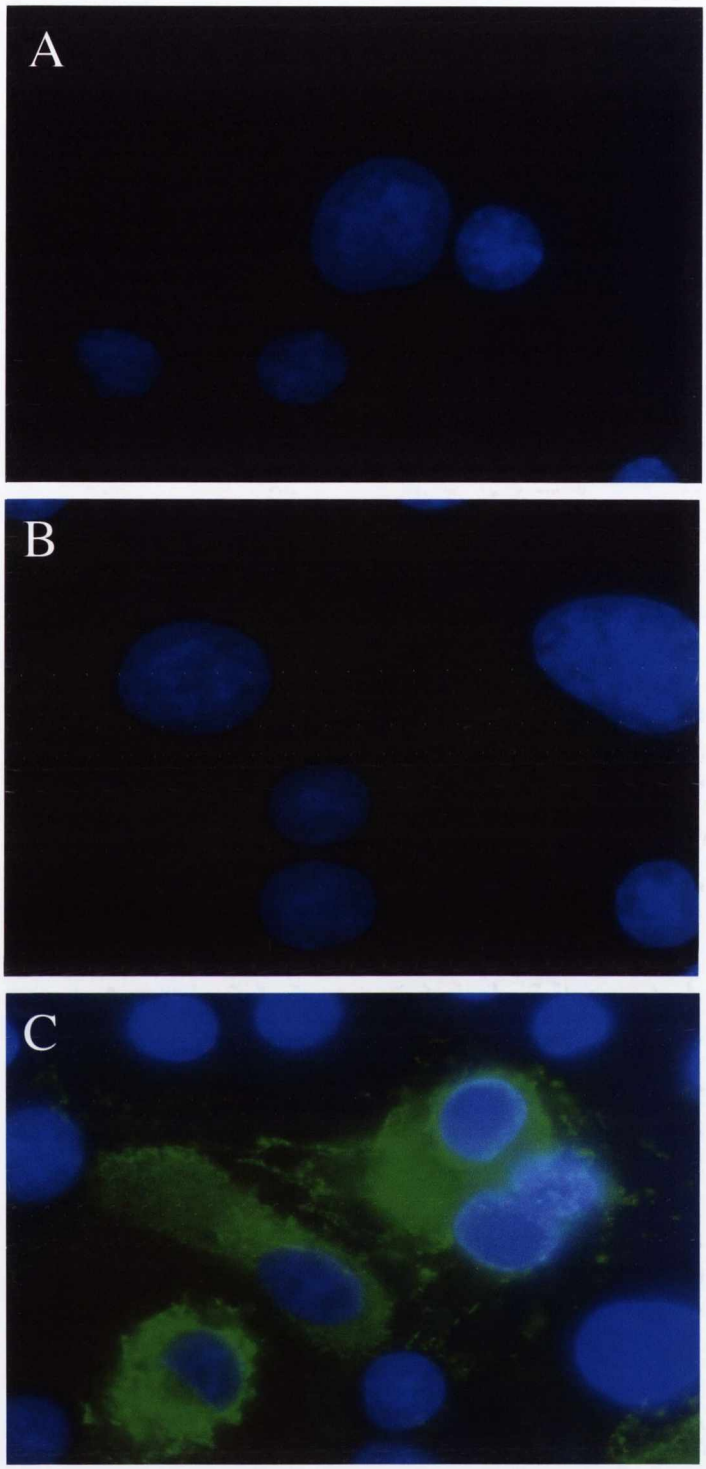

Figure 2.38: IFN-β expression following transfection with SFV-Enh-IFNβ mRNA.

S-BHK cells were electroporated with PBS, SFV-Enh mRNA or SFV-Enh-IFNβ mRNA. 18 hours later cells were stained with anti-rat IFN-β antibody followed by FITC conjugated secondary antibody. Image is 1000x DAPI/FITC merge of rat IFN-β stained mock electroporated (**A**) SFV-Enh mRNA electroporated (**B**) and SFV-Enh-IFNβ mRNA electroporated cells (**C**) S-BHK cells.

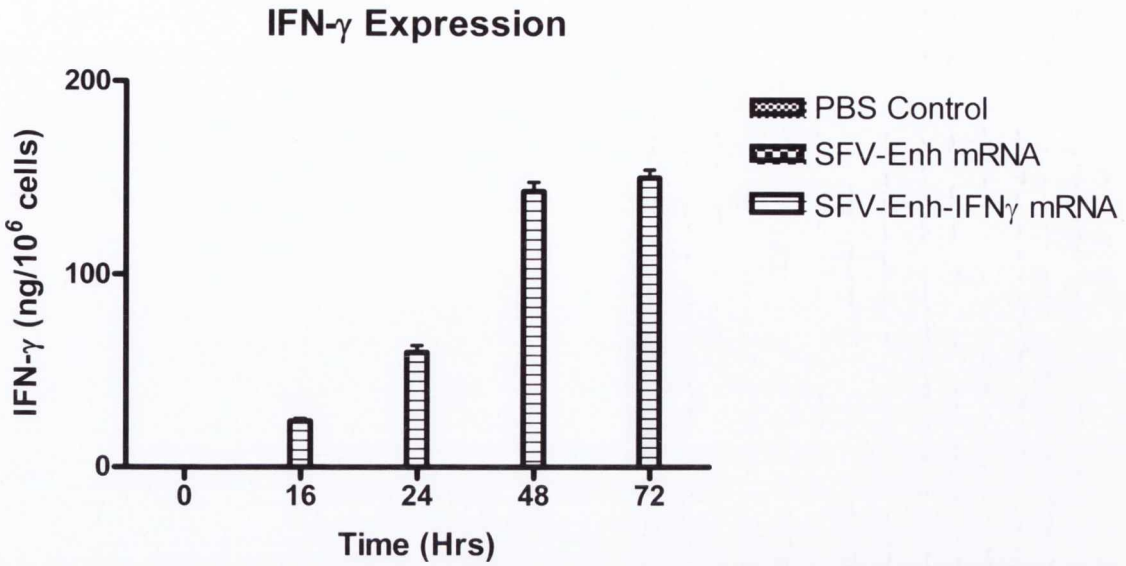

Figure 2.39: IFN-γ expression following transfection with SFV-Enh-IFNγ mRNA.

S-BHK cells were electroporated with PBS, SFV-Enh mRNA or SFV-Enh-IFNγ mRNA. Supernatant was harvested at 0, 16, 24, 48 and 72 hours post electroporation and examined for the presence of IFN-γ by ELISA. IFN-γ concentrations were adjusted to nanograms per 10^6 cells.

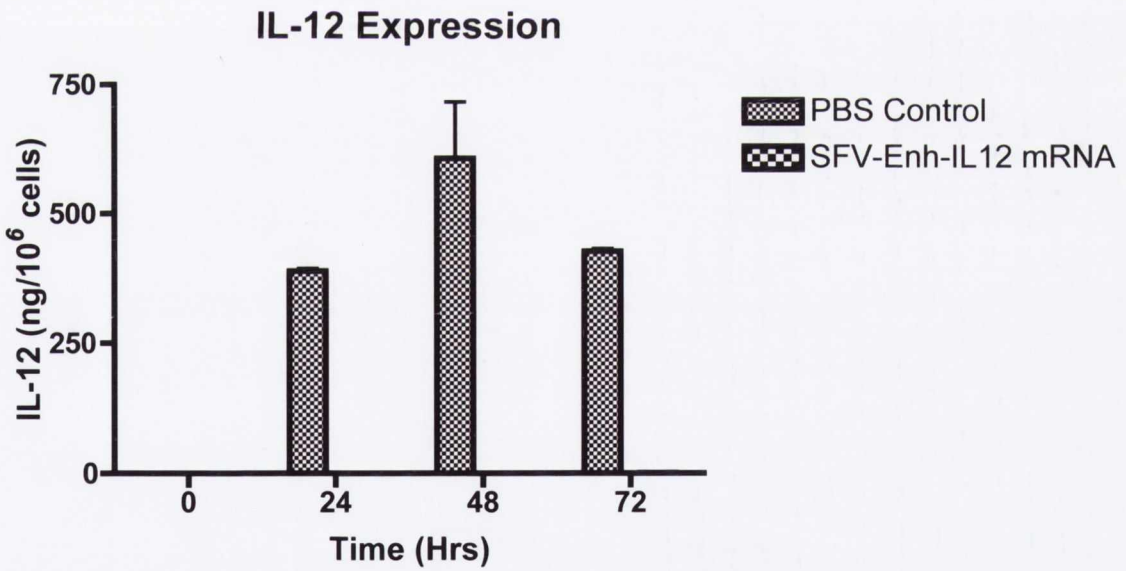

Figure 2.40: IL-12 expression following transfection with SFV-Enh-IL12 mRNA.

S-BHK cells were electroporated with PBS or SFV-Enh-IL12 mRNA. Supernatant was harvested at 0, 24, 48 and 72 hours post electroporation and examined for the presence of IL-12 by ELISA. IL-12 concentrations were adjusted to nanograms per 10^6 cells.

2.4 Discussion

PCR amplification of the IFN-γ, IFN-β and IL-12 p40 coding regions was carried out using the TripleMaster® PCR amplification system. PCR amplification and cloning produced a number of insert-positive clones for each plasmid. Three IFN-β insert-positive clones were sequenced; all three clones contained mutations although one had only a single synonymous mutation, which did not require correction by site-directed mutagenesis, and was used for further experimentation. Two IFN-γ insert-positive clones were sequenced and both demonstrated mutations although one contained only a single synonymous mutation; the absence of an amino acid sequence change did not warrant correction and this clone was used for further work. Three IL-12 p40 insert-positive clones were sequenced; of these, two contained a number of synonymous mutations and one contained only a single inversion at the 505th and 506th base. This inversion resulted in a V125R amino acid change and was present in all 3 sequenced clones suggesting it may have been a genuine polymorphism; in addition, the genomic *Rattus* norvegicus IL-12 p40 DNA nucleotide sequence (Pubmed accession number NW_047334) also contained this inversion providing further support that the inversion was not incorporated during PCR amplification. Initial attempts using the TripleMaster® PCR system failed to amplify significant quantities of the p35 PCR product; as a result, the p35 sequence was amplified using Taq DNA polymerase. Unlike the TripleMaster® enzyme, Taq polymerase does not have proofreading ability, which may explain the increased number of mutations in the amplified p35 fragment. All p35 subunit insert-positive clones sequenced contained both synonymous and non-synonymous mutations. Clone 1 was chosen for site-directed mutagenesis because two of the three non-synonymous mutations altered endonuclease recognition sites and as a result, correction could be confirmed by restriction digest avoiding repeated rounds of DNA sequencing. Site-directed mutagenesis was successfully carried out on the p35 subunit coding sequence. Following site-directed mutagenesis the p35 sequence was excised and re-cloned into pSFV-Enh that had not undergone PCR amplification; this was carried out as a precautionary measure as the introduction of mutations into the plasmid backbone during repeated PCR amplification, required for site-directed mutagenesis, could not be excluded.

The inclusion of the translational enhancer sequence within the enhanced expression plasmid required the incorporation of the co-translationally self-cleaving FMDV 2A protease sequence to remove the N terminal capsid sequence. There remains

however, a minimum of a single proline at the N terminus of the contiguously translated transgene. Depending upon the 5' cloning site used for ligation and the inclusion of additional nucleotides to maintain frame, a total of 10 amino acids may precede the N terminus of the transgene protein product. Although effects detrimental to protein folding, protein stability or targeting/secretion cannot be completely excluded as a result of these additional bases, this system has been used for the production of a multitude of proteins and the author is not aware of any published or otherwise documented problems associated with these additional residues. As a result of the production of the IFN-β SFV plasmid, three residues (PSS) were included into the N terminus of the translated IFN-β protein while the translated IFN-γ protein was preceded by the additional PSAS amino acid sequence. Both IL-12 subunits included additional residues; p35 contained the additional N terminal PAG sequence and PGP preceded the p40 subunit amino acid sequence. The genes cloned into the SFV-Enh plasmid used in this study all encode secreted proteins and as such contain signal sequences in the N terminus of the translated proteins that result in the co-translational sequestering of the nascent protein and traffic towards the endoplasmic reticulum. These N terminal signal sequences are removed prior to protein secretion (Nothwehr and Gordon, 1990; Murphy *et al.*, 2000) and as such remove the extra N terminal residues included as a result of cloning. Protein secretion is thus indicative of proper protein expression and removal of the non-structural N terminus residues.

The IL-12 double construct was cloned to encode both the p35 and p40 subunits. In order to produce both subunits in equimolar quantities, the p35 and p40 subunits were cloned under the control of individual subgenomic promoters. Following initial 42S minus strand ($42S^-$) RNA synthesis, both positive-sense genomic (42S) and subgenomic (26S) RNAs are transcribed by the SFV RNA-dependent RNA polymerase. Consequently, following transfection of cells by the SFV-Enh-IL-12 mRNA, three positive-sense RNA species are produced, one genomic $42S^+$ RNA and two subgenomic RNA species. The two subgenomic RNA species derive from the first 5' subgenomic promoter encoding both the p35 and p40 subunits, here termed the $26S^{p70}$ mRNA, and the second from the 3' subgenomic promoter encoding only the p40 subunit, here termed the $26S^{p40}$ mRNA (Figure 2.41).

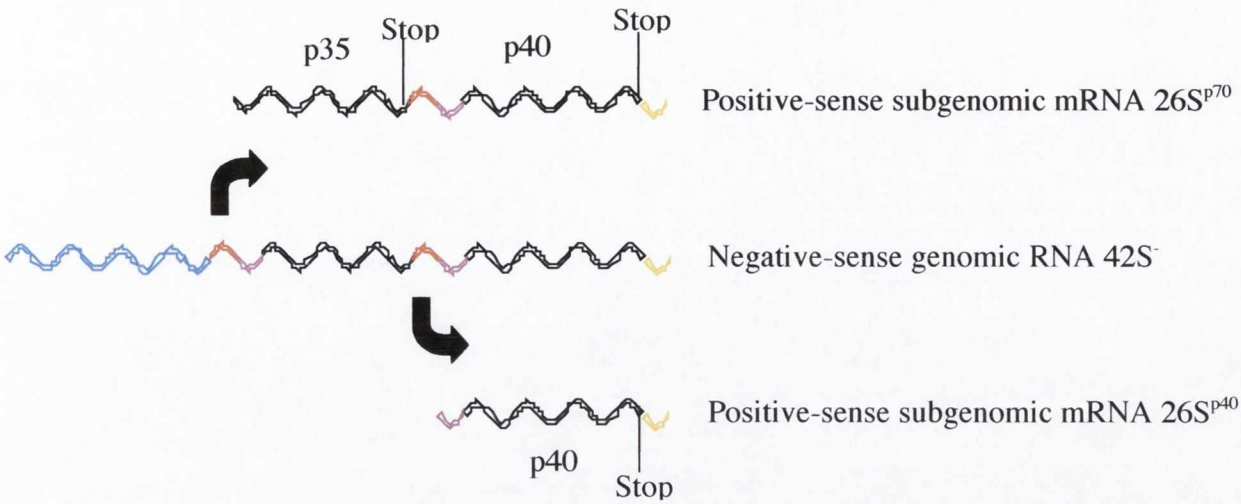

Figure 2.41: Schematic of SFV-Enh-IL-12 RNA replication.

Red – subgenomic promoter, blue – non-structural protein coding region, yellow – poly(A) tail, purple – translational enhancer and start codon.

The $26S^{p70}$ RNA is thus a polycistronic mRNA containing translation promoters and enhancers for each IL-12 subunit. This raises the potential for the over production of the p40 subunit, which may produce secreted p40 dimers that are IL12R antagonists however, this is unlikely considering that translation of the subgenomic mRNA appears to be cap-dependant and as such only the open reading frame initiated by the 5' most ATG is translated (reviewed in Lopez-Lastra *et al.*, 2005).

Following the successful cloning of each cytokine into the pSFV-Enh vector, expression of the protein product was verified. *In vitro* transcribed SFV-Enh mRNA is identical to that encapsidated into the VLP virion and electroporation allows for analysis of transgene expression without VLP production. IL-12 and IFN-γ expression from vectors was analysed by commercial ELISA; this confirmed protein expression, processing and secretion of the encoded proteins. The absence of a commercial rat IFN-β ELISA meant protein expression in the supernatant could not be easily confirmed. For this reason indirect immunofluorescence was used and although it did not show IFN-β secretion, this was confirmed by viral inhibition assay in later work. Although ELISA analysis allowed for the quantitative analysis of protein production, the qualitative demonstration of protein expression was of more importance as quantitative analyses using the VLP system will be examined in the next chapter.

Chapter 3

In vitro analysis of the expression and activity of SFV VLP encoded cytokines

3.1 Introduction

The Semliki Forest virus virus-like particle system is a suicidal expression system which involves the production of virus particles containing a single genomic RNA species comprising a truncated structural ORF into which transgenes, of up to 6.5kb in length, can be cloned (Ehrengruber *et al.*, 2001). The absence of the structural genes precludes productive infection although the VLPs retain the ability to transfect cells, induce RNA amplification, mediate transgene expression and initiate cell death. During VLP production the structural proteins are supplied *in trans* encoded by the helper mRNA molecules transcribed from the helper DNA plasmids. The helper plasmids lack the non-structural ORF and packaging signal and as a result, helper plasmid RNA is not packaged into the newly synthesised virion. The helper plasmid has undergone a number of revisions, the primary role of which was to improve biosafety by the restriction of replication-competent virus (RCV) production. RCVs are thought to occur via template switching of the viral RNA-dependent RNA polymerase during genomic replication (U Geigenmüller-Gnirke *et al.*, 1991) resulting in the generation of RNA species containing both SFV ORFs and capable of initiating productive infection. Initially, the structural proteins were provided *in trans* on a single RNA molecule transcribed from pSFV-helper-1. Production of VLPs using the helper-1 plasmid resulted in relatively high-titer VLPs, however the rate of RCV generation was approximately 10^{-3}-10^{-5} (Berglund *et al.*, 1993). In an attempt to reduce the production of RCVs, the helper-1 plasmid was modified to produce the helper-2 plasmid. The helper-2 plasmid contains a number of amino acids substitutions in the structural ORF, which abolish p62 cleavage and render the budded VLPs non-infectious (Salminen *et al.*, 1992). As a result, helper-2 produced VLPs require activation by α-chymotrypsin digestion treatment prior to use. Although VLPs production using the helper-2 plasmid resulted in decreased RCV production, the activation step was inconvenient and the development of true reversion or off-site reversion mutations was still possible. In an effort to further enhance biosafety, Smerdou *et al.* (1999) devised a helper packaging strategy which split the structural proteins into two helper plasmids, pSFV-Capsid and pSFV-Spike. In this split helper system the capsid protein is encoded by pSFV-Capsid and contains additional substitution mutations, which introduce a 3' stop codon and abrogate the capsid self-cleavage activity. The remainder of the structural polyprotein gene, encoding the p62, 6k and E1 proteins, was cloned into pSFV-Spike. The absence of the capsid gene from the spike polyprotein sequence meant the translation enhancement was lost and as a result the

p62-6k-E1 sequence is 5' flanked by the capsid translational enhancer sequence and the FMDV 2A auto-protease sequence. The split helper VLP production system is used in this project and involves the co-transfection of cells, by electroporation, with each of the capsid, spike and expression mRNA molecules (Figure 1.2). The non-structural proteins, comprising the replicase complex, are directly translated from the expression mRNA molecule and amplify all three RNA species followed by subgenomic RNA transcription and translation of the capsid and spike proteins. Virion production then follows a route identical to that of replicating SFV although, importantly, only the expression mRNA is encapsidated. This mRNA is translated into the transgene protein product and accounts for approximately 30-40% of cellular protein production (Ventoso *et al.*, 2006). The split helper system allows for the production of high-titer VLPs with a frequency of RCV generation of approximately 10^{-13} or about 1 RCV in every 100 - 1000 batches of particles (Smerdou and Liljestrom, 1999). Additionally, all the hallmarks of replicating virus infection are preserved including host protein shutdown and apoptosis induction mediated by dsRNA production (Jacobs and Langland, 2000) and RNA replication (Urban *et al.*, 2008) respectively.

The SFV VLP system has been used for the expression of a variety of antigenic or bioactive molecules. This study utilises three immunomodulatory cytokines individually cloned into the enhanced SFV expression plasmid (pSFV-Enh) for the production of cytokine-encoding VLPs. The production of bioactive molecules in this manner is reliant upon the correct secretion and activity of the encoded transgenes. For this reason secreted cytokines were examined for their activity *in vitro*. As mentioned, the major downstream mediator of IL-12 activity is through IFN-γ, expression of which is induced upon IL-12R binding. This induction of IFN-γ allows for the indirect assessment of VLP encoded IL-12 activity. Both IFN-γ and IFN-β are potent anti-viral cytokines and their expression is stimulated by numerous factors including viral infection or antigen-presenting cell activation. Both interferons initiate the upregulation of key mediators of the cellular antiviral response and include, among others, the dsRNA-dependant protein kinase R (PKR) and the 2'-5' oligoadenylate synthetase systems, involved in the suppression of cellular translation and RNA degradation respectively (Goodbourne *et al.*, 2000). This antiviral state primes cells against subsequent infection and is the premise for the viral inhibition assay.

3.2 Experimental Procedures

3.2.1 New Materials

3.2.1.1 Cell lines and bacterial cultures

F98 and RG2 glioma cells were obtained from the ATCC and maintained in DMEM (4,500g/L glucose) supplemented with 10% (v/v) FCS, 1mM sodium pyruvate, 0.1mM non-essential amino acids (NEAA), 2mM L-glutamine and 100 units/ml penicillin/streptomycin. Splenocytes were maintained in DMEM (4,500g/L glucose), 10% (v/v) heat-inactivated FCS, 0.1mM NEAA, 20mM hepes, 1mM sodium pyruvate, 2mM L-glutamine and 100 units/ml penicillin/streptomycin. L929 cells were purchased from the European collection of cell cultures (ECACC, UK) and maintained in DMEM (4,500 g/L glucose) supplemented with 10% FCS, 2mM L-glutamine and 100 units/ml penicillin/streptomycin. Hank's buffered salt solution (HBSS) was purchased from Invitrogen. BD Falcon™ 40μm cell strainers were purchased from BD Biosciences. Red blood cell lysis buffer was sourced from eBioscience, USA. Concanavalin A (Con A) was purchased from Sigma-Aldrich. The CellTiter 96® aqueous non-radioactive cell proliferation assay (MTS) was purchased from Promega.

3.2.1.2 Semliki Forest virus and SFV expression vectors

SFV-A7 and the helper plasmids pSFV-Spike, and pSFV-Capsid were a gift from Prof. P. Liljeström. pSFV-Enh-IFNγ, pSFV-Enh-IFNβ and pSFV-Enh-IL12 were cloned from pSFV-Enh (**2.2**).

3.2.1.3 SFV virus-like particle production

Tris(hydroxymethyl)aminomethane (Tris) and sucrose were purchased from BDH. Ultracentrifugation was performed in the Optima™ L-100 XP ultracentrifuge using Beckman Ultra-Clear™ (25 x 89mm) centrifugation tubes (Beckman Coulter, USA). Nunc® CryoTubes™ were purchased from ThermoFischer.

3.2.1.4 Immunofluorescence reagents

Polyclonal rabbit IgG anti-SFV nSP2 antibody was a kind gift from Prof. A. Hinkkanen (Åbo Akademi University, Finland). Neutralising polyclonal mouse IgG_1 anti-rat interferon gamma antibody (clone M99012622) was purchased from Fitzgerald Industries International, USA. Neutralising polyclonal rabbit IgG anti-rat interferon beta antibody (cat. ab-25470) was purchased from Abcam (UK) and polyclonal goat IgG anti-rat IL-12 antibody (cat. AF1760) was purchased from R&D Systems, USA. Biotinylated rabbit anti-goat IgG antibody was purchased from Dako-Cytomation.

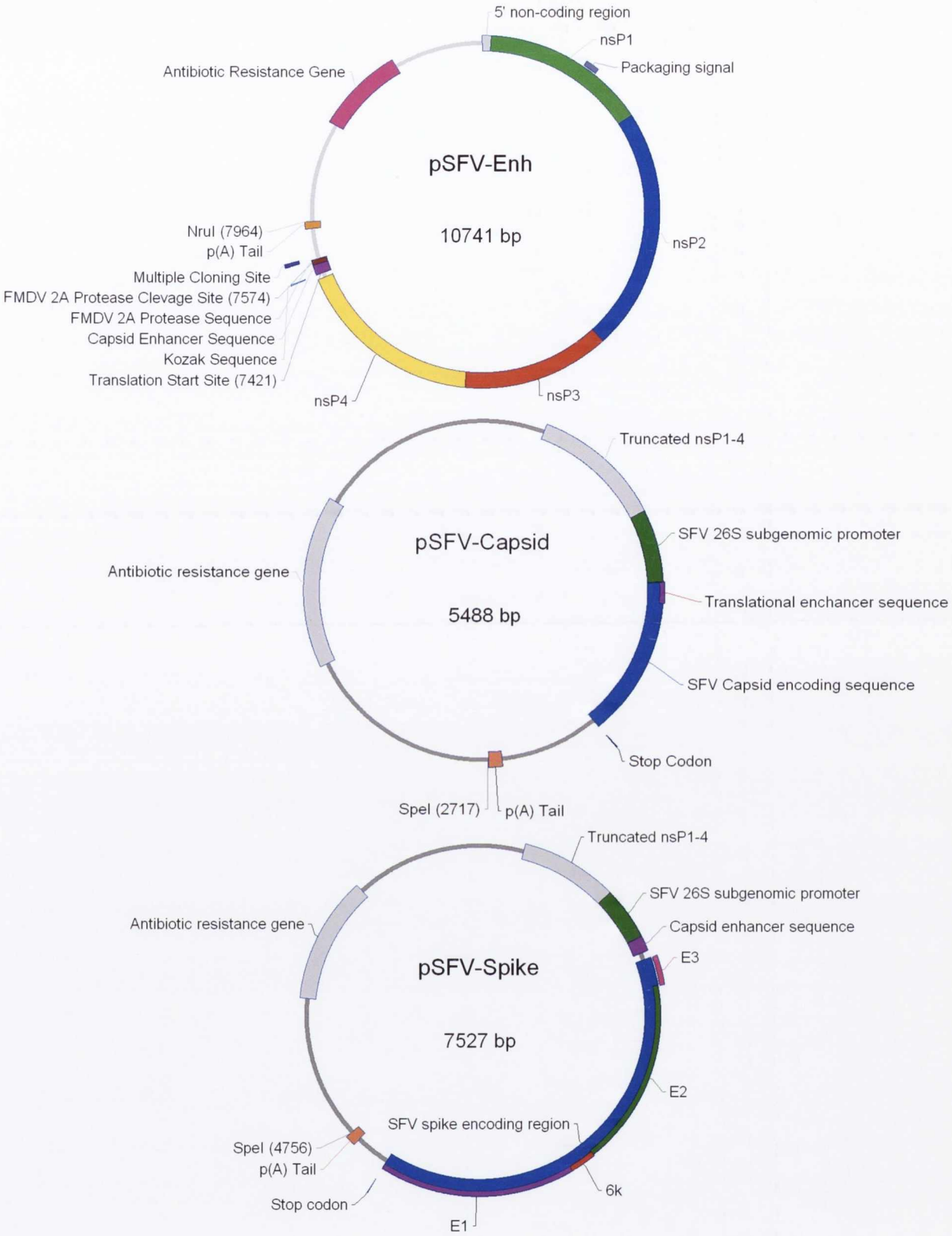

Figure 3.1: Schematic of split helper system plasmids.

Schematic of plasmids used for VLP production. Indicated are the structural ORF, non-structural ORF, multiple cloning site and poly(A) tail. Additionally the endonuclease restriction site used for linearisation, located downstream of the poly(A) tail, is indicated.

3.2.2 New Methods

3.2.2.1 Production of SFV VLPs

3.2.2.1.1 SFV VLP spilt helper system

SFV VLPs are produced by the co-electroporation of 3 mRNA species *in vitro* transcribed from pSFV-Capsid, pSFV-spike and pSFV-Enh. Figure 3.1 is a schematic of the plasmids used for VLP production and indicates the restriction site used for plasmid linerisation.

3.2.2.1.2 Linearisation of plasmids

pSFV-Capsid and pSFV-Spike were linearised by SpeI digestion. pSFV-Enh, pSFV-Enh-IFNβ, pSFV-Enh-IFNγ and pSFV-Enh-IL12 were linearised with NruI for the production of empty, IFN-β, IFN-γ and IL-12 encoding SFV VLPs respectively.

3.2.2.1.3 *In vitro* transcription of DNA

For each set of SFV particles 9μg of capsid, spike and expression plasmid was linearised. Plasmids were purified with the QIAquick® nucleotide removal kit and resuspended in nuclease free water. *In vitro* transcription was carried out as per **2.2.2.4.1** in a final volume of 300μl. 1μl of the reaction was run on a 0.6% agarose gel to confirm adequate RNA for electroporation.

3.2.2.1.4 Electroporation of RNA

Electroporation was carried out as per **2.2.2.4.2** with some minor alterations. Three 150cm^2 flasks of 90-95% confluent S-BHK cells were used for each set of particles; cells were trypsinised, washed, centrifuged and resuspended in 3.9ml of PBS. 300µl of each transcription reaction product was pooled and added to cells prior to electroporation in six 4mm electroporation cuvettes. Following electroporation, cells were pooled in a total volume of 50ml divided into two 150cm^2 tissue culture flasks and incubated for 36-40 hours at 33°C (5% CO_2, 100% RH).

3.2.2.1.5 VLP harvesting and purification

Electroporated cell supernatant was decanted, divided into two sterile 50ml Falcon™ tubes and centrifuged at 4°C for 10 minutes at 4,000rpm (2934.4g). Supernatant was pooled, filtered through a 0.22µm filter and divided into two Beckman ultracentrifuge tubes. 5ml of sterile filtered sucrose (20% w/v in TNE) was gently pipetted into the base of each tube and the volume adjusted with D-PBS. Tubes were centrifuged at 25,000rpm (112,700g) for 2 hours 15 minutes under vacuum at 4°C. After centrifugation supernatant was discarded, the tubes dried and the pellet resuspended in 200µl of sterile TNE (50mM Tris, 0.1M NaCl, 0.1mM EDTA) on ice for 2 hours. VLPs were pooled and tubes washed with a further 200µl of TNE. VLPs were aliquoted into sterile Nunc® CryoTubes™ and frozen at –80°C.

3.2.2.2 Titration of virus-like particles

3.2.2.2.1 Titration of empty virus-like particles

Six-well tissue culture dishes, with 22x22mm coverslips placed on the floor, were seeded with S-BHK cells and grown to 90-95% confluence. VLPs were 10-fold serially diluted in infection medium and used to infect wells in duplicate. Infection proceeded for 1 hour at 37°C with gentle rocking every 15 minutes followed by the addition of 2ml of S-BHK medium per well and incubation at 37°C. 16-20 hours later supernatant was removed and cells washed twice with D-PBS (with Ca^{2+}/Mg^{2+}), fixed for 5 minutes in cold acetone at –20°C and washed twice with PBS. Cells were blocked in 5% NMS in PBS for 1 hour in a

humidified chamber and incubated with a 1/200 dilution of rabbit anti-SFV nSP2 antibody in blocking buffer for 1 hour at RT. Cells were washed twice in PBS-T for 5 minutes each and incubated with biotinylated mouse anti-rabbit IgG antibody (1/1000 in blocking buffer) for 1 hour followed by two washes in PBS-T, as before. Coverslips were incubated with a 1/100 dilution of streptavidin/FITC in PBS for 40 minutes at RT. Coverslips were washed twice for 15 minutes each in high-salt/hepes buffer (0.5M NaCl, 10mM hepes) followed by two 7.5 minute washes in PBS-T, two 5 minute washes in PBS and dipped in distilled water before mounting with VECTASHIELD® Hard Set™ mountant with DAPI.

FITC positive cells were examined by fluorescent microscopy and ten 400x (40x objective, 10x eyepiece) fields counted from each VLP dilution. VLP titers were determined as follows;

VLP titer per ml = $^{1}4035 * ^{2}2 * 10^{x}$

1 – number of 400x fields per well of 6-well tissue culture dish

2- adjust to 1 ml (infection was carried out in 500µl)

x – dilution factor

3.2.2.2.2 Titration of IL-12 encoding virus-like particles

IL-12 encoding SFV VLP titration was carried out as per **3.2.2.2.1** with minor alterations. Cells were first fixed with 4% PFA, washed twice with PBS and permeabilised with cold ethanol:acetic acid (1:2) for 5 minutes at –20°C. Cells were washed twice with PBS and blocked with 5% NRS for 1 hour followed by incubation with a 1/100 dilution of goat anti-rat IL-12 p70 antibody in blocking buffer. A 1/200 dilution of biotinylated rabbit anti-goat IgG antibody and a 1/100 dilution of streptavidin/FITC were used as per **3.2.2.2.1**.

3.2.2.2.3 Titration of IFN-β encoding virus-like particles

IFN-β encoding SFV VLPs were titrated using a 1/1000 dilution of mouse anti-rat IFN-β antibody and remaining reagents as per **3.2.2.2.2**.

3.2.2.2.4 Titration of IFN-γ encoding virus-like particles

IFN-γ encoding VLP titration was carried out as per **3.2.2.2.2**. Cells were blocked with 5% NRS for 1 hour. The primary antibody used was mouse anti-rat IFN-γ (1/100 dilution) and remaining steps were as per **3.2.2.2.2**.

3.2.2.3 Analysis of transgene expression and activity

3.2.2.3.1 Analysis of SFV-Enh-IL12 VLP expression and activity

3.2.2.3.1.1 IL-12 expression

96-well tissue culture plates were seeded with 1 x 10^4 F98, RG2 or BHK cells and allowed to adhere overnight. Cells were recounted and infected in triplicate with empty or IL-12 encoding VLPs (MOI 50). Mock infection was carried out with infection medium alone. Cells were infected in a total volume of 25μl for 1 hour with gentle rocking every 15 minutes. Cell supernatant was harvested at 0, 24, 48 and 72 hours post-infection by placing the appropriate plate at –80°C until assayed.

3.2.2.3.1.2 IL-12 ELISA

The IL-12 ELISA was carried out as per **2.2.2.4.5.**

3.2.2.3.1.3 Splenocyte harvesting

Two 250-300g Fischer 344 rats were killed by anesthetic overdose and cervical dislocation. Spleens were sterilely transferred into 10ml HBSS medium on ice, divided in 3, teased through a 40μm cell strainer and washed 3 times with 4ml of cold HBSS into a sterile 50ml falcon tube. Cells were centrifuged at 1,500rpm (412.65g) for 5 minutes at 4°C, the supernatant discarded, the pellet gently agitated and allowed to stand for 2 minutes before resuspension in 2ml of red blood lysis buffer. Cells were incubated for a further two minutes at RT, centrifuged as before, the supernatant discarded and the pellet resuspended in 10ml of HBSS buffer. Resuspended cells were washed through a 40μm strainer and pelleted as before. The pellet was resuspended in splenocyte maintenance medium,

counted and diluted to $1x10^4$ cells/200µl. $1x10^4$ cells were added to each well of four 96-well tissue culture plates and placed at 37°C.

3.2.2.3.1.4 IL-12 activity

Freshly harvested rat splenocytes were induced in triplicate with a 1/50 or 1/500 dilution of cell supernatant from IL-12 encoding SFV VLP infected BHK cells. Additionally, splenocytes were incubated with a 1/50 dilution of cell supernatant from empty VLP or mock-infected BHK cells. Concanavalin A (5µg/ml) was used as a positive control. Supernatant was harvested at 0, 24, 48 and 72 hours by placing the appropriate plate at –80°C until assayed.

3.2.2.3.2 Analysis of IFN-β expression from IFN-β encoding VLPs

3.2.2.3.2.1 IFN-β expression

IFN-β expression was carried out in 6-well tissue culture dishes. Each well was seeded with $1x10^4$ BHK cells and allowed to adhere overnight. Cells were infected with IFN-β encoding VLPs, empty VLPs (MOI 50) or medium alone in 0.5ml of infection medium. Infection proceeded for 1 hour with gentle rocking every 15 minutes. Each well was supplemented with 2.5ml of BHK medium and supernatant harvested at 0, 24, 48 and 72 hours, spun at 14,000rpm (2934.4g) for five minutes, snap frozen in liquid nitrogen and stored at –80°C.

3.2.2.3.2.2 IFN-β viral inhibition assay

The interferon beta bioassay was carried out as previously described (Quinn, K., 2006), with some minor alterations. L929 cells were grown to confluence, trypsinised, used to seed three 96-well dishes at $1x10^4$ cells/well in 100µl and allowed to adhere overnight. The outer 36 wells were filled with 300µl of PBS and only the inner 60 wells used in order to reduce variation due to evaporation. To each plate, twenty neutralising units of anti-mouse interferon beta antibody (2µg/ml), neutralising anti-mouse interferon gamma antibody (2µg/ml) or medium alone was added in a total volume of 50µl. 10-fold dilutions of mouse interferon beta standard, ranging from 500 to 0.05 units/ml and two-fold dilutions of cell

supernatant from IFN-β, empty and mock infected BHK cells was added to the medium in a total volune of 50µl. Cells were incubated for 24 hours at 37°C, cell supernatant removed, cells washed twice with PBS and infected with SFV-A7 (MOI 100) in 25µl of infection medum. One hour after infection, the inoculum was removed and 100µl of L929 maintenance medium added to each well. 48 hours post-infection, when control wells displayed conplete CPE, 10µl of MTS was added to each well, incubated for 2 hours at 37°C and read at 490nm to determine cell viability.

3.2.2.3.3 Analysis of IFN-γ expression from IFN-γ encoding VLPs

3.2.2.3.3.1 IFN-γ expression

IFN-γ expression was carried out as per **3.2.2.3.2.1** and cells were infected with IFN-γ encoding VLPs, empty VLPs (MOI 50) or medium alone in 0.5ml of infection medium.

3.2.2.3.3.2 IFN-γ ELISA

The IFN-γ ELISA was carried out as per **2.2.2.4.4**

3.2.2.3.3.3 IFN-γ viral inhibition assay

The IFN-γ viral inhibition assay was carried out as **3.2.2.3.2.2**, with some minor alterations. IFN-γ activity was assayed only at a single expression time point (72 hours p.i.). Standard mouse interferon gamma was used in 10-fold dilutions and twenty neutralising units of anti-mouse interferon gamma antibody (0.8µg/ml), neutralising anti-mouse interferon beta antibody (0.8µg/ml) or medium alone was added in a total volume of 50µl to each well of the triplicate plates.

3.3 Results

3.3.1 *In vitro* transcription of plasmid DNA

pSFV-Capsid and pSFV-Spike helper plasmids were linearised by SpeI digestion and the enhanced expression plasmid linearised by NruI digestion. Following *in vitro* transcription, 1μl of each reaction product were examined by agarose gel electrophoresis. The resultant gel demonstrated the presence of two bands for each reaction product (Figure 3.2). The higher molecular weight band indicates template DNA and a lower molecular weight band is the mRNA product. mRNA was considered sufficient for electroporation if 1μl of reaction product had an mRNA band twice the intensity of the 3,000 bp (125ng) DNA band.

3.3.2 Titration of SFV virus-like particles

Cytokine encoding particles were titered using antibodies directed against the encoded transgene and visualised using a FITC-conjugated secondary antibody. Empty VLPs were titered using an anti-SFV or anti-nsP2 antibody. Figure 3.3 is an example of SFV VLP titration by immunoflourescent staining. Ten 400x fields (10x eyepiece, 40x objective) from dilutions amenable to counting were used for VLP titre determination.

3.3.3 Analysis of transgene expression and activity

3.3.3.1 SFV VLP encoded IL-12 expression and activity

Following infection of S-BHK cells with IL-12 encoding VLPs, supernatant was harvested at 0, 24, 48 and 72 hours p.i. and frozen at –80°C until assayed. A commercial IL-12 ELISA was used for the determination of IL-12 in supernatant samples; values were adjusted to $\mu g/10^6$ cells. IL-12 levels were detected at all time points following VLP infection and maximum expression was seen at 48 and 72 hours in all cell lines with no statistical difference between either time point for any cell line ($p=0.9925$, Two-Way ANOVA). Mock and empty VLP infected cells demonstrated no detectable IL-12 expression in any cell line at any time point. Figure 3.4 includes the average IL-12 levels among the three cells line following mock or empty VLP infection. At 72 hours post-infection, levels of IL-12 from infected BHK cells were 1.5-fold (1.53±0.26-fold, $p<0.05$, One-Way ANOVA) that of RG2 cells and four-fold that of F98 cells (4.169±0.712-fold, $p<0.001$, One-Way ANOVA).

The VLP encoded IL-12 p70 protein was examined for activity by incubation of freshly harvested rat splenocytes with dilutions of supernatant from VLP infected BHK cells. Splenocytes ($1x10^4$/well) were incubated with a 1/50 dilution of mock or empty VLP infected BHK cell supernatant or a 1/50 or 1/500 dilution of IL-12 encoding VLP infected BHK cell supernatant. Additionally, concanavalin A (5μg/ml) and a 1/50 dilution of BHK medium were used as a positive and negative control respectively. Splenocyte medium was harvested at 0, 24, 48 and 72 hours after incubation and assayed by commercial IFN-γ ELISA for the presence of IFN-γ. The presence of IFN-γ was detected at all time points measured for both dilutions of IL-12 containing supernatant and con A stimulated cells (Figure 3.5). There was no statically significant difference in IFN-γ levels between a 1/50 and 1/500 dilution of IL-12 encoding VLP infected BHK cell supernatant at any time point measured ($p=0.8697$, Two-Way ANOVA).

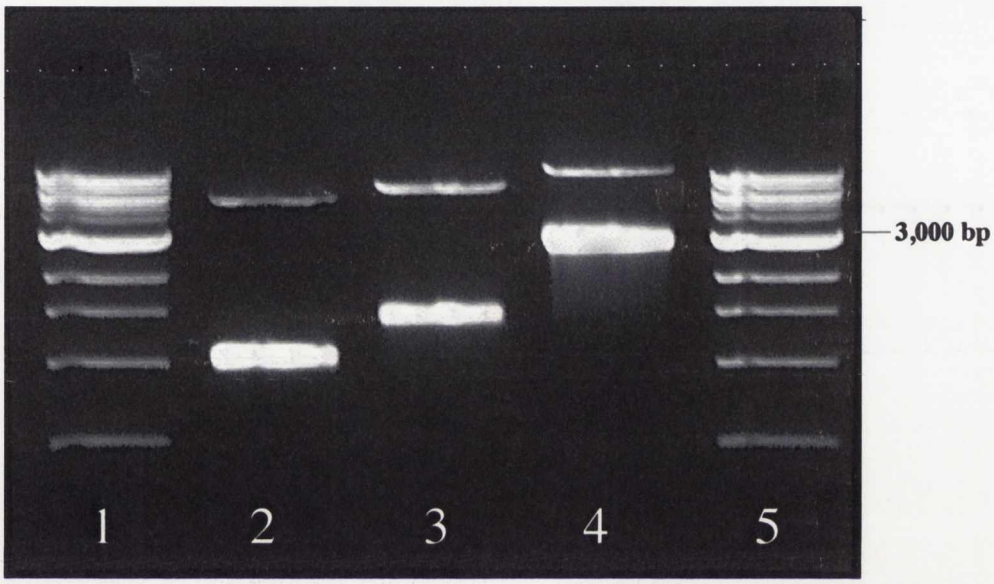

Figure 3.2: *In vitro* transcribed capsid, spike and expression vector mRNA prior to electroporation.

Lanes 1 and *5* are 1 kb DNA marker. *Lanes 2, 3* and *4* are 1µl of *in vitro* transcription products from capsid, spike and expression vector reactions respectively. In all cases the higher molecular weight band is DNA template and the lower molecular weight band mRNA product. An mRNA band twice the intensity of the 3,000 bp DNA band is considered sufficient for electroporation

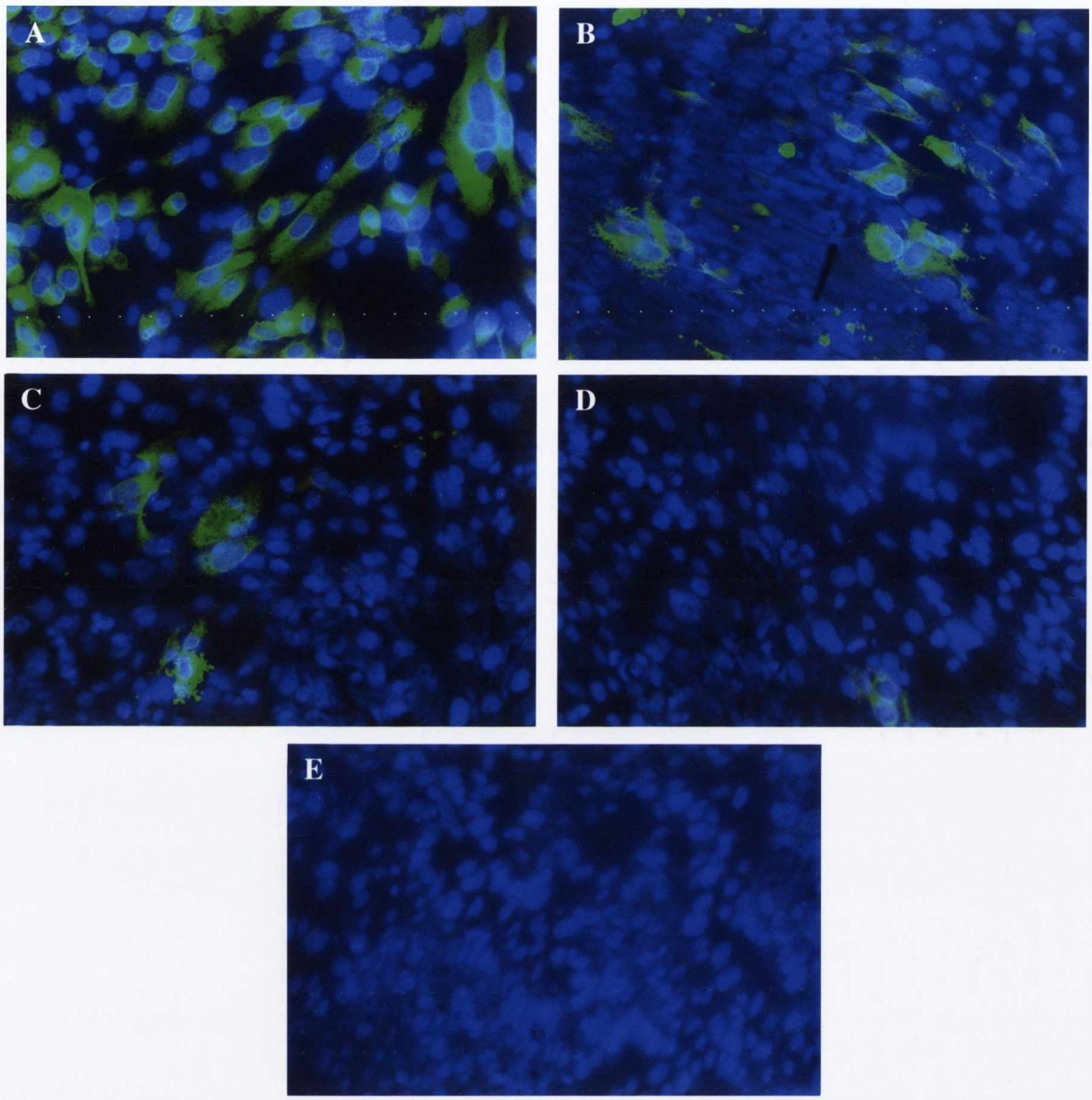

Figure 3.3: Titration of SFV VLPs by immunoflourescent staining.

SFV VLPs were titered by immunoflourescent staining of the encoded transgene or nsP2 protein. S-BHK cells were infected with 10-fold serial dilutions and dilutions amenable to counting were used to determine VLP titer. Images **A** – **D** represent ten-fold serial dilutions of SFV VLPs from 10^{-3}-10^{-6}. Image **E** represents mock-infected cells.

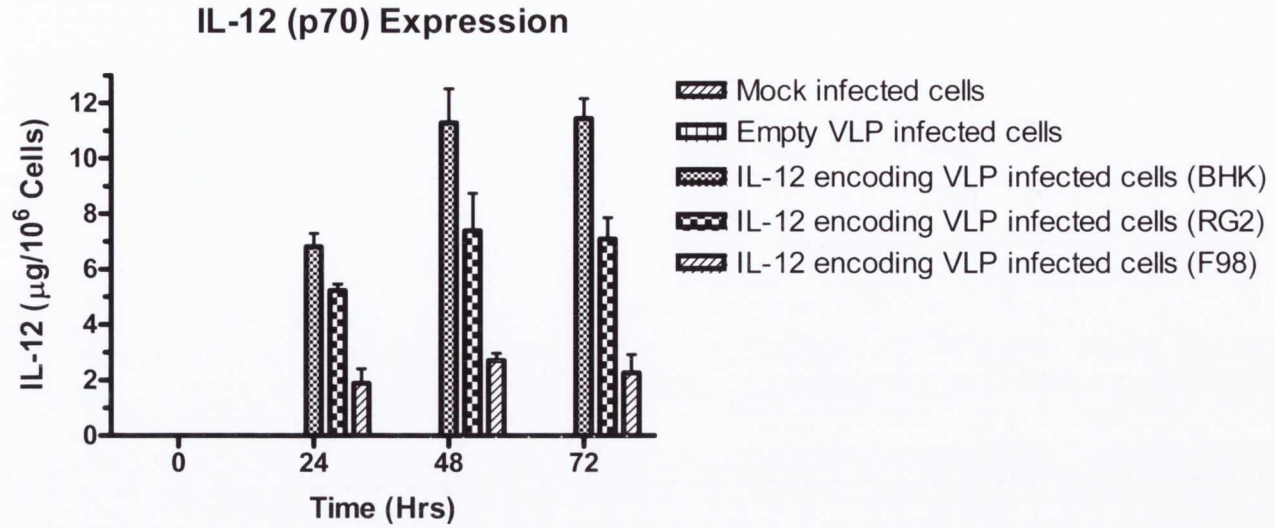

Figure 3.4: IL-12 expression by IL-12 encoding VLPs.

BHK, F98 or RG2 cells were mock infected or infected with empty or IL-12 encoding VLPs at MOI 50. IL-12 levels were adjusted to $\mu g/10^6$ cells. Empty VLP and mock infected IL-12 levels represent the average among the 3 cell lines tested and were negligible at all time points assayed.

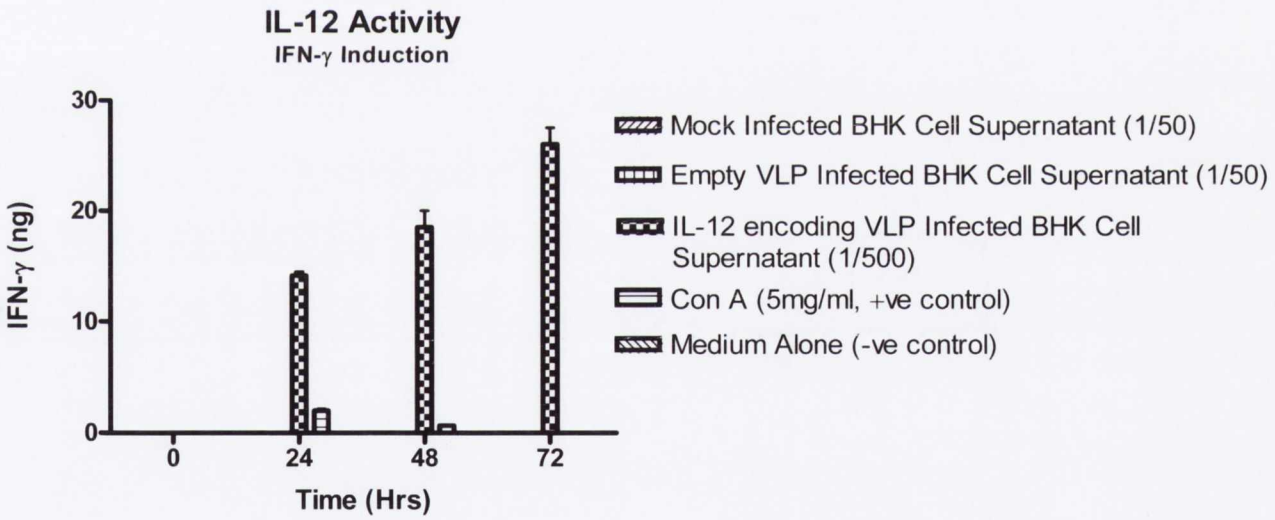

Figure 3.5: IFN-γ induction by SFV VLP encoded IL-12.

Splenocytes ($1x10^4$ cells/well) were incubated with medium from mock, empty VLP or IL-12 VLP infected BHK cells. Medium was harvested at 0, 24, 48 and 72 hours and assayed for the presence of IFN-γ by ELISA. IFN-γ induction by Con A was low relative to IL-12 incubated splenocytes although IFN-γ was present at all time points measured.

3.3.3.2 SFV VLP encoded IFN-β expression and activity

The IFN-β viral inhibition assay was used for the simultaneous quantification of IFN-β expression and confirmation of activity. Standard IFN-β ($3.9x10^7$ IU/mg), in 10-fold serial dilutions, was included and the IFN-β concentration that produced 50% protection from SFV infection was used to extrapolate the amount of IFN-β in each sample (Table 3.1). As additional controls, neutralising anti-IFN-β antibody (20 neutralising units per ml, 2μg/ml), anti-IFN-γ antibody (2μg/ml) or medium alone was added to each well. The viral inhibition assay results were used to determine levels of IFN-β from VLP infected cells and values adjusted to units/10^6 cells (Figure 3.6).

IFN-β expression was detected at all time points assayed with maximum expression at 24 hours at 320,000 units/10^6 cells. Mean levels decreased until 72 hours with a statistical decrease between 24 and 72 hours ($p<0.05$, One-Way ANOVA). Negligible IFN-β levels were detected in mock or empty VLP infected cell supernatant. The addition of anti-IFN-β antibody reduced the apparent concentration of IFN-β by approximately one dilution (two-fold) while the addition of the IFN-γ antibody had no effect (data not shown). IFN-β levels as measured by bioassay corresponded approximately to 8.2μg per 10^6 cells at 24 h.p.i.

3.3.3.3 SFV VLP encoded IFN-γ expression and activity

IFN-γ expression from VLP infected BHK cells was measured by commercial ELISA. BHK cells were infected with medium alone, empty VLPs or IFN-γ encoding VLPs (MOI of 50). Supernatant was harvested at 0, 24, 48 and 72 hours p.i. and assayed for the presence of IFN-γ (Figure 3.7). IFN-γ expression was observed at all time points post-infection in IFN-γ encoding VLP infected BHK cell supernatant. Maximum expression was observed at 48 and 72 hours p.i. at approximately 20μg/10^6 cells with no significant difference between either time point (p=0.6337, Two-Sample T test).

IFN-γ activity was measured by viral inhibition assay at a single time point (72 h.p.i.) to confirm IFN-γ activity. The viral inhibition assay was carried out similarly to **3.3.3.2** and standard IFN-γ (1x10^7 IU/mg), in 10-fold serial dilutions, was included and the IFN-γ concentration that produced 50% protection from SFV infection used to extrapolate IFN-γ in samples. Controls included neutralising anti-IFN-γ antibody (20 neutralising units per ml, 0.8μg/ml), anti-IFN-β antibody (0.8μg/ml) or medium alone. The viral inhibition assay results were used to determine levels of IFN-γ from infected cells and were adjusted to IU/10^6 cells (Figure 3.8). IFN-γ activity was demonstrated in supernatant from IFN-γ VLP infected BHK cells correlating to 533,333 (± 76,700) IU per 10^6 cells. Negligible IFN-γ levels were detected in mock or empty VLP infected cell supernatant. The addition of anti-IFN-γ antibody reduced the apparent concentration of IFN-γ by approximately 1 dilution while the addition of the IFN-β antibody had no effect (data not shown). IFN-γ levels as measured by viral inhibition assay corresponded to approximately 53.33 (± 7.67) μg per 10^6 cells, similar to levels measured by ELISA.

		Standard IFN-β	IFN-β VLPs	Empty VLPs	Mock infected
0 hrs	Dilution exhibiting 50% CPE	1/220,000	< 1/10	< 1/10	< 1/10
	IFN-β (U/ml)	0.5	< 5	< 5	< 5
24 hrs	Dilution exhibiting 50% CPE	1/220,000	1/2133	1/20	1/10
	IFN-β (U/ml)	0.5	1066.5	10	5
48 hrs	Dilution exhibiting 50% CPE	1/220,000	1/1778	1/16	1/16
	IFN-β (U/ml)	0.5	889	8	8
72 hrs	Dilution exhibiting 50% CPE	1/220,000	1/1422	< 1/10	1/16
	IFN-β (U/ml)	0.5	711	< 5	8

Table 3.1: IFN-β viral inhibition assay.

IFN-β viral inhibition assay was used to determine IFN-β expression from BHK cells infected with IFN-β encoding, empty or TNE and values represent averages. Standard IFN-β was included to quantify, in terms of international units, IFN-β in samples.

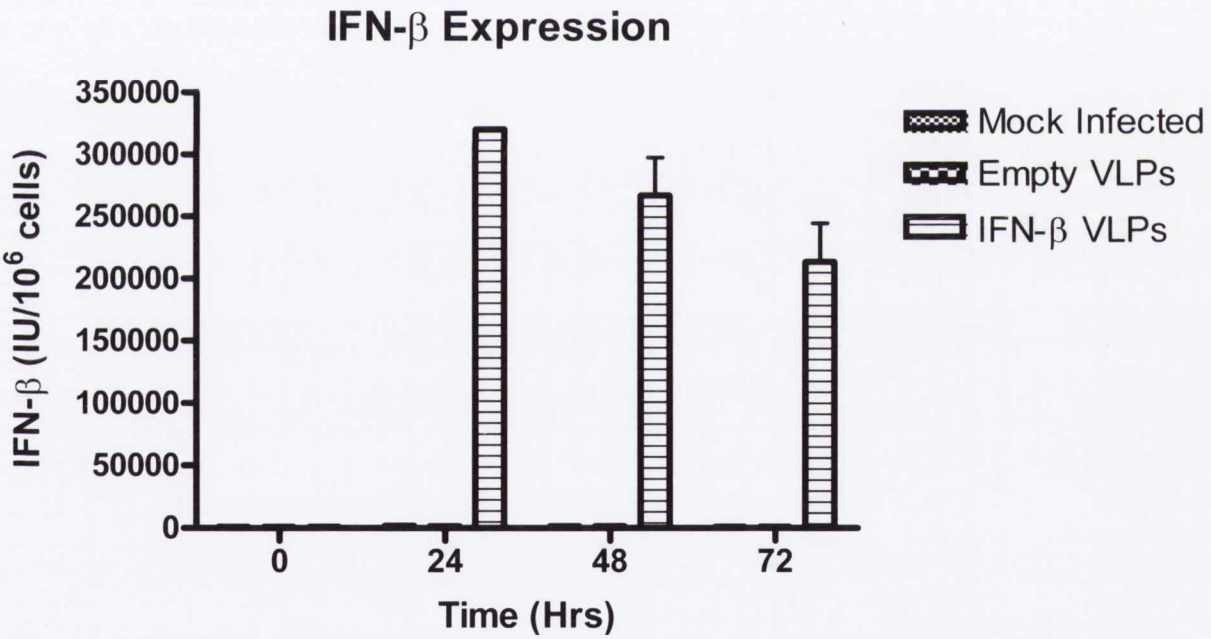

Figure 3.6: IFN-β expression by IFN-β VLPs.

Viral inhibition assay results were used to determine IFN-β expression from mock, empty VLP or IFN-β encoding VLP infected BHK cells at an MOI of 50. Values were adjusted to international units (IU) per 10^6 cells.

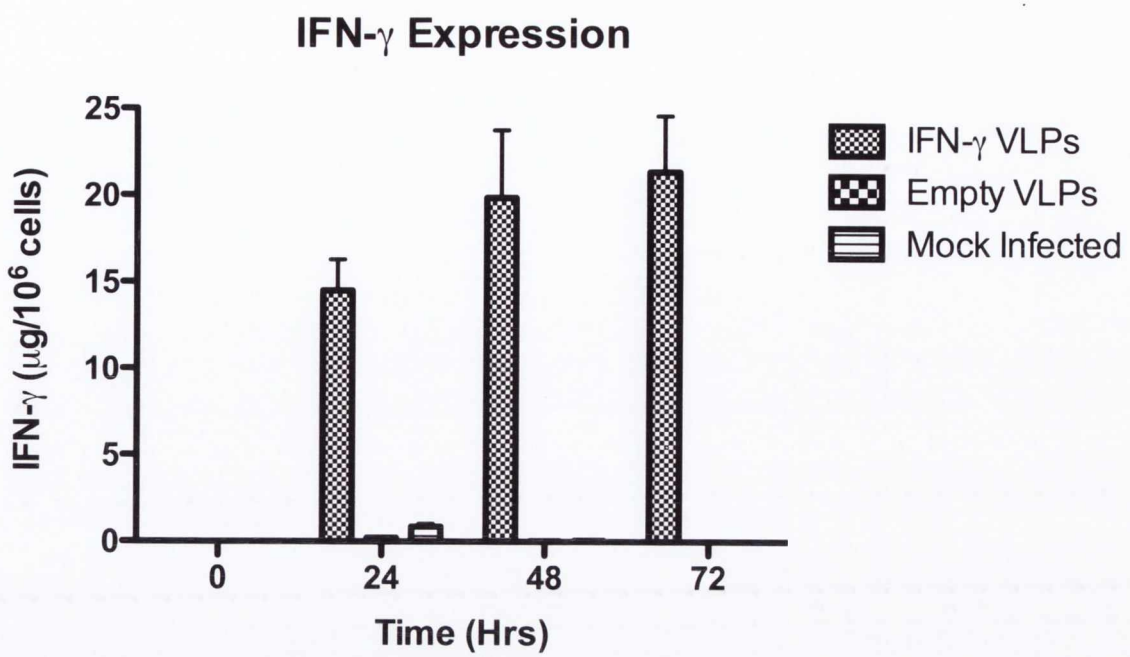

Figure 3.7: IFN-γ expression from IFN-γ encoding VLPs.

BHK cells were mock infected or infected with empty VLPs or IFN-γ VLPs at an MOI of 50. IFN-γ expression was assayed by commercial ELISA and results were adjusted to $\mu g/10^6$ cells.

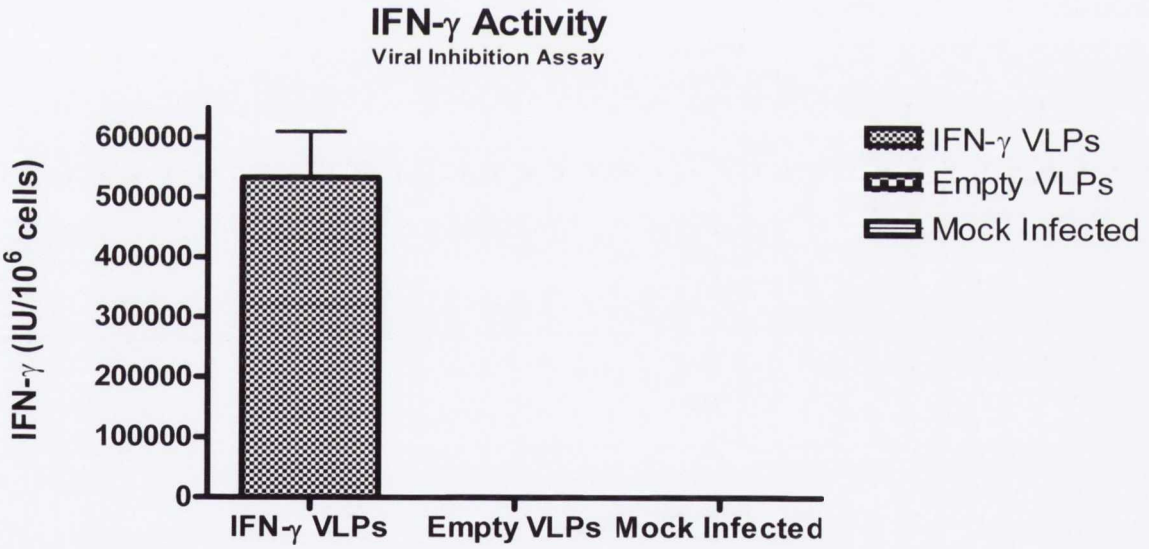

Figure 3.8: IFN-γ viral inhibition assay.

Viral inhibition assay results were used to determine IFN-γ expression from mock, empty VLP or IFN-β encoding VLP infected BHK cells (MOI 50, 72 h.p.i). Values were adjusted to international units (IU) per 10^6 cells.

3.4 Discussion

Virus-like particles encoding each of the IFN-γ, IFN-β and IL-12 transgenes were produced and titered by indirect immunofluorescence directed against the encoded transgene. Titers of 10^{10} were routinely obtained in volumes of 0.6 - 1ml. IFN-β expression was examined in cell supernatant at a number of time points following infection of BHK cells with IFN-β encoding VLPs. IFN-β expression and activity were examined concurrently by viral inhibition assay. Due to an absence of an international unit calibration for rat IFN-β, samples were titrated against a mouse IFN-β standard, as used by other commercial bioassays (PBL Interferon Source, USA). IFN-β expression was present at all time points assayed with maximal expression at 24 hours at 320 $x10^3$ IU/10^6 cells, corresponding to 8.2μg of IFN-β per 10^6 cells. Incubation of samples with either anti-mouse IFN-β antibody (standard) or anti-rat IFN-β antibody (samples) demonstrated a negation of inhibition indicating that the anti-viral effect was due to the presence of IFN-β.

Expression of IFN-γ was examined in cell supernatant following infection of BHK cells with IFN-γ encoding VLPs. Supernatant was harvested at a number of time point after infection and examined for the presence of IFN-γ by commercial ELISA. IFN-γ expression was evident at all time points tested post-infection and peaked at 48-72 hours p.i. at 21.37 (±1.86) μg per 10^6 cells. IFN-γ activity was measured at a single time point (72 hrs p.i.) by viral inhibition assay using mouse IFN-γ as a standard for sample titration. At 72 hours p.i., 533 $x10^3$ IU/10^6 cells of IFN-γ was detected by viral inhibition assay, corresponding to 53.33 (±4.42) μg, similar to levels estimated by ELISA.

IL-12 encoding VLPs were used to infect BHK, F98 or RG2 cells; medium was harvested at 0, 24, 48 and 72 hours p.i. and examined for the presence of rat IL-12 by commercial ELISA. IL-12 expression was evident from 24 hours with maximal levels detected at 48 and 72 hours, at approximately 11 μg/10^6 cells. This is comparable with expression levels previously described for IL-12 expressed from the enhanced expression vector in our laboratory (Chikkanna-Gowda, CP., 2005). However, Rodriguez-Madoz *et al.* (2005) demonstrated expression of murine IL-12 from SFV-Enh corresponding to approximately 124 μg/10^6 BHK cells; although the cloning strategy used for the production of pSFV-Enh-IL12, constructed in this project, and the strategy used in the above mentioned publication are essentially identical, the disparity in expression levels is unknown. The activity of VLP encoded IL-12 was confirmed by incubation of freshly harvested rat splenocytes with supernatant from SFV VLP infected cells. Dilutions of 1/50

and 1/500 of IL-12 containing supernatant showed similar levels of IFN-γ induction; although this suggests a saturation effect it is nonetheless indicative of the production of biologically active IL-12. Thus the SFV VLP system was successfully used to express biologically active IFN-γ, IFN-β and IL-12 *in vitro*.

Chapter 4

Characterisation of SFV VLP infection and apoptosis induction in two rat glioma cell lines

4.1 Introduction

The alphaviruses mediate cell entry by receptor-mediated endocytosis; studies to elucidate the specific receptors responsible have demonstrated a number of salient points. Firstly, the alphaviruses have a large host-range and there are a wide variety of permissive cells within each host. Secondly, the receptors used are, or are partially, proteinaceous in nature and viruses may use one or several receptors, potentially shared by other members of the alphavirus genus (Strauss and Strauss, 1994). A number of minor and major Sindbis (SIN) virus receptors have been identified and include the high affinity laminin receptor, considered the major SIN receptor in mammalian cells (Wang *et al.*, 1992). Although it had previously been reported that SFV bound cell-surface MHC antigens (Helenius *et al.*, 1978) their putative role as the sole or necessary receptors for SFV entry has since been refuted (Oldstone *et al.*, 1980) and the major cell receptors for SFV entry remain to be elucidated. Despite the ignorance of specific receptors, SFV is known to infect a large variety of mammalian cells *in vitro* and *in vivo* (Strauss and Strauss, 1994) and a number of studies have demonstrated infection of neoplastic cells lines (Murphy *et al.*, 2000; Smyth *et al.*, 2005; Chikkanna-Gowda *et al.*, 2006).

Whatever the specific cellular factors determining permissiveness, the fate of cells infected with SFV VLPs is almost certainly apoptosis, initiated either by the cell itself or cytotoxic immune cells. Apoptosis is an energy-dependant cell death process and a number of comprehensive reviews are available on the subject (Schultz and Harrington, 2003; Zhang *et al.*, 2004a; Elmore, S., 2007). Cell death by apoptosis is an essential element in growth and development, the control of cell populations and as a defensive response to noxious stimuli. Apoptosis is characterised by a number of morphological and biochemical changes including cell shrinkage, nuclear condensation and fragmentation, protease activation, plasma membrane blebbing and apoptotic body budding. Apoptosis is distinct from necrosis in so far as it does not result in an inflammatory process or direct release of cytoplasmic factors into the surrounding interstitial fluid. There are three major pathways leading to the induction of apoptotic cell death: the intrinsic, extrinsic and granzyme pathways. The extrinsic and granzyme pathways rely on external factors for the induction of cell death with the former mechanism primarily reliant on ligand/receptor binding including, but not limited to, the FasL/FasR and TNF-α/TNFR1 interactions. The granzyme/perforin pathway is an apoptosis inducing mechanism induced by cytotoxic T cells on aberrant cells such as tumor or virus-infected cells. The intrinsic pathway, the

mechanism most pertinent to virus-infected cells, particularly in tissue culture, is initiated by internal cellular signals such as virus infection, toxins and other noxious stimuli. Although the initiation and initial propagation of these pathways differ, there is significant crosstalk between them and they eventually converge upon the activation of a family of cellular cystine-aspartic acid proteases, called caspases. The activation of executioner caspases including caspase-3, 6 and 7 results in cleavage of a variety of cellular substrates ultimately leading to the morphological changes apparent in apoptotic cells.

The induction of apoptosis by SFV VLPs is in an important consideration in the use of SFV VLPs *in vivo*. Although apoptosis will limit transgene expression, in a tumor therapy model, apoptosis induction in tumor cells may provide some temporary reduction in tumor volume and potentially provide tumor-derived antigens to the immune system via cross-presentation, presumably the mechanism of an adaptive immune response induction, where it occurs, in replicating SFV tumor therapy. It is also noteworthy that unlike mosquito cell infection, which results in a persistent infection, almost all permissive mammalian cells undergo apoptosis following alphavirus infection, the primary exception being mature neurons. Several studies have examined the mechanism of SFV-induced apoptosis; it had previously been demonstrated that the SFV-mediated induction of apoptosis was not dependant on the structural genes but upon viral replication and was independent of cellular p53 status (Glasgow *et al.*, 1998). Furthermore, Urban *et al.* (2008) demonstrated that apoptosis induction was initiated via the intrinsic pathway involving the loss of mitochondrial potential, cytochrome c release into the cytosol followed by caspase activation. Additionally, it was established that members of the extrinsic pathway were activated downstream of cytochrome c release able to mediate apoptosis in the absence of key members of the intrinsic pathway.

This chapter examines the ability of the SFV VLP system to infect two rat glioma cell lines *in vitro* and induce apoptosis in infected cells. Additionally, the ability of the VLP system to infect cells *in vivo* and mediate transgene expression therefrom will be examined.

4.2 Experimental Procedures

4.2.1 New Materials

4.2.1.1 Flow cytometry

VLP infected cells were analysed for the presence of GFP fluorescence on an Epics XL flow cytometer using the EXPO™ 32 ADC software v1.1c Beckman Coulter (USA).

4.2.1.2 Immunofluorescence reagents

Biotinylated polyclonal rabbit IgG anti-active caspase-3 antibody (cat. 557038) was purchased from BD Biosciences. DakoCytomation pen was purchased from DakoCytomation. Triton X-100 and sodium citrate were purchased from Sigma-Aldrich.

4.2.1.3 Immunohistochemistry reagents

Frozen sections were processed on a Leica CM1900 cryostat (Leica Microsystems, Germany). SuperFrost® slides were purchased from Menzel-Gläser®. Hydrogen peroxide, Tris buffered saline tablets, normal serum, 3,3'-diaminobenzidine (DAB), trypsin tablets, phosphatase inhibitor cocktail I and II, and protease inhibitor cocktail were purchased from Sigma-Aldrich. Mayer's haematoxylin was purchased from DakoCytomation. VECTASTAIN® ABC kits were purchased from Vector Laboratories. Tissue-Tek® O.C.T. compound, methanol, hydrochloric acid (HCL), xylene and D.P.X. mountant were purchased from BDH.

4.2.1.4 Miscellaneous

Cells were centrifuged using a Shandon Cytospin 2 centrifuge and cytofunnel® disposable sample chambers (ThermoScientific). Poly-L-lysine coated glass slides were purchased from Sigma-Aldrich. Tissue samples were homogenised using a RZR1 homogeniser from Heidolph (Germany). Bradford reagent was purchased from Sigma-Aldrich.

4.2.1.5 Reagents for *in vivo* experimentation

The stereotaxic apparatus was purchased from Stoelting, USA. BD Plastipak™ syringes and BD Mircolance™ 3 needles were purchased from Becton Dickinson (USA). Baytril® (2.5% enrofloxacin) and Rompun® (2.33% w/v xylazine hydrochloride) were purchased from Bayer Healthcare, Germany. Vetalar™ V (10% ketamine hydrochloride) was purchased from Pharmacia, Sweden. Rimadyl® solution (5% carpofen) was purchased from Pfizer, USA. Simplex Rapid™ dental cement was purchased from Kemdent®, UK. SURGIPRO™ VPF-735 polypropylene sutures were purchased from Covidine (USA). Vidisic® 0.2% (w/w) carbomer gel was purchased from Pharma-Global (Germany). Betadine® (7.5% w/v povidone-iodine) surgical scrub was purchased from Steon Healthcare group (UK). IsoFlo® isoflourane inhalation anaesthetic was purchased from Abbot Laboratories Ltd., UK. Fused silica guide cannulas (23 gauge, 1.6mm projection below pedestal), dummy cannulas (cut to fit guide cannulas) and nylon microscrews (2.25mm head diameter, 2.4mm shaft length) were purchased from Plastics One® Inc. (USA). Lignospan special solution for injection (20mg/ml lidocain hydrochloride and 12.5μg/ml epinephrine bitartate) was purchased from Septodont, USA. Cicatrin™ powder (3,300 units/g neomycin sulphate and 250 units/g bacitacin zinc) was purchased from GSK, USA.

4.2.2 New Methods

4.2.2.1 *In vitro* experimentation

4.2.2.1.1 EGFP encoding VLP production

EGFP encoding SFV VLPs were produced as per **3.2.2.1**.

4.2.2.1.2 Titration of EGFP encoding VLPs

Six-well tissue culture dishes, with 22x22mm cover slips placed on the floor, were seeded with S-BHK cells and allowed grow to 90-95% confluence. 10-fold dilutions of VLPs were made in infection medium and used to infect wells in duplicate. Infection was carried out in a total volume of 0.5ml and proceeded for 1 hour at 37°C with gentle rocking every 15 minutes followed by the addition of 2ml of S-BHK medium per well. Cells were placed at 37°C for 16-20 hours, the supernatant removed and the cells washed twice with D-PBS (with Ca^{2+}/Mg^{2+}), fixed for 20 minutes in the dark with 4% PFA and washed twice further with PBS. Coverslips were mounted and examined by fluorescent microscopy.

4.2.2.1.3 Analysis of glioma cell line infection by the SFV VLP system

4.2.2.1.3.1 SFV VLP infection of glioma cell lines

F98, RG2 and BHK cells were used to seed 6-well tissue culture dishes at $1x10^5$ cells per well and allowed to adhere overnight. Cells were recounted, washed twice with PBS and infected with EGFP encoding VLPs at an MOI of 0, 1, 10, 50 and 100. Infection was carried out in a total volume of 0.5ml for 1 hour with gentle rocking every 15 minutes. Following infection, 2.5ml of maintenance medium was added to each well and incubated for 18 hours at 37°C. Cells were trypsinised and supernatant and trypsinised cells pooled, spun at 1,500rpm (412.65g) for 8 minutes and resuspended in 1ml of 4% PFA. Cells were incubated at 4°C until examined by flow cytometry.

4.2.2.1.3.2 Flow cytometric analysis of EGFP encoding VLP infected cells

10,000 cells were analysed in each sample, in triplicate, and results expressed as percentage GFP positive cells compared to uninfected controls.

4.2.2.1.4 Analysis of VLP induced apoptosis in glioma cell lines

4.2.2.1.4.1 Infection of glioma cells

F98, RG2 or BHK cells were used to seed 6-well tissue culture dishes at a concentration of $1x10^5$ cells per well and allowed to adhere overnight. Cells were then recounted and infected with empty, IL-12 encoding VLPs, SFV4 replicating virus (MOI 50) or medium alone. Cells were harvested at 0, 24, 48 and 72 hours post-infection.

4.2.2.1.4.2 Harvesting of cells

Cell supernatant from infected cells was removed to a 7ml bijoux tube, cells were trypsinised and the wells washed twice with PBS. Supernatant, cells and wash PBS were pooled, diluted to 50ml with PBS and centrifuged at 1,500rpm (412.65g) for 8 minutes at 4°C, resuspended in 1ml of 4% PFA and incubated in the dark at RT for at least 20 minutes. Cells were placed in a cytofunnel® disposable sample chamber and spun at 1,500rpm (412.65g) for 10 minutes on a Cytospin® 2 centrifuge onto poly-L-lysine coated glass slides.

4.2.2.1.4.3 Immunoflourescent detection of active caspase-3.

Cells were analysed for the presence of active caspase 3 as previously described (Smyth, 2004). After centrifugation onto poly-L-lysine slides, cells were outlined using a DakoCytomation pen, washed for 5 minutes in PBS and permeabilised for 2 minutes in a 0.1% solution of Triton X-100 in 0.1% sodium citrate in PBS at 4°C. Cells were then washed twice in PBS for 5 minutes each, blocked in 5% NRS in PBS for 1 hour at RT in a humidified chamber. Cells were washed briefly in PBS and incubated with 40µl of a 1/40 dilution of biotinylated anti-active caspase-3 antibody for 18 hours at 4°C in a humidified chamber. Cells were washed twice for 5 minutes each in PBS and incubated with a 1/100

dilution of streptavidin/FITC in PBS for 40 minutes followed by two 15 minute washes in high salt/hepes buffer, two 7.5 minute washes in PBS-T, two 5 minute washes in PBS and dipped in distilled water before mounting with VECTASHIELD® mountant with DAPI. FITC fluorescence was analysed by fluorescent microscopy.

4.2.2.1.4.4 Immunoflourescent detection of viable cells

Cells were prepared as per **4.2.2.1.4.3** and viable nuclei enumerated by fluorescent microscopy.

4.2.2.2 *In vivo* experimentation

4.2.2.2.1 Surgical implantation of cannula

250-300g Fischer 344 rats were anesthetised by i.p. injection with xylazine/ketamine mix (0.3ml per 100g of 17.5mg/ml ketamine, 3.75mg/ml xylazine). Animals received Rimadyl™ (50mg carpofen per kg) as analgesia prior to surgery. The scalp was shaved, swabbed with iodine/ethanol solution and 100µl of lidocain/adrenalin was delivered under the scalp. The initial incision was made along the midline, the scalp cleaned and the bregma identified. The implant site was stereotaxically measured 3.9mm back and 2.5mm right from the bregma. Three holes were drilled around the implant site and plastic microscrews screwed into the skull. A plastic cannula was placed into the implant hole and fixed in place with dental cement. Animals were recovered under a heat lamp until the reappearance of a pedal reflex.

4.2.2.2.2 Inoculation of glioma cells

Passage 6 to 8 F98 or RG2 cells were trypsinised, resuspended in 10ml of glioma cell maintenance medium and counted with a haemocytometer. Cells were diluted to 50ml in PBS and centrifuged at 1,500rpm (412.65g) for 8 minutes. The supernatant was discarded, cells resuspended to 5,000cells/µl in PBS, and stored on ice for no more than 1 hour. Implanted rats were anesthetised by inhalation with 5% isoflourane vaporised with 100% medical oxygen. Animals were maintained with 3% isoflourane on a heated pad for the duration of the experiment. Animals were placed in a stereotaxic rig, the dummy cannula

removed and the cannula cleared of any obstructions using a 25-gauge sterile needle. 0.4μl (2000 cells) of glioma cells were then injected into the hippocampal coordinates (3.5mm down from the skull) with a 10μl 26s-gauge sterile Hamilton syringe. The syringe was held in place for 5 minutes, withdrawn and the dummy cannula replaced before the animal was recovered from anaesthetic.

4.2.2.2.3 Intracerebral delivery of SFV VLPs.

SFV VLPs were delivered similarly to **4.2.2.2.2**. Animals were anesthetised with 5% isoflourane and maintained with 3% isoflourane on a heated pad throughout the experiment. The animal was placed in a stereotaxic rig, the particles thawed immediately prior to use and 5μl injected into the coordinates used for glioma implantation at a rate of 1μl/min. The syringe was then held in place for 3 minutes, withdrawn and the animal recovered.

4.2.2.2.4 Culling of animals and tissue processing

48 hours after VLP delivery, animals were culled by isoflourane overdose, the head removed and brain extracted. For ELISA cytokine analysis the area containing the tumor was excised, two volumes of Krebs buffer added (136mM NaCl, 2.56mM KCl, 1.18mM KH_2PO_4, 2.24mM $MgSO_4$, 16mM $NaHCO_3$ 10mM Glucose, 13.24mM $CaCl_2$ with protease and phosphatase inhibitors) and homogenised. Samples were stored at –80°C until assayed at which point samples were thawed, spun at 14,000rpm (2934.4g) for 5 minutes and analysed by commercial rat IL-12 ELISA.

For immunohistochemical analysis, animals were culled by isoflourane overdose, the brain extracted and divided sagittally into both hemispheres. A coronal section of approximately 1-2 mm anterior and posterior to the inoculation site was excised embedded in O.C.T. compound and frozen in liquid nitrogen-cooled isopentane before storage at –80°C. OCT embedded brains were allowed to warm to –20°C and 4μm sections cut and placed onto glass slides. Sections were air-dried and stored at –20°C until immunohistochemical analysis.

4.2.2.2.5 ELISA analysis of *in vivo* IL-12 expression

IL-12 was quantified by commercial ELISA and carried out as per **2.2.2.4.5**. Total soluble protein concentration was determined by Bradford assay and IL-12 expression standardised per mg of total soluble protein.

4.2.2.2.6 Immunohistochemical detection of SFV antigen

Frozen sections were thawed, air-dried and fixed in 4% NBF in the dark for 20 minutes. Slides were washed three times for 5 minutes each in PBS and sections outlined using a DakoCytomation pen. Antigen retrieval was carried out by trypsin digestion for 7 minutes at 37°C followed by two PBS washes as above. Endogenous peroxidase quenching was carried out by incubation of slides with 0.9% H_2O_2 in 100% methanol for 30 minutes in the dark at RT. Sections were blocked with 5% NGS at RT for 30 minutes. Blocking serum was decanted and slides incubated with a 1/200 dilution of rabbit anti-SFV4 or anti-nSP2 antibody at 4°C for 18 hours. Slides were washed twice for 5 minutes each with PBS and incubated for 30 minutes at RT with goat anti-rabbit IgG biotinylated secondary antibody supplied with the VECTASTAIN® Elite ABC kit, as per manufacturer's instructions. Slides were washed twice further with PBS for 5 minutes each and incubated with ABC reagent for 30 minutes at RT. Slides were washed twice for 5 minutes each in PBS and incubated for approximately 2 minutes with DAB substrate. Slides were washed in running water for 2 minutes, stained for 30 seconds with Mayer's haematoxylin and washed for 2 minutes in running water. Slides were clarified by incubation for 10 seconds in acid-alcohol (2.5% conc. HCl in 70% EtOH) and rinsed in running water for 2 minutes. Slides were dehydrated by incubation for 2 minutes each in 80% EtOH, twice in 100% EtOH and twice in 100% xylene before mounting with D.P.X. mountant.

4.2.2.2.7 Immunohistochemical detection of IL-12

Frozen sections were fixed/permeabilised in cold ethanol:acetic acid (2:1) for 5 minutes at –20°C. Sections were blocked with 5% NRS at RT for 30 minutes. Blocking serum was decanted and slides incubated with a 1/1000 dilution of goat anti-rat IL-12 antibody at 4°C for 18 hours. Slides were washed twice for 5 minutes each with PBS and incubated for 30 minutes at RT with rabbit anti-goat IgG biotinylated secondary antibody supplied with the

VECTASTAIN® Elite ABC kit, as per manufacturer's instructions. The remaining steps were carried out as per **4.2.2.2.6**.

4.3 Results

4.3.1 *In vitro* analysis

4.3.1.1 SFV VLP infection efficiency of glioma cell lines

BHK, F98 and RG2 cells were infected with EGFP encoding or empty VLPs at an MOI of 0, 1, 10, 50 and 100. 18 hours post-infection, cells were trypsinised and resuspended in 4% PFA. Cells were analysed by flow cytometry for GFP expression (Figure 4.1). Results demonstrated that BHK and RG2 cells have similar infection efficiencies with BHK cells demonstrating a slightly higher infection rate at the majority of MOIs ($p<0.001$, Two-Way ANOVA). F98 cells demonstrated infection levels approximately two-fold lower than that of BHK cells at MOI of 100 (-2.29±0.06-fold, $P<0.0001$ Two-Sample T-test). Maximum transfection was observed at an MOI of 100.

4.3.1.2 Analysis of VLP induced apoptosis in glioma cell lines

4.3.1.2.1 Immunoflourescent detection of active caspase-3 and viable cells

Cells were harvested 0, 24, 48 and 72 hours p.i. and examined for the presence of active caspase-3 by immunofluorescence. Figure 4.2 demonstrates the presence of active caspase-3 in BHK cells. Anuclear cells or cells displaying nuclear blebbing and fragmentation were not considered viable. Figure 4.3 demonstrates nuclear blebbing indicative of apoptosis in BHK cells. The percentage caspase-3 positive cells and viable cells were tabulated for BHK (Figure 4.4), RG2 (Figure 4.5) and F98 (Figure 4.6) cells. Additionally, the transfection level for each cell line is indicated, as determined in **4.3.1.1**.

Percentage active caspase-3 positive cells were calculated as;
% Positive cells = 100 * $FITC^{pos}$ / ($DAPI^{pos}$ + $DAPI^{neg}FITC^{pos}$)

Percentage viable cells were calculated as;
% Viable Cells = 100 * viable nuclei / (viable nuclei + nonviable nuclei + anuclear cells)

BHK cells demonstrated apoptosis induction following infection with empty, IL-12 encoding VLPs and replicating SFV4 virus. No statistically significant difference in the frequency of apoptosis induction was observed between IL-12 encoding or empty VLP infected cells ($p=0.3057$, Two-Way ANOVA). Apoptosis induction in SFV4 infected cells was apparent at all time points following infection with 100% of cells displaying active caspase-3 presence at 48 and 72 hours. The analysis of cell viability mirrored those of apoptosis induction with no statically significant difference between IL-12 encoding and empty VLP infected cells ($p=0.1698$, Two-Way ANOVA). Additionally, no SFV4 infected cells were viable at 48 or 72 hours post-infection. The infection efficiency of BHK cells was previously determined as 60.00 (± 1.633)% at MOI 50. Maximum apoptosis induction was observed at 72 hours post-infection at levels of 73.50 (± 10.93)% and 96.00 (± 1.85)% for empty and IL-12 encoding VLPs respectively. Although there was no statistically significant difference between empty and IL-12 encoding VLPs, the latter was significantly different from the expected transfection level ($p<0.0001$, Two-Sample T-Test).

RG2 cells demonstrated apoptosis induction following infection with empty, IL-12 encoding VLPs and replicating SFV4 virus. No statistically significant difference in apoptosis induction was observed between IL-12 encoding and empty VLP infected cells

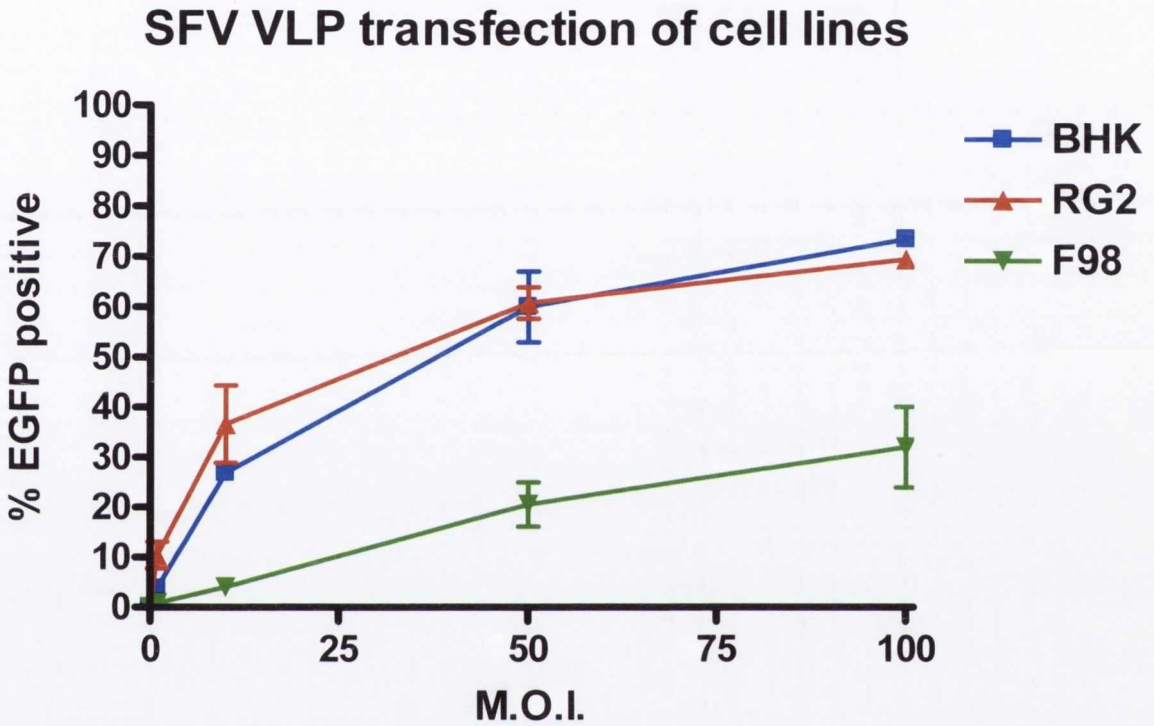

Figure 4.1: SFV transfection of BHK, RG2 and F98 cells.

Cells were infected with empty or EGFP encoding SFV VLPs at an MOI of 0, 1, 10, 50 or 100. Cells were analysed for EGFP fluorescence by flow cytometry at 18 hours post infection. Empty VLP infected cells were negative at all MOIs. Values represent mean ± SEM.

(p=0.7548, Two-Way ANOVA). Apoptosis induction in SFV4 infected cells was apparent at all time points following infection with approximately 90% of cells displaying active caspase-3 presence at 48 and 72 hours and no statistical difference between the two time points (p=0.3704, Two-Sample T-Test). The analysis of cell viability mirrored those of apoptosis induction with no statistically significant difference between IL-12 encoding and empty VLP infected cells (p=0.2176, Two-Way ANOVA). Additionally, no SFV4 infected cells were viable at 48 or 72 hours post infection. The infection efficiency of RG2 cells was previously determined as 60.83 (± 0.73)% at MOI 50. Maximum apoptosis induction was observed at 72 hours post-infection at levels of 49.88 (± 3.30)% and 51.95 (± 2.09)% for empty and IL-12 encoding VLPs respectively. Although there was no statistically significant difference between empty and IL-12 encoding VLPs both displayed slightly lower levels of apoptosis induction than expected from the previously determined infection efficiency (p=0.0318 and 0.0160) for empty and IL-12 encoding VLPs respectively (Two-Sample T-Test).

F98 cells demonstrated apoptosis induction following infection with empty, IL-12 encoding VLPs and replicating SFV4 virus. Interestingly, unlike BHK and RG2 cells there was a statistically significant difference between apoptosis induction following infection with IL-12 encoding and empty VLPs. Empty VLPs displayed a slightly higher rate of apoptosis induction at all time points compared to IL-12 encoding VLP infected cells (p=0.0455 Two-Way ANOVA). Apoptosis induction in SFV4 infected cells was apparent at all time points following infection with approximately 85% of cells displaying active caspase-3 presence at 24 and 48 hours peaking at 72 hours with 100% of cells undergoing apoptosis. The analysis of cell viability mirrored those of apoptosis induction with a significantly lower percentage of viable cells following infection with empty VLPs compared to IL-12 encoding VLPs (p=0.0002, Two-Way ANOVA). Additionally, no SFV4 infected cells were viable after 24 hours post-infection. The infection efficiency of F98 cells was previously determined at 20.54 (± 1.03)% at MOI 50. Maximum apoptosis induction was observed at 24 hours post-infection at levels of 32.44 (± 2.71)% and 24.75 (± 3.56)% for empty and IL-12 encoding VLPs respectively. Empty VLP infection resulted in levels of apoptosis statistically greater than expected by infection levels (p=0.0148, Two-Sample T-Test) while IL-12 encoded VLP infected cells demonstrated levels of apoptosis statistically similar to levels expected by infection levels (p=0.3192, Two-Sample T-Test).

4.3.2 *In vivo* analysis

4.3.2.1 ELISA detection of IL-12 expression

Four animals were implanted with RG2 glioma cells and were treated 17 days later with IL-12 encoding VLPs (two animals) or empty VLPs (two animals). Animals were culled 48 hours later, the brain section containing the tumor excised, homogenised and examined for IL-12 presence by ELISA. IL-12 levels were adjusted per mg of soluble protein. IL-12 levels in the brains of IL-12 encoding VLP treated animals were 140.9 ± 30.25 (mean ± SEM) ng of IL-12 per mg of total soluble protein. IL-12 levels in empty VLP treated animals were below the limit of detection.

4.3.2.3 Immunohistochemical detection of SFV antigen

For each glioma cell line, tumor-bearing animals were inoculated with IL-12 encoding VLPs (three animals) or TNE (two animals) via the implanted cannula 17 days after glioma cell inoculation. 48 hours later, brains were examined for the presence of SFV antigen using either an anti-SFV4 or anti-nsP2 antibody. In all cases sections were negative for the presence of SFV antigen (data not shown).

4.3.2.4 Immunohistochemical detection of IL-12

Frozen sections were examined for the presence of IL-12 using a goat anti-rat IL-12 antibody. All animals treated with IL-12 encoding VLPs were positive for IL-12 antigen at the inoculation site while staining was absent on the contralateral side of IL-12 treated animals and in the brains of TNE treated animals. Staining was located only at the inoculation site and largely absent from the needle tract. Staining was evident in tumor and non-tumor tissue depending on the specific inoculation site. Figure 4.7 demonstrates IL-12 staining following anti-IL-12 immunohistochemistry. Additionally, cells in areas of VLP infection displayed cellular fragmentation indicative of cell death.

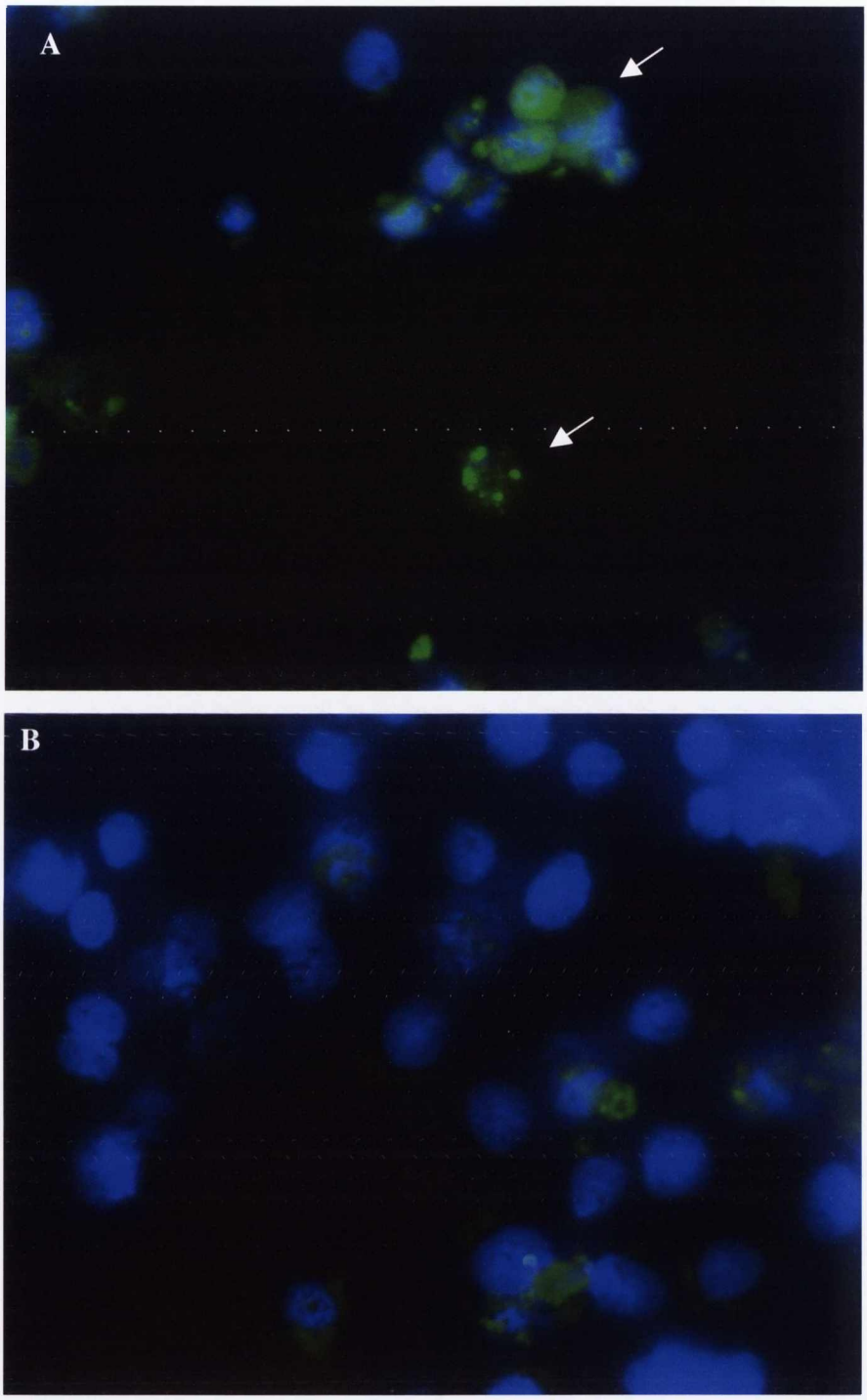

Figure 4.2: Immunohistochemical detection of active caspase-3 by indirect immunofluorescence.

BHK cells infected with replicating SFV4 (**A**) or IL-12 encoding VLPs (**B**), 48 hours post infection. Arrows indicate active caspase-3 presence as detected by indirect immunofluorescence.

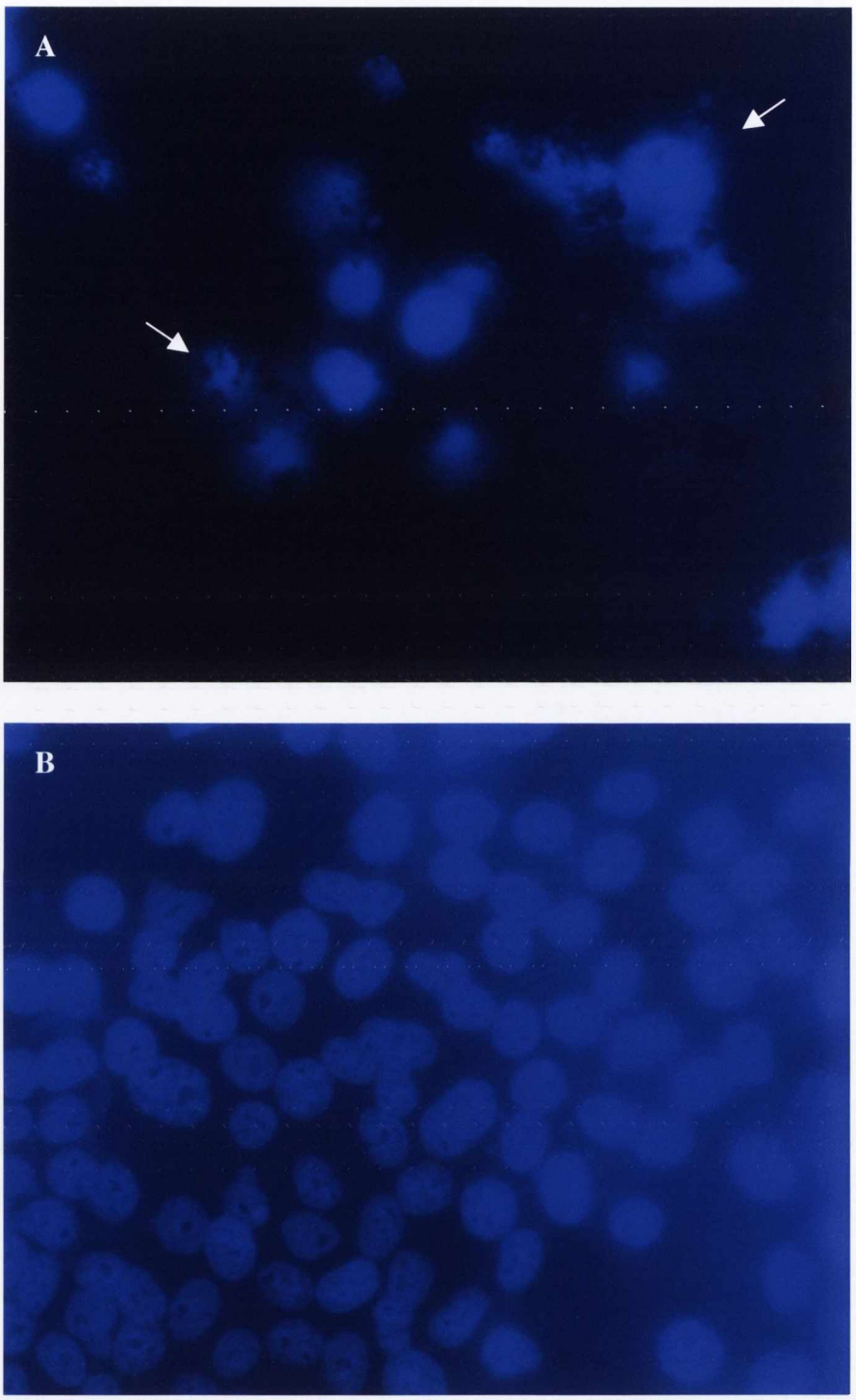

Figure 4.3: Detection of viable cells by DAPI staining.

BHK cells infected with replicating SFV4 (**A**) or mock-infected (**B**), 48 hours post infection. Arrows indicate nuclear blebbing and fragmentation indicative of apoptotic cells.

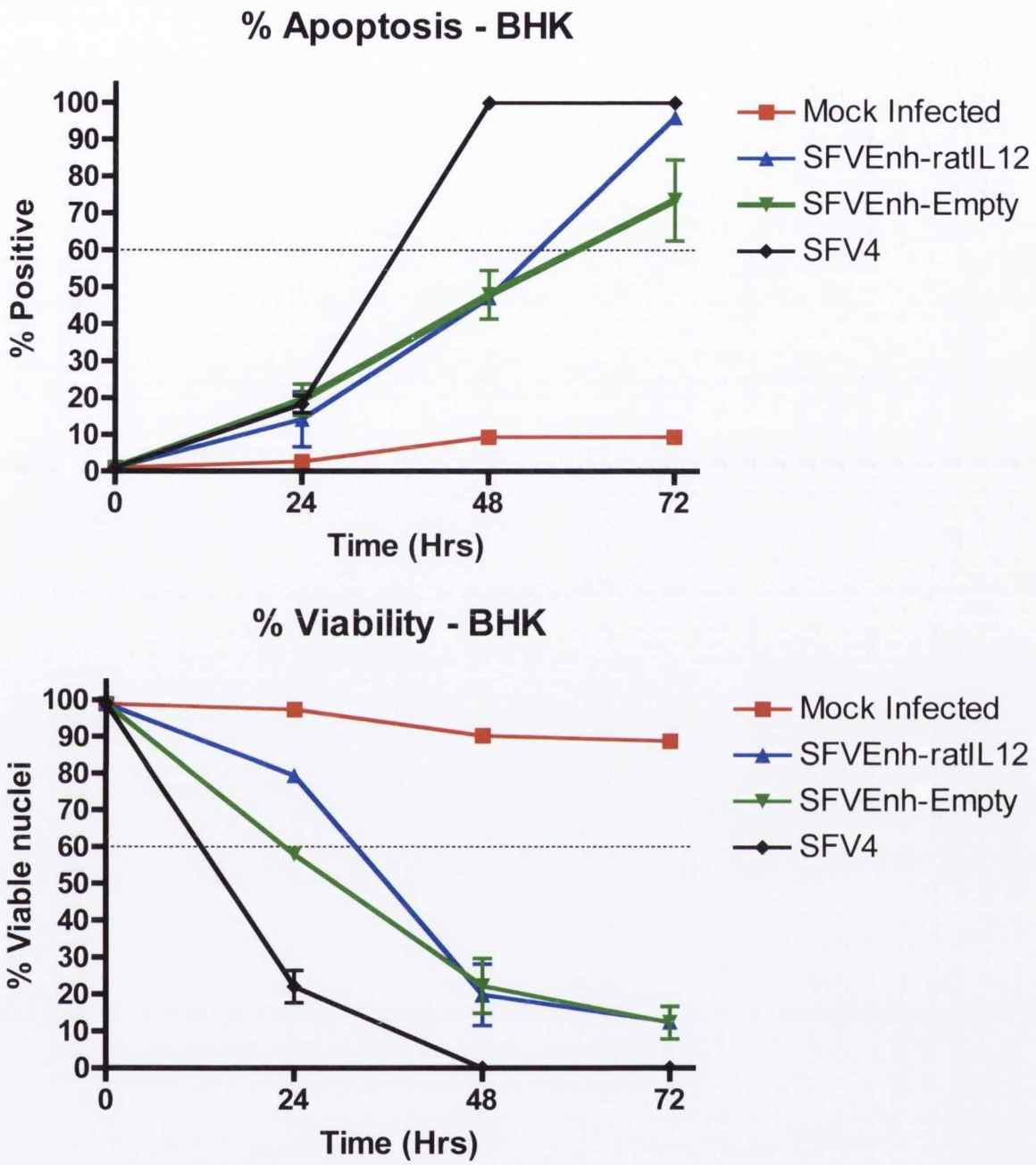

Figure 4.4: Apoptosis induction by VLPs in BHK cells.

BHK cells were mock infected or infected with empty, IL-12 encoding VLPs or replicating SFV4 at an MOI of 50. Active caspase-3 presence was detected by immunofluorescence (**top**) and viable cells assessed by DAPI staining (**bottom**). The dashed line represents the transfection efficiency for BHK cells at an MOI of 50. Values represent mean ± SEM.

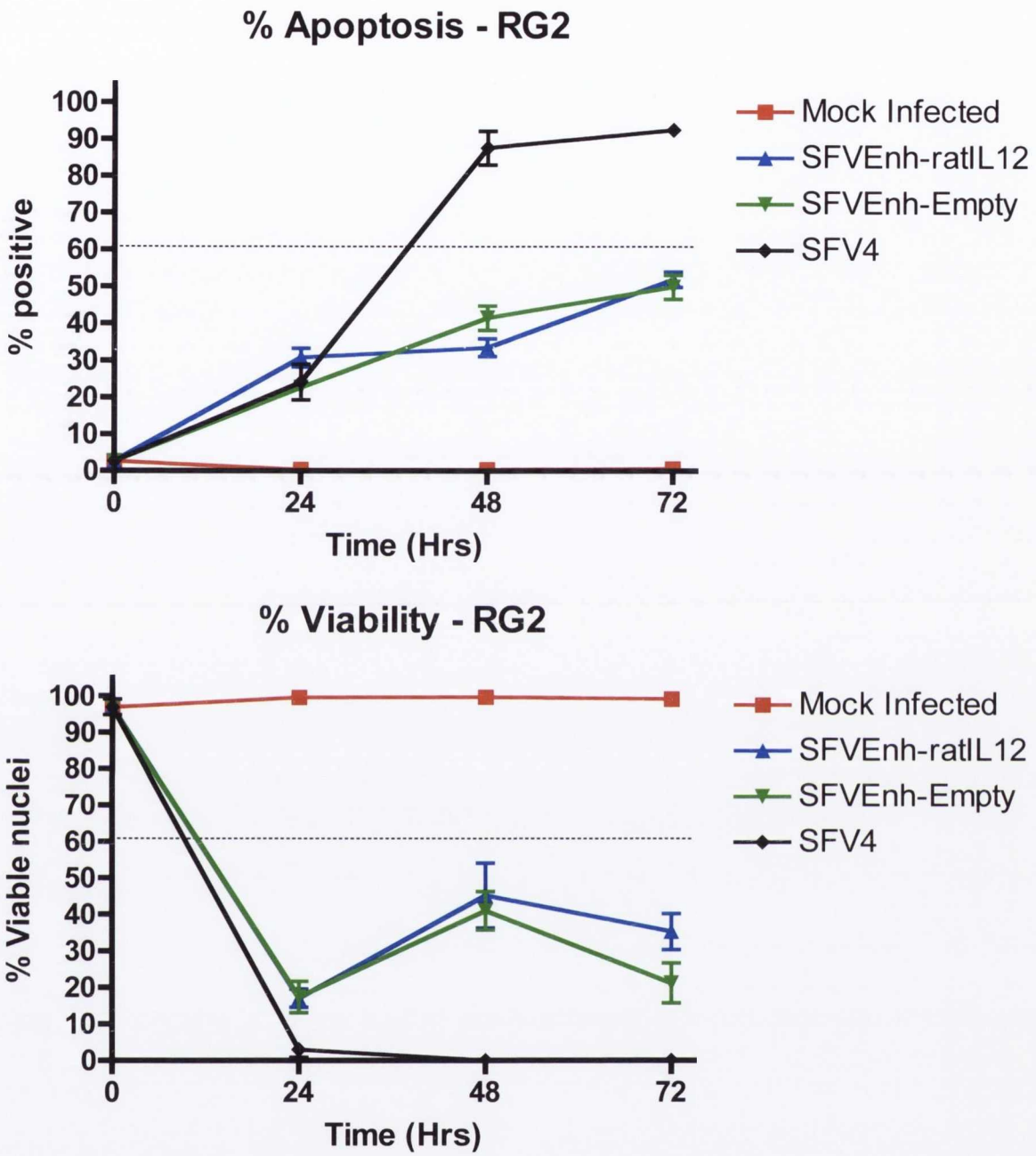

Figure 4.5: Apoptosis induction by VLPs in RG2 cells.

RG2 cells were mock infected or infected with empty, IL-12 encoding VLPs or replicating SFV4 at an MOI of 50. Active caspase-3 presence was detected by immunofluorescence (**top**) and viable cells assessed by DAPI staining (**bottom**). The dashed line represents the transfection efficiency for RG2 cells at an MOI of 50. Values represent mean ± SEM.

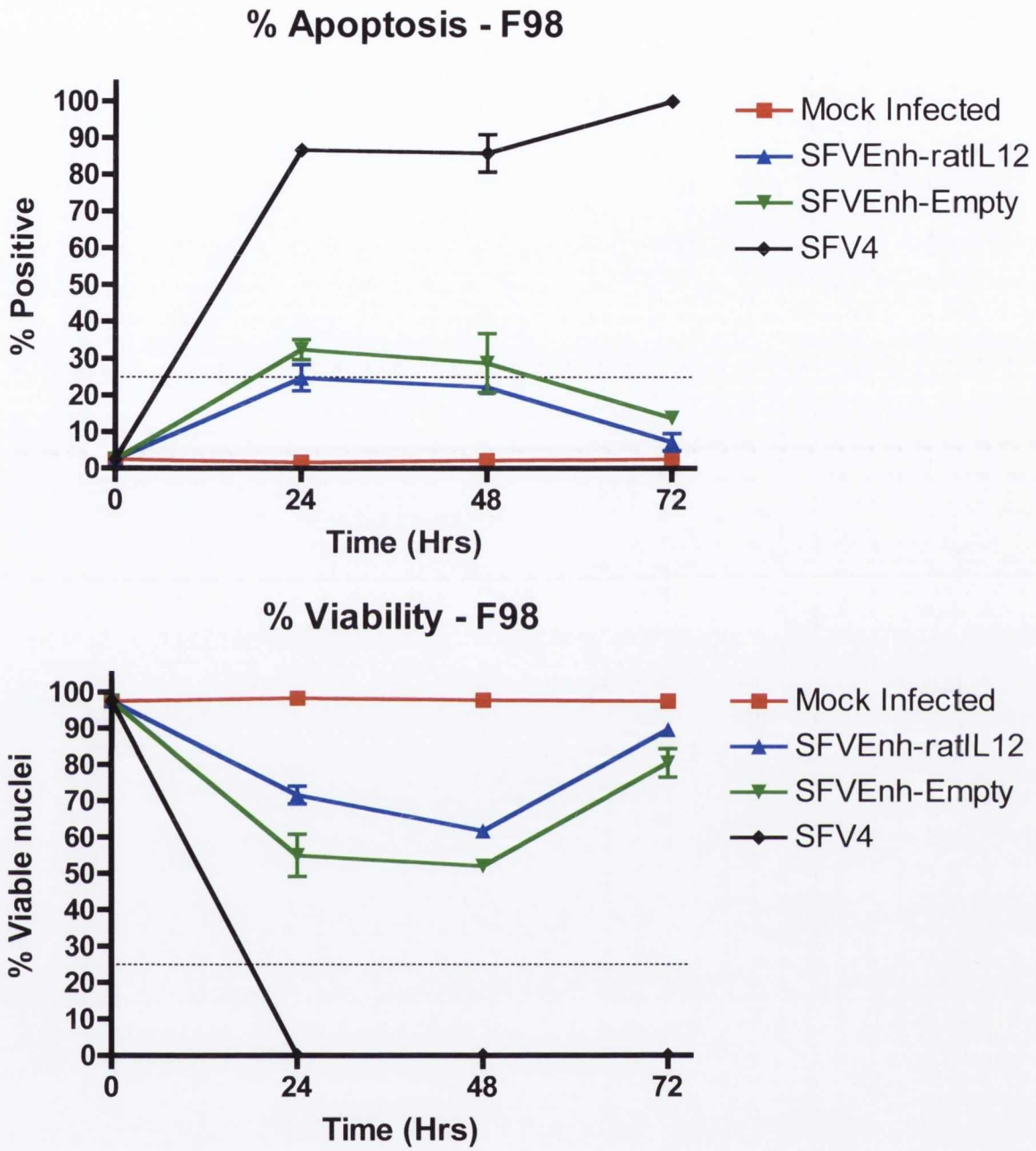

Figure 4.6: Apoptosis induction by VLPs in F98 cells.

F98 cells were mock infected or infected with empty, IL-12 encoding VLPs or replicating SFV4 at an MOI of 50. Active caspase-3 presence was detected by immunofluorescence (**top**) and viable cells assessed by DAPI staining (**bottom**). The dashed line represents the transfection efficiency for F98 cells at an MOI of 50. Values represent mean ± SEM.

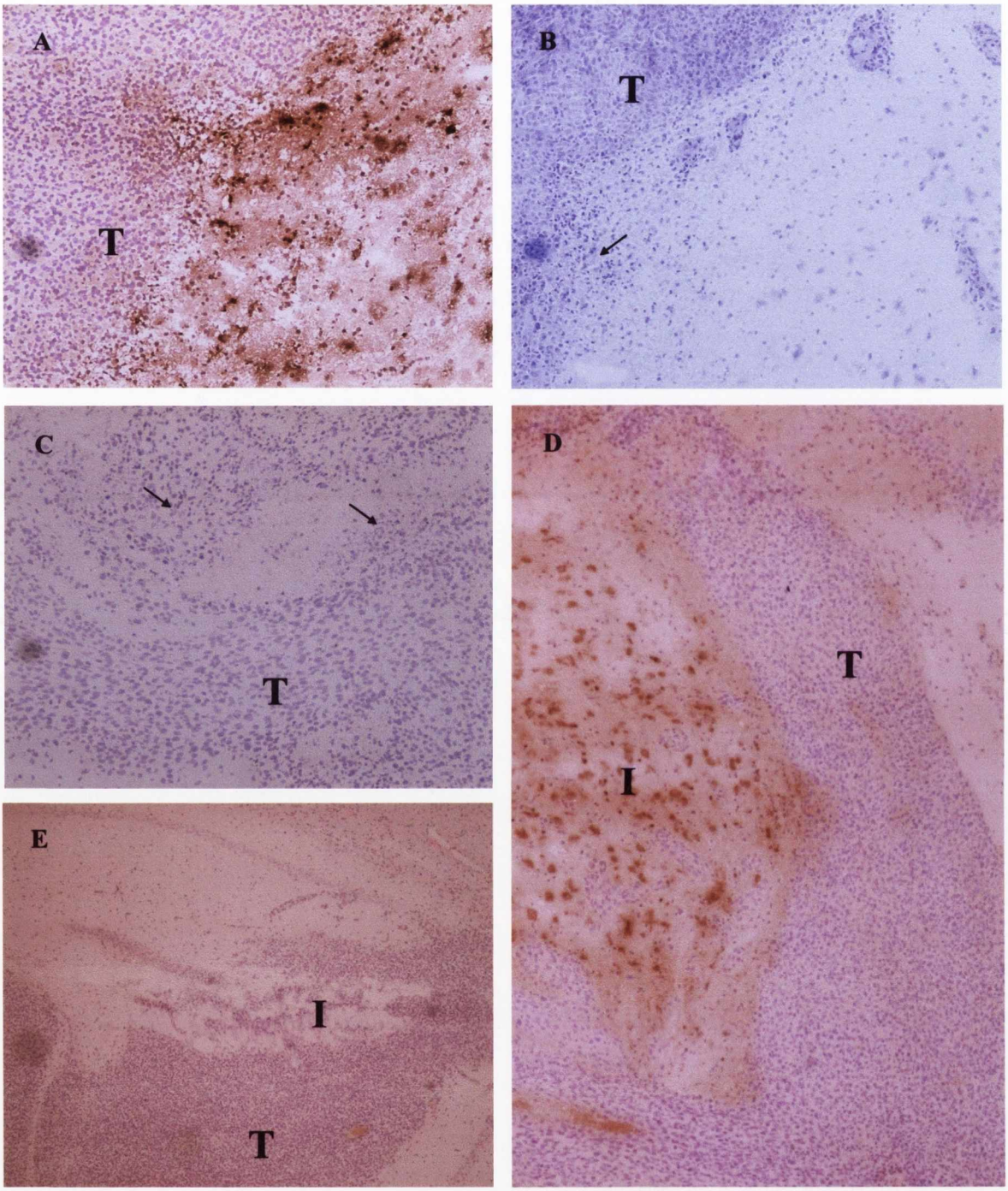

Figure 4.7: Immunohistochemical detection of *in vivo* IL-12.

A - IL-12 encoding VLP treated RG2 tumor 48 h.p.i. stained with anti-IL-12 antibody; IHC, 100x. **B** - consecutive section of (A) stained with PBS (negative primary control); IHC, 100x. **C** - haematoxylin stained IL-12 encoding VLP treated F98 tumor 48 h.p.i.; 100x. **D** - IL-12 encoding VLP treated F98 tumor 48 h.p.i. stained with anti-IL-12 antibody; IHC, 40x. **E** - TNE treated RG2 tumor treated 48 h.p.i. stained with anti-IL-12 antibody; IHC, 40x. Tumor (T) and approximate inoculation site (I) are also indicated where applicable. Arrows represent areas of cell fragmentation indicative of cell death.

4.4 Discussion

The ability of the SFV VLP system to infect two glioma cell lines *in vitro* was examined. In order to determine the infection efficiency following a single round of VLP infection, cells were infected with EGFP encoding SFV VLPs and analysed for the presence of GFP expression by flow cytometry. Results demonstrated that BHK and RG2 cells had similar infection efficiencies while F98 cells had an infection efficiency two-fold lower than that of BHK and RG2 cells. Previous studies in our laboratory have indicated that infection of neoplastic cells, including rat prostate cancer, human lung carcinoma and murine sarcoma cell lines, with the SFV VLP system is far less efficient than BHK or S-BHK cells (Murphy *et al.*, 2000; Smyth *et al.*, 2005; Chikkanna-Gowda *et al.*, 2006). In fact, infection efficiencies equivalent to BHK cells were rarely observed in tumor cell lines following a single round of infection with VLPs. Interestingly, from the analysis of apoptosis induction by the VLP system, complete infection of all cell lines was observed following infection with replicating SFV. This suggested that despite a single round of infection only infecting a proportion of cells, those uninfected cells were not completely resistant to infection and permissiveness may be related to temporal changes in the cell, possibly related to cell cycle.

The induction of apoptosis following infection with VLPs or replicating virus was examined by indirect IHC against active caspase-3, a marker of ongoing apoptosis. While one hundred percent of BHK and F98 cells were positive for active caspase-3 at 72 hrs p.i. some RG2 cells (approximately 5-10%) remained negative. The observation that all cells appeared non-viable by 72 hours suggested that cells had been completely infected but, at that point may not have been positive for active caspases-3, which appeared delayed relative to nuclear blebbing and fragmentation. Interestingly, F98 cells appeared to undergo apoptosis more rapidly than either BHK or RG2 cells following infection with SFV4 virus or VLPs as measured by active caspase-3 presence or cell viability. This indicated that F98 cells maybe more sensitive to apoptosis induction than the other cell line tested although the reason for this is unknown. Two of the three cell lines examined showed no significant difference in apoptosis induction following infection with IL-12 encoding or empty VLPs, suggesting that the production of the encoded transgene did not affect virus-initiated apoptosis induction. This observation was expected as it has previously been determined that high-level protein expression of the structural proteins was not required for apoptosis induction (Glasgow *et al.*, 1998). In contrast, F98 cells

demonstrated a significantly higher induction of apoptosis following infection with empty VLPs compared to IL-12 encoding VLPs. The fact that maximum empty VLP apoptosis induction was greater than expected as estimated by infection efficiency suggests that there may have been some variation between the titers of IL-12 encoding and empty VLPs and that this observation was not due to the inherent ability of empty VLPs to induce greater levels of cell death. The lower than expected percentage of active caspase-3 positive cells at 72 hours in F98 and RG2 cells is presumably the result of ongoing growth of non-infected cells reducing the apparent proportion of apoptotic cells. At 72 hours post-infection, BHK cells demonstrated apoptosis induction at levels greater than expected and this observation was mirrored by cell viability. The reason for this is unknown but maybe a result of the bystander effect possibly more pronounced in BHK cells which form a more compact monolayer in tissue culture than the F98 and RG2 cell lines.

The ability of the VLP system to infect cells and induce transgene expression *in vivo* was also examined. Following intracerebral inoculation of IL-12 encoding VLPs into tumor bearing animals, the IL-12 protein could be readily detected by indirect immunohistochemistry. Cellular expression was observed in IL-12 encoding VLP infected animals; expression was limited to the site of inoculation and absent from TNE treated animals in both the F98 and RG2 glioma models. At the inoculation site, both tumor and non-tumor tissue was positive for IL-12 expression, indicative of IL-12 encoding VLP infection, suggesting that both tumor cells and cells of the CNS were permissive to infection and that the site of inoculation was an important determinant in the precise cell populations infected. Additionally, IL-12 presence was rarely detected along the needle tract or at the dorsal surface of the brain indicating that the flow rate of VLP delivery was not causing backflow of VLPs away from the intended inoculation site. Cellular fragmentation was also observed at the inoculation site indicating that the infected cells were undergoing cell death, an expected consequence of VLP infection. The presence of IL-12 was also examined by ELISA 48 hours after intracerebral inoculation. IL-12 p70 levels of 140.9 (±30.25) ng per mg of total soluble protein were detected in IL-12 encoding VLP treated animals while IL-12 levels were undetectable following empty VLP administration. As mentioned previously, Rodriguez-Madoz *et al.* had constructed a similar SFV based IL-12 encoding vector that resulted in *in vitro* IL-12 levels approximately 10-fold greater than the vector constructed here. Interestingly, *in vivo* IL-12 levels measured in this model were at least 15-fold greater than observed by Rodriguez-Madoz who inoculated tumors with a two-fold greater dose of VLPs. This is likely a result

of the VLP transfection efficiency and may be related to the presence of cells capable of mediating a positive feedback loop via interferon gamma and highlights the potential disparity between *in vitro* and *in vivo* expression levels.

Thus, the SFV VLP system has been shown to infect glioma cells *in vitro* and efficiently initiate apoptosis induction. Also, *in vivo* studies indicated that the VLP system is capable of infecting tumor cells and inducing transgene expression.

Chapter 5

Intracerebral treatment of glioma models using the SFV VLP system

treatment modalities. Chikkanna-Gowda *et al.* (2005) and Rodriguez-Madoz *et al.* (2005) have demonstrated the ability of SFV VLPs encoding murine IL-12 to induce complete tumor regression in murine colon adenocarcinoma and mammary carcinoma models, accompanied by the induction of adaptive immunity and protection from subsequent rechallenge.

The IL-12 based immuno-gene therapy models mentioned involved the use of subcutaneous tumor implantation and intratumoral delivery of IL-12 encoding VLPs. The model undertaken in this study is similar to those discussed, however tumor implantation and VLP delivery is carried out within the brain. Similar models involving herpes simplex virus, adenovirus and vaccinia virus vectors encoding IL-12 have demonstrated the induction of tumor regression and protection from re-challenge (Chen *et al.*, 2001; Parker *et al.*, 2000; Liu *et al.*, 2002). Additionally, Yamanaka *et al.* (2000) demonstrated the induction of an anti-tumor immune response to i.c. 203-gliomas using the SFV VLP system encoding IL-12, which resulted in complete tumor regression and long-term survival. It should be noted however that these intracerebral models involved the use of antigenic glioma models, to which protection is possible by vaccination; it does however, demonstrate that the afferent and efferent immune functions are capable of eliminating tumors located within the CNS following viral vector-based IL-12 gene therapy.

The model undertaken in this study uses the non- and weakly immunogenic RG2 and F98 glioma models and the ability of the SFV VLP system encoding IL-12 examined as an anti-tumor therapy.

5.2 Experimental Procedures.

5.2.1 New Materials

5.2.1.1 Surgical instrumentation

All surgical instrumentation were as per **4.2.1.5**.

5.2.1.2 Immunohistochemistry

Goat anti-pecam-1 (CD31) antibody was purchased from Santa Cruz Biotechnology, Inc (USA). Mouse anti-human CD3 antibody (clone F7.2.38, cat no. M7254) was purchased from DakoCytomation. Harris haematoxylin, eosin aqueous solution and dichromate eosin were purchased from BDH.

5.2.1.3 Miscellaneous

Images were analysed using the Image-Pro® Plus software (Media Cybernetics® inc. USA).

5.2.2 New Methods

5.2.2.1 Preparation of virus-like particles for intracerebral inoculation.

VLPs were diluted to $1x10^7$ or $1x10^8$ VLPs/μl in TNE for the low and high-dose i.c. experiments respectively. Particles were aliquoted, snap frozen in liquid nitrogen and stored at –80°C until used.

5.2.2.2 Surgical implantation of cannulas.

Implantation of cannula was carried out as per **4.2.2.2.1**.

5.2.2.3 Inoculation of glioma cells.

Glioma cells were inoculated as per **4.2.2.2.2**.

5.2.2.4 Intracerebral delivery of SFV VLPs.

SFV VLPs were delivered out as per **4.2.2.2.3**.

5.2.2.5 Culling of animals.

Animals were anesthetised by i.p. injection of xylazine/ketamine mix and culled by perfusion via the transcardiac route. Animals were perfused with 100ml of PBS followed by 400ml of 10% NBF, the brain and organs excised and placed in 50ml of NBF for 48 hours before processing. For extended storage, samples were stored in 1% NBF until processed. When required, blood was harvested with a 19-gauge needle prior to the initiation of transcardiac perfusion. Blood was stored at RT for 1 hour and centrifuged at 1,500rpm (412.65g) for 10 minutes at 4°C. Plasma was aliquoted and frozen at –80°C until assayed.

5.2.2.6 Cytopathic effect assay of brain homogenates

Animals were culled by isoflourane overdose, the head removed, the brain aseptically excised and used to produce a 20% homogenate in infection medium using a RZR1 homogeniser. The homogenate was centrifuged at 4°C and 4,000rpm (2934.4g) and the supernatant aliquoted, snap frozen in liquid nitrogen and stored at –80°C until use. A 75cm^2 flask of BHK cells was grown to 25% confluence and infected at 37°C for 1 hour with 1ml of homogenate. 14mls of maintenance medium was added and the cells incubated at 37°C (5% CO_2, 100% RH). 72 hours later 1ml of medium was removed and used to infect a 75cm^2 flask of BHK cells, as before. This process was carried out a further 4 times and cells examined for CPE every 24 hours.

5.2.2.7 Cytopathic assay of VLP stocks

To determine if replication-competent virus was present in VLP stocks, a 25% confluent 150cm^2 flask of BHK cells were infected with empty or IL-12 encoding VLPs (MOI 100) in a total volume of 2ml of infection medium. Cells were incubated for 48 hours and 1ml of medium used to infect a 75 cm^2 sub-confluent flask of BHK cells for 72 hours. Cells were examined for CPE every 24 hours, medium was passaged an additional 4 times and cells examined for CPE every 24 hours.

5.2.2.8 *In vivo* cytokine detection

Plasma and brain homogenates were assayed from the presence of IL-12 or IFN-γ by commercial ELISA as per **2.2.2.4.4** and **2.2.2.4.5**, respectively.

5.2.2.9 Histopathology and immunohistochemistry

Histological examination was performed by Prof. Brian Sheahan (Veterinary Pathology Laboratory, University College Dublin).

5.2.2.9.1 Haematoxylin and eosin staining

Paraffin-embedded brain sections were examined by haematoxylin and eosin (H&E) staining. Sections were heated at 55°C for 10 minutes, de-waxed with three 10 minutes washes in 100% xylene followed by hydration with 100%, 95%, 70% ethanol for 5 minutes each followed by distilled water. Sections were stained in Harris' haematoxylin for 10 minutes, rinsed under running tap water until cleared, differentiated in 1% acid alcohol and 'blued-up' by dipping three times in 3% ammonia water. Sections were counterstained in 1% dichromate eosin for 2 minutes and washed under running tap water until cleared. Stained sections were dehydrated and mounted with D.P.X. mountant. Routine embedding and processing of brains was carried out by Mrs. Alex Whelan-Buckley (Veterinary Pathology Laboratory, University College Dublin).

5.2.2.9.2 Determination of tumor size

H&E stained brain sections were digitised and tumor size determined using the Image-Pro® Plus program. For each animal, the section containing the largest tumor area was imaged and measured. Within each experiment the average tumor size for TNE treated animals was determined and all tumors expressed as a percentage of this value. Necrotic area was measured as above.

5.2.2.9.3 Immunohistochemical detection of SFV antigen

Paraffin-embedded sections were heated to 55°C for 10 minutes and incubated twice in 100% xylene for 20 minutes each. Sections were then incubated in 100% EtOH twice for 5 minutes, running water for 5 minutes and PBS twice for 2 minutes each. Sections were processed as per **4.2.2.2.6.**

5.2.2.9.4 Immunohistochemical detection of IL-12

Paraffin-embedded sections were hydrated as per **5.2.2.9.3**. Endogenous peroxidase blocking was carried out as per **4.2.2.2.6** and antigen retrieval carried out by incubation of samples in 1mM EDTA at 121°C for 6 minutes followed by 20 minutes cooling. Samples were stained for IL-12 as per **4.2.2.2.7**.

5.2.2.9.5 Immunohistochemical detection of vessel density

Paraffin-embedded sections were hydrated as per **5.2.2.9.3**. Endogenous peroxidase blocking and antigen retrieval was carried out as per **5.2.2.9.4**. Samples were blocked overnight in 10% NRS in PBS at 4°C followed by avidin/biotin blocking using the Vector Laboratories avidin/biotin blocking kit, as per manufacture's instructions. Samples were incubated with a 1/200 dilution of goat anti-PECAM-1 (CD31) antibody in 5% NRS for one hour at RT. Remaining steps were carried out as per **4.2.2.2.6**.

5.2.2.9.6 Immunohistochemical detection of CD3 positive cells

Paraffin-embedded sections were hydrated as per **5.2.2.9.3.** Endogenous peroxidase blocking and antigen retrieval was carried out as per **5.2.2.9.4**. Samples were blocked overnight in 10% NHS in PBS at 4°C followed by avidin/biotin blocking using the Vector Laboratories avidin/biotin blocking kit, as per manufacture's instructions. Samples were incubated with a 1/50 dilution of mouse anti-CD3 antibody in 5% NHS for one hour at RT. Remaining steps were carried out as per **4.2.2.2.6**.

5.3 Results

5.3.1 The RG2 and F98 glioma models

To determine the growth characteristics of both glioma cell lines *in vivo,* RG2 and F98 glioma cells were inoculated directly into the right hippocampus of male Fischer 344 rats. Groups of 6 animals were implanted with RG2 or F98 cells and two animals from each group were culled at one, two and three weeks p.i. Brains were removed for gross and routine histological examination, the latter using sections stained with haematoxylin and eosin (H&E). Both cell lines produced macroscopically visible tumors with replacement and distortion of brain tissue at two and three weeks p.i. (Figures 5.1 and 5.2). Histologically, F98 tumors were highly infiltrative with poorly defined margins and central areas of necrosis and haemorrhage. Cords of polyhedral tumor cells showing marked nuclear pleomorphism and frequent mitotic forms extended into the surrounding parenchyma, primarily in perivascular spaces. Tumor cell invasion of the ventricles and subarachnoid space was common (Figures 5.1E and 5.1F). The histological appearance of RG2 tumors was of well-circumscribed, expansile masses mostly composed of spindle-shaped cells. Tumor cell invasion of the parenchyma and meninges was not a feature. Central necrosis and haemorrhage in large RG2 tumors were less extensive than in F98 tumors. Small accumulations of lymphocytes and macrophages, some laden with hemosiderin, were present together with oedema at the interface with the surrounding neuropil (Figures 5.2E and 5.2F).

For intracerebral treatment experiments, animals were implanted with a cannula at stereotaxic coordinates above the hippocampus. One week later, RG2 or F98 glioma cells were stereotaxically inoculated, via the implanted cannula, into the right hippocampus. Treatment was initiated one week after glioma cell implantation. Animals were briefly anesthetised, for approximately 20 minutes, and TNE buffer or VLPs delivered, in a total volume of 5µl, into the same coordinates as the glioma cell implants. Treatment was carried out every second day for a total of 6 treatments and repeated anaesthesia was not associated with toxicity (data not shown). Oedema, haemorrhage and macrophages were present at the inoculation sites in animals from all treatment groups.

Figure 5.1: *In vivo* characterisation of F98 gliomas.

A - RG2 tumor, 3 weeks p.i.; dorsally located tumor mass (T) contains areas of haemorrhage. The caudal lobe of the cerebellar vermis (V) protrudes over the medulla oblongata indicating brain swelling.

B - F98 tumour with irregular margins and central necrosis (N) in the hippocampus, cords of tumour cells extend into the parenchyma and the third ventricle (V); H&E, x20.

C - Higher magnification of (B) showing disruption of the ependymal epithelium and infiltration of the choroid plexus; H&E, x100.

D - F98 tumour cell metastasis in the subarachnoid and perivascular spaces; H&E, x100.

E - Perivascular proliferations of F98 tumour cells; H&E, x200.

F - Perivascular and parenchymal proliferations of F98 tumour cells. The tumour cells are polyhedral with round to oval vesicular nuclei; there are numerous mitotic figures (arrowheads); H&E, x200.

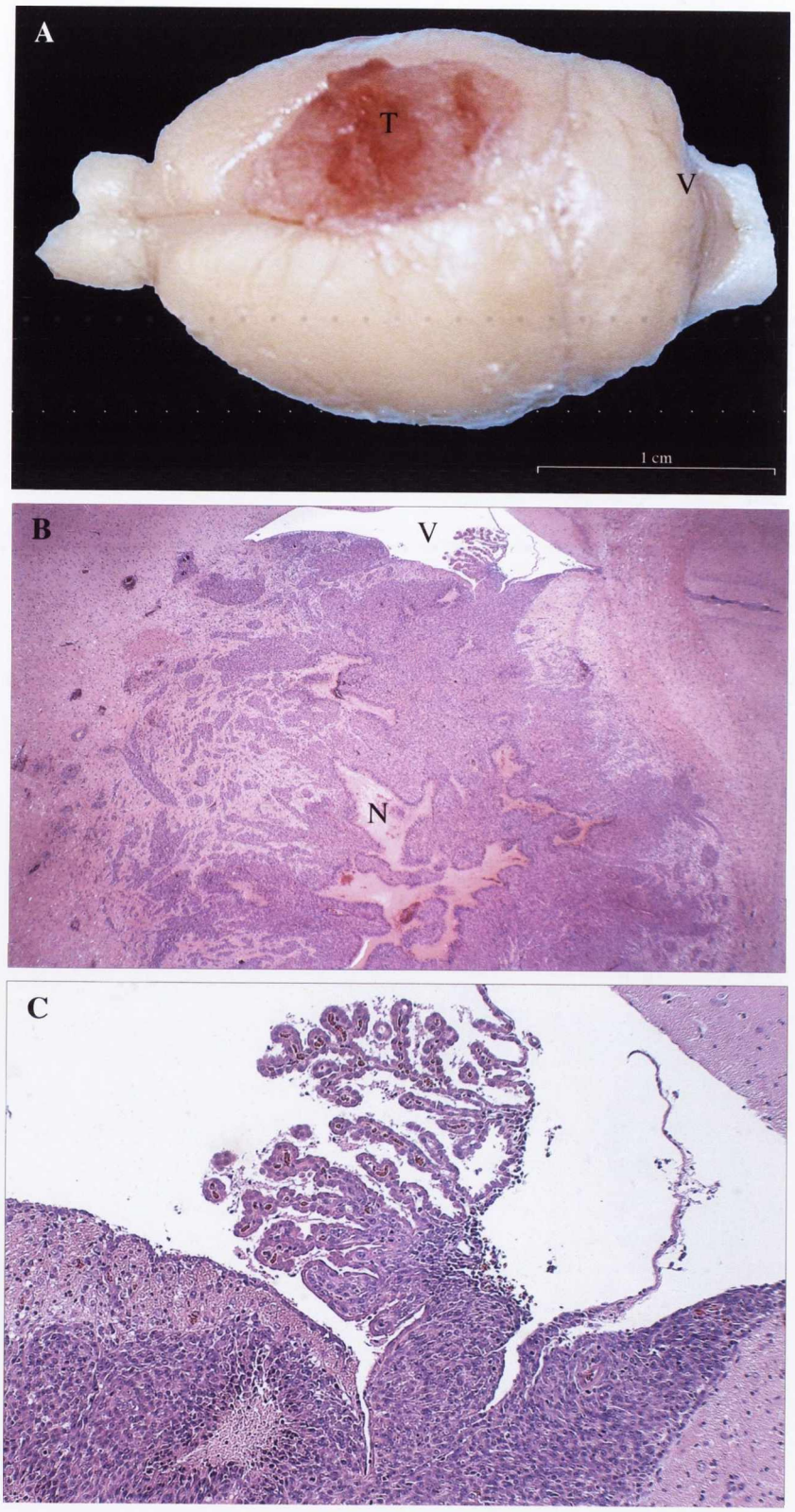

Figure 5.1: *In vivo* characterisation of F98 gliomas (A-C).

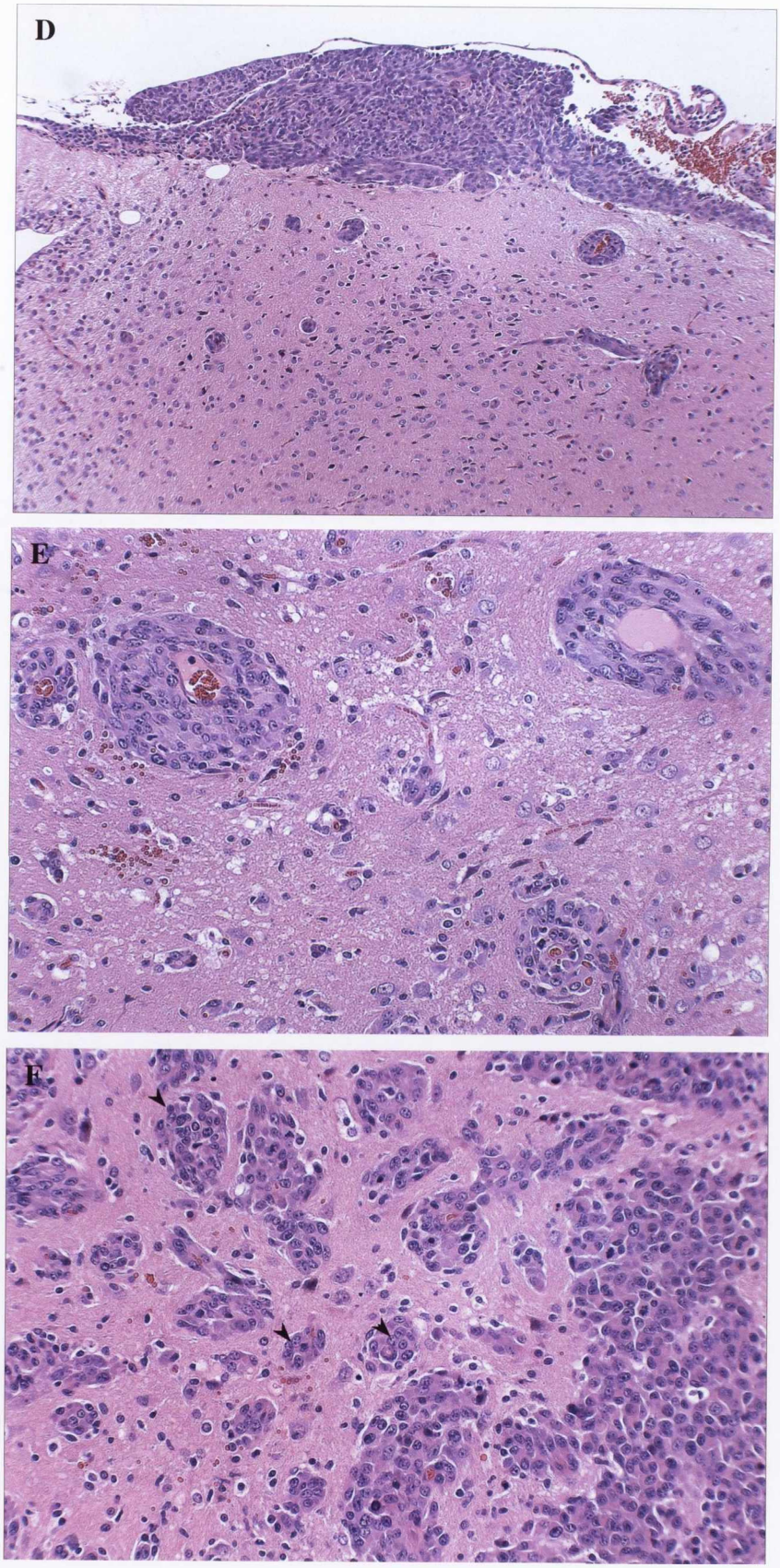

Figure 5.1: *In vivo* characterisation of F98 gliomas (D-F).

Figure 5.2: *In vivo* characterisation of RG2 gliomas.

A – RG2 tumour in the right cerebrum of a rat 21 days following inoculation with RG2 tumour cells.

B - Coronal section of the brain illustrated in (A) showing massive distortion of the cerebrum and extension of the tumour mass through the corpus callosum into the putamen.

C - RG2 tumour 14 days p.i. well-circumscribed tumor cell mass (T) adjoining the hippocampus (H); H&E, x40.

D - Spindle-shaped tumor cells and thin-walled blood vessels (BV); H&E, x400.

E - Localised area of oedema (O) and macrophage infiltration at the interface with the surrounding neuropil (N); H&E, x200.

F - Haemosiderin laden macrophages (blue) and haemorrhage (H) at the periphery; Prussian Blue, x400.

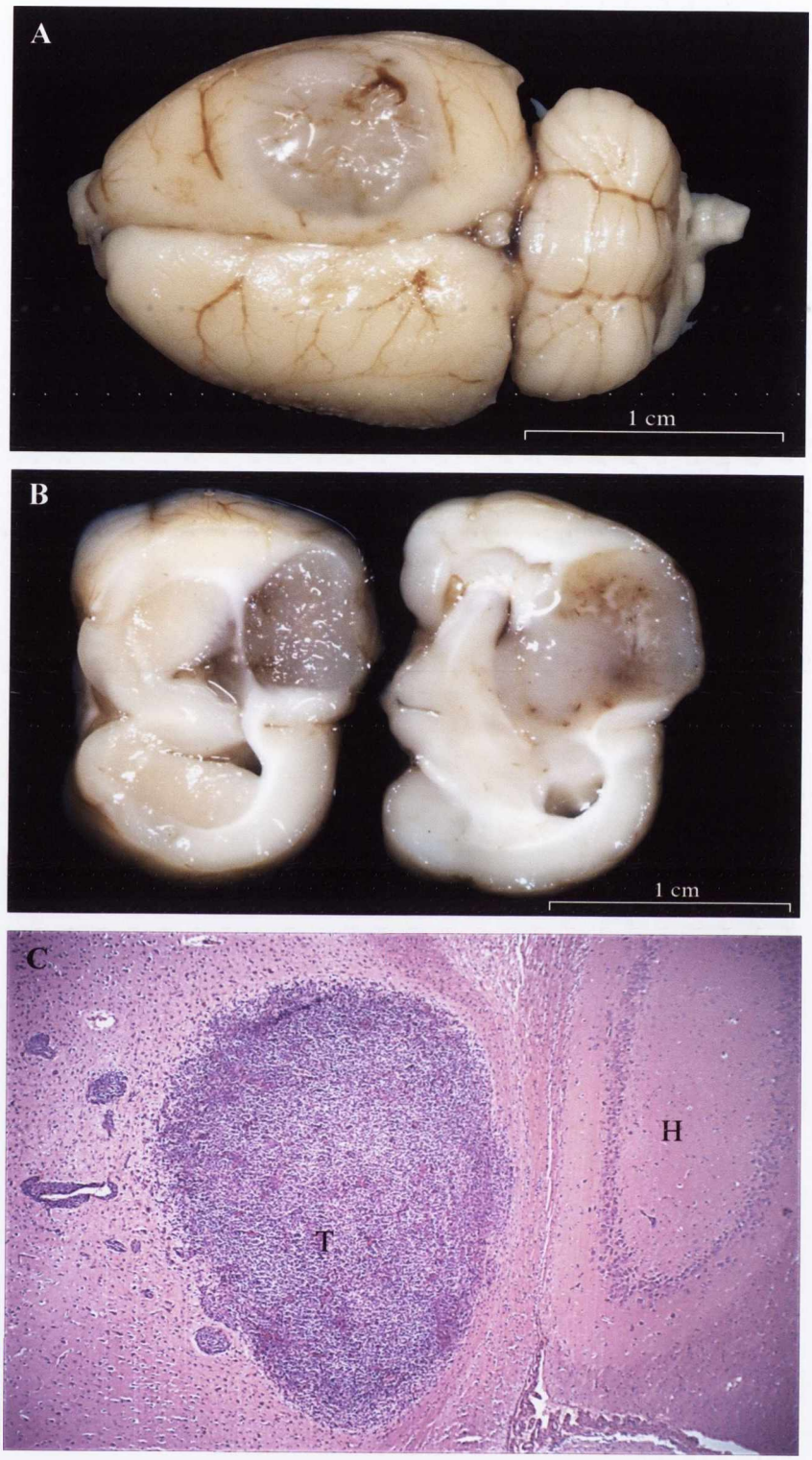

Figure 5.2: *In vivo* characterisation of RG2 gliomas (A-C).

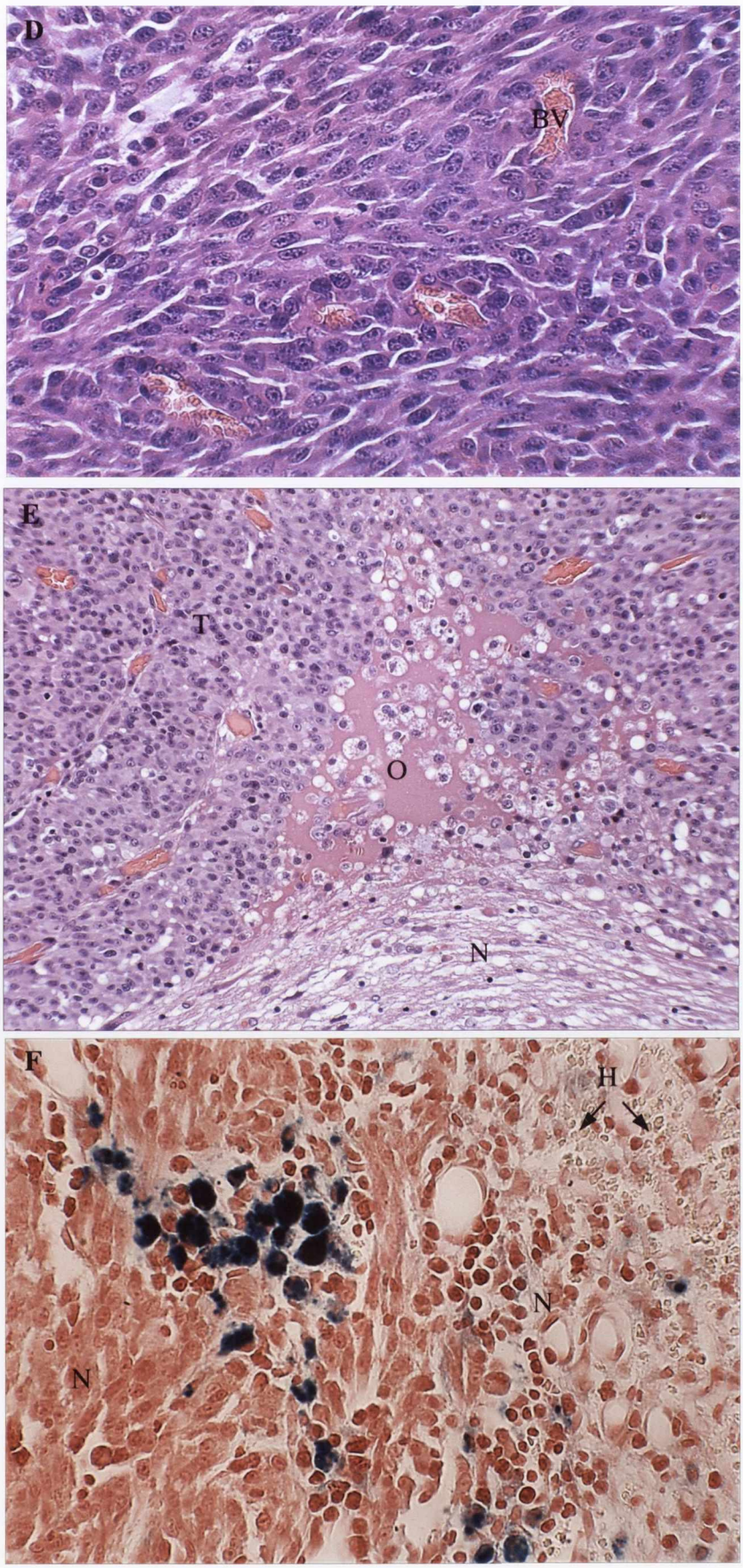

Figure 5.2: *In vivo* characterisation of RG2 gliomas (D-F).

5.3.2 Low-dose treatment of RG2 gliomas

5.3.2.1 Intracerebral treatment of RG2 gliomas with low-dose VLPs

Low-dose treatment was divided into 3 blocks of 6-8 animals per block. Treatments were assigned randomly such that, where possible, each block contained at least two members from each treatment group. Animals were implanted with cannulas and, one-week later, RG2 glioma cells were inoculated into the right hippocampus, via the implanted cannula. Treatment was initiated one-week after glioma cell inoculation. Animals were anesthetised with isoflourane and treated with TNE buffer, IL-12 encoding or empty SFV VLPs ($5x10^7$ VLPs/μl), in a total volume of 5μl. Animals received six treatments every second day, as per Figure 5.3. The experimental endpoint for each experimental block was determined by the onset of clinical signs in any animal, which occurred at 21 days (+/- 1 day) p.i. At the experimental endpoint, animals were anesthetised with xylazine/ketamine and perfused through the left ventricle with PBS followed by 10% NBFS; the brain and samples of liver, kidney and spleen were excised, placed in 10% NBFS and processed for histological examination. Throughout all three low-dose RG2 experiments three animals displayed clinical signs prior to the completion of treatment; one empty VLP (1/14, 7.14%) and two IL-12 encoding VLP (2/23, 8.7%) treated animals were culled prior to completion of treatment and were excluded from statistical analyses.

Low-dose VLP treatment was carried out in duplicate, using two independent batches of male Fischer 344 rats and independently prepared and titered batches of empty and IL-12 encoding SFV VLPs. RG2 tumors were roughly spherical and ranged from 4mm to 7mm in diameter in TNE treated animals. Tumors were measured and standardised against the mean TNE tumor volume. Tumor volumes were compared between blocks, where possible, and no statistically significant differences were detected; as a result, blocks were pooled and all statistical comparisons represent Two-Sample T-tests, unless otherwise stated. Figures 5.4 and 5.5 demonstrate the effect of low-dose VLP treatment at the experimental endpoint. Statistically significant differences between treatment groups were similar in both experiments. Results demonstrated no statistical difference between TNE and empty VLP treated animals (-16.89 ± 12.25%, p=0.2012 and -30.58 ± 20.65%, p=0.1728). IL-12 encoding VLP treated tumors demonstrated a highly significant reduction in tumor volume compared to TNE treated tumors (-60.37 ± 9.812%, p=0.0002 and -73.39 ± 15.69%, p=0.0007). Additionally, IL-12 encoding VLP treated tumors

demonstrated a statistically significant reduction in tumor volume compared to empty VLP treated tumors (-43.48 ± 11.26%, p=0.0032 and -42.81 ± 14.16, p=0.0106).

Within one low-dose RG2 experiment, the IL-12 treated group displayed a bimodal distribution that could be divided into two statistically dissimilar groups, termed IL-12_1 and IL-12_2. IL-12_1 (n=4, 45.36% ± 4.037) and IL-12_2 (n=4, 7.868% ± 2.008) were statistically different (-37.49 ± 4.508%, p=0.0002) and both groups had significantly smaller tumors compared to TNE treated animals (-54.64 ± 18.75, p=0.0225 and -92.13 ± 18.50, p=0.0016 respectively). IL-12_2 tumors were significantly smaller than empty VLP treated tumors (-61.56% ± 16.52, p=0.0058); however IL-12_1 tumors were not (24.06% ± 16.75, p=0.1887). Tumors from the IL-12_1 and IL-12_2 treatment groups were of similar histological appearance.

To determine if the reduction in tumor volume, as a result of therapy, resulted in an extension in survival, an additional RG2 low-dose treatment experiment was carried out. Only TNE and IL-12 treatments were examined and the experimental endpoint for each animal was the presentation of clinical signs, at which point animals were culled. Eleven animals survived until the end of treatment; five TNE treated and six IL-12 encoding VLP treated animals. A Kaplan-Meier survival curve analysis (Figure 5.6) demonstrated a moderate but highly significant survival benefit following IL-12 encoding VLP treatment (22.4 days vs. 26.5 days, p=0.0011). Tumors from IL-12 treated and TNE treated groups were of similar dimensions at the experimental endpoint and no histological differences were detected.

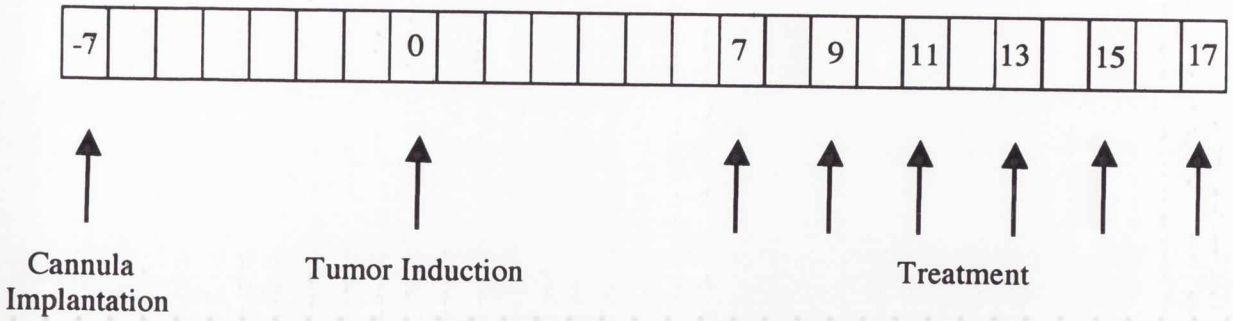

Figure 5.3: Schematic of treatment strategy for intracerebral SFV VLP delivery.

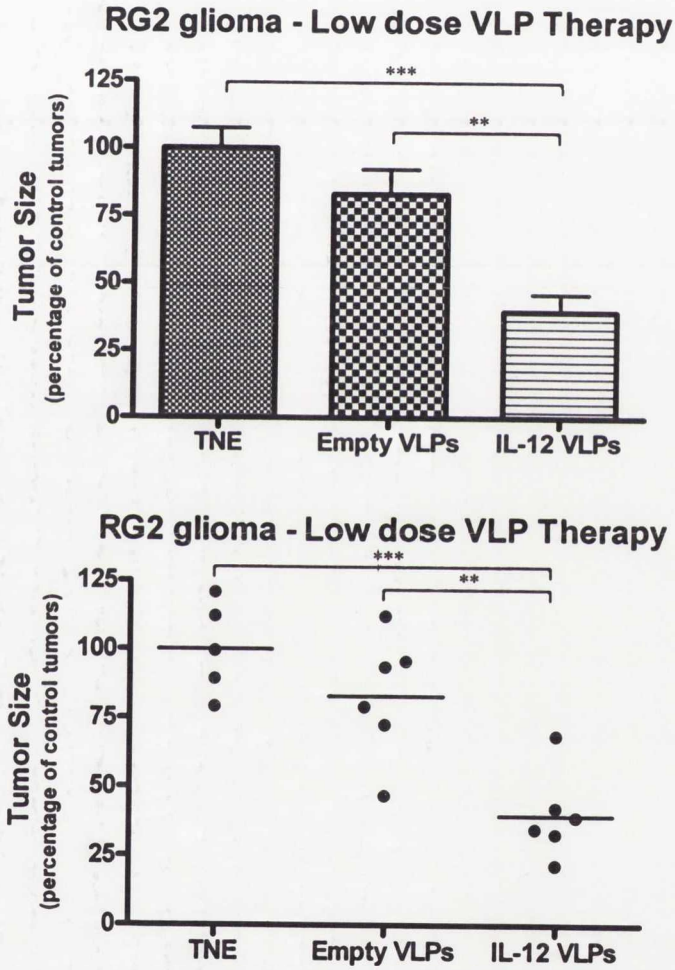

Figure 5.4: Low-dose VLP treated RG2 glioma.

Animals were treated intracerebrally with TNE (n=5), empty VLPs (n=6) or IL-12 encoding VLPs (n=6). Tumor volumes were standardised against the mean TNE tumor volume. Error bars represent SEM. ** - $p < 0.01$, *** - $p < 0.001$.

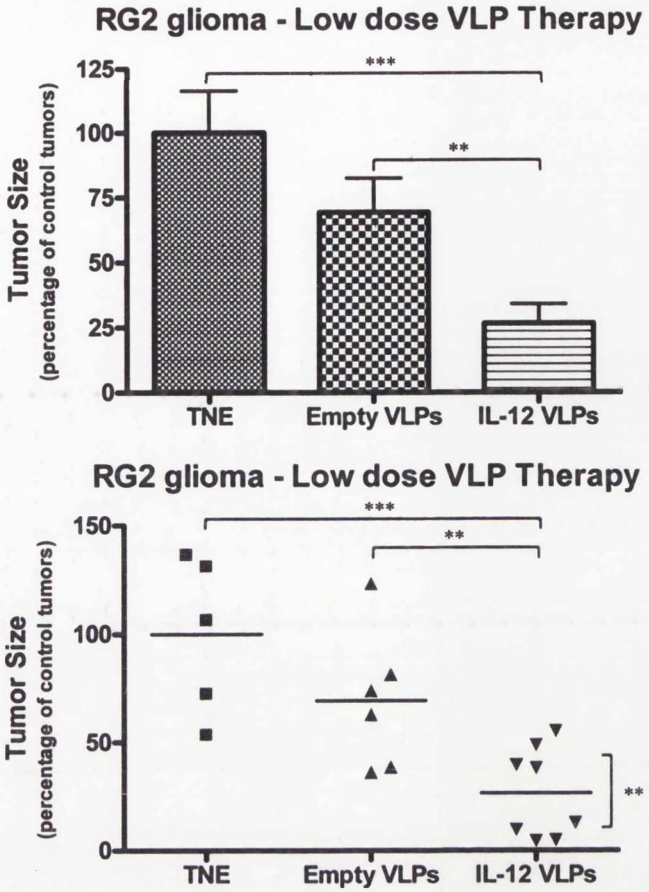

Figure 5.5: Low-dose VLP treated RG2 glioma.

Animals were treated intracerebrally with TNE (n=5), empty VLPs (n=6) or IL-12 encoding VLPs (n=8). Tumor volumes were standardised against the mean TNE tumor volume. Error bars represent SEM. ** - $p < 0.01$, *** - $p < 0.001$.

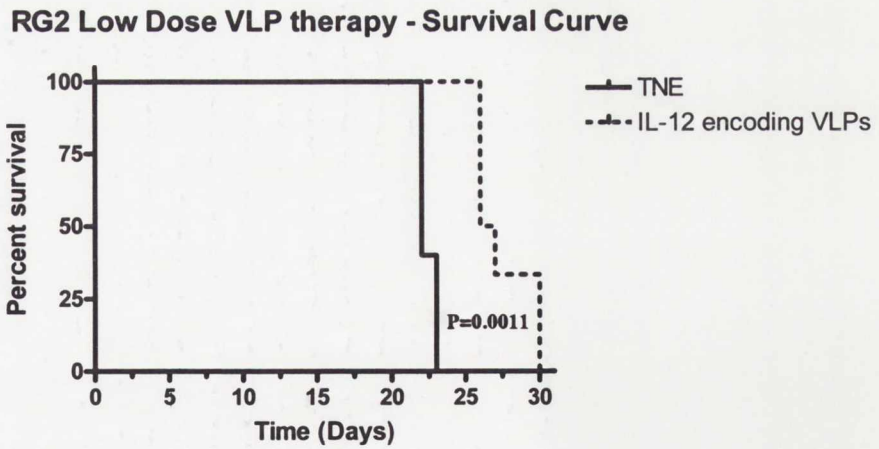

Figure 5.6: Survival curve analysis of low-dose VLP treated RG2 bearing animals.

Animals were treated intracerebrally with TNE (n=5) or IL-12 encoding VLPs (n=6). Animals were culled upon presentation of clinical signs. IL-12 encoding VLPs demonstrated a statistical enhancement in survival (22.4 days vs. 27.5 days, p=0.0011).

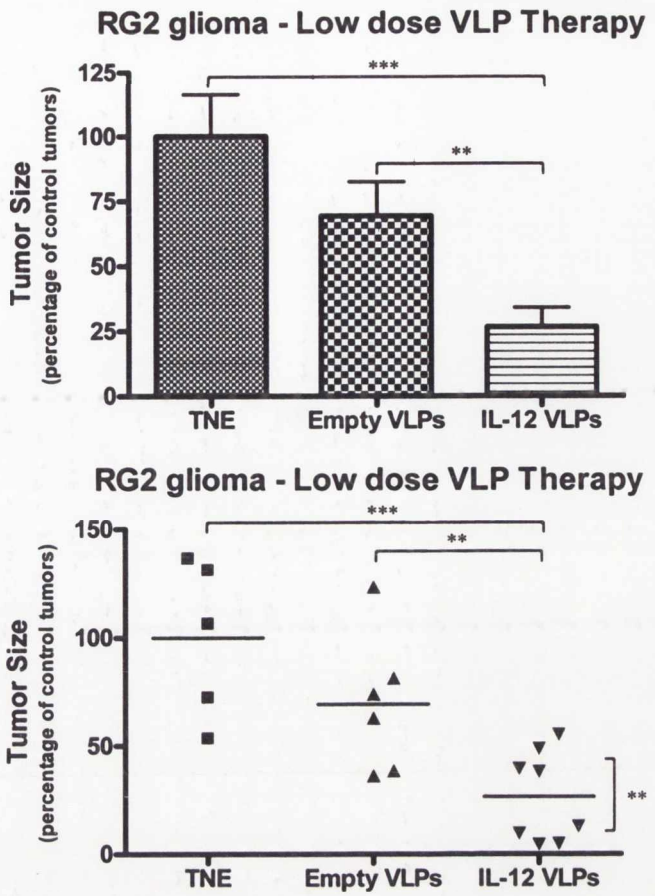

Figure 5.5: Low-dose VLP treated RG2 glioma.

Animals were treated intracerebrally with TNE (n=5), empty VLPs (n=6) or IL-12 encoding VLPs (n=8). Tumor volumes were standardised against the mean TNE tumor volume. Error bars represent SEM. ** - $p < 0.01$, *** - $p < 0.001$.

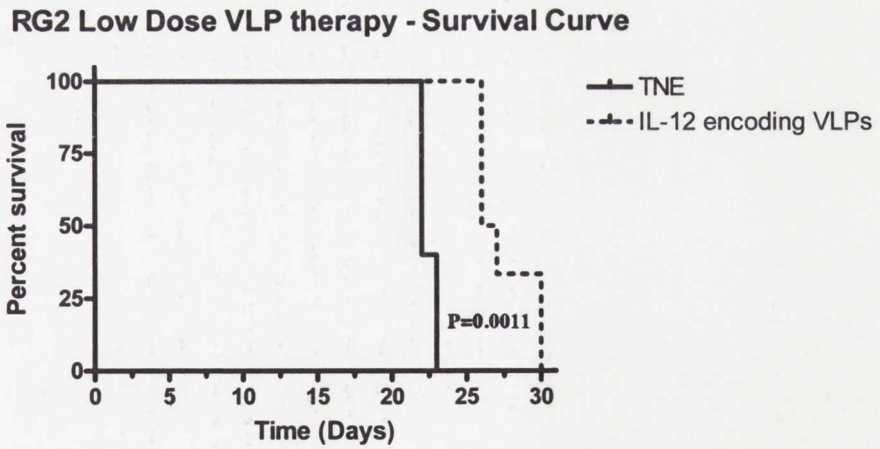

Figure 5.6: Survival curve analysis of low-dose VLP treated RG2 bearing animals.

Animals were treated intracerebrally with TNE (n=5) or IL-12 encoding VLPs (n=6). Animals were culled upon presentation of clinical signs. IL-12 encoding VLPs demonstrated a statistical enhancement in survival (22.4 days vs. 27.5 days, p=0.0011).

5.3.2.2 Characterisation of peritumoral lymphocytes

Anti-CD3 immunohistochemistry was performed on formalin-fixed brain sections from five empty VLP and five IL-12 encoding VLP treated tumors. Small numbers of $CD3^+$ cells were present at the inoculation site and the tumor perimeter in both empty and IL-12 encoding VLP treated tumors (Figure 5.7). $CD3^+$ cells were largely absent from the tumor bulk and the pattern and intensity of staining of $CD3^+$ cells was similar in both empty VLP and IL-12 encoding VLP treated tumors.

5.3.2.3 Analysis of tumor microvessel density

Anti-CD31 immunohistochemistry was performed on formalin-fixed brain sections from five TNE, five empty VLP and five IL-12 encoding VLP treated tumors (Figure 5.8A). Microvessel density was assessed by enumerating the number of $CD31^+$ vessels in ten 400x (40x objective, 10x eyepiece) fields per tumor. The tumor microvessel density between groups was compared by Two-Sample T-test and no significant differences were demonstrated (Figure 5.8B).

5.3.3 Low-dose treatment of F98 gliomas

5.3.3.1 Intracerebral treatment of F98 glioma with low-dose VLPs

Low-dose VLP treatment of F98 gliomas was carried out as **5.3.2**. Treatments were randomly assigned such that, where possible, each block contained at least two members from each treatment group. Each block was culled at the onset of clinical signs in any animal. Moribund animals that demarcated the experimental endpoint were members of all treatment groups and occurred at 21 days (+/- 1 day).

Four animals displayed clinical signs prior to the completion of treatment; one empty VLP treated animal (1/9, 11.11%) and three IL-12 encoding VLP treated animals (3/9, 33.33%) were culled and excluded from statistical analyses. Figure 5.9 demonstrates the effects of low-dose VLP treatment on F98 glioma volume at the experimental endpoint. There was no statistical difference between TNE and empty VLP or TNE and IL-12 encoding VLP treated tumors ($p=0.1699$ and $p=0.1871$, respectively). There was however a statistically significant difference in tumor volume between IL-12 encoding VLP treated and empty VLP treated animals ($-56.77 \pm 16.20\%$, $p=0.0057$).

Because of the high level of necrosis and haemorrhage in F98 tumors, areas of necrosis and haemorrhage were measured to determine possible associations with treatment. Levels of necrosis and haemorrhage correlated well with tumor volume (Figure 5.10, $r^2=0.6903$) and statistical significances between treatment groups were unaffected when total tumor volume, or tumor volume less necrotic area were compared (data not shown).

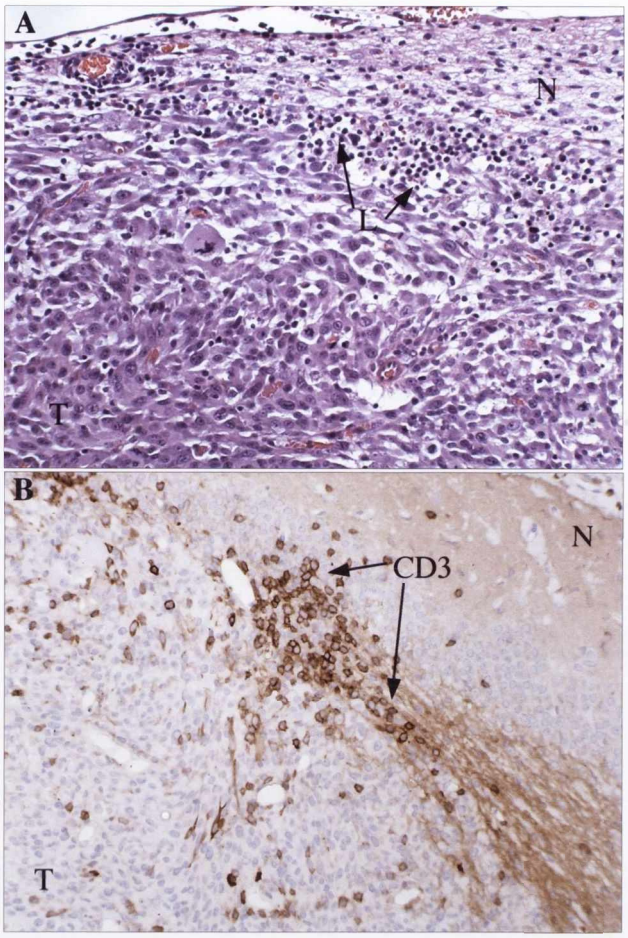

Figure 5.7: Immunohistochemical characterisation of peritumoral lymphocytes.

A - RG2 tumour showing low-grade lymphocytic infiltration (L) at the interface of the tumor (T) and the surrounding neuropil (N). H&E, x200. **B** - Serial section immunolabelled for $CD3^+$ T lymphocytes (CD3); IHC, x200.

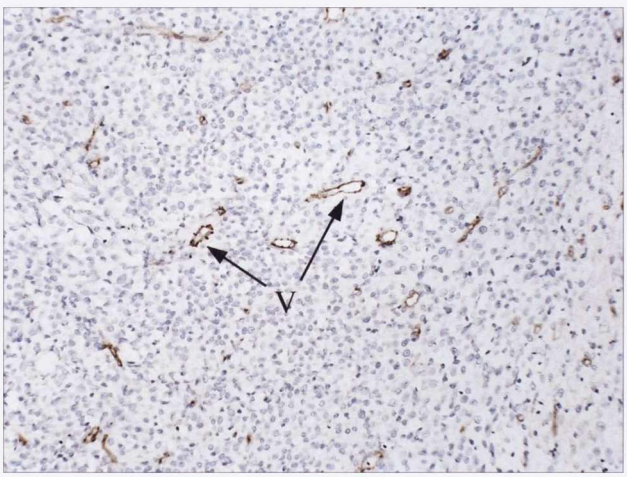

Figure 5.8: Analysis of tumor microvessel density.

Immunohistochemical localization of CD31 in vascular endothelial cells (V) in an RG2 tumor following low dose treatment with empty VLPs; IHC, x200.

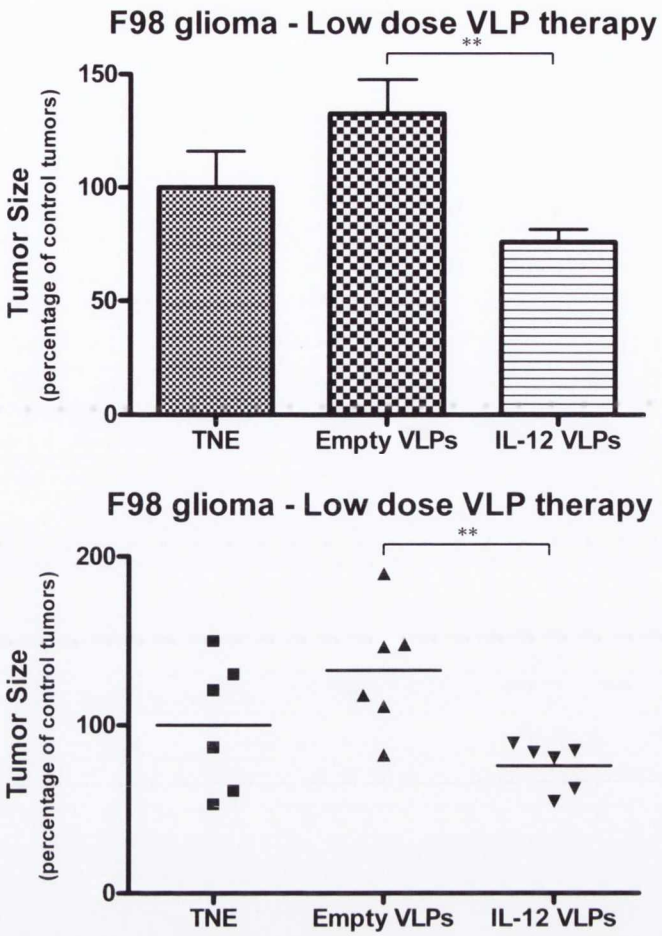

Figure 5.9: Low-dose VLP treated F98 glioma.

Animals were treated intracerebrally with TNE (n=6), empty VLPs (n=6) or IL-12 encoding VLPs (n=6). Tumor volumes were standardised against the mean TNE tumor volume. Error bars represent SEM. ** - $p < 0.01$.

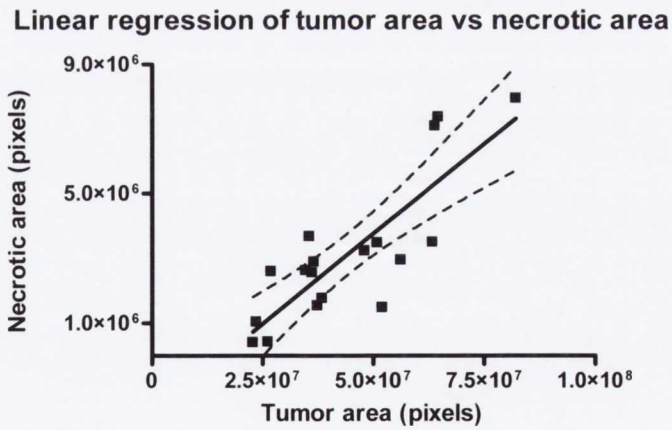

Figure 5.10: Linear regression analysis of tumor and necrotic area

A total of 18 data points were analysed representing tumors from 3 treatment groups, TNE (n=6), empty VLPs (n=6) and IL-12 encoding VLPs (n=6). The square of the correlation co-efficient (r^2) was 0.6903, dashed lines represent 95% confidence interval.

5.3.4 High-dose treatment of RG2 gliomas

5.3.4.1 Intracerebral treatment of RG2 glioma with high-dose VLPs

High-dose VLP treatment of RG2 gliomas was carried out as **5.3.2** and $1x10^8$ VLPs/μl were delivered per treatment. Seven animals comprising two empty VLP treated animals (2/6, 33.33%) and five IL-12 encoding VLP treated animals (5/8, 62.5%) were culled prior to completion of treatment and were excluded from statistical analyses. Figure 5.11 demonstrates the effect of high-dose VLP treatment on RG2 glioma volume at the experimental endpoint. There was a statistically significant reduction in tumor volume between TNE and empty VLP treated tumors (-72.93 ± 14.85%, p=0.0027) and between TNE and IL-12 encoding VLP treated tumors (-87.11 ± 17.95%, p=0.0047). No statistical difference between empty and IL-12 encoding VLP treated tumors (-14.18 ± 6.431%, p=0.0786) was observed although the p value approached significance.

Histologically, tumors in animals treated with empty and IL-12 encoding VLPs were markedly reduced in size with some animals showing only tumor remnants. Extensive cavitation and necrosis accompanied by oedema and leucocytic infiltrates, mostly composed of macrophages and neutrophils, was observed at the inoculation site of both empty and IL-12 encoding VLP treated animals (Figure 5.12).

5.3.5 Analysis of treatment-related deaths

A total of 94 animals were used in intracerebral VLP experiments. All animals that displayed lethargy, ruffled fur or discomfort prior to the completion of treatment, at 17 days post tumor cell inoculation, were considered to have died as a result of treatment. In no case did TNE treated animals display clinical signs before the experimental endpoint. Table 5.1 is a summary of the animals culled before the experimental endpoint stratified by group and treatment. Figure 5.13 is a Kaplan-Meier survival curve analysis of the data summarised in Table 5.1; all days represent time post-inoculation of tumor cells and animals surviving until the experimental endpoint were censored.

Within each experiment, F98 low-dose, RG2 low-dose and RG2 high-dose VLP treatment, there was no statistically significant difference between the frequencies of VLP related deaths as a result of empty or IL-12 encoding VLP treatment ($p=0.2383$, 0.848 and 0.4379 respectively). As a result, empty and IL-12 encoding VLP treated animals were pooled for comparison of treatment-related deaths between experiments (Figure 5.14). High-dose treated RG2 and low-dose treated F98 animals demonstrated treatment-related death rates statistically different from TNE treated animals ($p<0.0001$ and $p=0.0137$, respectively) while low-dose treated RG2 tumor-bearing animals did not ($p=0.1413$). Additionally, a statistically significant difference in the frequency of treatment-related deaths was observed between high-dose and low-dose treated RG2 tumor bearing animals ($p=0.0005$) although no other inter-experimental comparisons were significant ($p>0.05$).

Samples of liver, spleen and kidney harvested from animals treated with TNE, empty VLPs and VLPs encoding IL-12 were examined histologically and no significant changes were detected.

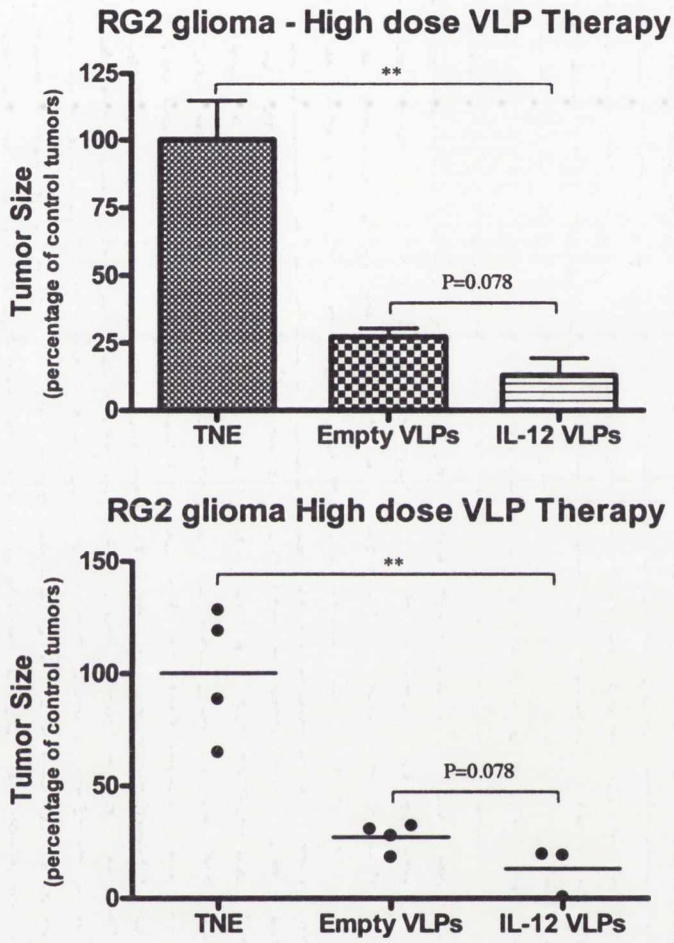

Figure 5.11: High-dose VLP treated RG2 glioma.

Animals were treated intracerebrally with TNE (n=4), empty VLPs (n=4) or IL-12 encoding VLPs (n=3). Tumor volumes were standardised against the mean TNE tumor volume. Error bars represent SEM. ** - $p < 0.01$.

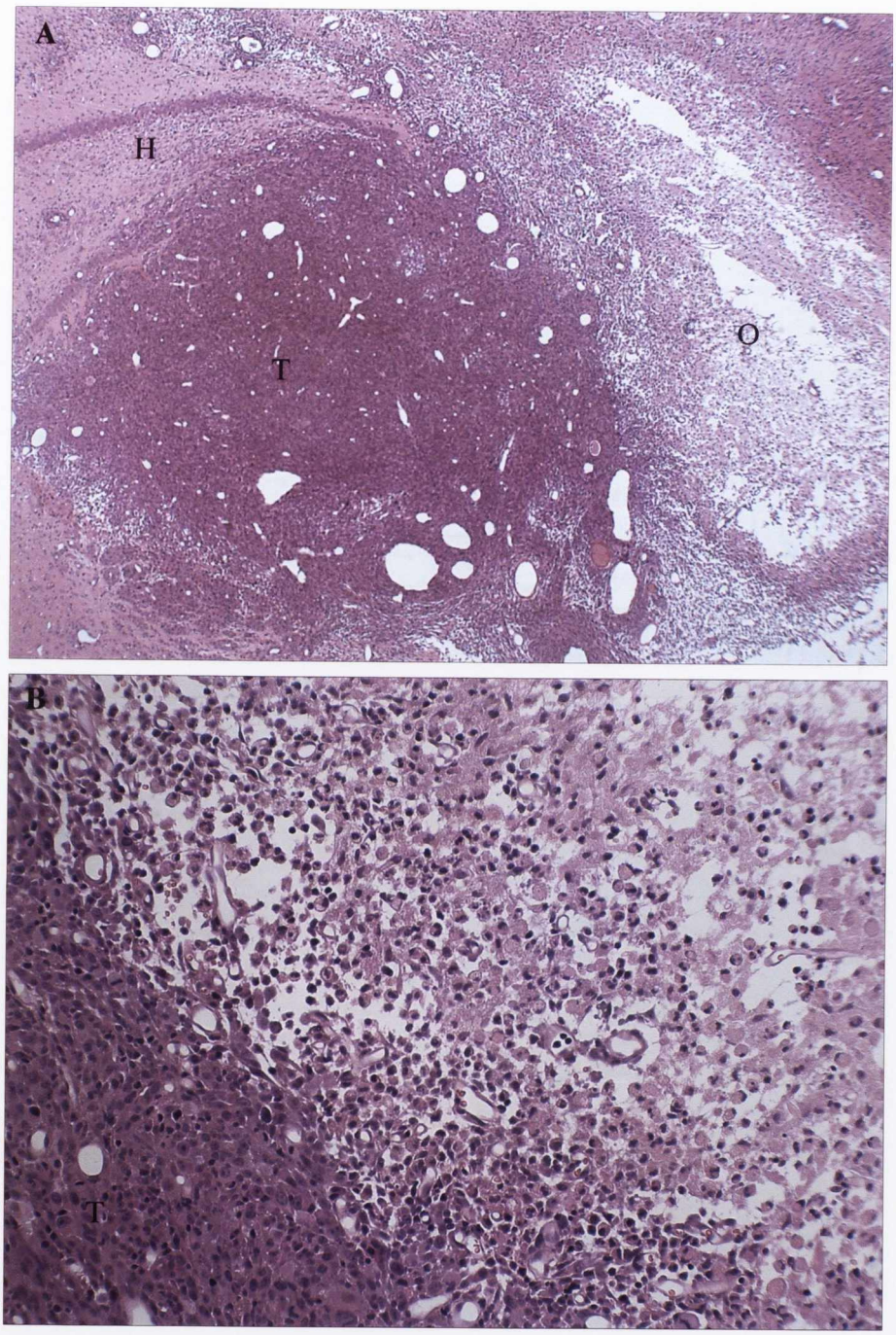

Figure 5.12: RG2 glioma treated with high-dose IL-12 encoding VLPs

A – An area of cavitation and oedema (O) adjoins a tumour mass (T) in the hippocampus (H) 5 days after final (6^{th}) intratumoural treatment with IL-12 encoding VLPs; H&E, x40. **B** – Higher magnification of (A) showing macrophages and neutrophils at the periphery of the tumor mass (T); H&E, x200.

Experiment	Treatment	N	Toxicities (%)
RG2 Low dose	TNE	15	0 (0)
	Empty VLPs	14	1 (7.14)
	IL-12 VLPs	23	2 (8.7)
F98 Low Dose	TNE	5	0 (0)
	Empty VLPs	9	1 (11.11)
	IL-12 VLPs	9	3 (33.33)
RG2 High Dose	TNE	5	0 (0)
	Empty VLPs	6	2 (33.33)
	IL-12 VLPs	8	5 (62.5)

Table 5.1: Summary of the animals culled due to apparent toxicity stratified by group and treatment.

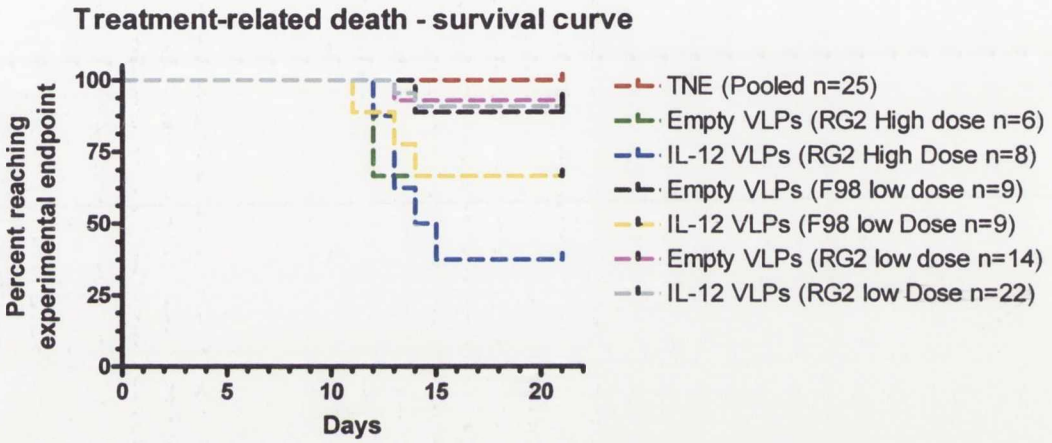

Figure 5.13: Kaplan-Meier survival curve analysis of VLP related toxicity.

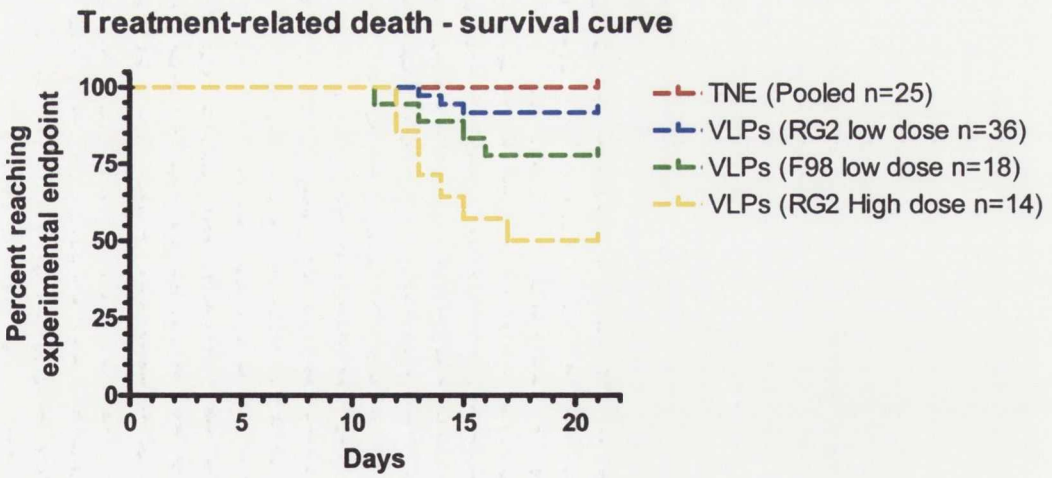

Figure 5.14: Kaplan-Meier survival curve analysis of VLP related toxicity.

Within each experiment, empty and IL-12 encoding VLP treatments were combined for analysis between experiments.

5.3.5.1 Detection of replication competent virus

Six animals treated with high-dose VLPs (four IL-12 encoding VLP and two empty VLP treated animals) were examined for replication-competent virus. Brains were homogenised in infection medium (50% w/v) and 1ml of each homogenate used to infected one 75cm^2 flask of sub-confluent BHK cells for 1 hour with gentle rocking every 15 minutes. Following infection, 14 ml of maintenance medium was added and cells incubated for 72 hours at 37°C. Cells were examined for cytopathic effect every 24 hours and 72 hours p.i. 1ml supernatant was used to infect a sub-confluent 75 cm^2 flask, as before. This procedure was carried out a further four times and at no time was cytopathic effect observed in cells from the brain homogenate of any animal. Additionally, RCV could not be detected in VLP stocks by cytopathic effect assay.

5.3.5.2 Analysis of SFV antigen expression in VLP treated animals

Using antibodies raised against the SFV nsP2 protein or replicating SFV4 virus, brains from eleven animals were analysed by anti-SFV immunohistochemistry (Table 5.2). The positive control was known SFV4-positive brain sections from infected mice. Although the positive control was strongly positive using anti-SFV4 or anti-nsP2 antibodies (Figure 5.15), all brain and tumor samples were negative for SFV antigen using both antibodies. Additionally, brain regions shown to be positive for SFV VLPs, as demonstrated by IL-12 expression (**5.3.3.2**), were negative when serial sections were examined for SFV antigen expression (data not shown).

5.3.3.3 Immunohistochemical detection of IL-12 in VLP treated animals

Due to the inability to detect SFV antigen in the brains of VLP treated animals, a panel of eleven brains was examined by immunohistochemistry for the expression of the VLP encoded transgene, IL-12 (Table 5.2). IL-12 was readily detectable in all animals treated with IL-12 encoding VLPs and culled because of clinical signs prior to the completion of treatment. Expression of IL-12 was localised at the inoculation sites in neurons and neuronal cell processes in the hippocampus (Figure 5.16). IL-12 expression was absent in culled empty treated animals and in empty or IL-12 encoding VLP treated animals surviving until the experimental endpoint.

Tumor	Treatment	Death*	IL-12	SFV antigen
(F98 low-dose)	Empty VLPs	No	No	No
(F98 low-dose)	IL-12 encoding VLPs	No	No	No
(F98 low-dose)	IL-12 encoding VLPs	No	No	No
(RG2 low-dose)	IL-12 encoding VLPs	No	No	No
(RG2 low-dose)	IL-12 encoding VLPs	No	No	No
(F98 low-dose)	Empty VLPs	Yes	No	No
(RG2 low-dose)	Empty VLPs	Yes	No	No
(F98 low-dose)	IL-12 encoding VLPs	Yes	Yes	No
(F98 low-dose)	IL-12 encoding VLPs	Yes	Yes	No
(F98 low-dose)	IL-12 encoding VLPs	Yes	Yes	No
(RG2 high-dose)	IL-12 encoding VLPs	Yes	Yes	No

Table 5.2: Results of anti-SFV and anti-IL-12 immunohistochemistry on a panel of samples from VLP treated animals.

* – occurring before the experimental endpoint.

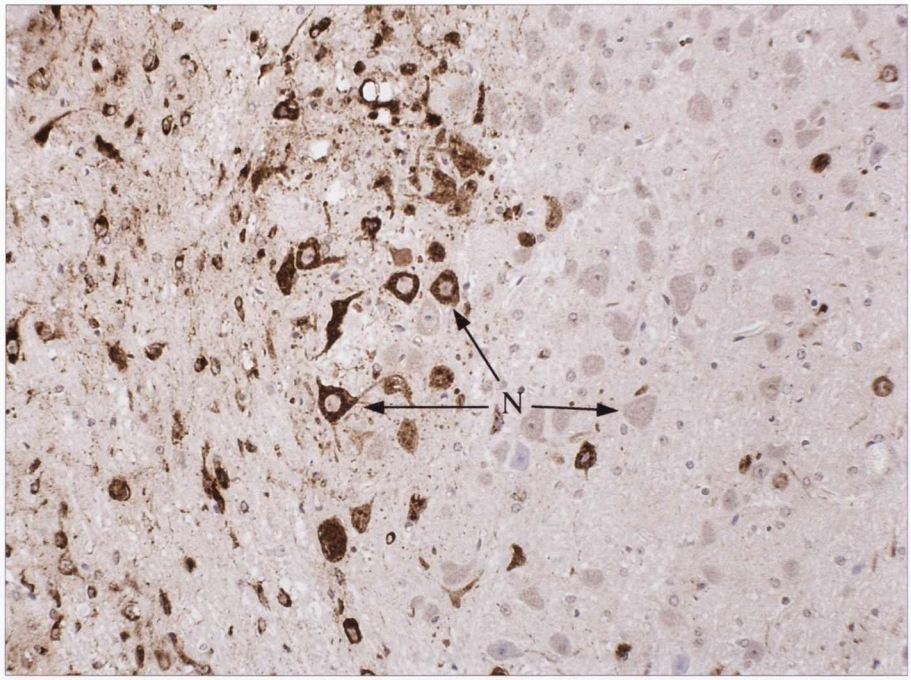

Figure 5.15: Immunohistochemical detection of SFV antigen expression.

Thalamus of a BALB/c mouse 4 days following i.p. inoculation with SFV4. SFV antigen is localised in the cytoplasm of neurons (N) and in neuronal cell processes; IHC, x200.

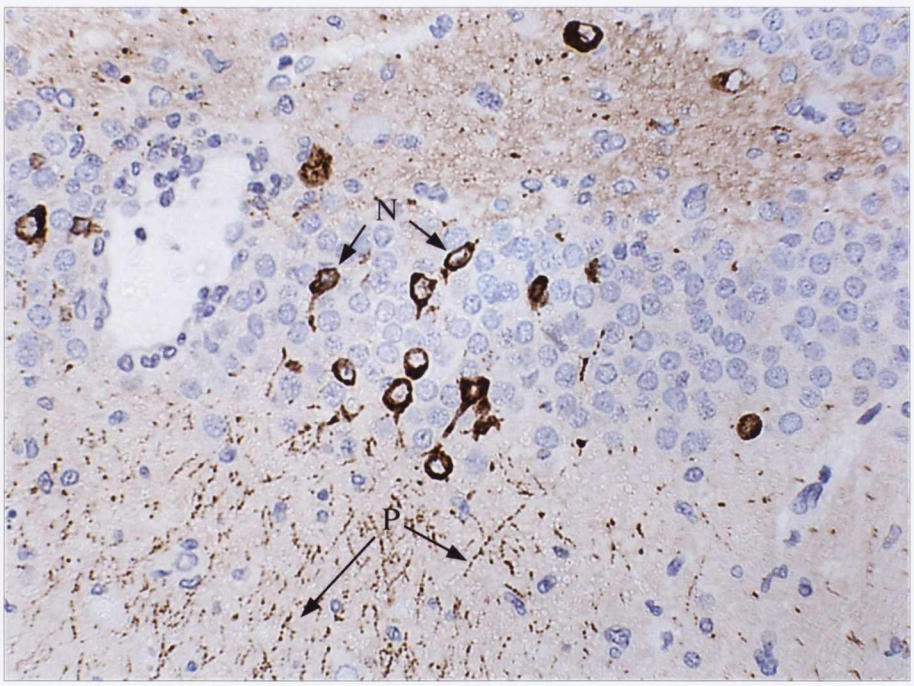

Figure 5.16: Immunohistochemical analysis of IL-12 antigen expression.

Hippocampus of a rat bearing an RG2 tumour treated with IL-12 encoding SFV VLPs. Neurons (N) and neuronal cell processes (P) show positive expression of IL-12; IHC, x400.

5.4 Discussion

Initial experimentation demonstrated that intracerebral inoculation of 2,000 glioma cells resulted in tumors with a survival time of approximately three weeks. Initial observations also confirmed published data on tumor growth rates (Seitz *et al.*, 1988). Negligible tumor masses were present at one week and small macroscopic tumors at two weeks p.i; the majority of tumor growth occurred between two and three weeks p.i. leading to the rapid onset of clinical signs, at which point animals were culled. Both RG2 and F98 glioma cell lines produced reproducible and lethal tumors, noticeable differences were observed in the growth patterns of both glioma models. RG2 gliomas were well defined, roughly spherical, expansile and infrequently extended beyond the main tumor mass. Necrosis and haemorrhage was confined to the center of large tumors and represented only a small percentage of the tumor area. In contrast, F98 tumors were highly infiltrative and necrosis and haemorrhage were prominent features, additionally observed by Wechsler *et al.* (1989). F98 tumors also frequently extended beyond the main tumor mass into the brain parenchyma, particularly in perivascular spaces, and nodular masses were located in the ventricular system and in the meninges. Traumatic lesions in the brain associated with the i.c. microinjections were well tolerated and did not appear to impact negatively upon the welfare of the animals. Additionally, repeated anesthesia, required for i.c. treatment was also well-tolerated and regular histological examination of samples of liver, spleen and kidneys showed no evidence of toxicity.

Previous experimentation in our laboratory using the SFV VLP system encoding IL-12 (Chikkanna-Gowda *et al.*, 2005) demonstrated that maximum therapeutic effect was achieved following multiple treatments and as a result, six treatments were delivered every other day over eleven days. Treatment modalities involving intratumoral delivery of viral vectors are typically initiated once the tumor has reached a defined size, which can be easily assessed in subcutaneous tumors. Given the location of tumors in this model and the technical problems associated with repeated measurement of tumors by MRI, treatment was initiated, similarly to published literature, one week after glioma cell inoculation. Although this approach may have resulted in greater variation in tumor size at the experimental endpoint, it did not adversely affect statistical inferences. The i.c. location of tumors in this treatment model also imposed limits on the treatment strategy. Subcutaneous tumor models have previously been treated with a total volume of approximately 50 μl/treatment (Chikkanna-Gowda *et al.*, 2005; Rodriguez-Madoz *et al.*, 2005). Given the

tumor volume at the initiation of treatment and the location of the tumor within the subcutis, large delivery volumes were possible and did not cause significant problems. In the intracerebral model employed in this project however, the use of large delivery volumes would have increased the spread of VLPs into delicate, non-renewable brain tissue, which VLPs can readily infect and damage. Additionally, given the rate of delivery used (1 μl/min), large delivery volumes would have either required prolonged anesthesia and would have been excessively labor intensive if increased intracranial pressure were to be avoided. As a result of the factors mentioned above and the volumes used in published literature, a delivery volume of five microliters per treatment was chosen; as a direct consequence of the limited delivery volume, the limit of VLP delivery was 1 x 10^8 VLPs/μl (high-dose treatment).

Low-dose VLP treatment of RG2 tumors produced statistically significant results. Empty VLP treated tumors demonstrated an approximately 20% reduction in tumor volume; although this was not statistically significant, it is likely a real effect because of VLP delivery alone. This effect was previously observed by Chikkanna-Gowda *et al.* (2005) and Rodriguez-Madoz *et al.* (2005) and is likely due to the oncolytic effect of the VLPs and the induction of pro-inflammatory cytokines and innate cell activation, although the relative contributions of each are unknown. IL-12 encoding VLP treatment of RG2 tumors resulted in a statistically significant reduction in tumor volume compared to both TNE (67%) and empty VLP (43%) treated tumors. In order to correlate the reduction in tumor volume with survival benefit, animals were treated with TNE or IL-12 encoding VLPs and individual animals culled upon presentation of clinical signs. Results demonstrated a moderate survival advantage of 4 days (20.5%) although all animals eventually succumbed to tumor burden and were culled. Low-dose treatment of F98 tumors did not demonstrate a significant difference in tumor size between TNE and any treatment group; the observation that animals that demarcated the experimental endpoint were members of all treatment groups further supported the observation of no therapeutic effect. IL-12 treated tumor volumes were significantly reduced compared to empty VLP treated tumors. The reason for this observation is unknown but may be related to the difficulty in accurately measuring tumors, as a result of the extensive necrosis, poorly defined margins and infiltrative growth. The presence of necrosis in the F98 tumors also raised the question as to whether the development of necrosis was related to treatment. Necrotic areas correlated well with tumor volume suggesting that necrosis was unrelated to treatment and instead resulted from tumor expansion and ischemia.

To determine the mechanism responsible for the reduction in tumor volume following treatment, a number of immunohistochemical (IHC) analyses were performed. Reduction in tumor volume attributable to direct lysis of tumor cells or pro-inflammatory cytokine induction by the VLP system, although playing some part in the overall reduction in tumor volume, was not the major factor in reducing tumor volume, as determined by empty VLP controls. IL-12 has, in previous studies, been shown to influence T cell infiltration and tumor angiogenesis. To determine the effect of IL-12 encoding VLP treatment on T cell infiltration, empty and IL-12 encoding VLP treated tumors were labeled for $CD3^+$ lymphocytes. Low levels of $CD3^+$ lymphocytes were observed towards the perimeter of all tumors and differences in the patterns or concentrations of expression were not detected. Additionally, few CD3 positive cells were present within the tumor mass, a feature that has previously been demonstrated in our laboratory following the induction of anti-tumor adaptive immunity (Chikkanna-Gowda *et al.*, 2005; Smyth, 2005). To determine the effect of IL-12 treatment upon tumor angiogenesis, microvessel density was examined by CD31, an antigen expressed on vascular endothelial cells, staining of TNE, IL-12 encoding VLP and empty VLP treated tumors. The mean number of microvessels per high power field in control, IL-12 encoding VLP and empty VLP treated tumors was not statistically different. Seitz *et al.* (1988) examined the vascularisation of the RG2 gliomas during development in the CNS of syngeneic animals and demonstrated that while vessel density remained constant, mean vessel diameter increased concomitantly with tumor growth (independently confirmed by Valable *et al.*, 2008). Since vessel area can also be affected by pro-angiogenic factors such as VEGF-C and angiopoiten-1 (Carmeliet, 2000), the analysis of mean vessel area may have provided a possible explanation of the inhibitory effects of IL-12. Unfortunately, the analysis of tumor vessels was limited to vessel counts. In any event, the growth inhibitory effect of IL-12 treatment was short lived and tumors rapidly re-grew following the cessation of treatment, ultimately leading to lethal tumor formation. In fact, at the time points analyzed in the initial experimentation, the tumor size would have predicted a further survival of less than one week assuming tumor growth resumed at a rates similar to controls, following the cessation of treatment.

These results demonstrate a disparity between the two glioma models in terms of their sensitivity to IL-12 therapy. Given that F98 glioma cells are considered more immunogenic that the RG2 model, in terms of immune effector functions as determined by vaccination, it would further support the absence of a specific anti-tumor adaptive immune

response for the growth inhibitory effects of IL-12 treatment. Interestingly, despite there being no difference between the absolute size of RG2 or F98 gliomas, F98 gliomas demonstrated extensive necrosis and infiltration, the latter being particularly evident in perivascular regions. Additionally, Seitz *et al.* (1988), when comparing both glioma models, demonstrated a lower vessel density and mean vessel surface area and an increased intercapillary distance in F98 gliomas compared to RG2 gliomas. This decreased vascularisation is though responsible for the increased necrotic potential of F98 gliomas compared to RG2 gliomas and is presumably related to insufficient angiogenic factor production. It is possible, given the infiltrative behaviour of F98 gliomas, that angiogenic factor production is a redundant mechanism in this model. Under the assumption that the inhibitory effect of IL-12 was related to reduced vascularisation as demonstrated directly and indirectly, following treatment with SFV VLP encoding IL-12 (Asselin-Paturel *et al.*, 1998; Chikkanna-Gowda *et al.*, 2005) it is also possible then that the lower reliance of F98 gliomas upon angiogenic factors would have rendered an anti-angiogenic treatment ineffective.

High-dose treatment was examined using the RG2 glioma model. Unlike both low-dose treatments, tumors treated with both IL-12 encoding and empty VLPs had significantly reduced volumes compared to TNE controls. Although there was no significant difference between the IL-12 encoding and empty VLP treated tumors, the p value was very close to significance (-14.18 ± 6.431, $p=0.078$) and would likely have been significant had group numbers, surviving until the experimental endpoint, been larger. The results demonstrated that VLPs alone were capable of significantly reducing tumor size and high-dose empty VLP treated RG2 tumors were significantly reduced compared to RG2 tumors treated with low-dose empty VLPs. Direct lysis of tumor cells is clearly an important factor in the reduction in size of the tumors. The induction of an inflammatory response accompanied by oedema may also have provided an environment, somewhat localized to the tumor, that was not conducive to tumor growth. The inhibitory effect of VLPs alone probably comprised elements of both mechanisms mentioned but was nonetheless non-specific and, as mentioned later, resulted in considerable treatment-related deaths. Presumably, the enhanced effect of the VLP encoded IL-12 was similar to the low-dose tumor treatment regiment although, in contrast, the major effect of high-dose treatment was related to effects of the VLP system and not the encoded transgene. Interestingly, there was no significant difference in tumor size at the experimental endpoint between high-dose and low-dose IL-12 encoding VLP treated RG2 tumors (-17.79 ± 10.78,

p=0.1212) although this is again probably due to the low group number (n=3) of high-dose IL-12 encoding VLP treated animals surviving until the experimental end-point. Because of the considerable number of deaths that occurred before the completion of treatment high-dose VLP treatment of F98 tumors was not examined.

A number of VLP treated animals from all experiments displayed clinical signs prior to the completion of treatment. Clinical signs occurred as early as one day after the second treatment (ten days after inoculation of glioma cells). These animals were considered to have died as a result of treatment as tumor size was negligible at this time. At no point did TNE treated animals demonstrate clinical signs before the experimental endpoint indicating that treatment-related death was unrelated to i.c. inoculation alone. Within each experiment, there was no significant difference between the frequencies of toxicities following empty or IL-12 encoding VLP treatment and, as a result, numbers were pooled for inter-experiment analysis. This observation indicated that IL-12 expression was not toxic *per se*; given that previous experimentation has demonstrated the toxicity of i.c. IFN-γ expression (Ehtesham *et al.*, 2002) it suggested that, despite high levels of IL-12 expression, toxic levels of IFN-γ induction was not the cause of treatment-related death, which was additionally suggested by IFN-γ ELISA of brain homogenates. High-dose RG2 and low-dose F98 experiments demonstrated significant differences between TNE and VLP treated animals. Low-dose RG2 treatment did not demonstrate a significant difference between TNE and VLP treated animals although this conclusion may be related to the sensitivity of the statistical analysis.

To investigate further the cause of death following VLP treatment, the brains of treated animals were examined using anti-SFV IHC. Detection of SFV antigen was not possible using either polyclonal anti-SFV4 antibody or polyclonal anti-nsP2 antibody. This is not surprising given that the structural proteins are the main antigenic proteins of SFV4, and are present at negligible levels in the VLP system and not expressed following infection. Additionally, the non-structural proteins are expressed at low levels, approximately 4,000 – 6,000 copies per cell and are difficult to detect by IHC (Fragkoudis *et al.*, 2008). This finding indicated that the deaths were unrelated to RCV, which was readily detected in positive controls, due to the presence of the structural proteins. This conclusion is also supported by the inability to detect RCV in brain homogenates or VLP stocks.

To determine the location of VLP infection, IHC was carried out against the encoded transgene, IL-12. Detection of IL-12 was limited to IL-12 encoding VLP treated

animals and, because IL-12 expression is eliminated as a result of cellular apoptosis, it was confined to animals culled within 2-3 days of treatment. Expression of IL-12 was detectable only at the inoculation sites and was mostly confined to neurons and associated cell processes in the hippocampus. These neurons were histologically normal and showed no evidence of retraction or necrosis. While the possibility cannot be excluded that VLP infection of neurons contributed to the deaths of the high-dose treated animals, it is more likely that the majority of deaths were directly associated with lysis of the tumors. The histological studies demonstrated that necrotizing changes were accompanied by severe inflammatory oedema involving the tumor tissue and the surrounding brain parenchyma. Increased intracranial pressure invariably leads to cerebral oedema and brain swelling and is often life-threatening because of the limited ability for accommodation of increased volume within the confines of the cranial cavity. The significance of these changes in varied disease circumstances in animals and human beings is well recognized (Summers *et al.*, 1995).

Chapter 6

Intranasal treatment of glioma models using the SFV VLP system

6.1 Introduction

Therapeutic drug delivery to central nervous system tumors is complicated by a number of factors, some of which are unique the CNS while other are prevalent in all anti-cancer therapies. The blood brain barrier restricts accession of certain drugs to the CNS potentially limiting optimal drug concentration and efficacy. Secondly, when delivered systemically, anti-cancer therapeutics can have serious adverse effects, of particular concern for chemotherapy agents, which may not discriminate between tumor and non-tumor tissue, and bioactive compounds, which can be toxic at high systemic levels. Additionally, systemic delivery allows for first-pass metabolism in the liver leading to potential degradation or removal of therapeutics. Given that clinical primary CNS neoplasms rarely metastasis outside the CNS (Castro *et al.*, 2006) delivery of therapeutics directly to the CNS has a number of benefits above systemic delivery. Direct intracerebral or intratumoral delivery is an effective mechanism for direct delivery to the CNS; however, it is extremely invasive and not necessarily suitable for continuous or long-term delivery. The olfactory route of drug administration has been explored in recent years and has shown excellent potential for the delivery of therapeutics directly into the CNS. Delivery via this route results in rapid access to the CNS with maximum therapeutic concentrations occurring in the brain parenchyma approximately 4 hours after administration while resulting in negligible systemic dissemination (Hashizume *et al.*, 2007).

Semliki Forest virus is a neurotropic virus capable of efficiently penetrating the CNS following intranasal administration in mice. Replicating SFV has been shown to enter the CNS via the olfactory route by infection of olfactory neurons (receptor cells) present in the nasal epithelium followed by transport along the neuronal axon, which terminates in the olfactory bulb, where continuous rounds of infection result in virus dissemination into the brain parenchyma (Sheahan *et al.*, 1996). For this reason the applicability of the SFV VLP system for the delivery of the VLP encoded transgenes into the CNS following intranasal administration has been previously explored (Jerusalmi *et al.*, 2003; Quinn *et al.*, 2006). The primary focus of previous experimentation using the SFV VLP system has been the delivery of anti-inflammatory cytokines to the CNS in an attempt to ameliorate the symptoms of experimental autoimmune encephalomyelitis, a commonly used murine model of relapsing and remitting multiple sclerosis. In mice, the SFV VLP system has demonstrated the ability to infect cells of the nasal mucosa and mediate transport of the encoded protein to the olfactory bulb and CNS, without viral replication beyond the nasal

mucosa. Although the mechanism for SFV VLP mediated protein delivery to the CNS has not been fully elucidated it is suspected to be mediated by a mechanism similar to replicating SFV infection, involving initial infection of neurons of the nasal mucosa which extend into the olfactory bulb as far as the glomerular layer (Jerusalmi, 2004). Although using the VLP system, new virus production and subsequent rounds of infection do not occur, once protein has been expressed from neurons in the glomerular layer it may simply diffuse into the CNS. Additionally, initial studies in mice demonstrated no apparent toxicity associated with intranasal delivery of VLPs, which is consistent with the transient infection and regenerative capacity of olfactory nerve cells.

Although there is obviously an absence of direct glioma cell infection and lysis, as occurs following intracerebral delivery of VLPs, this non-invasive method has a number of advantages especially in the delivery of tumorostatic agents which has the potential to inhibit tumor growth and extend survival while allowing for other therapeutic interventions. The VLP expression system, when delivered intranasally, also allows for prolonged production of transgene products in the olfactory bulb and thus protein traffic into the brain. Previous studies have demonstrated that IFN-β therapy was most effective when protein concentrations were maintained over a period of time rather than a single delivery of protein which has a relatively short half life (Yoshida *et al.*, 2004). The use of interferons as an anti-glioma therapeutic has been examined in a number of pre-clinical models; both interferon gamma and interferon beta have been delivered via intracerebral viral vector gene therapy (Kanno *et al.*, 1999; Saleh *et al.*, 2000; Chiocca *et al.*, 2008) or as recombinant protein (Oshiro *et al.*, 2001) with extremely promising results.

The IN treatment modality will be explored as a non-invasive alternative to intracerebral delivery in a rodent glioma model. The effect of SFV VLPs encoding IFN-β, IFN-γ or IL-12 delivered intranasally will be examined on tumor growth *in vivo*.

6.2 Experimental Procedures

6.2.1 New Materials

6.2.1.1 Animals

Male Fischer 344 rats were obtained from Harlan and housed in a Scantainer (Scanbar, Denmark), maintained at 25°C and given food and water *ad libitum*.

6.2.1.2 Virus

rSFV4-EGFP26MCS was constructed by Dr. Sareen Galbraith and produced and titered in house by Ms. Guniz Iskender.

6.2.2 New Methods

6.2.2.1 Preparation of VLPs for intranasal delivery

VLPs were diluted in TNE buffer, aliquoted, snap frozen in liquid nitrogen and stored at –80°C.

6.2.1.2 Surgical implantation of glioma cells

Passage 6 to 8 RG2 cells were trypsinised, resuspended in 10ml of glioma cell maintenance medium and counted. Cells were diluted with PBS and centrifuged at 1,500rpm (412.65g) for 8 minutes at 4°C. The supernatant was discarded and the cells resuspended to 5,000 cells/μl in PBS and stored on ice for no more than 1 hour before inoculation.

250-300g Fischer 344 rats were anesthetised by i.p. injection with xylazine/ketamine mix (0.3ml per 100g of 17.5mg/ml ketamine, 3.75mg/ml xylazine). Animals received Rimadyl™ (50mg carpofen per kg) as analgesia prior to surgery and anesthetised animals were placed on a stereotaxic rig. The scalp was shaved, swabbed with Betadine®, the initial incision made along the midline, the scalp cleaned and the bregma identified. The inoculation site was stereotaxically measured 3.9mm back and 2.5mm right

from the bregma and a single hole drilled into the skull. 0.4µl (2000 cells) of glioma cells were stereotaxically injected into the hippocampal coordinates (3.5mm down from the skull) using with a sterile 10µl Hamilton syringe. The syringe was held in place for 5 minutes, withdrawn, the drill hole filled with dental wax and the scalp sutured and covered in Cicatrin™ powder. Animals were recovered from anesthetic under a heat lamp until the reappearance of a pedal reflex.

6.2.1.3 Intranasal treatment of glioma bearing rats

For VLP treatment, SFV VLPs were thawed and 20µl inoculated onto each nostril every 3 days starting one week after RG2 glioma cell implantation. Animals were held on their backs and a 2-5µl droplet placed on the nostril, animals were allowed inhale it completely before the addition of the next droplet. Animals were held on their backs and gently rocked for an additional two minutes before being returned into their cages.

6.2.1.4 Culling of animals

Animals were culled by isoflourane overdose, the brain removed and placed in 50ml of NBF. The olfactory bulbs were removed and placed in Krebs buffer (136mM NaCl, 2.56mM KCl, 1.18mM KH_2PO_4, 2.24mM $MgSO_4$, 16mM $NaHCO_3$ 10mM glucose, 13.24mM $CaCl_2$, 0.2% protease inhibitor cocktail), homogenised and frozen at –80°C.

6.2.1.5 Analysis of cytokine expression in the olfactory bulb of intranasally treated animals

Rat IL-12 and IFN-γ protein was measured by commercial ELISA as per **2.2.2.4.5** and **2.2.2.4.4** respectively. To enhance the detection limit, samples were incubated overnight at 4°C and all other steps carried out as before. Total soluble protein was determined by Brandford assay.

6.2.1.6 Histological analysis of tumor size

Brains were processed, H&E stained and tumors measured as previously described in **5.2.2.9.1** and **5.2.2.9.2**.

6.2.1.7 Processing of tissue for immunofluorescence

48 hours after intranasal treatment, animals were culled by isoflourane overdose, the head removed and olfactory bulbs excised. Olfactory bulbs were placed on a small amount of frozen OCT compound on a cork disk, covered in OCT compound and frozen in liquid nitrogen cooled iso-pentane. Samples were stored at –80°C until processed. For safety reasons, rats infected intranasally with replicating SFV-EGFP were first perfused via the trans-cardiac route with 10% NFB. Twenty minutes after perfusion the olfactory bulbs were excised and frozen as before. All frozen olfactory bulbs were warmed to –20°C and sectioned on a cryostat no longer that 3 hours after culling. 6-8 micron sagittal sections were cut though the entire olfactory bulb. Sections were briefly air-dried, stained with VECTASHIELD® Hard Set™ mountant with DAPI and examined for EGFP/DAPI fluorescence.

6.3 Results

6.3.1 Intranasal treatment of RG2 glioma with SFV VLPs

Intranasal treatments were divided into 10 blocks of 3 animals per block. Surgical implantation of RG2 glioma cells was carried out on each block on a single day and each block randomly assigned a treatment. The remaining 5 animals were randomly assigned treatments. For VLP treatment, SFV VLPs were thawed and 20µl ($1x10^8$ VLPs) used to inoculate each nostril every 3 days starting one week after glioma cell implantation (Figure 6.1). Animals were held on their backs, a 2-5µl droplet placed on the nostril and the animal allowed to inhale it completely before the addition of the next droplet. The experimental end point was the development of clinical symptoms in any animal which occurred at 18 days post tumor inoculation and all animals were culled at this time after glioma cell implantation. Animals were culled, the brain excised and placed in 50ml of 10% NBFS for 48 hours. Tumor sizes were measured and standardised against the mean TNE tumor size (Figure 6.2). Throughout the intranasal treatment no animals displayed apparent signs of toxicity related to VLP delivery.

All statistical analyses represent Two-Sample T-Tests and results indicate mean difference (± SEM), unless otherwise stated. No statistically significant differences were observed between blocks of treatments in any of the treatment groups ($p>0.05$, Two-Sample T-Test between blocks of each treatment group). No statistically significant difference was observed between TNE and IL-12 encoding VLP treated animals ($p=0.2701$) while empty VLPs and IFN-β encoding VLPs showed statistically lower tumor volumes compared to TNE treated animals (-42.36 ± 19.22%, $p=0.0462$ and -45.23 ± 19.48%, $p=0.0386$, respectively). IFN-γ encoding VLPs demonstrated a 36.98 (± 18.03)% reduction in tumor volume compared to TNE treated controls, although this was not statistically significant ($p=0.0610$) the reduction indicated a trend toward a lower tumor volume. IL-12, IFN-β and IFN-γ encoding VLPs demonstrated no significant difference compared to empty VLP treated tumors ($p=0.5168$, $p=0.8509$ and $p=0.7059$ respectively). No obvious differences, such as changes in necrosis, were observed between any treatments following inspection of H&E stained tumors.

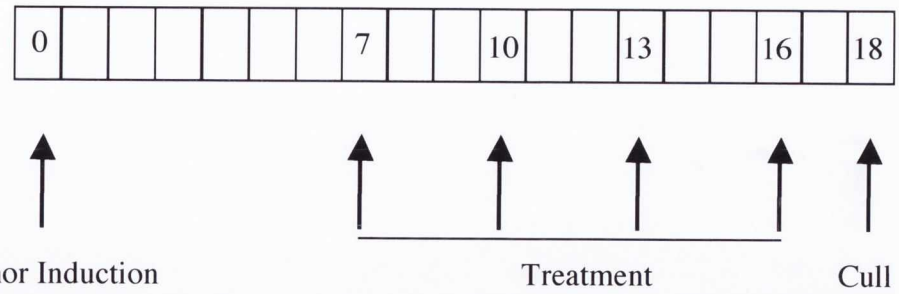

Figure 6.1: Schematic of the treatment schedule for intranasal SFV VLP delivery.

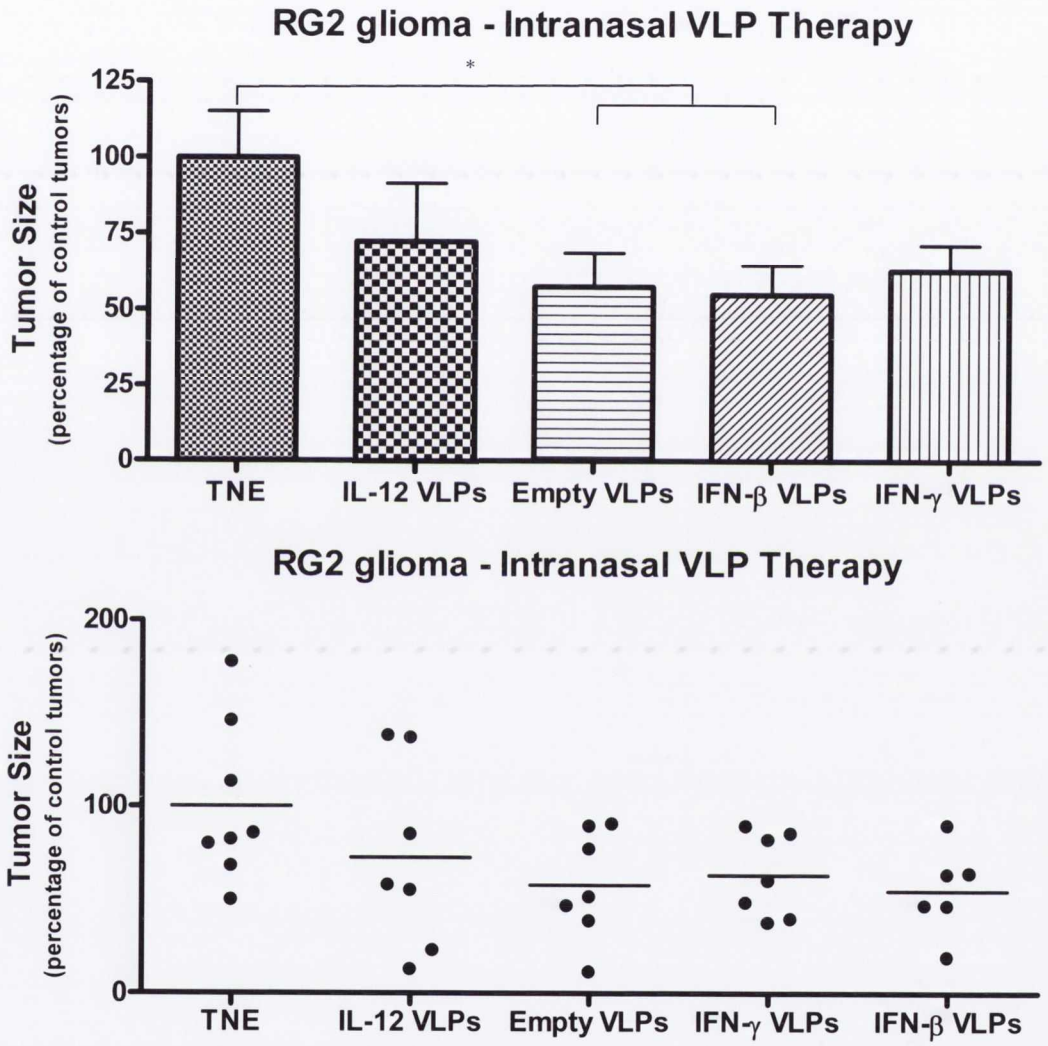

Figure 6.2: Intranasal VLP treated RG2 glioma.

Animals were treated intranasally with TNE (n=8), Empty VLPs (n=7), IL-12 (n=7), IFN-β (n=7) or IFN-γ encoding VLPs. Tumor volumes were standardised against the mean TNE tumor volume. Error bars represent SEM. * - $p < 0.05$.

6.3.2 Analysis of cytokine expression following intranasal VLP treatment

At the experimental endpoint, olfactory bulbs were removed, homogenised and examined for the presence of IL-12 in the olfactory bulbs of IL-12 encoding VLP, empty VLP or TNE treated animals. IFN-γ presence was analysed in the olfactory bulbs of IFN-γ encoding VLP, empty VLP or TNE treated animals. In no animals could IL-12 or IFN-γ be detected in the olfactory bulbs of VLP treated animals.

Twelve additional animals were treated intranasally with TNE buffer, empty VLPs, IL-12 encoding or IFN-γ encoding VLPs (n=3 per group). 48 hours later, animals were culled, the olfactory bulbs and brains homogenised and examined for the presence of the VLP encoded cytokine. No detectable levels of IL-12 or IFN-γ was demonstrated in the olfactory bulbs or brains of any VLP treated animals.

6.3.3 Analysis of EGFP expression following intranasal VLP treatment with EGFP encoding particles or replicating virus

Due to the inability to detect VLP encoded cytokines in the olfactory bulbs or brains of treated animals, animals were treated intranasally with EGFP encoding VLPs and the presence of EGFP in the olfactory bulbs examined by fluorescent microscopy. A total of 10 animals were used and received escalating dose of EGFP encoding VLPs. Olfactory bulbs were harvested, frozen and the entire bulb sectioned and examined for DAPI/EGFP flouresence. 2 animals each received 20μl of TNE per nostril, $1x10^8$ EGFP VLPs (in 20μl per nostril), $1x10^9$ EGFP VLPs (in 20μl per nostril), $1x10^9$ EGFP VLPs (in 100μl per nostril), $5x10^9$ (in 100μl per nostril) or $1x10^8$ p.f.u. of rSFV-EGFP26MCS replicating virus (in 20μl per nostril). Figure 5.3 shows the olfactory bulbs from TNE and rSFV-EGFP26MCS treated animals. Additionally indicated are the relevant areas of the olfactory bulb. No EGFP florescence was observed in the olfactory bulbs of animals treated with EGFP encoding VLPs or EGFP encoding replicating virus.

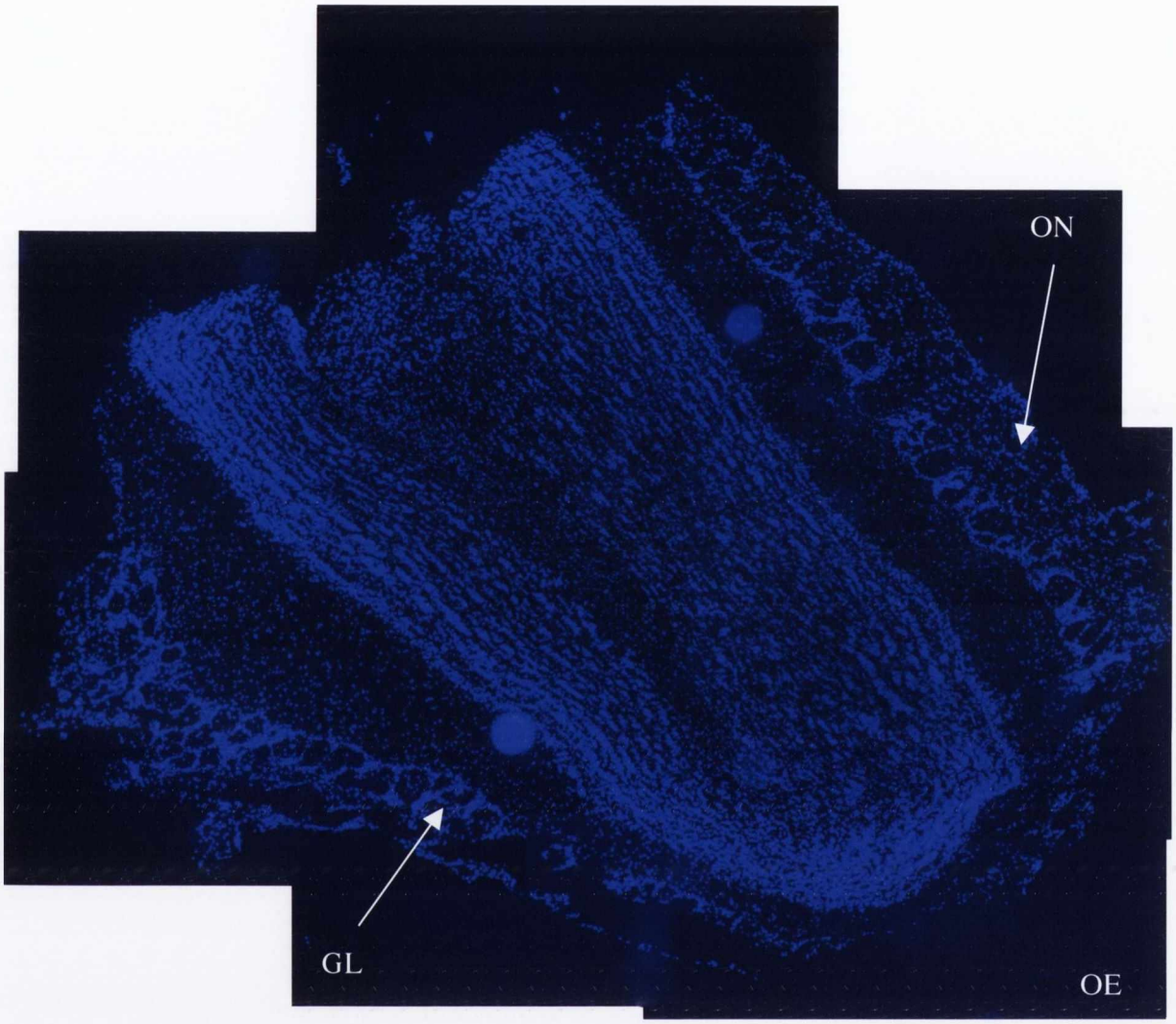

Figure 6.3-A: Olfactory bulb from rat intranasally treated with TNE buffer.

Image of olfactory bulb from rat inoculated intranasally with TNE (negative control). Image is DAPI/FITC merge and is a composite of approximately ten 40x images. The olfactory nerve layer (ON) surrounds the bulb and contains incoming axons from the receptor cells in the olfactory epithelium which terminate in the glomerular layer (GL). Also indicated is the area where the olfactory epithelium (OE) adjoined the olfactory bulb.

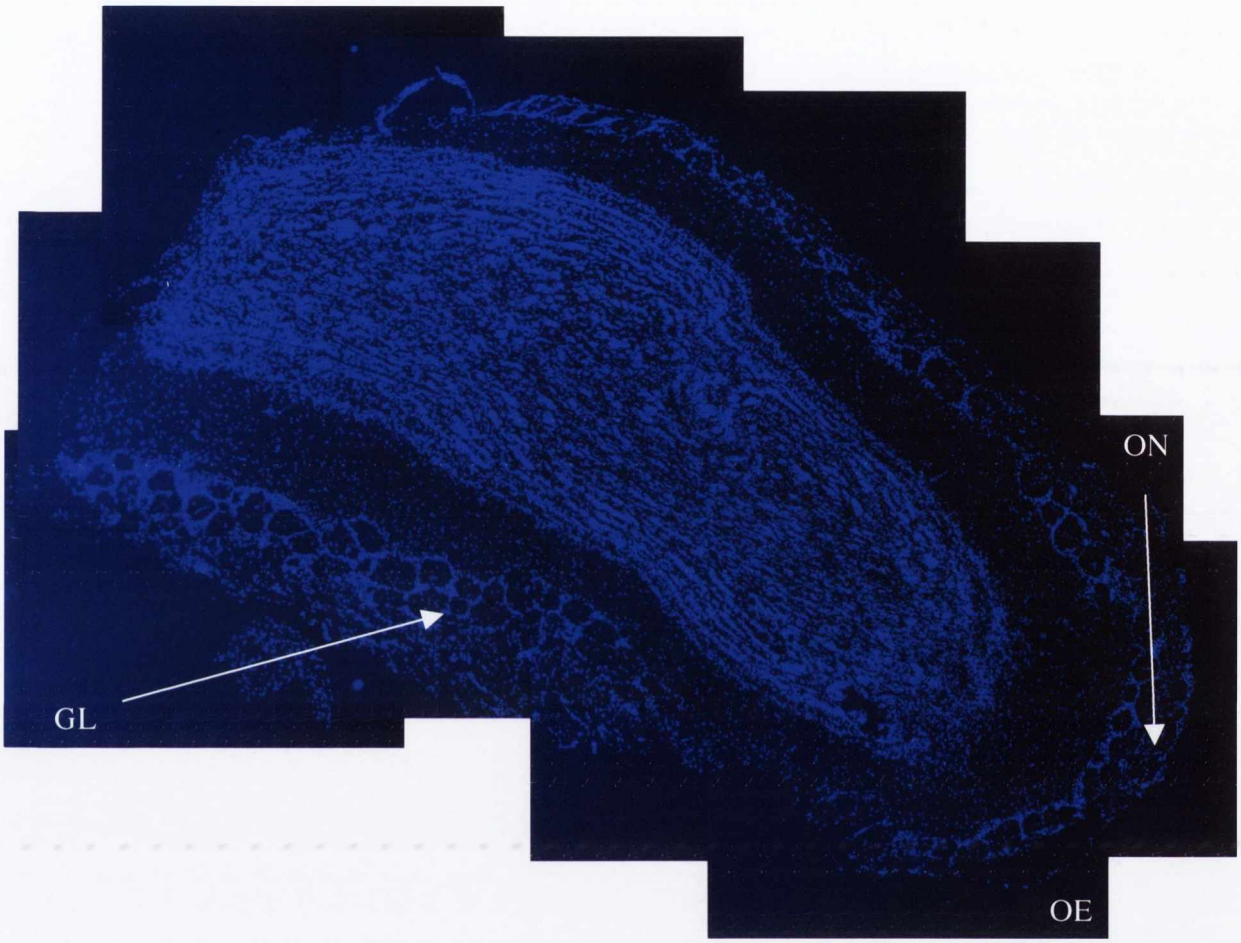

Figure 6.3-B: Olfactory bulb from rat intranasally treated with SFV-EGFP26MCS.

Image of olfactory bulb from rat inoculated intranasally with replicating SFV-EGFP26MCS virus. Image is DAPI/FITC merge and is a composite of approximately ten 40x images. The olfactory nerve layer (ON) surrounds the bulb and contains incoming axons from the receptor cells in the olfactory epithelium which terminate in the glomerular layer (GL). Also indicated is the area where the olfactory epithelium (OE) adjoined the olfactory bulb.

6.4 Discussion

Comparatively, animals treated intranasally had a shorter time to clinical symptoms than observed in intracerebral treated animals suggesting that the intracerebral inoculation procedure had some effect on tumor growth. The effect of treatment upon glioma growth was assessed compared to TNE controls and statistically significant results were obtained following intranasal delivery of empty and IFN-β encoding VLPs. Additionally, IFN-γ treated animals demonstrated reduced tumor volumes compared to TNE treated animals, which was close to significance ($p=0.0610$). Interestingly, neither IFN-γ nor IFN-β encoding VLP treated animals had tumor volumes significantly different from empty VLP treated animals. This suggested that growth inhibition was independent of the VLP encoded transgene and possibly related to the pro-inflammatory cytokine milieu induced by VLP infection. Jerusilami *et al.* (2003) and Quinn (2006) have also reported similar observations following empty VLP treatment, resulting in an enhancement of EAE symptoms. Weather these cytokines diffused via the olfactory route to the CNS or acted systemically with a knock-on effect on the CNS is unknown although Hidmark *et al.* (2006) demonstrated that the pro-inflammatory cytokine stimulation required for the VLP adjuvant effect acted systemically and its effect was observable even when VLPs and antigens were injected at different sites. In an attempt to address whether VLP induced cytokines were present at insufficient levels within the CNS to have an anti-tumor effect or were not in fact trafficked to the brain, cytokine analysis was carried out by commercial ELISA. Attempts to detect VLP encoded cytokines in the olfactory bulbs or brains of animals 48 hours after the fourth intranasal VLP treatment or 48 hours after a single intranasal VLP treatment were not successful. Both Quinn and Jerusilami *et al.* demonstrated the presence of VLP encoded cytokines in the olfactory bulbs and brain of VLP treated mice; however, levels were low at approximately 10-20 pg per mg of soluble cell protein. The ELISAs used in this study for the detection of IL-12 and IFN-γ had working limits of detection of approximately 200 pg/ml, equivalent to 100pg/mg of total soluble protein, which may have explained the inability to detect VLP encoded cytokines following intranasal delivery. As a result, EGFP encoding VLPs were used in an attempt to detect transgene expression in the olfactory bulb. This method was successfully employed for VLP expression analysis in mice (Jerusalmi, 2004) and demonstrated EGFP fluorescence in the incoming axons from the nasal mucosa that terminated, as did EGFP fluorescence, in the glomerular layer of the olfactory bulb (Figure 3). In the rat model used

in this study EGFP expression could not be detected in the olfactory bulbs of any VLP treated animals. As an additional control, rats were infected with replication competent EGFP encoding SFV, however EGFP expression was not observed in any of the animals examined. Previous work using replicating SFV intranasally (Sammin *et al.*, 1999) demonstrated that SFV intranasal infection was far less efficient in rats than mice, requiring a 100-fold greater virus inoculum for CNS infection, which was still not sufficient to infect all animals.

These results suggest that the use of SFV VLPs for intranasal treatment in rats is less effective than previous studies in mice. It is unknown as to what parameters are responsible for the observed differences although it appears to be related to the inefficient infection of the nasal mucosa. RG2 tumor therapy involving cytokine delivery has previously shown some efficacy in retarding glioma growth (Oshiro *et al.*, 2001; Tjuvajev *et al.*, 1995) indicating that RG2 tumors are sensitive to cytokine therapy and that if any VLP-encoded cytokine were penetrating the CNS it was not at sufficient levels to induce a distinguishable effect compared to empty VLPs alone. It is obvious then that the SFV VLP intranasal treatment regimen needs to be investigated further as a method of therapeutic CNS transgene delivery and the disparate results observed between rat and mice models be explored.

Chapter 7

General discussion

7.1 General Discussion

The experimentation undertaken in this study employed two strategies for the treatment of intracerebral gliomas using the SFV VLP expression system. The SFV expression system was engineered to encode the immunomodulatory cytokines IFN-β, IFN-γ and IL-12. The VLP system was able to induce the expression and secretion of biologically active cytokines from transfected cells. Additionally, the induction of apoptosis, a consequence of VLP infection, was demonstrated in both glioma cell lines.

7.1.1 *In vivo* glioma models

In vivo experimentation initially involved the characterisation of the intracerebral glioma models; to this end, glioma cells were inoculated into the right hippocampus of male Fischer 344 rats. Glioma cell inoculation resulted in the induction of gliomas in all animals and was associated with a survival time of approximately three weeks. Additionally, histological examination of tumors demonstrated that growth characteristics, including the pattern and rate of growth, were similar to those in published literature (Seitz *et al.*, 1988; Wechsler *et al.*, 1989).

The requirement for repeated access to the tumor during treatment necessitated the use of a cannula system, implanted into the skull above the hippocampus. Surgical implantation was well tolerated and cannulas remained intact for the duration of the experiment. One-week after cannula implantation, glioma cells were inoculated into the right hippocampus, using a stereotaxic apparatus, via the implanted cannula.

The i.c. delivery of the SFV VLPs was examined by a single inoculation of low-dose ($5x10^7$ VLPs in 5μl TNE) IL-12 encoding VLPs or empty VLPs into tumor-bearing animals. Treatment was delivered 17 days after glioma cell inoculation and animals were culled 48 hours later. Treatment was delayed until near the experimental endpoint to ensure that a tumor mass of sufficient size for examination was present. Immunohistochemical analysis demonstrated the presence of IL-12 positive cells, indicative of IL-12 encoding VLP infection, at the inoculation site. IL-12 staining was limited to the inoculation site and not observed in the contralateral hemisphere or in the brains of TNE treated animals. Additionally, IL-12 expression in IL-12 encoding VLP treated animals was limited to the inoculation site and not observed along the needle tract or at the dorsal surface of the brain. This indicated that the flow rate was not resulting in backflow of the inoculum along the

needle tract and that delivery was to the intended inoculation site. Interestingly, despite VLP infection being limited to the inoculation site, infection was observed in both tumor and non-tumor tissue. This demonstrated, as would have been expected, that the SFV VLP system was capable of infecting both tumor and normal cells of the CNS. However, the pattern of infection appeared to depend upon the precise inoculation site; normal CNS cells were infected primarily when the inoculation site was close to the tumor border and less so when the inoculation site was located within the centre of large tumors.

This highlights at least one potential problem with the use of the VLP system in an i.c. tumor model; the ability of the VLP system to infect and induce death in non-tumor cells. In peripheral tumor models, infection of non-tumor cells is largely acceptable and inconsequential in terms of adverse effects; however, the low renewal potential and importance of cells of the CNS mean that off-target infection can result in unacceptable damage. Unlike s.c. tumor models, in which the tumor is relatively large and accessible upon the initiation of treatment and VLP delivery can be easily directed to the area of interest; i.c. tumors are small, particularly during initial treatments, and given the variability in the growth and location of tumors, even though inoculation was stereotaxically guided, it is likely that VLPs will infect normal CNS tissue to some degree. This is of particular relevance considering the treatment-related toxicity observed during experiments, not only because of adverse effects but also because it limits the use of the system to potentially sub-optimal doses. It is likely however that problems relating to inoculation, primarily the size and location of tumors, are inherent in this model and may not be easily overcome. Real-time imaging of tumors before and during treatment is possible, as is carried out in clinical therapies, although in pre-clinical models this has obvious limitations.

7.1.2 Intracerebral therapy of rat glioma models

Intracerebral therapy was carried out using either low- or high-dose VLPs. Low-dose treatment was examined in both glioma models; however, as a result of high-rates of treatment-related death, high-dose VLP therapy was only examined using the RG2 glioma model. Low-dose treatment of RG2 gliomas with IL-12 encoding SFV VLPs resulted in a significant reduction in tumor volume compared to TNE or empty VLP controls, which produced a statistically significant enhancement in survival. However, this effect was not observed using the F98 glioma model.

In an attempt to determine the mechanism responsible for the anti-tumor effect observed, a number of immunohistochemical analyses were performed. Empty VLP treated controls demonstrated that the anti-tumor effect was dependant upon IL-12 expression and appeared transient, as all animals eventually succumbed to tumor burden following the cessation of treatment. IHC demonstrated the presence of $CD3^+$ cells at the tumor border however, there was no difference in the pattern or concentration of $CD3^+$ cells between empty and IL-12 encoding VLP treated tumors. IHC analysis of microvessels was also performed; although this did not demonstrate a significant change in mean vessel density between empty and IL-12 treated tumors, this may not have been the most appropriate measure of blood vessel development using the RG2 glioma model, as discussed in section **5.4**. The assumption of an anti-angiogenic effect may also explain the disparate observations between the RG2 and F98 models. However, an anti-angiogenic effect is only one possibility and the exact mechanism remains to be defined. Conceivably, IL-12 stimulation and activation of microglia resulting in the production of factors, such as TNF-related apoptosis-inducing ligand (TRAIL), which possess some direct anti-tumor activity, such as the induction of apoptosis, may be responsible for this effect. Given that the F98 tumor cell line demonstrated a lower infection efficiency and lower IL-12 expression than RG2 cells *in vitro* this may provide an explanation for the absence of an effect using the F98 model. However, it would need to be determined if the relative expression levels *in vivo* reflected those *in vitro*.

High-dose treatment of the RG2 glioma model was complicated by the fact that numerous VLP treated animals were culled before the experimental endpoint and group numbers were not optimal. Despite this, both empty and IL-12 encoding VLPs demonstrated a statistically significant reduction in tumor volume. However, the major mechanism responsible for this effect appeared to be related to the VLP system alone although IL-12 expression provided some additional reduction in tumor volume. It is likely that high-dose VLP therapy with IL-12 encoding VLPs produced an enhanced effect above low-dose VLP therapy but group numbers made statistical inference difficult.

Interestingly, one effect of IL-12 therapy demonstrated in a number of *in vivo* s.c. and i.c tumor models is the induction of a specific anti-tumor adaptive immune response capable of eliminating the primary tumor mass, residual tumor cells and mediating protection from re-challenge. The advantages of this are obvious especially considering the infiltrative potential of gliomas and the fact that residual tumor cells rapidly regrow, ultimately being fatal, following treatment. A number of *in vivo* models have demonstrated

the ability of IL-12 gene therapy to eliminate i.c. located gliomas (Yamanaka *et al.*, 2000; Liu *et al.*, 2002) demonstrating, at least, that i.c. IL-12 gene therapy is capable of arming an immune response capable of efficiently eliminating i.c. located tumors. However, the vast majority of IL-12 glioma therapies have involved the use of inherently immunogenic glioma cell lines, such as GL-26/1 known to express melanoma-associated antigens, in which protection is possible by peripheral vaccination. The antigenicity of the RG2 and F98 glioma models has been studied extensively. Initial experiments demonstrated that peripheral vaccination with autologous tumor cells did not protect animals or enhance survival following i.c. challenge with RG2 glioma cells (Tzeng *et al.*, 1991). An equivalent protocol using the F98 glioma cell line demonstrated a small enhancement in survival although all animals eventually succumbed to tumor burden. Interestingly, the RG2 glioma cell line displays a significantly altered sensitivity to systemic immune responses when inoculated in the subcutis; spontaneous regression has been observed in female Fischer 344 rats, the syngeneic species, and regression has been induced in male Fischer 344 rats when treated with the innate immune stimulants Zymosan A or LPS. Regression was associated with the induction of an adaptive immune response that protected animals from s.c. rechallenge although protection from i.c. challenge was not examined (Mariani *et al.*, 2007).

Despite the success in s.c. models of F98 or RG2 gliomas, this has not translated into i.c. models. Previous experimentation using the F98 glioma model has achieved complete eradication of established tumors but these therapies have incorporated a fundamentally different strategy involving the i.c. infusion of radio-enhancers combined with high-dose radiation; although long-term survival was achieved, an investigation into the immunological responses of survivors was not examined. Immunotherapeutic strategies against the F98 and RG2 glioma models have also been inefficacious whether attempting to enhance glioma immunogenicity by gene transfer of co-stimulatory molecules (Paul *et al.*, 2000) or direct i.c. gene transfer-mediated cytokine expression (Tjuvajev *et al.*, 1995). In fact, this resilience to therapy is one of the factors for which these glioma models are considered as suitable representations of human GBM. It is possible that variables associated with the treatment strategy used in this study were responsible for the absence of a host anti-tumor response, such as the initiation and length of therapy and the i.c. levels of IL-12 achieved; however, previous experimentation also implicates this model, particularly the i.c. location of tumors, in the resistance to the induction of an effective adaptive immune response. Further investigation of these glioma models may elucidate

aspects of these observations and provide novel approaches for overcoming these issues and, given their similarities to human GBM, may be directly related to clinical investigations.

7.1.3 Treatment-related death

Animals which displayed clinical signs prior to the completion of treatment were considered to have been culled as a result of treatment-related effects. This occurred in all treatment experiments although more frequently in high-dose RG2 treated animals than low-dose RG2 treated animals. The induction of treatment-related death was not the result of replication-competent virus production and did not appear to be related to the expression of IL-12. VLP therapy, high-dose VLP treatment in particular, resulted in significant cavitation and oedema at the inoculation site. Additionally, IHC detected infection of neurons in the hippocampus of all animals culled following IL-12 encoding VLP treatment. The relative contribution of each of these elements to the induction of clinical signs is unknown. It is well known that brain haemorrhage and oedema can be fatal as a result of increased intracranial pressure and damage to the delicate architecture in the brain suggesting that this may be the probable cause of death although infection and necrosis of neurons may be a contributing factor.

The observation of treatment-related death raises the obvious question as to the suitability of this vector system in an i.c. glioma model, at least in its current form. Since stereotaxic inoculation is the only mechanism for 'targeting' VLP infection and there is inherent variability in this approach, as discussed, there would be obvious advantages in engineering the expression system to overcome or reduce off-target effects. A number of attenuating mutations have been described for both replicating SFV and the SFV expression system and may provide a mechanism for such an approach. An ideal SFV based expression vector for i.c. glioma therapy would allow for high-level transgene expression and demonstrate limited infection, or at least non-cytopathic infection, of neurons and oligodendrocytes, while retaining the ability to infect and induce apoptosis in tumor cells. The etiology of gliomas and their close resemblance to astrocytes and/or oligodendrocytes means that it is probably impossible to target only transformed cells by the introduction of attenuating mutations alone; however, sparing neurons would have obvious advantages in limiting disruption of important neural pathways.

Lundstrom *et al.* (1999, 2001 and 2003) created a panel of modified SFV expression vectors harbouring mutations in the nsP2 coding sequence. The resultant vectors SFV(PD), SFV(PDE_{153}), SFV(PDTE) and SFV(PD713P) displayed varying degrees of attenuation. However, despite advantages of the vector being reported, such as increase transgene expression, these were primarily observed *in vitro* and at permissive temperatures (31°C); accompanied by their neuron-specific infection (Lundstrom *et al.*, 2001) the *in vivo* use of these vectors would hold no particular advantages above the vector used in this study. Casales *et al.* (2008) isolated a novel non-cytopathic vector containing two nsP2 mutations (P718T and R649H). Although, relative to the parental vector, the attenuated vector demonstrated equivalent expression levels, infection was far less efficient. Additionally, the production of VLPs using this expression vector was greater than four logs lower than the parental vector, severely limiting its use as a VLP vector system. If similar non-cytopathic vectors could be produced that retained the infection efficiency and VLP-production capability of the parental vector they would hold a number of advantages above the current vector system. Additionally, a non-cytopathic vector system would allow for determination of the contribution of tumor cell lysis to SFV based immunogene therapy, which may prove redundant in anti-angiogenic therapies.

Probably the most suitable expression vector currently reported is based upon the avirulent SFV strain A7(74) which demonstrates an attenuated phenotype both *in vitro* and *in vivo*. Additionally, A7(74) displays restricted replication in the CNS of adults rodents (Fazakerley *et al.*, 2006) while retaining the ability to infect and induce apoptosis in a number of neoplastic cell lines, including rat glioma cells (Määttä *et al.*, 2007). Ehrengruber *et al.* (2003) produced a modified non-replicating expression vector encoding EGFP which included the A7(74) non-structural sequence, responsible for the attenuated phenotype of A7(74). The resultant vector, SFV(A774nsP)-EGFP, demonstrated attenuation similar to the parental virus including restricted infection of neurons. This attenuated expression vector thus provides a mechanism for restricting infection in neurons while retaining its ability to induce tumor cells lysis. However, neurons represent a small proportion of cells in the CNS and as such, some off-target infection of the remaining cell populations would be likely. This would however, allow for determination of the relative contribution of neuronal infection to VLP-related death and probably should be considered as a precautionary measure for the future use of the SFV expression system in the CNS, although a direct comparison of both expression vectors *in vivo* would be required.

An alternative approach is provided by the positive-sense RNA genome of SFV coupled with the cell's inherent regulatory mechanisms. MicroRNAs (miRNAs) are 20-25 nucleotide single-stranded RNA species intimately involved in the regulation of host-cell gene expression (review by Bartel, 2004). Mature miRNAs act by binding a complementary sequence present in 3' untranslated region of cellular mRNAs and regulate gene expression by either translational repression or initiating mRNA degradation. A single miRNA is capable of acting upon a diverse range of cellular mRNAs and this pleiotropic nature is an important aspect of their function, particularly during the development and differentiation of tissues and cells. It has been suggested that each metazoan cell type and developmental stage has a distinct miRNA expression profile and this cell and tissue specific profile of miRNA expression may provide a mechanism for limiting VLP infection in non-target cells. Brown *et al.* (2007) successfully exploited this mechanism to restrict lentiviral vector-mediated transgene expression in various cell/tissue types. The mRNA nature of SFV allows not just for the elimination of transgene expression but also mRNA replication, which produces the cytotoxic effects of VLP infection. The inclusion of a neuron specific miRNA into the genome of the positive-sense mRNA poliovirus was capable of restricting infection in the CNS (Barnes *et al.*, 2008). This strategy could be incorporated into the SFV expression vector system to limit infection in non-target cells and may avoid some of the problems associated with the current vector system. This is however contingent upon the identification of miRNA(s) with expression limited to cell types of interest and the ability to include complementary sequences in the viral genome without adversely affecting replication and transgene expression in miRNA negative cells. It is likely that both these obstacles are surmountable and may vastly contribute to the biosafety and versatility of the SFV expression system.

Targeting of SFV and other alphaviruses has been attempted by the modification of virus envelope proteins (reviewed by Lundstrom, 2001) which has produced some success in broadly altering host-cell specificity. If this strategy could be further developed and refined, it may provide another potential mechanism for engineering the VLP system to circumvent the limitations demonstrated in this study.

7.1.4 Intranasal therapy of rat glioma model

The intranasal delivery of VLPs was also examined in this study as a method of cytokine delivery to the CNS. This method of delivery has a number of advantages and limitations

compared to intracerebral VLP delivery; i.n. delivery circumvents direct intracerebral delivery and the resultant infection of, and damage to, the delicate structures of the CNS while potentially maintaining cytokine delivery into the CNS. However, cytokine delivery to the CNS is likely to be less efficient than direct i.c. delivery and the potential advantages of tumor cell lysis are absent. Despite this, the potential tumorostatic effects of the cytokines used in this study and the non-invasive method of delivery may have provided an adjuvant therapy while still allowing for additional therapeutic intervention.

Although a significant reduction in tumor volume was observed in IFN-β encoding VLP treated animals, and an almost significant reduction following IFN-γ encoding VLP treatment, there was no statistical difference between either treatment compared to empty treated animals. Follow-up experiments to determine the significance of these observations demonstrated that the protein products encoded by the VLP system could not be detected in the olfactory bulbs or brains of i.n. treated animals. To further investigate this observation, EGFP encoding VLPs and replicating virus-encoding EGFP were delivered intranasally. Neither the expression vector nor replicating virus resulted in detectable levels of EGFP expression in the olfactory bulb of inoculated rats. This indicated that the inability to detect cytokine expression may have been the result of inefficient transfection of the nasal mucosa and resultant cytokine expression into the olfactory bulbs. The inefficient infection of rats with replicating SFV, via the intranasal route, has previously been described although the reasons for this have not been elucidated (Sammin *et al.*, 1999).

The experiments carried out in this study represent essentially preliminary investigations into the use of the VLP system as an i.n. cytokine delivery system. Additionally, there remains to be elucidated a number of elements in the use of the VLP system in both mouse and other animal models. Obviously, the disparate observations between the mouse and rat model would need to be addressed and the reason for these observations determined. Additionally, the analysis of transgene expression from the nasal mucosa/olfactory bulb has been somewhat limited. Intranasal EGFP encoding VLP delivery limited detection to initially infected cells, a consequence of the VLP's replication incompetence and the intracellular expression of EGFP. In murine models, quantitative transgene expression in the olfactory bulbs and brain was examined using the VLP system encoding IFN-β or IL-10; although both are extracellularly expressed, quantification was complicated by their endogenous expression and their potential involvement in amplification loops. Additionally, measured cytokine expression was low and close to the

limit of detection of the detection ELISAs. An alternative strategy could incorporate the luciferase gene from *Cypridina* noctiluca, secreted from mammalian cells (Nakajima *et al.*, 2004), into the VLP vector system. This system would allow for *in vitro* and *ex vivo* quantification of VLP mediated expression using a cheaper, less laborious and more sensitive detection system. Additionally, although dependent upon sensitivity, real time *in vivo* expression can be assessed repeatedly without culling and processing of animals.

For the VLP system to be used in the manner examined in this and previous studies, repeated administration of VLPs would be required, as transgene expression is limited by the induction of host cell death. This does however raise a number of questions that have not been addressed using this vector system. Given that the SFV VLP system induces a robust immunity following i.n. VLP delivery (Berglund *et al.*, 1999) it is likely that host anti-SFV immune responses will impact upon the efficiency of repeated VLP delivery. Stimulation of the innate immune system following infection of the nasal mucosa, resulting in interferon production and the induction of anti-viral state in uninfected cells may reduce the efficiency of re-administration, at least in the short-term. Additionally, the incorporation of cytokines, which possess antiviral activity, into the vector system may further affect the efficiency of readministration and transgene expression. The adaptive immune system, resulting in the development of neutralising antibodies, is also of particular importance for the long-term administration of VLPs. Interestingly, the mucosal route of vector delivery has been demonstrated as an effective method of inoculation in the presence of pre-existing immunity when using the adenoviral vectors (Santosusso *et al.*, 2005; Croyle *et al.*, 2008). Whether or not this is the case using the SFV based system and whether this effect will change after repeated i.n. administration remains to be explored. Additionally, armed effector cells of the adaptive immune system may enhance the elimination of transgene expressing cells once T cell priming has occurred. The deleterious effects of cytokine induction because of VLP infection or VLP encoded cytokine expression may be overcome by altering the frequency and timing of administration; however, and particularly when using VLPs encoding antiviral cytokines, this may limit administration to sub-optimal doses by compromising the duration of therapy and i.c. cytokine levels achieved during treatment. The effects of neutralising antibodies may be negated by encapsulating VLPs in various inert materials, such as PEGylation, successfully employed by Croyle *et al.* (2008), or lipid complexes.

Despite these concerns, the i.n. delivery system has demonstrated efficacy in cytokine delivery into the CNS in murine models and some or none of the effects

mentioned above may be of importance. However, the mechanism of VLP encoded cytokine transfer into the brain remains to be elucidated. Jerusalmi *et al.* (2003) demonstrated that although expression of EGFP was detected in the incoming axons of the nasal mucosa following i.n. delivery of EGFP encoding VLPs, vector mRNA could not be detected at any time point after infection. It was proposed that infection of migratory cells, which traffic into the olfactory bulb after infection, were the source of cytokine production following i.n. treatment although only neurons were identified as GFP positive by fluorescent microscopy. Interestingly, intranasal therapy using an adenoviral vector demonstrated a strikingly similar expression pattern to that observed by Jerusalmi *et al.* (Zhao *et al.*, 1996), which was later demonstrated to be positive for adenovirus DNA (Damjanovic *et al.*, 2008). It is possible that because first strand synthesis was carried out using poly(T) primers, which produce cDNA molecules for all cellular mRNAs, and that the frequency of EGFP positive cells was low, particularly as the entire both olfactory bulb was used for RNA extraction, that there may have been a saturation effect during the reverse transcription process. If this is not the case however, then the precise mechanism should be examined as this may also explain the apparent absence of efficacy using the system in a rat model.

7.1.5 Conclusion

The aim of this experimentation was to examine the efficacy of SFV-mediated cytokine therapy in two rat glioma models. The intranasal route of cytokine delivery has numerous advantages compared to intracerebral treatment but, unlike murine models, it was not successful in the delivery of cytokines to the CNS of rats. This is an important point as it may reflect an inherent limitation in the use of the SFV expression system, via the i.n route, in larger animal models and should be explored to examine if this is in fact the case.

The intracerebral delivery of low-dose SFV VLPs encoding IL-12 effectively inhibited tumor growth in the RG2 glioma model and this inhibition correlated with enhanced survival. High-dose VLP treatment resulted in an impressive reduction in tumor volume, however it was also associated with considerable VLP-induced toxicity. The previous successes of *in vivo* glioma treatment using an immunotherapeutic approach have invariably involved immunogenic cell lines or allogeneic host strains and for this reason the 'non-immunogenic' RG2 and F98 glioma models were used in this study. Therapeutic treatment of the RG2 glioma model has had extremely limited success and this study extends the current research to include the use of IL-12 as an immunotherapeutic agent. Despite the inability to induce an effective host anti-tumor response, the inhibition of tumor growth and survival of IL-12 treated animals has not previously been demonstrated in the RG2 glioma model incorporating an immunogene therapy approach. Additionally, the absence of cytokine-related toxicity is particularly noteworthy as it has been demonstrated in similar i.c. gene therapy strategies as well as in systemic cytokine therapy. However, the VLP vector system resulted in the induction of treatment-related clinical signs in some animals and is an inherent limitation in the use of SFV VLPs intracerebrally. If VLP-mediated toxicity could be reduced or overcome, the SFV VLP system may provide a good candidate in future therapeutic interventions against malignant glioma.

Chapter 8

Bibliography

Adams, G. P. and Weiner, L. M. 2005. Monoclonal antibody therapy of cancer. *Nat Biotechnol* **23**(9): 1147-57.

Afkarian, M., Sedy, J. R., Yang, J., Jacobson, N. G., Cereb, N., Yang, S. Y., Murphy, T. L. and Murphy, K. M. 2002. T-bet is a STAT1-induced regulator of IL-12R expression in naive CD4+ T cells. *Nat Immunol* **3**(6): 549-57.

Aloisi, F., Ria, F., Columba-Cabezas, S., Hess, H., Penna, G. and Adorini, L. 1999. Relative efficiency of microglia, astrocytes, dendritic cells and B cells in naive CD4+ T cell priming and Th1/Th2 cell restimulation. *Eur J Immunol* **29**(9): 2705-14.

Aloisi, F., Ria, F. and Adorini, L. 2000. Regulation of T-cell responses by CNS antigen-presenting cells: different roles for microglia and astrocytes. *Immunol Today* **21**(3): 141-7.

Altman, J. and Das, G. D. 1965. Autoradiographic and histological evidence of postnatal hippocampal neurogenesis in rats. *J Comp Neurol* **124**(3): 319-35.

Amor, S., Scallan, M. F., Morris, M. M., Dyson, H. and Fazakerley, J. K. 1996. Role of immune responses in protection and pathogenesis during Semliki Forest virus encephalitis. *J Gen Virol* **77** (**Pt 2**): 281-91.

Asselin-Paturel, C., Lassau, N., Guinebretiere, J. M., Zhang, J., Gay, F., Bex, F., Hallez, S., Leclere, J., Peronneau, P., Mami-Chouaib, F. and Chouaib, S. 1999. Transfer of the murine interleukin-12 gene in vivo by a Semliki Forest virus vector induces B16 tumor regression through inhibition of tumor blood vessel formation monitored by Doppler ultrasonography. *Gene Ther* **6**(4): 606-15.

Bachoo, R. M., Maher, E. A., Ligon, K. L., Sharpless, N. E., Chan, S. S., You, M. J., Tang, Y., DeFrances, J., Stover, E., Weissleder, R., Rowitch, D. H., Louis, D. N. and DePinho, R. A. 2002. Epidermal growth factor receptor and Ink4a/Arf: convergent mechanisms governing terminal differentiation and transformation along the neural stem cell to astrocyte axis. *Cancer Cell* **1**(3): 269-77.

Balkwill, F. and Mantovani, A. 2001. Inflammation and cancer: back to Virchow? *Lancet* **357**(9255): 539-45.

Barnes, D., Kunitomi, M., Vignuzzi, M., Saksela, K. and Andino, R. 2008. Harnessing endogenous miRNAs to control virus tissue tropism as a strategy for developing attenuated virus vaccines. *Cell Host Microbe* **4**(3): 239-48.

Bartel, D. P. 2004. MicroRNAs: genomics, biogenesis, mechanism, and function. *Cell* **116**(2): 281-97.

Barth, R. F., Yang, W., Rotaru, J. H., Moeschberger, M. L., Joel, D. D., Nawrocky, M. M., Goodman, J. H. and Soloway, A. H. 1997. Boron neutron capture therapy of brain tumors: enhanced survival following intracarotid injection of either sodium borocaptate or boronophenylalanine with or without blood-brain barrier disruption. *Cancer Res* **57**(6): 1129-36.

Barth, R. F. 1998. Rat brain tumor models in experimental neuro-oncology: the 9L, C6, T9, F98, RG2 (D74), RT-2 and CNS-1 gliomas. *J Neurooncol* **36**(1): 91-102.

Barzon, L., Zanusso, M., Colombo, F. and Palu, G. 2006. Clinical trials of gene therapy, virotherapy, and immunotherapy for malignant gliomas. *Cancer Gene Ther* **13**(6): 539-54.

Baumgartner, J. E., Rachlin, J. R., Beckstead, J. H., Meeker, T. C., Levy, R. M., Wara, W. M. and Rosenblum, M. L. 1990. Primary central nervous system lymphomas: natural history and response to radiation therapy in 55 patients with acquired immunodeficiency syndrome. *J Neurosurg* **73**(2): 206-11.

Beatty, G. and Paterson, Y. 2001. IFN-gamma-dependent inhibition of tumor angiogenesis by tumor-infiltrating CD4+ T cells requires tumor responsiveness to IFN-gamma. *J Immunol* **166**(4): 2276-82.

Benda, P., Someda, K., Messer, J. and Sweet, W. H. 1971. Morphological and immunochemical studies of rat glial tumors and clonal strains propagated in culture. *J Neurosurg* **34**(3): 310-23.

Bergers, G. and Benjamin, L. E. 2003. Tumorigenesis and the angiogenic switch. *Nat Rev Cancer* **3**(6): 401-10.

Berglund, P., Sjoberg, M., Garoff, H., Atkins, G. J., Sheahan, B. J. and Liljestrom, P. 1993. Semliki Forest virus expression system: production of conditionally infectious recombinant particles. *Biotechnology (N Y)* **11**(8): 916-20.

Berglund, P., Fleeton, M. N., Smerdou, C. and Liljestrom, P. 1999. Immunization with recombinant Semliki Forest virus induces protection against influenza challenge in mice. *Vaccine* **17**(5): 497-507.

Bernsen, H. J. and van der Kogel, A. J. 1999. Antiangiogenic therapy in brain tumor models. *J Neurooncol* **45**(3): 247-55.

Binder, G. K. and Griffin, D. E. 2001. Interferon-gamma-mediated site-specific clearance of alphavirus from CNS neurons. *Science* **293**(5528): 303-6.

Biston, M. C., Joubert, A., Adam, J. F., Elleaume, H., Bohic, S., Charvet, A. M., Esteve, F., Foray, N. and Balosso, J. 2004. Cure of Fisher rats bearing radioresistant F98 glioma treated with cis-platinum and irradiated with monochromatic synchrotron X-rays. *Cancer Res* **64**(7): 2317-23.

Boehm, U., Klamp, T., Groot, M. and Howard, J. C. 1997. Cellular responses to interferon-gamma. *Annu Rev Immunol* **15**: 749-95.

Bogdan, C. and Nathan, C. 1993. Modulation of macrophage function by transforming growth factor beta, interleukin-4, and interleukin-10. *Ann N Y Acad Sci* **685**: 713-39.

Bogdan, C., Mattner, J. and Schleicher, U. 2004. The role of type I interferons in non-viral infections. *Immunol Rev* **202**: 33-48.

Bos, J. L. 1989. ras oncogenes in human cancer: a review. *Cancer Res* **49**(17): 4682-9.

Brem, S., Cotran, R. and Folkman, J. 1972. Tumor angiogenesis: a quantitative method for histologic grading. *J Natl Cancer Inst* **48**(2): 347-56.

Brown, B. D., Venneri, M. A., Zingale, A., Sergi Sergi, L. and Naldini, L. 2006. Endogenous microRNA regulation suppresses transgene expression in hematopoietic lineages and enables stable gene transfer. *Nat Med* **12**(5): 585-91.

Bryan, T. M., Englezou, A., Dalla-Pozza, L., Dunham, M. A. and Reddel, R. R. 1997. Evidence for an alternative mechanism for maintaining telomere length in human tumors and tumor-derived cell lines. *Nat Med* **3**(11): 1271-4.

Buckner, J. C., Brown, P. D., O'Neill, B. P., Meyer, F. B., Wetmore, C. J. and Uhm, J. H. 2007. Central nervous system tumors. *Mayo Clin Proc* **82**(10): 1271-86.

Cao, G., Su, J., Lu, W., Zhang, F., Zhao, G., Marteralli, D. and Dong, Z. 2001. Adenovirus-mediated interferon-beta gene therapy suppresses growth and metastasis of human prostate cancer in nude mice. *Cancer Gene Ther* **8**(7): 497-505.

Car, B. D., Eng, V. M., Lipman, J. M. and Anderson, T. D. 1999. The toxicology of interleukin-12: a review. *Toxicol Pathol* **27**(1): 58-63.

Carmeliet, P., Ferreira, V., Breier, G., Pollefeyt, S., Kieckens, L., Gertsenstein, M., Fahrig, M., Vandenhoeck, A., Harpal, K., Eberhardt, C., Declercq, C., Pawling, J., Moons, L., Collen, D., Risau, W. and Nagy, A. 1996. Abnormal blood vessel development and lethality in embryos lacking a single VEGF allele. *Nature* **380**(6573): 435-9.

Carmeliet, P. 2000. Mechanisms of angiogenesis and arteriogenesis. *Nat Med* **6**(4): 389-95.

Carson, M. J., Doose, J. M., Melchior, B., Schmid, C. D. and Ploix, C. C. 2006. CNS immune privilege: hiding in plain sight. *Immunol Rev* **213**: 48-65.

Caruso, M., Pham-Nguyen, K., Kwong, Y. L., Xu, B., Kosai, K. I., Finegold, M., Woo, S. L. and Chen, S. H. 1996. Adenovirus-mediated interleukin-12 gene therapy for metastatic colon carcinoma. *Proc Natl Acad Sci U S A* **93**(21): 11302-6.

Casales, E., Rodriguez-Madoz, J. R., Ruiz-Guillen, M., Razquin, N., Cuevas, Y., Prieto, J. and Smerdou, C. 2008. Development of a new noncytopathic Semliki Forest virus vector providing high expression levels and stability. *Virology* **376**(1): 242-51.

Castro, M., Curtin, J., King, G., Candolfi, M., Czer, P., Kroeger, K., Sciascia, S., Xiong, W., Fakhouri, T., Honig, S., Kuoy, W., Kang, T., Johnson, S. and Lowenstein, P. 2006. *Gene Therapy for Neurological Disorders*, Taylor & Francis Group, LLC.

CBTRUS, C. B. T. R. o. t. U. S. 2009. CBTRUS Statistical Report: Primary Brain and Central Nervous System Tumors Diagnosed in the United States in 2004-2005. .

Chen, B., Timiryasova, T. M., Haghighat, P., Andres, M. L., Kajioka, E. H., Dutta-Roy, R., Gridley, D. S. and Fodor, I. 2001. Low-dose vaccinia virus-mediated cytokine gene therapy of glioma. *J Immunother* **24**(1): 46-57.

Chikkanna-Gowda, C. P., Sheahan, B. J., Fleeton, M. N. and Atkins, G. J. 2005. Regression of mouse tumours and inhibition of metastases following administration of a Semliki Forest virus vector with enhanced expression of IL-12. *Gene Ther* **12**(16): 1253-63.

Chikkanna-Gowda, C. P., McNally, S., Sheahan, B. J., Fleeton, M. N. and Atkins, G. J. 2006. Inhibition of murine K-BALB and CT26 tumour growth using a Semliki Forest virus vector with enhanced expression of IL-18. *Oncol Rep* **16**(4): 713-9.

Chin, Y. E., Kitagawa, M., Su, W. C., You, Z. H., Iwamoto, Y. and Fu, X. Y. 1996. Cell growth arrest and induction of cyclin-dependent kinase inhibitor p21 WAF1/CIP1 mediated by STAT1. *Science* **272**(5262): 719-22.

Chin, Y. E., Kitagawa, M., Kuida, K., Flavell, R. A. and Fu, X. Y. 1997. Activation of the STAT signaling pathway can cause expression of caspase 1 and apoptosis. *Mol Cell Biol* **17**(9): 5328-37.

Chiocca, E. A., Abbed, K. M., Tatter, S., Louis, D. N., Hochberg, F. H., Barker, F., Kracher, J., Grossman, S. A., Fisher, J. D., Carson, K., Rosenblum, M., Mikkelsen, T., Olson, J., Markert, J., Rosenfeld, S., Nabors, L. B., Brem, S., Phuphanich, S., Freeman, S., Kaplan, R. and Zwiebel, J. 2004. A phase I open-label, dose-escalation, multi-institutional trial of injection with an E1B-Attenuated adenovirus, ONYX-015, into the peritumoral region of recurrent malignant gliomas, in the adjuvant setting. *Mol Ther* **10**(5): 958-66.

Chiocca, E. A., Smith, K. M., McKinney, B., Palmer, C. A., Rosenfeld, S., Lillehei, K., Hamilton, A., DeMasters, B. K., Judy, K. and Kirn, D. 2008. A phase I trial of Ad.hIFN-beta gene therapy for glioma. *Mol Ther* **16**(3): 618-26.

Chiou, S. H., Sheu, B. C., Chang, W. C., Huang, S. C. and Hong-Nerng, H. 2005. Current concepts of tumor-infiltrating lymphocytes in human malignancies. *J Reprod Immunol* **67**(1-2): 35-50.

Colmenero, P., Liljestrom, P. and Jondal, M. 1999. Induction of P815 tumor immunity by recombinant Semliki Forest virus expressing the P1A gene. *Gene Ther* **6**(10): 1728-33.

Colmenero, P., Chen, M., Castanos-Velez, E., Liljestrom, P. and Jondal, M. 2002. Immunotherapy with recombinant SFV-replicons expressing the P815A tumor antigen or IL-12 induces tumor regression. *Int J Cancer* **98**(4): 554-60.

Copeland, D. D., Talley, F. A. and Bigner, D. D. 1976. The fine structure of intracranial neoplasms induced by the inoculation of avian sarcoma virus in neonatal and adult rats. *Am J Pathol* **83**(1): 149-76.

Croyle, M. A., Patel, A., Tran, K. N., Gray, M., Zhang, Y., Strong, J. E., Feldmann, H. and Kobinger, G. P. 2008. Nasal delivery of an adenovirus-based vaccine bypasses pre-existing immunity to the vaccine carrier and improves the immune response in mice. *PLoS ONE* **3**(10): e3548.

Csatary, L. K., Gosztonyi, G., Szeberenyi, J., Fabian, Z., Liszka, V., Bodey, B. and Csatary, C. M. 2004. MTH-68/H oncolytic viral treatment in human high-grade gliomas. *J Neurooncol* **67**(1-2): 83-93.

Damjanovic, D., Zhang, X., Mu, J., Fe Medina, M. and Xing, Z. 2008. Organ distribution of transgene expression following intranasal mucosal delivery of recombinant replication-defective adenovirus gene transfer vector. *Genet Vaccines Ther* **6**: 5.

Del Vecchio, M., Bajetta, E., Canova, S., Lotze, M. T., Wesa, A., Parmiani, G. and Anichini, A. 2007. Interleukin-12: biological properties and clinical application. *Clin Cancer Res* **13**(16): 4677-85.

Didenko, V. V., Ngo, H. N., Minchew, C. and Baskin, D. S. 2002. Apoptosis of T lymphocytes invading glioblastomas multiforme: a possible tumor defense mechanism. *J Neurosurg* **96**(3): 580-4.

Dropcho, E. J. and Soong, S. J. 1996. The prognostic impact of prior low grade histology in patients with anaplastic gliomas: a case-control study. *Neurology* **47**(3): 684-90.

Duff, T. A., Borden, E., Bay, J., Piepmeier, J. and Sielaff, K. 1986. Phase II trial of interferon-beta for treatment of recurrent glioblastoma multiforme. *J Neurosurg* **64**(3): 408-13.

Dunn, G. P., Koebel, C. M. and Schreiber, R. D. 2006. Interferons, immunity and cancer immunoediting. *Nat Rev Immunol* **6**(11): 836-48.

Dunn, G. P., Bruce, A. T., Sheehan, K. C., Shankaran, V., Uppaluri, R., Bui, J. D., Diamond, M. S., Koebel, C. M., Arthur, C., White, J. M. and Schreiber, R. D. 2005. A critical function for type I interferons in cancer immunoediting. *Nat Immunol* **6**(7): 722-9.

Ehrengruber, M. U., Hennou, S., Bueler, H., Naim, H. Y., Deglon, N. and Lundstrom, K. 2001. Gene transfer into neurons from hippocampal slices: comparison of recombinant Semliki Forest Virus, adenovirus, adeno-associated virus, lentivirus, and measles virus. *Mol Cell Neurosci* **17**(5): 855-71.

Ehrengruber, M. U., Renggli, M., Raineteau, O., Hennou, S., Vaha-Koskela, M. J., Hinkkanen, A. E. and Lundstrom, K. 2003. Semliki Forest virus A7(74) transduces hippocampal neurons and glial cells in a temperature-dependent dual manner. *J Neurovirol* **9**(1): 16-28.

Ehtesham, M., Kabos, P., Kabosova, A., Neuman, T., Black, K. L. and Yu, J. S. 2002. The use of interleukin 12-secreting neural stem cells for the treatment of intracranial glioma. *Cancer Res* **62**(20): 5657-63.

Ehtesham, M., Black, K. L. and Yu, J. S. 2004. Recent progress in immunotherapy for malignant glioma: treatment strategies and results from clinical trials. *Cancer Control* **11**(3): 192-207.

Elmore, S. 2007. Apoptosis: a review of programmed cell death. *Toxicol Pathol* **35**(4): 495-516.

Erpolat, O. P., Akmansu, M., Goksel, F., Bora, H., Yaman, E. and Buyukberber, S. 2009. Outcome of newly diagnosed glioblastoma patients treated by radiotherapy plus concomitant and adjuvant temozolomide: a long-term analysis. *Tumori* **95**(2): 191-7.

Esiri, M. 2000. Russell and Rubinstein's Pathology of Tumors of the Nervous System. Sixth Edition. *J Neurol Neurosurg Psychiatry* **68**(4): 538d-.

Farkkila, M., Jaaskelainen, J., Kallio, M., Blomstedt, G., Raininko, R., Virkkunen, P., Paetau, A., Sarelin, H. and Mantyla, M. 1994. Randomised, controlled study of intratumoral recombinant gamma-interferon treatment in newly diagnosed glioblastoma. *Br J Cancer* **70**(1): 138-41.

Farrar, M. A. and Schreiber, R. D. 1993. The molecular cell biology of interferon-gamma and its receptor. *Annu Rev Immunol* **11**: 571-611.

Fazakerley, J. K. 2002. Pathogenesis of Semliki Forest virus encephalitis. *J Neurovirol* **8 Suppl 2**: 66-74.

Fazakerley, J. K. 2004. Semliki forest virus infection of laboratory mice: a model to study the pathogenesis of viral encephalitis. *Arch Virol Suppl*(18): 179-90.

Fazakerley, J. K., Cotterill, C. L., Lee, G. and Graham, A. 2006. Virus tropism, distribution, persistence and pathology in the corpus callosum of the Semliki Forest virus-infected mouse brain: a novel system to study virus-oligodendrocyte interactions. *Neuropathol Appl Neurobiol* **32**(4): 397-409.

Fecci, P. E., Mitchell, D. A., Whitesides, J. F., Xie, W., Friedman, A. H., Archer, G. E., Herndon, J. E., 2nd, Bigner, D. D., Dranoff, G. and Sampson, J. H. 2006. Increased regulatory T-cell fraction amidst a diminished CD4 compartment explains cellular immune defects in patients with malignant glioma. *Cancer Res* **66**(6): 3294-302.

Fecci, P. E., Ochiai, H., Mitchell, D. A., Grossi, P. M., Sweeney, A. E., Archer, G. E., Cummings, T., Allison, J. P., Bigner, D. D. and Sampson, J. H. 2007. Systemic CTLA-4 blockade ameliorates glioma-induced changes to the CD4+ T cell compartment without affecting regulatory T-cell function. *Clin Cancer Res* **13**(7): 2158-67.

Fischer, I., Gagner, J. P., Law, M., Newcomb, E. W. and Zagzag, D. 2005. Angiogenesis in gliomas: biology and molecular pathophysiology. *Brain Pathol* **15**(4): 297-310.

Folkman, J. 1971. Tumor angiogenesis: therapeutic implications. *N Engl J Med* **285**(21): 1182-6.

Folkman, J. 2003. Fundamental concepts of the angiogenic process. *Curr Mol Med* **3**(7): 643-51.

Folkman, J. 2006. Angiogenesis. *Annu Rev Med* **57**: 1-18.

Fragkoudis, R., Ballany, C. M., Boyd, A. and Fazakerley, J. K. 2008. In Semliki Forest virus encephalitis, antibody rapidly clears infectious virus and is required to eliminate viral material from the brain, but is not required to generate lesions of demyelination. *J Gen Virol* **89**(Pt 10): 2565-8.

Fujii, S., Huang, S., Fong, T. C., Ando, D., Burrows, F., Jolly, D. J., Nemunaitis, J. and Hoon, D. S. 2000. Induction of melanoma-associated antigen systemic immunity upon intratumoral delivery of interferon-gamma retroviral vector in melanoma patients. *Cancer Gene Ther* **7**(9): 1220-30.

Gabrilovich, D. 2004. Mechanisms and functional significance of tumour-induced dendritic-cell defects. *Nat Rev Immunol* **4**(12): 941-52.

Galli, R., Binda, E., Orfanelli, U., Cipelletti, B., Gritti, A., De Vitis, S., Fiocco, R., Foroni, C., Dimeco, F. and Vescovi, A. 2004. Isolation and characterization of tumorigenic, stem-like neural precursors from human glioblastoma. *Cancer Res* **64**(19): 7011-21.

Garber, J. E. and Offit, K. 2005. Hereditary cancer predisposition syndromes. *J Clin Oncol* **23**(2): 276-92.

Gelati, M., Corsini, E., Frigerio, S., Pollo, B., Broggi, G., Croci, D., Silvani, A., Boiardi, A. and Salmaggi, A. 2003. Effects of thalidomide on parameters involved in angiogenesis: an in vitro study. *J Neurooncol* **64**(3): 193-201.

Gilboa, E. 2007. DC-based cancer vaccines. *J Clin Invest* **117**(5): 1195-203.

Glasgow, G. M., McGee, M. M., Tarbatt, C. J., Mooney, D. A., Sheahan, B. J. and Atkins, G. J. 1998. The Semliki Forest virus vector induces p53-independent apoptosis. *J Gen Virol* **79 (Pt 10)**: 2405-10.

Goh, P. P., Sze, D. M. and Roufogalis, B. D. 2007. Molecular and cellular regulators of cancer angiogenesis. *Curr Cancer Drug Targets* **7**(8): 743-58.

Goldstein, D. and Laszlo, J. 1986. Interferon therapy in cancer: from imaginon to interferon. *Cancer Res* **46**(9): 4315-29.

Goodbourn, S., Didcock, L. and Randall, R. E. 2000. Interferons: cell signalling, immune modulation, antiviral response and virus countermeasures. *J Gen Virol* **81**(Pt 10): 2341-64.

Graeber, M. B., Scheithauer, B. W. and Kreutzberg, G. W. 2002. Microglia in brain tumors. *Glia* **40**(2): 252-9.

Guillemin, G. J. and Brew, B. J. 2004. Microglia, macrophages, perivascular macrophages, and pericytes: a review of function and identification. *J Leukoc Biol* **75**(3): 388-97.

Harrow, S., Papanastassiou, V., Harland, J., Mabbs, R., Petty, R., Fraser, M., Hadley, D., Patterson, J., Brown, S. M. and Rampling, R. 2004. HSV1716 injection into the brain adjacent to tumour following surgical resection of high-grade glioma: safety data and long-term survival. *Gene Ther* **11**(22): 1648-58.

Hashizume, R., Ozawa, T., Gryaznov, S. M., Bollen, A. W., Lamborn, K. R., Frey, W. H., 2nd and Deen, D. F. 2008. New therapeutic approach for brain tumors: Intranasal delivery of telomerase inhibitor GRN163. *Neuro Oncol* **10**(2): 112-20.

Helenius, A., Morein, B., Fries, E., Simons, K., Robinson, P., Schirrmacher, V., Terhorst, C. and Strominger, J. L. 1978. Human (HLA-A and HLA-B) and murine (H-2K and H-2D) histocompatibility antigens are cell surface receptors for Semliki Forest virus. *Proc Natl Acad Sci U S A* **75**(8): 3846-50.

Hess, K. R., Broglio, K. R. and Bondy, M. L. 2004. Adult glioma incidence trends in the United States, 1977-2000. *Cancer* **101**(10): 2293-9.

Hidmark, A. S., McInerney, G. M., Nordstrom, E. K., Douagi, I., Werner, K. M., Liljestrom, P. and Karlsson Hedestam, G. B. 2005. Early alpha/beta interferon production by myeloid dendritic cells in response to UV-inactivated virus requires viral entry and interferon regulatory factor 3 but not MyD88. *J Virol* **79**(16): 10376-85.

Hidmark, A. S., Nordstrom, E. K., Dosenovic, P., Forsell, M. N., Liljestrom, P. and Karlsson Hedestam, G. B. 2006. Humoral responses against coimmunized protein antigen but not against alphavirus-encoded antigens require alpha/beta interferon signaling. *J Virol* **80**(14): 7100-10.

Hoelzinger, D. B., Demuth, T. and Berens, M. E. 2007. Autocrine factors that sustain glioma invasion and paracrine biology in the brain microenvironment. *J Natl Cancer Inst* **99**(21): 1583-93.

Hoffmann, T. K., Nakano, K., Elder, E. M., Dworacki, G., Finkelstein, S. D., Appella, E., Whiteside, T. L. and DeLeo, A. B. 2000. Generation of T cells specific for the wild-type sequence p53(264-272) peptide in cancer patients: implications for immunoselection of epitope loss variants. *J Immunol* **165**(10): 5938-44.

Hussain, S. F., Yang, D., Suki, D., Aldape, K., Grimm, E. and Heimberger, A. B. 2006. The role of human glioma-infiltrating microglia/macrophages in mediating antitumor immune responses. *Neuro Oncol* **8**(3): 261-79.

Immonen, A., Vapalahti, M., Tyynela, K., Hurskainen, H., Sandmair, A., Vanninen, R., Langford, G., Murray, N. and Yla-Herttuala, S. 2004. AdvHSV-tk gene therapy with intravenous ganciclovir improves survival in human malignant glioma: a randomised, controlled study. *Mol Ther* **10**(5): 967-72.

Iwashita, Y., Ogawa, T., Goto, S., Nakanishi, M., Goto, T. and Kitano, S. 2004. Effective transfer of interleukin-12 gene to solid tumors using a novel gene delivery system, poly [D,L-2,4-diaminobutyric acid]. *Cancer Gene Ther* **11**(2): 103-8.

Jack, C. S., Arbour, N., Manusow, J., Montgrain, V., Blain, M., McCrea, E., Shapiro, A. and Antel, J. P. 2005. TLR signaling tailors innate immune responses in human microglia and astrocytes. *J Immunol* **175**(7): 4320-30.

Jacobs, B. L. and Langland, J. O. 1996. When two strands are better than one: the mediators and modulators of the cellular responses to double-stranded RNA. *Virology* **219**(2): 339-49.

Jerusalmi, A., Morris-Downes, M. M., Sheahan, B. J. and Atkins, G. J. 2003. Effect of intranasal administration of Semliki Forest virus recombinant particles expressing reporter and cytokine genes on the progression of experimental autoimmune encephalomyelitis. *Mol Ther* **8**(6): 886-94.

Jerusalmi, A. 2004. *Development of the recombinant Semliki Forest virus vector as a gene therapy agent for the central nervous system*. PhD thesis. Dublin, Trinity College.

Jungbluth, A. A., Busam, K. J., Kolb, D., Iversen, K., Coplan, K., Chen, Y. T., Spagnoli, G. C. and Old, L. J. 2000. Expression of MAGE-antigens in normal tissues and cancer. *Int J Cancer* **85**(4): 460-5.

Kang, W. K., Park, C., Yoon, H. L., Kim, W. S., Yoon, S. S., Lee, M. H., Park, K., Kim, K., Jeong, H. S., Kim, J. A., Nam, S. J., Yang, J. H., Son, Y. I., Baek, C. H., Han, J., Ree, H. J., Lee, E. S., Kim, S. H., Kim, D. W., Ahn, Y. C., Huh, S. J., Choe, Y. H., Lee, J. H., Park, M. H., Kong, G. S., Park, E. Y., Kang, Y. K., Bang, Y. J., Paik, N. S., Lee, S. N., Kim, S., Robbins, P. D., Tahara, H., Lotze, M. T. and Park, C. H. 2001. Interleukin 12 gene therapy of cancer by peritumoral injection of transduced autologous fibroblasts: outcome of a phase I study. *Hum Gene Ther* **12**(6): 671-84.

Kanno, H., Hattori, S., Sato, H., Murata, H., Huang, F. H., Hayashi, A., Suzuki, N., Yamamoto, I., Kawamoto, S., Minami, M., Miyatake, S., Shuin, T. and Kaplitt, M. G. 1999. Experimental gene therapy against subcutaneously implanted glioma with a herpes simplex virus-defective vector expressing interferon-gamma. *Cancer Gene Ther* **6**(2): 147-54.

Khorana, A. A., Rosenblatt, J. D., Sahasrabudhe, D. M., Evans, T., Ladrigan, M., Marquis, D., Rosell, K., Whiteside, T., Phillippe, S., Acres, B., Slos, P., Squiban, P., Ross, M. and Kendra, K. 2003. A phase I trial of immunotherapy with intratumoral adenovirus-interferon-gamma (TG1041) in patients with malignant melanoma. *Cancer Gene Ther* **10**(4): 251-9.

Kito, T., Kuroda, E., Yokota, A. and Yamashita, U. 2002. Enhancement of macrophage cytotoxicity against murine gliomas by interferon beta: increase in nitric oxide production in response to glioma-derived soluble factors. *J Neurosurg* **97**(3): 619-26.

Knobbe, C. B., Merlo, A. and Reifenberger, G. 2002. Pten signaling in gliomas. *Neuro Oncol* **4**(3): 196-211.

Ko, L., Koestner, A. and Wechsler, W. 1980. Morphological characterization of nitrosourea-induced glioma cell lines and clones. *Acta Neuropathol* **51**(1): 23-31.

Korkolopoulou, P., Kaklamanis, L., Pezzella, F., Harris, A. L. and Gatter, K. C. 1996. Loss of antigen-presenting molecules (MHC class I and TAP-1) in lung cancer. *Br J Cancer* **73**(2): 148-53.

Kruse, C. A., Molleston, M. C., Parks, E. P., Schiltz, P. M., Kleinschmidt-DeMasters, B. K. and Hickey, W. F. 1994. A rat glioma model, CNS-1, with invasive characteristics similar to those of human gliomas: a comparison to 9L gliosarcoma. *J Neurooncol* **22**(3): 191-200.

Kumar, R., Kamdar, D., Madden, L., Hills, C., Crooks, D., O'Brien, D. and Greenman, J. 2006. Th1/Th2 cytokine imbalance in meningioma, anaplastic astrocytoma and glioblastoma multiforme patients. *Oncol Rep* **15**(6): 1513-6.

Lang, F. F., Bruner, J. M., Fuller, G. N., Aldape, K., Prados, M. D., Chang, S., Berger, M. S., McDermott, M. W., Kunwar, S. M., Junck, L. R., Chandler, W., Zwiebel, J. A., Kaplan, R. S. and Yung, W. K. 2003. Phase I trial of adenovirus-mediated p53 gene therapy for recurrent glioma: biological and clinical results. *J Clin Oncol* **21**(13): 2508-18.

Laperriere, N., Zuraw, L. and Cairncross, G. 2002. Radiotherapy for newly diagnosed malignant glioma in adults: a systematic review. *Radiother Oncol* **64**(3): 259-73.

Lebbink, R. J. and Meyaard, L. 2007. Non-MHC ligands for inhibitory immune receptors: novel insights and implications for immune regulation. *Mol Immunol* **44**(9): 2153-64.

Lemke, D. M. 2004. Epidemiology, diagnosis, and treatment of patients with metastatic cancer and high-grade gliomas of the central nervous system. *J Infus Nurs* **27**(4): 263-9.

Leung, S. Y., Wong, M. P., Chung, L. P., Chan, A. S. and Yuen, S. T. 1997. Monocyte chemoattractant protein-1 expression and macrophage infiltration in gliomas. *Acta Neuropathol* **93**(5): 518-27.

Levine, B. and Griffin, D. E. 1992. Persistence of viral RNA in mouse brains after recovery from acute alphavirus encephalitis. *J Virol* **66**(11): 6429-35.

Liljestrom, P. and Garoff, H. 1991. A new generation of animal cell expression vectors based on the Semliki Forest virus replicon. *Biotechnology (N Y)* **9**(12): 1356-61.

Ling, P., Gately, M. K., Gubler, U., Stern, A. S., Lin, P., Hollfelder, K., Su, C., Pan, Y. C. and Hakimi, J. 1995. Human IL-12 p40 homodimer binds to the IL-12 receptor but does not mediate biologic activity. *J Immunol* **154**(1): 116-27.

Liu, Y., Ehtesham, M., Samoto, K., Wheeler, C. J., Thompson, R. C., Villarreal, L. P., Black, K. L. and Yu, J. S. 2002. In situ adenoviral interleukin 12 gene transfer confers potent and long-lasting cytotoxic immunity in glioma. *Cancer Gene Ther* **9**(1): 9-15.

Lopez-Lastra, M., Rivas, A. and Barria, M. I. 2005. Protein synthesis in eukaryotes: the growing biological relevance of cap-independent translation initiation. *Biol Res* **38**(2-3): 121-46.

Louis, D. N. 2006. Molecular pathology of malignant gliomas. *Annu Rev Pathol* **1**: 97-117.

Louis, D., Ohgaki, H., Wiestler, O., Cavenee, W., Burger, P., Jouvet, A., Scheithauer, B. and Kleihues, P. 2007. The 2007 WHO classification of tumours of the central nervous system. *Acta Neuropathol*. **114**(2): 97-109.

Lu, W., Fidler, I. J. and Dong, Z. 1999. Eradication of primary murine fibrosarcomas and induction of systemic immunity by adenovirus-mediated interferon beta gene therapy. *Cancer Res* **59**(20): 5202-8.

Luft, T., Pang, K. C., Thomas, E., Hertzog, P., Hart, D. N., Trapani, J. and Cebon, J. 1998. Type I IFNs enhance the terminal differentiation of dendritic cells. *J Immunol* **161**(4): 1947-53.

Lundstrom, K., Schweitzer, C., Richards, J., MU., E., Jenck, F. and Mulhardt, C. 1999. Semliki Forest virus vectors for in vitro and in vivo applications. *Gene Ther Mol Biol*(4): 23-31.

Lundstrom, K. 2001. Novel developments for applications of alphavirus vectors in gene therapy *Gene Ther Mol Biol* **6**: 25-31.

Lundstrom, K., Rotmann, D., Hermann, D., Schneider, E. M. and Ehrengruber, M. U. 2001. Novel mutant Semliki Forest virus vectors: gene expression and localization studies in neuronal cells. *Histochem Cell Biol* **115**(1): 83-91.

Lundstrom, K., Abenavoli, A., Malgaroli, A. and Ehrengruber, M. U. 2003. Novel Semliki Forest virus vectors with reduced cytotoxicity and temperature sensitivity for long-term enhancement of transgene expression. *Mol Ther* **7**(2): 202-9.

Lyons, J. A., Sheahan, B. J., Galbraith, S. E., Mehra, R., Atkins, G. J. and Fleeton, M. N. 2006. Inhibition of angiogenesis by a Semliki Forest virus vector expressing VEGFR-2 reduces tumour growth and metastasis in mice. *Gene Ther* **14**(6): 503-13.

Maatta, A. M., Liimatainen, T., Wahlfors, T., Wirth, T., Vaha-Koskela, M., Jansson, L., Valonen, P., Hakkinen, K., Rautsi, O., Pellinen, R., Makinen, K., Hakumaki, J., Hinkkanen, A. and Wahlfors, J. 2007. Evaluation of cancer virotherapy with attenuated replicative Semliki forest virus in different rodent tumor models. *Int J Cancer* **121**(4): 863-70.

Mahaley, M. S., Jr., Bertsch, L., Cush, S. and Gillespie, G. Y. 1988. Systemic gamma-interferon therapy for recurrent gliomas. *J Neurosurg* **69**(6): 826-9.

Mantovani, A. 1994. Tumor-associated macrophages in neoplastic progression: a paradigm for the in vivo function of chemokines. *Lab Invest* **71**(1): 5-16.

Mariani, C. L., Rajon, D., Bova, F. J. and Streit, W. J. 2007. Nonspecific immunotherapy with intratumoral lipopolysaccharide and zymosan A but not GM-CSF leads to an effective anti-tumor response in subcutaneous RG-2 gliomas. *J Neurooncol* **85**(3): 231-40.

Marincola, F. M., Jaffee, E. M., Hicklin, D. J. and Ferrone, S. 2000. Escape of human solid tumors from T-cell recognition: molecular mechanisms and functional significance. *Adv Immunol* **74**: 181-273.

Martin-Villalba, A., Okuducu, A. F. and von Deimling, A. 2008. The evolution of our understanding on glioma. *Brain Pathol* **18**(3): 455-63.

Mathiot, C. C., Grimaud, G., Garry, P., Bouquety, J. C., Mada, A., Daguisy, A. M. and Georges, A. J. 1990. An outbreak of human Semliki Forest virus infections in Central African Republic. *Am J Trop Med Hyg* **42**(4): 386-93.

McHeyzer-Williams, M. G., Altman, J. D. and Davis, M. M. 1996. Tracking antigen-specific helper T cell responses. *Curr Opin Immunol* **8**(2): 278-84.

Mehlen, P. and Puisieux, A. 2006. Metastasis: a question of life or death. *Nat Rev Cancer* **6**(6): 449-58.

Merits, A., Vasiljeva, L., Ahola, T., Kaariainen, L. and Auvinen, P. 2001. Proteolytic processing of Semliki Forest virus-specific non-structural polyprotein by nsP2 protease. *J Gen Virol* **82**(Pt 4): 765-73.

Mesnil, M. and Yamasaki, H. 2000. Bystander effect in herpes simplex virus-thymidine kinase/ganciclovir cancer gene therapy: role of gap-junctional intercellular communication. *Cancer Res* **60**(15): 3989-99.

Murphy, F. J., Hayes, M. P. and Burd, P. R. 2000. Disparate intracellular processing of human IL-12 preprotein subunits: atypical processing of the P35 signal peptide. *J Immunol* **164**(2): 839-47.

Nakajima, Y., Kobayashi, K., Yamagishi, K., Enomoto, T. and Ohmiya, Y. 2004. cDNA cloning and characterization of a secreted luciferase from the luminous Japanese ostracod, Cypridina noctiluca. *Biosci Biotechnol Biochem* **68**(3): 565-70.

Nastala, C. L., Edington, H. D., McKinney, T. G., Tahara, H., Nalesnik, M. A., Brunda, M. J., Gately, M. K., Wolf, S. F., Schreiber, R. D., Storkus, W. J. and et al. 1994. Recombinant IL-12 administration induces tumor regression in association with IFN-gamma production. *J Immunol* **153**(4): 1697-706.

Natsume, A., Tsujimura, K., Mizuno, M., Takahashi, T. and Yoshida, J. 2000. IFN-beta gene therapy induces systemic antitumor immunity against malignant glioma. *J Neurooncol* **47**(2): 117-24.

Nguyen, K. B., Salazar-Mather, T. P., Dalod, M. Y., Van Deusen, J. B., Wei, X. Q., Liew, F. Y., Caligiuri, M. A., Durbin, J. E. and Biron, C. A. 2002A. Coordinated and distinct roles for IFN-alpha beta, IL-12, and IL-15 regulation of NK cell responses to viral infection. *J Immunol* **169**(8): 4279-87.

Nguyen, M. D., Julien, J. P. and Rivest, S. 2002B. Innate immunity: the missing link in neuroprotection and neurodegeneration? *Nat Rev Neurosci* **3**(3): 216-27.

Nishikawa, H., Kato, T., Tawara, I., Ikeda, H., Kuribayashi, K., Allen, P. M., Schreiber, R. D., Old, L. J. and Shiku, H. 2005. IFN-gamma controls the generation/activation of CD4+ CD25+ regulatory T cells in antitumor immune response. *J Immunol* **175**(7): 4433-40.

Nyberg, P., Xie, L. and Kalluri, R. 2005. Endogenous inhibitors of angiogenesis. *Cancer Res* **65**(10): 3967-79.

O'Byrne, K. J., Dalgleish, A. G., Browning, M. J., Steward, W. P. and Harris, A. L. 2000. The relationship between angiogenesis and the immune response in carcinogenesis and the progression of malignant disease. *Eur J Cancer* **36**(2): 151-69.

Ohgaki, H. and Kleihues, P. 2005. Epidemiology and etiology of gliomas. *Acta Neuropathol* **109**(1): 93-108.

Ohgaki, H. 2009. Epidemiology of brain tumors. *Methods Mol Biol* **472**: 323-42.

Oldstone, M. B., Tishon, A., Dutko, F. J., Kennedy, S. I., Holland, J. J. and Lampert, P. W. 1980. Does the major histocompatibility complex serve as a specific receptor for Semliki Forest virus? *J Virol* **34**(1): 256-65.

Olson, M. V., Lee, J., Zhang, F., Wang, A. and Dong, Z. 2006. Inducible nitric oxide synthase activity is essential for inhibition of prostatic tumor growth by interferon-beta gene therapy. *Cancer Gene Ther* **13**(7): 676-85.

Oshiro, S., Liu, Y., Fukushima, T., Asotra, K. and Black, K. L. 2001. Modified immunoregulation associated with interferon-gamma treatment of rat glioma. *Neurol Res* **23**(4): 359-66.

Packer, R. J., Prados, M., Phillips, P., Nicholson, H. S., Boyett, J. M., Goldwein, J., Rorke, L. B., Needle, M. N., Sutton, L., Zimmerman, R. A., Fitz, C. R., Vezina, L. G., Etcubanas, E., Wallenberg, J. C., Reaman, G. and Wara, W. 1996. Treatment of children with newly diagnosed brain stem gliomas with intravenous recombinant beta-interferon and hyperfractionated radiation therapy: a childrens cancer group phase I/II study. *Cancer* **77**(10): 2150-6.

Pannetier, C., Even, J. and Kourilsky, P. 1995. T-cell repertoire diversity and clonal expansions in normal and clinical samples. *Immunol Today* **16**(4): 176-81.

Parker, J. N., Gillespie, G. Y., Love, C. E., Randall, S., Whitley, R. J. and Markert, J. M. 2000. Engineered herpes simplex virus expressing IL-12 in the treatment of experimental murine brain tumors. *Proc Natl Acad Sci U S A* **97**(5): 2208-13.

Parkin, D. M., Bray, F., Ferlay, J. and Pisani, P. 2005. Global cancer statistics, 2002. *CA Cancer J Clin* **55**(2): 74-108.

Paul, D. B., Barth, R. F., Yang, W., Shen, G. H., Kim, J. and Triozzi, P. L. 2000. B7.1 expression by the weakly immunogenic F98 rat glioma does not enhance immunogenicity. *Gene Ther* **7**(12): 993-9.

Paulus, W. and Tonn, J. C. 1994. Basement membrane invasion of glioma cells mediated by integrin receptors. *J Neurosurg* **80**(3): 515-9.

Pecora, A. L., Rizvi, N., Cohen, G. I., Meropol, N. J., Sterman, D., Marshall, J. L., Goldberg, S., Gross, P., O'Neil, J. D., Groene, W. S., Roberts, M. S., Rabin, H., Bamat, M. K. and Lorence, R. M. 2002. Phase I trial of intravenous administration of PV701, an oncolytic virus, in patients with advanced solid cancers. *J Clin Oncol* **20**(9): 2251-66.

Peto, J. 2001. Cancer epidemiology in the last century and the next decade. *Nature* **411**(6835): 390-5.

Pisani, P., Parkin, D. M., Munoz, N. and Ferlay, J. 1997. Cancer and infection: estimates of the attributable fraction in 1990. *Cancer Epidemiol Biomarkers Prev* **6**(6): 387-400.

Portielje, J. E., Gratama, J. W., van Ojik, H. H., Stoter, G. and Kruit, W. H. 2003. IL-12: a promising adjuvant for cancer vaccination. *Cancer Immunol Immunother* **52**(3): 133-44.

Quinn, K. 2006. *Effect of intranasal administration of Semliki Forest virus recombinant particles expressing interferon-beta on the progression of experimental autoimmune encephalomyelitis*. PhD thesis. Trinity College, Dublin.

Rao, J. S. 2003. Molecular mechanisms of glioma invasiveness: the role of proteases. *Nat Rev Cancer* **3**(7): 489-501.

Roberts, R. O., Lynch, C. F., Jones, M. P. and Hart, M. N. 1991. Medulloblastoma: a population-based study of 532 cases. *J Neuropathol Exp Neurol* **50**(2): 134-44.

Rodriguez-Madoz, J. R., Prieto, J. and Smerdou, C. 2005. Semliki forest virus vectors engineered to express higher IL-12 levels induce efficient elimination of murine colon adenocarcinomas. *Mol Ther* **12**(1): 153-63.

Rodriguez-Madoz, J. R., Prieto, J. and Smerdou, C. 2007. Biodistribution and tumor infectivity of semliki forest virus vectors in mice: effects of re-administration. *Mol Ther* **15**(12): 2164-71.

Rosenberg, S. A., Restifo, N. P., Yang, J. C., Morgan, R. A. and Dudley, M. E. 2008. Adoptive cell transfer: a clinical path to effective cancer immunotherapy. *Nat Rev Cancer* **8**(4): 299-308.

Roth, P., Mittelbronn, M., Wick, W., Meyermann, R., Tatagiba, M. and Weller, M. 2007. Malignant glioma cells counteract antitumor immune responses through expression of lectin-like transcript-1. *Cancer Res* **67**(8): 3540-4.

Rousseau, J., Boudou, C., Barth, R. F., Balosso, J., Esteve, F. and Elleaume, H. 2007. Enhanced survival and cure of F98 glioma-bearing rats following intracerebral delivery of carboplatin in combination with photon irradiation. *Clin Cancer Res* **13**(17): 5195-201.

Russel, D. S. and Rubinstein, L. T. 2007. Pathology of Tumours of the Nervous System, 7th edn. *British Journal of Neurosurgery* **21**(1): 82-83.

Ryman, K. D. and Klimstra, W. B. 2008. Host responses to alphavirus infection. *Immunol Rev* **225**: 27-45.

Saleh, M., Jonas, N. K., Wiegmans, A. and Stylli, S. S. 2000. The treatment of established intracranial tumors by in situ retroviral IFN-gamma transfer. *Gene Ther* **7**(20): 1715-24.

Salminen, A., Wahlberg, J. M., Lobigs, M., Liljestrom, P. and Garoff, H. 1992. Membrane fusion process of Semliki Forest virus. II: Cleavage-dependent reorganization of the spike protein complex controls virus entry. *J Cell Biol* **116**(2): 349-57.

Sammin, D. J., Butler, D., Atkins, G. J. and Sheahan, B. J. 1999. Cell death mechanisms in the olfactory bulb of rats infected intranasally with Semliki forest virus. *Neuropathol Appl Neurobiol* **25**(3): 236-43.

Sandmair, A. M., Loimas, S., Puranen, P., Immonen, A., Kossila, M., Puranen, M., Hurskainen, H., Tyynela, K., Turunen, M., Vanninen, R., Lehtolainen, P., Paljarvi, L., Johansson, R., Vapalahti, M. and Yla-Herttuala, S. 2000. Thymidine kinase gene therapy for human malignant glioma, using replication-deficient retroviruses or adenoviruses. *Hum Gene Ther* **11**(16): 2197-205.

Santosuosso, M., McCormick, S. and Xing, Z. 2005. Adenoviral vectors for mucosal vaccination against infectious diseases. *Viral Immunol* **18**(2): 283-91.

Schmidek, H. H., Nielsen, S. L., Schiller, A. L. and Messer, J. 1971. Morphological studies of rat brain tumors induced by N-nitrosomethylurea. *J Neurosurg* **34**(3): 335-40.

Schottenfeld, D. and Beebe-Dimmer, J. L. 2005. Advances in cancer epidemiology: understanding causal mechanisms and the evidence for implementing interventions. *Annu Rev Public Health* **26**: 37-60.

Schroder, K., Hertzog, P. J., Ravasi, T. and Hume, D. A. 2004. Interferon-gamma: an overview of signals, mechanisms and functions. *J Leukoc Biol* **75**(2): 163-89.

Schultz, D. R. and Harrington, W. J., Jr. 2003. Apoptosis: programmed cell death at a molecular level. *Semin Arthritis Rheum* **32**(6): 345-69.

Schwartzbaum, J. A., Fisher, J. L., Aldape, K. D. and Wrensch, M. 2006. Epidemiology and molecular pathology of glioma. *Nat Clin Pract Neurol* **2**(9): 494-503; quiz 1 p following 516.

Seitz, R. J., Deckert, M. and Wechsler, W. 1988. Vascularization of syngenic intracerebral RG2 and F98 rat transplantation tumors. A histochemical and morphometric study by use of ricinus communis agglutinin I. *Acta Neuropathol* **76**(6): 599-605.

Shay, J. W. and Bacchetti, S. 1997. A survey of telomerase activity in human cancer. *Eur J Cancer* **33**(5): 787-91.

Sheahan, B., Ibrahim, M. and Atkins, G. 1996. Demyelination of olfactory pathways in mice following intranasal infection with the avirulent A7 strain of Semliki Forest virus. *European Journal of Veterinary Pathology* **2**(3): 117-125.

Sherr, C. J. and McCormick, F. 2002. The RB and p53 pathways in cancer. *Cancer Cell* **2**(2): 103-12.

Shurin, M. R., Lu, L., Kalinski, P., Stewart-Akers, A. M. and Lotze, M. T. 1999. Th1/Th2 balance in cancer, transplantation and pregnancy. *Springer Semin Immunopathol* **21**(3): 339-59.

Sibenaller, Z. A., Etame, A. B., Ali, M. M., Barua, M., Braun, T. A., Casavant, T. L. and Ryken, T. C. 2005. Genetic characterization of commonly used glioma cell lines in the rat animal model system. *Neurosurg Focus* **19**(4): E1.

Smerdou, C. and Liljestrom, P. 1999. Two-helper RNA system for production of recombinant Semliki forest virus particles. *J Virol* **73**(2): 1092-8.

Smithburn, K. C. and Haddow, J. A. 1944. Semliki Forest Virus I. Isolation and Pathogenic Properties. *The Journal of Immunology* **43**(3): 141-157.

Smyth, M. J., Taniguchi, M. and Street, S. E. 2000A. The anti-tumor activity of IL-12: mechanisms of innate immunity that are model and dose dependent. *J Immunol* **165**(5): 2665-70.

Smyth, M. J., Thia, K. Y., Street, S. E., Cretney, E., Trapani, J. A., Taniguchi, M., Kawano, T., Pelikan, S. B., Crowe, N. Y. and Godfrey, D. I. 2000B. Differential tumor surveillance by natural killer (NK) and NKT cells. *J Exp Med* **191**(4): 661-8.

Smyth, J. W. P. 2004. Inhibition of K-BALB murine tumours using semliki forest virus and its derived vector.

Smyth, J. W., Fleeton, M. N., Sheahan, B. J. and Atkins, G. J. 2005. Treatment of rapidly growing K-BALB and CT26 mouse tumours using Semliki Forest virus and its derived vector. *Gene Ther* **12**(2): 147-59.

Stark, G. R., I. M. Kerr, et al. (1998). How cells respond to interferons. *Annu Rev Biochem* **67**: 227-64.

Strauss, J. H. and Strauss, E. G. 1994. The alphaviruses: gene expression, replication, and evolution. *Microbiol Rev* **58**(3): 491-562.

Stupp, R., Mason, W. P., van den Bent, M. J., Weller, M., Fisher, B., Taphoorn, M. J., Belanger, K., Brandes, A. A., Marosi, C., Bogdahn, U., Curschmann, J., Janzer, R. C., Ludwin, S. K., Gorlia, T., Allgeier, A., Lacombe, D., Cairncross, J. G., Eisenhauer, E. and Mirimanoff, R. O. 2005. Radiotherapy plus concomitant and adjuvant temozolomide for glioblastoma. *N Engl J Med* **352**(10): 987-96.

Summers, B., Cummings, J. and De Lahunta, A. 1995. Veterinary Pathology.

Tahara, H., Zitvogel, L., Storkus, W. J., Zeh, H. J., 3rd, McKinney, T. G., Schreiber, R. D., Gubler, U., Robbins, P. D. and Lotze, M. T. 1995. Effective eradication of established murine tumors with IL-12 gene therapy using a polycistronic retroviral vector. *J Immunol* **154**(12): 6466-74.

Takaoka, A., Hayakawa, S., Yanai, H., Stoiber, D., Negishi, H., Kikuchi, H., Sasaki, S., Imai, K., Shibue, T., Honda, K. and Taniguchi, T. 2003. Integration of interferon-alpha/beta signalling to p53 responses in tumour suppression and antiviral defence. *Nature* **424**(6948): 516-23.

Tjuvajev, J., Gansbacher, B., Desai, R., Beattie, B., Kaplitt, M., Matei, C., Koutcher, J., Gilboa, E. and Blasberg, R. 1995. RG-2 glioma growth attenuation and severe brain edema caused by local production of interleukin-2 and interferon-gamma. *Cancer Res* **55**(9): 1902-10.

Toda, M., Martuza, R. L., Kojima, H. and Rabkin, S. D. 1998. In situ cancer vaccination: an IL-12 defective vector/replication-competent herpes simplex virus combination induces local and systemic antitumor activity. *J Immunol* **160**(9): 4457-64.

Trinchieri, G. 1998. Immunobiology of interleukin-12. *Immunol Res* **17**(1-2): 269-78.

Trojan, J., Cloix, J. F., Ardourel, M. Y., Chatel, M. and Anthony, D. D. 2007. Insulin-like growth factor type I biology and targeting in malignant gliomas. *Neuroscience* **145**(3): 795-811.

Tsung, K., Meko, J. B., Peplinski, G. R., Tsung, Y. L. and Norton, J. A. 1997. IL-12 induces T helper 1-directed antitumor response. *J Immunol* **158**(7): 3359-65.

Tzeng, J. J., Barth, R. F., Orosz, C. G. and James, S. M. 1991. Phenotype and functional activity of tumor-infiltrating lymphocytes isolated from immunogenic and nonimmunogenic rat brain tumors. *Cancer Res* **51**(9): 2373-8.

Tuteja, N. and Tuteja, R. 2001. Unraveling DNA repair in human: molecular mechanisms and consequences of repair defect. *Crit Rev Biochem Mol Biol* **36**(3): 261-90.

U Geigenmüller-Gnirke, B Weiss, R Wright and Schlesinger, S. 1991. Complementation between Sindbis viral RNAs produces infectious particles with a bipartite genome. *PNAS* **88**: 3253-3257.

Urban, C., Rheme, C., Maerz, S., Berg, B., Pick, R., Nitschke, R. and Borner, C. 2008. Apoptosis induced by Semliki Forest virus is RNA replication dependent and mediated via Bak. *Cell Death Differ* **15**(9): 1396-407.

Valable, S., Lemasson, B., Farion, R., Beaumont, M., Segebarth, C., Remy, C. and Barbier, E. L. 2008. Assessment of blood volume, vessel size, and the expression

of angiogenic factors in two rat glioma models: a longitudinal in vivo and ex vivo study. *NMR Biomed* **21**(10): 1043-56.

Vasiljeva, L., Merits, A., Golubtsov, A., Sizemskaja, V., Kaariainen, L. and Ahola, T. 2003. Regulation of the sequential processing of Semliki Forest virus replicase polyprotein. *J Biol Chem* **278**(43): 41636-45.

Ventoso, I., Sanz, M. A., Molina, S., Berlanga, J. J., Carrasco, L. and Esteban, M. 2006. Translational resistance of late alphavirus mRNA to eIF2alpha phosphorylation: a strategy to overcome the antiviral effect of protein kinase PKR. *Genes Dev* **20**(1): 87-100.

Vermeulen, K., Van Bockstaele, D. R. and Berneman, Z. N. 2003. The cell cycle: a review of regulation, deregulation and therapeutic targets in cancer. *Cell Prolif* **36**(3): 131-49.

Vogelstein, B. and Kinzler, K. W. 2004. Cancer genes and the pathways they control. *Nat Med* **10**(8): 789-99.

Von Deimling, A., Eibl, R. H., Ohgaki, H., Louis, D. N., von Ammon, K., Petersen, I., Kleihues, P., Chung, R. Y., Wiestler, O. D. and Seizinger, B. R. 1992. p53 mutations are associated with 17p allelic loss in grade II and grade III astrocytoma. *Cancer Res* **52**(10): 2987-90.

Wagner, S., Czub, S., Greif, M., Vince, G. H., Suss, N., Kerkau, S., Rieckmann, P., Roggendorf, W., Roosen, K. and Tonn, J. C. 1999. Microglial/macrophage expression of interleukin 10 in human glioblastomas. *Int J Cancer* **82**(1): 12-6.

Walker, P. R., Calzascia, T., de Tribolet, N. and Dietrich, P. Y. 2003. T-cell immune responses in the brain and their relevance for cerebral malignancies. *Brain Res Brain Res Rev* **42**(2): 97-122.

Wan, Y. Y. and Flavell, R. A. 2006. The roles for cytokines in the generation and maintenance of regulatory T cells. *Immunol Rev* **212**: 114-30.

Wang, K. S., Kuhn, R. J., Strauss, E. G., Ou, S. and Strauss, J. H. 1992. High-affinity laminin receptor is a receptor for Sindbis virus in mammalian cells. *J Virol* **66**(8): 4992-5001.

Watford, W. T., Moriguchi, M., Morinobu, A. and O'Shea, J. J. 2003. The biology of IL-12: coordinating innate and adaptive immune responses. *Cytokine Growth Factor Rev* **14**(5): 361-8.

Watts, R. G. and Merchant, R. E. 1992. Cerebrovascular effects and tumor kinetics after a single intratumoral injection of human recombinant interleukin-2 alone or in

combination with intravenous chemotherapy in a rat model of glioma. *Neurosurgery* **31**(1): 89-98; discussion 98-9.

Wechsler, W., Szymas, J., Bilzer, T. and Hossmann, K. A. 1989. Experimental transplantation gliomas in the adult cat brain. 1. Experimental model and neuropathology. *Acta Neurochir (Wien)* **98**(1-2): 77-89.

Weinberg, R. A. 1995. The retinoblastoma protein and cell cycle control. *Cell* **81**(3): 323-30.

Weinberg, R. A. 2006. *The Biology of Cancer*.

Wesseling, P., Ruiter, D. J. and Burger, P. C. 1997. Angiogenesis in brain tumors; pathobiological and clinical aspects. *J Neurooncol* **32**(3): 253-65.

Whiteside, T. L. 2002. Tumor-induced death of immune cells: its mechanisms and consequences. *Semin Cancer Biol* **12**(1): 43-50.

Willems, W. R., Kaluza, G., Boschek, C. B., Bauer, H., Hager, H., Schutz, H. J. and Feistner, H. 1979. Semliki forest virus: cause of a fatal case of human encephalitis. *Science* **203**(4385): 1127-9.

Williams, K., Jr., Ulvestad, E., Cragg, L., Blain, M. and Antel, J. P. 1993. Induction of primary T cell responses by human glial cells. *J Neurosci Res* **36**(4): 382-90.

Windbichler, G. H., Hausmaninger, H., Stummvoll, W., Graf, A. H., Kainz, C., Lahodny, J., Denison, U., Muller-Holzner, E. and Marth, C. 2000. Interferon-gamma in the first-line therapy of ovarian cancer: a randomized phase III trial. *Br J Cancer* **82**(6): 1138-44.

Xu, L., Xie, K. and Fidler, I. J. 1998A. Therapy of human ovarian cancer by transfection with the murine interferon beta gene: role of macrophage-inducible nitric oxide synthase. *Hum Gene Ther* **9**(18): 2699-708.

Xu, X., Fu, X. Y., Plate, J. and Chong, A. S. 1998B. IFN-gamma induces cell growth inhibition by Fas-mediated apoptosis: requirement of STAT1 protein for up-regulation of Fas and FasL expression. *Cancer Res* **58**(13): 2832-7.

Yamanaka, R., Zullo, S. A., Tanaka, R., Ramsey, J., Blaese, M. and Xanthopoulos, K. G. 2000. Induction of a therapeutic antitumor immunological response by intratumoral injection of genetically engineered Semliki Forest virus to produce interleukin-12. *Neurosurg Focus* **9**(6): e7.

Yang, S. Y., Liu, H. and Zhang, J. N. 2004. Gene therapy of rat malignant gliomas using neural stem cells expressing IL-12. *DNA Cell Biol* **23**(6): 381-9.

Yoshida, J., Mizuno, M. and Wakabayashi, T. 2004. Interferon-beta gene therapy for

cancer: basic research to clinical application. *Cancer Sci* **95**(11): 858-65.

Yung, W. K., Castellanos, A. M., Van Tassel, P., Moser, R. P. and Marcus, S. G. 1990. A pilot study of recombinant interferon beta (IFN-beta ser) in patients with recurrent glioma. *J Neurooncol* **9**(1): 29-34.

Yung, W. K., Prados, M., Levin, V. A., Fetell, M. R., Bennett, J., Mahaley, M. S., Salcman, M. and Etcubanas, E. 1991. Intravenous recombinant interferon beta in patients with recurrent malignant gliomas: a phase I/II study. *J Clin Oncol* **9**(11): 1945-9.

Yung, W. K., Prados, M. D., Yaya-Tur, R., Rosenfeld, S. S., Brada, M., Friedman, H. S., Albright, R., Olson, J., Chang, S. M., O'Neill, A. M., Friedman, A. H., Bruner, J., Yue, N., Dugan, M., Zaknoen, S. and Levin, V. A. 1999. Multicenter phase II trial of temozolomide in patients with anaplastic astrocytoma or anaplastic oligoastrocytoma at first relapse. Temodal Brain Tumor Group. *J Clin Oncol* **17**(9): 2762-71.

Zhang, A., Wu, Y., Lai, H. W. L. and Yew, D. T. 2004A. Apoptosis -- A Brief Review. *Neuroembryology and Aging* **3**(1): 47-59.

Zhang, R., Zhang, Z., Zhang, C., Zhang, L., Robin, A., Wang, Y., Lu, M. and Chopp, M. 2004B. Stroke transiently increases subventricular zone cell division from asymmetric to symmetric and increases neuronal differentiation in the adult rat. *J Neurosci* **24**(25): 5810-5.

Zhao, H., Otaki, J. M. and Firestein, S. 1996. Adenovirus-mediated gene transfer in olfactory neurons in vivo. *J Neurobiol* **30**(4): 521-30.

Zitvogel, L., Tahara, H., Robbins, P. D., Storkus, W. J., Clarke, M. R., Nalesnik, M. A. and Lotze, M. T. 1995. Cancer immunotherapy of established tumors with IL-12. Effective delivery by genetically engineered fibroblasts. *J Immunol* **155**(3): 1393-403.

Zou, W. 2005. Immunosuppressive networks in the tumour environment and their therapeutic relevance. *Nat Rev Cancer* **5**(4): 263-74.